To the Graduate Council:

I am submitting herewith a dissertation written by Ali Vatansever entitled "Thermal Aging and Morphology of High Voltage Crosslinked Polyethylene Cables". I have examined the final copy of this dissertation for form and content and recommend that it be accepted in partial fulfillment of the requirements for the degree of Doctor of Philosophy, with a major in Polymer Engineering.

Paul J. Phillips, Major Professor

We have read this dissertation
and recommend its acceptance:

Accepted for the Council:

Vice Provost
and Dean of The Graduate School

THERMAL AGING AND MORPHOLOGY OF HIGH VOLTAGE CROSSLINKED POLYETHYLENE CABLES

A Dissertation

Presented for the

Doctor of Philosophy

Degree

The University of Tennessee, Knoxville

Ali Vatansever

March 1987

To My Wife Nurhan

ACKNOWLEDGEMENTS

The author wishes to thank his advisor, Professor Paul J. Phillips for his contributions, suggestions, guidance and constructive criticism throughout this work.

The author thanks The Electric Power Research Institute for the financial support.

The author would like to express his appreciation to Dr. J.S. Lin at Oak Ridge National Laboratories for his help and useful discussions.

The author appreciates the discussions with fellow graduate students Young D. Lee, Galen C. Richeson and Deepak R. Parikh in the Department of MSE and Paul A. Flowers in the Department of Chemistry. The technical help provided by the departmental electronic and machine shops and by Dick Williams in The Biology Department is appreciated.

The author expresses his appreciation to his wife Nurhan Vatansever, who has been a graduate student coworker, for her input, discussions and encouragement throughout this work and her help in typing the thesis.

Finally, the author wishes to thank his committee members, Professors, P. J. Phillips, J. E. Spruiell, E. S. Clark and J. D. Kovac.

ABSTRACT

High Voltage polyethylene (PE) and crosslinked polyethylene (XLPE) cables extruded and cured under different conditions were obtained from major cable producing companies and studied to define their physical, chemical and morphological structures. All XLPE cables were found to comprise of crosslinked network (gel) and uncrosslinked extractable fractions (sol). The amount of extractables, crosslink density, melting characteristics as well as morphology were found to differ according to the method of heat transfer used during crosslinking. The effect of extractables on the melting of the original cables and on annealing process, especially at high annealing temperatures, was found to be different from one cable to another. The morphologies throughout the cables are sheaf-like and the appearance of those morphological entities upon annealing remained unchanged. An understanding was obtained of the annealing mechanisms operating at different temperatures which resulted in multiple melting behavior. One process was shown to be caused by a separation of sol from gel in the melt. On the other hand, morphological structure was found to be altered on a lamellar scale upon thermal and thermoelectrical aging in terms of the lamellar thickness and void content. Understanding of the complicated

multiple melting behavior and molecular changes taking place in field aged cables was deduced from knowledge of isothermal annealings carried out on the original cables. While a deterioration in the dielectric breakdown strength was observed for the laboratory cured XLPE samples annealed at temperatures up to 95 ^{o}C, the breakdown strength was found to increase for samples annealed between 100 ^{o}C and 107 ^{o}C.

SECTION PAGE

1. INTRODUCTION..... 1

2. LITERATURE REVIEW..... 8

2.1. Electrical Properties of Polymers..... 8

2.2. Dielectric Breakdown in Polymers 11

2.2.1. Thermal Breakdown 12

2.2.2. Electrical Breakdown..... 14

2.2.3. Electromechanical Breakdown..... 15

2.3. Aging of Polymeric Insulation..... 15

2.3.1. Treeing Phenomena..... 16

2.3.2. Factors Affecting Treeing..... 20

2.3.2.1. Molecular Structure..... 22

2.3.2.2. Morphology..... 23

2.3.3. Accelerated Aging 27

2.4. Polymers Used in High Voltage Applications..... 29

2.4.1. Polyethylene 30

2.4.2. Crosslinked Polyethylene..... 33

2.4.3. Manufacture of Cable Insulation 37

2.5. Polymer Crystallization and Morphology..... 39

2.5.1. Polymer Crystallization..... 39

2.5.1.1. Chain Folding..... 42

2.5.1.2. Bulk Crystallization..... 45

2.5.2. Polymer Morphology..... 47

2.5.2.1. Lamellar Crystals..... 47

2.5.2.2. Spherulites..... 48

2.5.2.3. Degree of Crystallinity..... 51
2.6. Thermal-Morphological Relationships..... 53
2.6.1. Melting..... 53
2.6.2. Annealing..... 56

3- EXPERIMENTATION..... 61
3.1. Materials..... 61
3.1.1. High Voltage Cables 61
3.1.2. Crosslinked Polyethylene Preparation.... 65
3.2. Characterization of Cables..... 68
3.2.1. Extraction 68
3.2.2. Crosslink Density Determination..... 72
3.2.3. Molecular Weight Determination..... 75
3.2.4. Infrared Spectroscopy Studies..... 77
3.3. Thermal Studies..... 79
3.3.1. Annealing..... 79
3.3.2. DSC Analysis..... 81
3.4. Thermo-Optical Studies..... 85
3.4.1. Instrumentation..... 85
3.4.2. In-Situ Annealing Studies..... 88
3.5. X-Ray Studies..... 89
3.5.1. Wide Angle X-Ray Studies 89
3.5.2. Small Angle X-Ray Studies..... 93
3.6. Morphology Studies..... 97
3.6.1. Microtoming..... 97
3.6.2. Etching..... 98

3.6.3. Replication..... 102

3.6.4. Microscopy..... 103

4. RESULTS..... 106

4.1. Crosslinking of LDPE..... 106

4.2. Original Cables..... 107

4.2.1. Extraction Studies..... 107

4.2.2. Crosslink Density Determination..... 116

4.2.3. Molecular Weight Studies of Extractables. 120

4.2.4. Spectroscopic Studies..... 123

4.2.5. DSC Studies..... 130

4.2.6. X-Ray Studies..... 148

4.2.7. Optical and Electron Microscopy..... 163

4.3. Thermally Aged Cables 177

4.3.1. DSC Studies..... 177

4.3.2. Thermo-Optical Studies..... 223

4.3.3. X-Ray Studies..... 235

4.3.4. Electron Microscopy 238

4.3.5. Electrical Breakdown Studies..... 245

4.4. Field Aged Cables..... 256

4.4.1. Extraction Studies..... 256

4.4.2. Molecular Weight Studies of Extractables. 259

4.4.3. Spectroscopic Studies..... 259

4.4.4. DSC Studies..... 265

4.4.5. X-Ray Studies..... 277

5. DISCUSSION..... 288

5.1. Original Cables..... 289

5.1.1. Sol-Gel Fractions..... 289

5.1.2. Molecular Structure 292

5.1.3. Thermal Behavior..... 298

5.1.4. Morphology..... 305

5.1.5. Evaluation of Original Cables..... 312

5.2. Thermally Aged Cables 314

5.2.1. Thermal Behavior..... 315

5.2.2. In-Situ Annealing Studies..... 324

5.2.3. Morphology..... 328

5.2.4. Electrical Breakdown Studies..... 331

5.3. Field Aged Cables..... 338

5.3.1. Changes in Molecular Structure..... 338

5.3.2. Thermal Behavior..... 341

5.3.3. Morphological Changes..... 347

6.CONCLUSIONS..... 349

7.SUGGESTIONS FOR FURTHER WORK 353

LIST OF REFERENCES..... 355

VITA..... 364

LIST OF TABLES

TABLE		PAGE
1	Specifications of HV transmission cables.....	62
2	Specifications of HV distribution cables.....	63
3	Thermoelectrical history of field aged cable E2 at the Waltz Mill aging facility.....	65
4	Crosslink density and molecular weight between crosslinks data for cables A1, C1 and E1.....	119
5	Viscosity average molecular weight of extractables from cables A1, E1 and C1.....	121
6	GPC results for extractables from different sections of cable A1.....	122
7	FTIR data of the indicated original transmission and distribution cables.....	129
8	DSC data of the original and gel fractions of the inner and outer radial sections of cable A1...	144
9	DSC results of the indicated original distribution cables.....	147
10	WAXS and SAXS results of the indicated original transmission and distribution cables.....	153
11	Percent crystalline material present at the indicated annealing temperatures for cable A1.....	237
12	SAXS results obtained from annealed transmission cables.....	244
13	Electrical breakdown data of XLPE thin films..	255
14	Percent extractables versus radial position for the indicated distribution cables.....	258
15	GPC results on extractables obtained from the indicated radial positions of field aged cable E2.....	261

16 FTIR data for the indicated field aged transmission and distribution cables..... 264

17 DSC results for the indicated field aged distribution cables.....276

18 SAXS results obtained from field aged cables....287

19 Breadth of the (110) crystalline peak at half maximum in HV XLPE transmission cables.....310

20 Rate of increase in percent crystallinity of the high temperature peak for cables A1-8 and E1-8 at the indicated annealing temperatures.....323

21 Recrystallization rates for the original and the gel fraction of the inner layer of cable A1....326

LIST OF FIGURES

FIGURE		PAGE
1	Cross-section of a typical single core three-polymeric layer cable insulation.....	38
2	Manufacture of conventional XLPE cable using catenary continuous vulcanization process.....	40
3	The simplest side-by-side arrangement of linear zig-zag chains.....	43
4	The fringed micelle model.....	44
5	Chain folding in lamellar crystals.....	46
6	Schematic representation of spherulites having lamellar structure and chain folding.....	49
7	Schematic representation of spherulitic growth (from Bassett 1981).....	52
8	A typical DSC melting curve for a semicrystalline polymer.....	55
9	A schematic representation of lamellar thickening (Dreyfuss and Keller 1970).....	58
10	Radial sectioning of HV cable insulation.....	70
11	Schematic representation of a typical DSC system....	82
12	A uniaxial crystal between cross-polars.....	86
13	Thermo-optical light transmission microscope set-up.	87
14	High temperature X-ray cell.....	92
15	Schematic drawings of the ORNL ten-meter SAXS spectrometer.....	94
16	Schematic representation of the rotary microtome with cold stage modification.....	99
17	Schematic of glass blade preparation.....	100
18	Diagram of the steps involved in morphological study using TEM.....	104

19 Experimental percent extractables versus calculated percent extractables for XLPEs prepared from the blends of 2 % DCP and LDPEs with different MWD.....108

20 Swelling ratio versus percent extractables for XLPEs prepared from the blends of 2 % DCP with LDPE (Union Carbide HFDE 4201), LDPE + 20 % sol and LDPE + 40 % sol.....109

21 Percent extractables versus radial position for the radial directions M, L and R of cable A1.....111

22 Percent extractables versus radial position for PEG cured cables A1 and A2.....112

23 Percent extractables versus radial position for steam cured cables B1, B2, B3 and B4.....113

24 Percent extractables versus radial position for cables A1, C1 and E1.....115

25 Swelling ratio versus radial position for cables A1, A2, C1 and E1.....117

26 Percent extractables versus swelling ratio for cables A1, A2, C1 and E1.....118

27 Molecular weight distributions for the extractables obtained from the indicated radial positions of cable A1.....124

28 Molecular weight distributions for the uncrosslinked Union Carbide HFDE 4201 LDPE.....125

29 FTIR spectra of HV cables in the 800-1000 cm^{-1} region.....126

30 FTIR spectra of HV cables in the 1600-2000 cm^{-1} region.....127

31 DSC thermograms obtained from the indicated radial positions of the narrow radial section of cable A1.....131

32 DSC thermograms obtained from the indicated radial positions of the wide radial section of cable A1.....132

33 DSC thermograms obtained from the indicated radial positions of cable C1.....133

34 DSC thermograms obtained from the indicated radial positions of cable E1.....134

35 Melting temperature, T_m, versus radial position for cables A1 narrow and broad regions C1 and E1.....135

36 Return to the base line temperature, T_{rb}, versus radial position for cables A1 narrow region, C1 and E1.....137

37 T_m and T_{rb} as a function of percent extractables for cable A1.....138

38 Percent crystallinity obtained from DSC as a function of radial position for cables A1, C1 and E1.....139

39 T_m and T_{rb} as a function of radial position for original and heat treated cables A1, C1 and E1.....141

40 DSC thermograms obtained from the outer (#1) and inner (#8) radial sections of the unextracted and gel versions of cable A1.....143

41 DSC thermograms obtained from the outermost (#1) and innermost (#4) layers of D1 and D3 LDPE distribution cables.....145

42 DSC thermograms obtained from the outermost (#1), the innermost (#3) and middle (#2) sections of D8 XLPE distribution cable.....146

43 Wide angle X-ray diffraction patterns of (a) the outermost and (b) the innermost layers of cable A1 in the radial direction obtained using a flat plate camera.....149

44 Representation of the direction nomenclature used in the cable analyses.....150

45 Intensity versus 2θ WAXS diffraction patterns obtained for the indicated cables.....151

46 SAXS contours obtained from (a) outer layer (b) inner layer of cable A1.....154

47 SAXS contours obtained from (a) outer layer (b) inner layer of cable C1.....155

48 SAXS contours obtained from (a) outer layer (b) inner layer of cable E1.....156

49 SAXS contours obtained from (a) gel fraction of inner layer of cable A1 and (b) outer layer of cable C1 quenched from the melt.....157

50 SAXS contours obtained for original distribution cables (a) D1 and (b) D8.....158

51 Circumferential average intensity versus scattering vector for the outer and inner layers of cable A1and A1-8 gel.....159

52 Circumferential average intensity versus scattering vector for the outer and inner layers of cable C1 and C1-1 Quenched.....160

53 Circumferential average intensity versus scattering vector for the outer and inner layers of cable E1.....161

54 Circumferential average intensity versus scattering vector for distribution cables D1 and D8.....162

55 Optical microscope pictures of a microtomed slice of cable A1 taken between cross-polars showing (a) concentric frozen-in stress lines (b) similar lines along the axial direction. Dotted line in (a) corresponds to blue line.....164

56 (a)(b)(c), optical microscope pictures of a microtomed slice of distribution cable D8 taken between cross-polars showing swirled features in the radial plane.....165

57 A higher magnification optical microscope picture of the area "A" in Figure 56-c.....167

58 Optical microscope picture of a microtomed thin slice of distribution cable D8 in the axial plane.....168

59 SEM picture showing the topography of the melt crystallized distribution cable D8.....170

60 (a)(b) TEM pictures of 2 % XLPE crystallized at 92 ^{o}C for two hours.....171

61 TEM picture of cable A1-8 crystallized at 92 °C for two hours.....173

62 (a)(b) TEM pictures of the inner radial section of original cable A1.....174

63 TEM picture showing worm-like lamellae with random orientation in the regions between sheaves for cable A1-8.....176

64 (a)(b) TEM pictures of the outer radial section of original cable E1.....178

65 (a)(b) TEM pictures of the inner radial section of original cable E1.....180

66 A histogram of the void size distribution of cable E1.....182

67 (a)(b) TEM pictures of the outer radial section of original cable C1.....183

68 (a)(b) TEM pictures of the outer radial section of cable C1 after it was quenched from the melt.....185

69 TEM picture of the inner radial section of original cable C1.....187

70 TEM picture of original distribution cable D1.....188

71 DSC thermograms obtained from the inner radial section of cable A1 annealed at 90 °C for the indicated periods of time.....190

72 DSC thermograms obtained from the inner radial section of cable A1 annealed at 92 °C for the indicated periods of time.....191

73 DSC thermograms obtained from the inner radial section of cable A1 annealed at 95 °C for the indicated periods of time.....192

74 DSC thermograms obtained from the inner radial section of cable A1 annealed at 97 °C for the indicated periods of time.....193

75 Comparative DSC thermograms obtained for cable A1 after annealing at 92 °C, 95 °C, 97 °C for (a) two hours (b) ten hours.....194

76 Melting peak temperatures as a function of annealing time for cable A1 annealed at 92, 95 and 97 °C.....195

77 DSC thermograms obtained from the inner radial section of cable A1 annealed at 100 °C, 103 °C and 107 °C for one hour.....197

78 High temperature peak width at half maximum versus annealing temperature.....198

79 DSC thermograms obtained from the inner radial section of cable A1 after annealing at 107 °C for (a) 2, (b) 7, (c) 15 and (d) 21 days.....199

80 Melting peak temperatures as a function of annealing time for cable A1 annealed at 103, 105 and 107 °C...200

81 Percentage of high temperature peak as a function of annealing time for cables A1 and E1 at indicated temperatures..... ..201

82 Percent of high temperature peak as a function of time for cable A1 annealed at 107 °C.....202

83 DSC thermograms of the outermost and innermost radial sections of cable A1 annealed at 90, 92,95 and 97 °C for one hour.....204

84 Melting temperatures as a function of annealing time for the outermost and innermost layers of cable A1 at 90, 95 and 97°C.....205

85 DSC thermograms of the outermost and innermost radial sections of cable A1 annealed at 100, 103 and 107 °C for one hour.....206

86 Melting temperatures as a function of annealing time for the outermost and innermost radial sections of cable A1 annealed at 100, 103, 105 and 107 °C for one hour.....207

87 DSC thermograms of the innermost radial section of cable A1 and its gel fraction at the indicated annealing temperatures.....209

88 DSC thermograms of the innermost radial section of cable A1 and its gel fraction annealed at 100, 103 and 107 °C for one hour.....210

89 Melting peak temperatures as a function of annealing time for the innermost radial section of cable A1 and its gel fraction annealed at 100, 103 and 107 °C.....211

90 Melting peak temperatures as a function of annealing time for the innermost radial section of cable A1 and its gel fraction annealed at 92, 95 and 97 °C.....212

91 DSC thermograms of the innermost radial sections of cables A1 and E1 annealed at 100, 103 and 107 °C for one hour.....213

92 DSC thermograms of the innermost radial sections of cables A1 and E1 annealed at 92, 95 and 97 °C for one hour.....214

93 Melting peak temperatures as a function of annealing time for cable E1 annealed at 100, 103, and 107 °C.....215

94 Percentage of high temperature peak as a function of annealing time for cable E1 at the indicated temperatures.....216

95 DSC thermograms of cable E1 after annealing at 90 °C for 8 days, 16 days, 24 days and 60 days.....217

96 DSC thermograms of cable E1 annealed at 90 °C after holding at 110 °C for four days and eight days.....219

97 DSC thermograms of cable E1 cooled to ambient temperature after holding at 110 °C for one day, four days and eight days.....220

98 DSC thermograms of cable E1 annealed at 107 and 100 °C successively for 60 minutes at each temperature.....221

99 DSC thermogram of cable E1 annealed at 107, 103, 100 and 95 °C successively for 30 min. and 60 min. at each temperature.....222

100 DSC thermograms of the innermost layers of cable A1 and cable C1 annealed at 92, 95 and 97 °C for two hours.....224

101 DSC thermograms of the innermost layers of cable A1 and cable C1 annealed at 100, 103 and 107 °C for one hour.....225

102 Melting peak temperature as a function of annealing time for the innermost radial section of cable C1 at the indicated annealing temperatures.....226

103 Percent of high temperature peak as a function of annealing time at the indicated temperatures for cable C1.....227

104 DSC thermograms of cable A1-8 cooled to ambient temperature at 0.2 deg./min and quenched after annealing at 107 ^{o}C for 30 minutes.....228

105 DSC thermograms of cable A1-8 cooled to ambient temperature at 0.2 deg./min and quenched after annealing at 97 ^{o}C for 30 minutes.....229

106 Light transmission intensity versus time plots of cable A1-8 annealed at the indicated temperatures.....230

107 Light transmission intensity versus temperature plots of 10 deg/min heating of cable A1-8 annealed at the indicated temperatures.....231

108 Light transmission intensity versus time plots of cable A1-8 gel annealed at the indicated temperatures.....232

109 Light transmission intensity versus temperature plots of 10 deg/min heating of cable A1-8 gel annealed at the indicated temperatures.....233

110 Wide angle X-ray diffraction patterns obtained at the indicated temperatures for cable A1-8.....236

111 SAXS contours of cable A1 (a) outer layer (b) inner layer annealed at 107 ^{o}C for two days.....239

112 SAXS contours of cable A1 annealed at (a) 90 and (b) 100 ^{o}C for two days.....240

113 Circumferential average intensity versus scattering vector for outer layer, inner layer and inner layer (quenched) of cable A1 annealed at 107 ^{o}C 241

114 Circumferential average intensity versus scattering vector for cable A1 annealed at 90 and 100 ^{o}C for two days.....242

115 Circumferential average intensity versus scattering vector for cable A1 annealed at 90 °C for 16 days and 40 days.....243

116 (a)(b) TEM pictures of cable A1-8 annealed at 107 °C for two days.....246

117 (a)(b) TEM pictures of cable A1-8 annealed at 100 °C for two days.....248

118 (a)(b) TEM pictures of LDPE samples air cooled from the melt.....250

119 (a)(b) TEM pictures of distribution cable D1 air cooled from the melt.....252

120 DSC thermograms of the XLPE thin films used in electrical breakdown tests annealed at a) 79, b) 85, c) 89, d) 93, e) 95, f) 100 and g) 107 °C for 30 minutes.....254

121 Percent extractables versus radial position for field aged cable E2 and original cable E1.....257

122 Molecular weight distributions of the extractables obtained from the inner and the outer radial sections of cable E2.....260

123 (a) (b) FTIR spectra of the field aged cables.....262

124 DSC thermograms obtained from the radial sections 1, 2 and 3 of field aged cable E2.....266

125 DSC thermograms obtained from the radial sections 4 and 5 of field aged cable E2.....267

126 DSC thermograms obtained from the radial sections 6, 7 and 8 of field aged cable E2.....268

127 DSC thermograms representative of each one-eighth fraction of radial section of cable E2.....269

128 Melting temperature versus radial position obtained from the DSC thermograms of radial sections, each being 1/32nd of the entire radial section of cable E2.....271

129 Percent crystallinity as a function of radial position for each 1/32nd fraction of the radial section of cable E2.....272

130 DSC thermograms of field aged distribution cables D2, D4, D6 and D7.....273

131 DSC thermograms of field aged distribution cables D9, D10, D11 and D12.....274

132 DSC thermograms of D5 field aged distribution cables.....275

133 SAXS contours obtained from (a) outer and (b) inner layers of cable E2 and (c) inner layer soaked in oil.....278

134 Circumferential average intensity versus scattering vector for (a) outer and (b) inner layer of cable E2.....279

135 Bow-tie trees from the inner layer of cable E2.....280

136 Angle average intensity versus scattering vector for (a) dry and (b) oil-soaked inner layer of cable E2.....281

137 (a)(b) TEM pictures obtained from the inner layer of cable E2.....282

138 SAXS contours obtained from distribution cables D2 and D9.....285

139 Circumferential average scattering intensity versus scattering vector obtained from distribution cables D2 and D9.....286

140 DSC thermograms of LDPE and its crosslinked version.....304

141 Schematic representation of multiple peaks generated from low and high temperature annealings of original crosslinked polyethylene.....317

142 (a)(b) log (ln-(1-p)) versus logE Weibull plots for electrical breakdown tests of XLPE thin films annealed at 79, 85, 89 and 93 ^{o}C for 30 minutes.....334

143 Calculated temperature distribution along the radial direction of cable E2 for 110-118°C and 120-80 ^{o}C temperature fields.....343

144 DSC thermograms from the inner and outer layer of cable E2 along with original cable E1.....345

1. INTRODUCTION

Since their introduction as insulating materials, polyethylene (PE), and crosslinked polyethylene (XLPE) have become the most widely used materials in high voltage (HV) cable insulation. They are preferred over the traditional oil impregnated paper insulation because of their better dielectric properties, low specific gravity, moderate melting range, good processability, economy and availability on a large scale. Despite their advantages, PE and XLPE are susceptible to a long term aging process usually referred to as "treeing" (Kitchin and Pratt 1958, Eichhorn 1977).

Several mechanisms have been proposed for the electrical breakdown process. Factors that affect treeing have long been studied and much effort has gone into attempting to clarify them and into minimizing their influence. Although accelerated aging tests were developed to predict the service life of insulation materials, still underground HV cables are facing unexpected failures. Therefore, increasing concern exists regarding the remaining service life of presently installed cables, both from the economic and safety points of view.

Besides operational factors such as voltage, stress, frequency, temperature and insulation environment, the material nature of the insulation plays a big role in the insulation performance. Molecular structure (Ieda 1978) and morphology have been found to influence the dielectric properties of polymeric insulation (Phillips 1978, Kolesov 1980, Ceres and Schultz 1984).

Breakdown is a physical process and is known to be related to the presence of heterogenous impurity particles and to the presence of voids. Although treeing is also a physical process which deteriorates the insulation, a definite relation between between treeing and breakdown has never been demonstrated. Treeing is a long term aging process resulting in physical and chemical deterioration of the electrical insulation. In the course of aging, electrical and thermal stresses are both in play; physical and chemical alterations induced by these stresses finally lead to the breakdown of the insulation. Because of its statistical nature and destruction of any physical evidence during its occurrance, it is difficult to study the origin of the breakdown process. Similarly, although the effects of aging can be studied and characterized, an in-situ test to determine the initiation site and the path followed is impossible. Therefore, understanding of the aging induced changes is important in resolving the processes leading to the breakdown of polymeric dielectrics. In electrical

insulations, thermal stress, being a major form of stress, is expected to play a major role in the degradation processes. In practice, the high levels of power used in HV cables produces heat in the conductor which causes thermal aging effects in the insulator. Therefore, our approach to the aging of electrical insulation is to attempt to understand the thermal aging characteristics of HV XLPE and PE cables along with the changes produced in their molecular and morphological properties.

The usual method of preparing XLPE from PE is either to vulcanize the polymer with organic peroxides in the melt state (chemical crosslinking) or to introduce crosslinks by high energy irradiation in the solid state (irradiational crosslinking). While chemical crosslinking in the melt state results in more evenly distributed crosslinks, solid state irradiational crosslinking results in preferential crosslinking of the amorphous phase. Still in chemical crosslinking, due to the statistical nature of the crosslinking reaction, some fraction of the base material does not participate in the crosslinking reaction and constitutes the extractables (sol) fraction of the crosslinked system. The amount of extractables depends on the amount of crosslinking agent, the extent of curing and the molecular structure of the base material. Thus, analysis of the amount of extractables is one of the ways of

characterizing the extent and the nature of the crosslinking reaction.

In this dissertation, research will be reported which considers the initial state of cable insulation and its response to thermal aging. Attempts at correlating the structure of field aged cables with structural changes occurring on thermal aging in the laboratory will be reported. Commercial cables prepared from the same LDPE and curing agent, dicumyl peroxide (DCP), where obtained from cable companies. In order to study the effectiveness of the cable curing method, cables were analyzed for the amount of extractables over their radial directions. Thus,the effectiveness of a curing method, e.g. steam cure, dry cure or polyethylene glycol (PEG) medium cure, was judged by the uniformity of the crosslink density and the level of extractables over the entire radial section of each cable. In order to comment further on the cable curing processes, XLPEs prepared in the laboratory from the same resin used in cable production containing the same amount of DCP (2 %) were analyzed for their percent extractables. Molecular weight and molecular weight distribution of the base LDPE were also changed by adding certain amounts of its low molecular weight fraction in order to have a better understanding of the crosslinking mechanism. Spectroscopic studies of the cables were also carried out in order to find

out if any structural variations resulted from different curing processes.

Thermal stress being a major form of stresses experienced in power cables, studying the thermal characteristics of the available HV XLPE transmission cables was regarded as essential. The effect of processing conditions on the thermal properties of the XLPE cable insulations (e.g. melting temperature, crystallinity, etc.) as a result of their molecular properties (e.g. sol-gel content) was studied using Differential Scanning Calorimetry (DSC). Despite the shapes of the thermograms from each original cable looking very much alike, differences in melting points and crystallinities were observed in parallel with changes in their molecular properties. After determining the effect of extractables on the thermal behavior of the original cables, annealing studies at temperatures in the melting range, especially at 107 ^{o}C, will be described, which were performed in order to follow the behavior of the extractables in thermal fields. In order to understand the effect of extractables on thermal behavior, thermal analyses of the original and gel fractions of the same cables were studied after they had acquired the same thermal history.

HV insulation cables are subjected to temperatures as high as 90 ^{o}C and occasionally above 100 ^{o}C due to Joule heating resulting from power losses in the conductor. This

heat is transferred to the insulator and the temperature of the insulator increases. Such high temperatures are within the effective annealing regions of LDPE and XLPE. Therefore it is critical to know the annealing characteristics of the insulating material. For this purpose, annealing experiments on various types of HV XLPE underground cables prepared using different curing processes have been performed under isothermal conditions. Thermal analyses of annealed cables show that different responses exist dependent on the annealing temperature. Microstructural differences between the original cables and their annealed versions were studied by utilizing SAXS and WAXS techniques.

The morphologies of LDPE and linear PE had been the subject of previous studies on morphology-electrical property relationships in cable insulation applications. While spherulitic morphologies are common for LDPE and linear PE, sheaf-like entities were found to be characteristic for XLPE morphology (Phillips and Gohil 1986). In this study, the effect of cable processing conditions and molecular structure on the morphology of the original cables, as well as the morphology of some of the annealed cables, was studied. Additionally electric breakdown strength tests of annealed XLPE thin films were performed in order to understand the relationships between electrical breakdown strength and microstructural changes taking place during annealing.

Since in-situ experimentation as a function of time with underground HV cables already in service is impractical and expensive, field aged distribution cables removed from the service line were subjected to analyses similar to those carried out for the original cables. An aged version of a steam cured cable, thermoelectrically aged in the Waltz Mill aging facilities was found to show multiple melting behavior. Various successive isothermal annealing studies were carried out on the original steam cured cable in order to reproduce similar thermal behavior. Further characterization of the field aged cables (e.g. MW and MWD, amount of extractables and FTIR and optical microscopy) were carried out in order to estimate the possible molecular changes accompanying the aging of the cable. Microscopy and SAXS studies were conducted to obtain an understanding of the changes taking place on a microstructural level.

2. LITERATURE REVIEW

2.1. Electrical Properties of Polymers

Chemical bonds between unlike atoms in molecules possess permanent dipole moments, which originate from the asymmetry of the positive and negative charge densities of the system. Positive charges arise from the nuclei and they are localized. Negative charge densities arise from the electronic systems which are delocalized. Many polymers with unlike atoms in their chemical structures can have bond moments that can vectorially accumulate into molecular or segmental moments depending on the molecular configurations and conformations. Polymers that have bond moments can be polarized by an electric field and they are said to be electrically active. In some chemical structures the bond moments vectorially add to zero and the polymer is said to be dielectrically inactive. Thus, the measurement of polarization in polymers has proven to be a useful method for understanding polymer structures and related physical properties.

Dielectric constant, dielectric loss, electric conductivity and dielectric strength each describe general features of the electrical behavior of a polymer. The

possible application of a polymer is judged by each or a combination of these parameters.

While some polymers with high dielectric constants are used as capacitors, polymers with low dielectric constants are used for insulation purposes. Polyethylene, PE, which does not have permanent dipole moments, has a low dielectric constant of about two Debyes resulting mainly from atomic and electronic polarizations and it is considered to be a good insulator. The introduction of polar functional groups, e.g. chlorine, fluorine, hydroxyl or carbonyl groups all increase the dielectric constant. Therefore, oxidative degradation of PE insulation during aging deteriorates the insulation performance.

Dielectric loss is a measure of the amount of energy dissipated by the insulation system when a voltage is applied. Most polymeric materials have lower loss factors than many other solid insulators. Dielectric loss and dielectric constant are known to be functions of temperature, frequency and voltage as well as the structural properties of the insulating material (McCrum et al. 1967).

In general, polymers have much lower conductivities than metals due to wide band gaps between the valence and conduction bands. Saturated polymers have a wide energy gap because of the strength of the σ-bonds. On the other hand, polymers with unsaturation have π bonding which can result in electron delocalization, thus increasing the

conductivity. This effect is even larger when there is conjugation of π bonds (Wintle 1983). The presence of ionic charge carriers, especially in condensation polymers, as remnants from the polymerization process, are known to cause conductivity (Seanor 1982). This indicates that additives for a designed plastic should be carefully chosen in order to keep the insulator properties under control.

The majority of polymers show an increase in conductivity with temperature. The morphology of polymers has also been found to influence conductivity. It has been shown that the volume conductivity in crystalline polymers decreases with increasing crystallinity (Sazhin 1964). Ionic charge carriers responsible for extrinsic conductivity are confined to the amorphous phase. Kargin et al.(1967) demonstrated that conduction was dependent on spherulite size and was taking place preferentially through spherulite boundaries. On a molecular level, intrinsic conduction is generally found to be along the chain direction via electron delocalization or, in some cases, normal to the chain direction via secondary bonds (e.g. hydrogen bonding, Seanor 1968, Miyoshi et al. 1968).

The dielectric strength, or more commonly the breakdown strength, is a measure of the resistance of an insulator to the applied electric field. It is the minimum voltage necessary to destroy its insulating properties and is expressed in volts or kilovolts per unit thickness of the

insulation at the point of failure. It is commonly expressed as volts per mil (one mil=$1x10^{-3}$ inches). Most generally it is the average of 10 or more voltage and thickness measurements. The AC voltage to be applied in the service life of an insulation should not exceed about one third of its dielectric strength determined in a short time testing procedure (usually a one minute voltage set-up). This rough guide should be applied only with careful consideration of testing design and conditions. The initial dielectric strength of unaged insulation is dependent on inherent and imposed factors such as the following (Clark 1962) : 1) breakdown strength, 2) ion content, 3) moisture content, 4) insulation thickness, 5) test area, 6) test conditions e.g. electrode or conductor shape and type, frequency and wave shape of the test voltage.

2.2. Dielectric Breakdown in Polymers

For each polymeric insulator there exists a critical voltage gradient across the material above which the polymer can no longer act as an insulator. A short circuit generated between the electrodes through the insulator reflects the breakdown of the dielectric. Dielectric breakdown may be instantaneous or the result of long term aging of the insulation. A clear distinction is necessary between the dielectric strength obtained in short

term laboratory testing and that obtained in service over a period of years. The effective dielectric strength of an insulator decreases over a period of several years due to deterioration of the insulation by thermal, mechanical, chemical and electrochemical activities. It is generally agreed that dielectric breakdown is a result of the field induced flow of charge carriers within the insulation (Schultz 1974). Critical breakdown in a crystalline material is reached when the insulation lattice becomes physically unstable through exchange of energy between the excessive amount of charge carrying electrons and the lattice phonons. Breakdown occurs through the breaking of chemical bonds and results in degradation on a molecular level (Patsch 1975).

Several mechanisms have been proposed to account for dielectric breakdown in polymers. Among these, thermal, electronic and electromechanical breakdown processes are the most discussed.

2.2.1. Thermal Breakdown

Thermal breakdown was the first breakdown theory of solid dielectrics and was presented by Wagner in 1922. Thermal breakdown simply results when the temperature rise due to conduction or dielectric losses in the material reaches the point at which the dielectric can no longer withstand the field. In this theory the dielectric breakdown

was discussed in terms of the thermal balance between joule heating due to the conduction current and its dissipation.

The theory postulates that the insulation breaks down if the temperature at some point in the dielectric exceeds a critical value, T_c. The rate of energy storage depends on the rate of field application. If the applied field is increased very slowly which is the case in continuously stressed dielectrics, the temperature of the insulator can stabilize below the critical value. The breakdown field strength in this type of application depends on the size and shape of the sample, on the geometry and thermal properties of the electrodes, and the ambient medium (Varlow 1980). The other limiting case occurs when the field is applied rapidly. In this case, dissipation of heat is limited and all the heat generated goes into raising the sample temperature. This type of thermal breakdown is often referred to as impulse thermal breakdown and the dielectric strength of the material very much depends on the duration of pulses, but not on the size or shape of the sample.

For most semicrystalline polymers the dielectric strength is found to decrease with temperature only over some finite temperature range extending below the melting temperature, T_m, of the polymer. At very low temperatures dielectric strength is almost independent of temperature (Ieda 1980).

2.2.2. Electrical Breakdown

Although the effect of temperature on dielectric strength at low temperatures was found to be negligible, the existence of dielectric breakdown in this region led to the recognition of electronic breakdown (O`Dwyer 1973). Theoretical description of the electronic breakdown process relies on the motion of the charge carriers in the dielectric material.

The intrinsic electric breakdown strength of a dielectric is obtained in a uniform electric field in the absence of discharges. Yet, this is not a precise definition since the word "intrinsic" suggests that the dielectric strength is a material property which is not affected by the dimensions of the sample, the nature of test conditions, etc. On the contrary, breakdown voltage is influenced by practically every experimental factor such as temperature, humidity, time of testing, frequency, type of electric field, area of test electrodes and sample thickness. Therefore, breakdown strength is not a design quantity but a guide for comparing materials for particular applications.

The extremely complex nature of the breakdown process complicates the formulation of theory and necessitates the making of diverse assumptions and approximations. Therefore, there is not any well established theory of electronic breakdown able to explain

satisfactorily the wide variety of experimental observations.

2.2.3. Electromechanical Breakdown

Electromechanical breakdown is the type of failure which represents an instability in the balance between mechanical and electrical forces. Stark and Garton (1955) suggested that similarity between electric strength and mechanical properties was a manifestation of electromechanical forces. They were able to show that in a soft elastic specimen an electromechanical pressure can significantly reduce the spacing between the electrodes and, in turn, enhance the electric field. This leads to mechanical instability and breakdown if the intrinsic electric strength is not reached first.

2.3. Aging of Polymeric Insulation

Polymeric dielectrics used in insulation applications are subjected to aging processes as a result of the nature of the insulation environment and operating conditions. While polymeric materials with tailored properties are designed to meet the desired dielectric performance, environmental factors make it difficult to predict the service performance of the material.

2.3.1. Treeing Phenomena

The breakdown of solid insulation has been shown to occur in stages that produce a tree-like structure (Rayner 1912) of channels which initiate from the high electric stress regions and propagate through the insulation. When a continuous path is formed between the electrodes, insulation breaks down (Mason 1955 and Baker 1956). The time it takes for breakdown depends on the material, environmental and operation factors.

Treeing is an electrical pre-breakdown phenomenon. Kitchin and Pratt (1958) described the breakdown process as "treeing" because the shape of the damage resembles a defoliated tree. Having all the trees initiating from interfaces, i.e. foreign particles, voids, protrusions etc., Eichhorn (1983) proved that tree initiation is not just determined by the electrical stresses but is influenced by the properties of interfaces.

In general, treeing phenomena are classified as being of two types, namely electrical and water trees. Electrochemical trees are accepted as another class by some researchers while many others accept electrochemical trees being within the water tree class (Bahder et al. 1973, Lanctoe et al. 1979).

Electrical trees grow in dry dielectrics by a periodic partial discharge mechanism. They are colored and composed of distinct hollow channels. Once they are

generated, they stay within the dielectric (Eichhorn 1977, 1983). On the other hand, water trees start and progress more slowly at lower dielectric stress in the presence of moisture. The stress levels experienced in high voltage underground cable insulation are usually within the range typical of water tree inception voltages. Therefore, water treeing is of major concern in high voltage underground cable aging.

Water trees tend to originate in areas where foreign substances or defects are present. They are diffuse and indistinct and have been reported to disappear upon drying. When they are immersed in hot water they take on their original appearance demonstrating a refractive index effect as the origin of their disappearance (Isshiki et al. 1974, McMahon 1978, Nunes and Shaw 1980). It is possible to render water trees permanently visible by the use of basic dyes (Ashcraft 1978). It has been claimed that they do not branch but have been described as strings of water filled cavities (Bamji et al. 1983). On the other hand, most researchers observed chain-link type microvoids all connecting back to the point from where the growth started (Tanaka and Fukuda 1974).

The water treeing mechanism may be roughly divided into two major stages; initiation and growth. Once water trees are initiated, it is believed that another mechanism takes over and controls the growth of trees (Ieda and Nawata

1972, Sletbak 1979). In the presence of water or humidity, electrical intensification on protrusions, contaminants and voids is enough to initiate water trees.

Initiation and growth of water trees normally takes a long time making it possible for it to be followed kinetically. Slow rates of initiation and growth of trees suggest that the number of trees and their maximum lengths are critical in determining the breakdown strength of a dielectric (McKean 1976, Mizukami et al. 1978). Since trees can be precursors of insulation failure, breakdown mechanisms discussed earlier may play a role in their formation.

Tanaka et al.(1976), and Birks and Hart (1965) proposed that water-filled cavities will enlarge when the water expands because of joule or dielectric heating. Generation of water trees was found to to be enhanced under gradient temperature and voltage fields (Tabata et al. 1972)

McMahon et al. (1964), Tanaka et al.(1973) and Pohl (1973) tried to explain water tree generation using electrokinetic effects, namely, dielectrophoresis. Dielectrophoresis considers the movement of uncharged but polarizable particles in a divergent field. This effect is much more pronounced when there is a sizable dielectric constant difference between the particles and the surrounding medium. This effect may well explain moisture aggregation and the movement of voltage stabilizers to the

regions of maximum stress. On the other hand, Auckland and Cooper (1974) and Nitta (1974) found a relationship between electric field and frequency inconsistent with dielectrophoresis and discounted this mechanism.

In a mechanical approach, expansion and contraction of water in micropores due to joule heating causes local fatigue and finally deteriorates the material mechanically (Sletbak and Erling 1974).

Due to the fact that water trees grow differently in different media, many researchers tried to understand the problem from the chemical point of view. In an interesting work carried out on radiation crosslinked PE, uncrosslinked PE and chemically crosslinked PE, Srinivas et al. (1976) explained such behavior as due to the presence of chemicals from the decomposition of the crosslinking agent dicumyl peroxide (DCP). Acetophenone, one of the decomposition products, was proven to be a good inhibitor of water tree initiation (Srinivas et al. 1976, Patsch 1979). When catalyst decomposition products were removed from chemically crosslinked PE, the material was found to be as susceptible to tree growth as uncrosslinked PE (Katz and Bernstein 1979). On the other hand, the effects of other chemicals such as H_2O, $CuSO_4$ and ethylene glycol were proved to be promotive in the creation of water trees (Bahder et al. 1974, Karakelle 1986). Blodgett (1979) claimed that the only reason a basic dye can stain the water trees is because of

the presence of oxidized states along the water tree walls and thus tried to correlate oxidation reactions with water tree growth. A similar correlation was attempted by Rye (1975) using the extent of hydroperoxy and carbonyl groups together with water tree growth.

Although all these proposed mechanisms approach the problem from different points of views, there are several well established factors that influence water treeing and should be considered in all theories.

2.3.2 Factors Affecting Treeing

The factors that influence water trees have long been known and much effort has gone into attempting to clarify them and minimize their influence. The presence of voltage stress and polar liquids are the most critical factors influencing water tree generation. All of the other parameters gain various levels of importance only in the presence of these two factors.

Factors influencing tree growth can be classified in two major groups, namely, operational factors and material factors. Operational factors, e.g. magnitude and type of stress, frequency, temperature and aging time, all affect tree growth. In general, the number and growth rates of water trees tend to increase with applied voltage and frequency reaching saturation with increasing time of voltage application (Noto 1980). The literature on

electrical breakdown is extensive. Often direct correlation between experiments carried out in different laboratories is difficult. Discrepancies between results are often due to different electrode systems, e.g. shape and electrode material, voltage source, material and environmental conditions, etc. In order to solve the physics of the problem one needs to return to the selection of materials and to investigate the basic requirements for better dielectric performance. It is necessary to understand the relation between the dielectric breakdown phenomenon and the material properties inherent to polymers, such as, chemical structure, morphology, impurities, additives, etc.

In trying to match the suitability of a material to the requirements for a given application there are a series of properties which should be compared with the requirements of the application. A balance of properties can be maintained by offsetting a lack in one area by a plus in another. Although, mechanical, thermal, environmental and electrical considerations, ease of fabrication and economic requirements can be regarded as the order of importance, economic factors usually override everything else. A particular polymer with outstanding dielectric properties may not serve the purpose if it does not have the appropriate mechanical and/or thermal stability required for a particular application. Therefore, one has to tailor the structural characteristics of a polymer, either chemically

or morphologically, in order to meet the electrical, physical and chemical requirements needed for a particular application.

2.3.2.1. Molecular Structure

As was stated earlier, the electrical properties of polymers (i.e., dielectric constant and loss, dielectric strength, conductivity) all depend on the chemical nature of the polymer molecules. The type of atoms and their spatial distribution not only determine the dielectric properties but also determine the physical and mechanical properties of the polymer. Isotactic and atactic polypropylenes (PP) having different molecular conformations have been found to have different electrical strengths depending on temperature (Artbauer and Griac 1966). At low temperatures isotactic PP was found to have a lower electrical strength than atactic PP. This was related to the difficulty of electron acceleration due to irregular conformation in atactic PP. Sabuni and Nelson (1976) showed that there is a close relationship between cohesive energy density, a measure of the strength of secondary bond forces between molecules, and electric strength. A decrease in electrical strength with increasing temperature reflects a reduction in secondary bonding forces, thus facilitating breakdown forces operating electromechanically.

Crosslinking was found to be one way of controlling the electrochemical forces generated during the breakdown process (Stark and Garton 1955). In general the electric strength of a thermoplastic was found to increase on crosslinking especially on high temperatures.

Oakes (1949) and Ball (1951) showed that electric strength is greater for polar polymers. Ball pointed out that this was due to dipoles acting as scattering centers for electrons thus reducing the electric damage.

Fisher and Nielsen (1976) studied the molecular weight dependence of breakdown strength in polyethylene and they found an increase in breakdown strength with molecular weight. Molecular flexibilities gained due to changes in chemical structure and due to temperature increase were found to affect the breakdown strength. Segmental molecular motions and/or increased rearrangements of free volume were found to enhance electron transport and facilitate breakdown processes (Ieda 1980). These observations have prompted the possible consideration of a dependence of electric strength on mechanical strength of polymers.

2.3.2.2. Morphology

Despite the existence of an extensive literature on dielectric properties and breakdown of polymers, the effect of microstructural variables on dielectric phenomena did not attract much attention until the subject was

effectively reviewed in detail by Phillips (1978, 1983). He pointed out the importance of having more than one phase in polymer systems. Fractions of phases, their sizes and shapes and their orientation all affect the ultimate electrical properties of polymers. Yahagi (1980) studied the dependence of the electrical strength of PE on the degree of crystallinity under dc voltage fields. Different levels of crystallinities were achieved by varying the annealing process on the same high density PE film. It was found that for temperatures below 80 ^{o}C electrical strength decreased with an increase in crystallinity, but above 80 ^{o}C the effect of crystallinity was reversed. Nagao et al. (1977) studied ethylene-vinyl acetate copolymers (EVA) and their blends. Electric strength was found to increase with VA content which reflected a decrease in crystallinity. This was thought to be possibly due to an increase in electron scattering with the increase in polar groups concentration compensating for the decrease in crystallinity. They also studied the effect of microcrystallite size on electrical breakdown strength and suggested that electron avalanching occurs over a region much greater than the size of microcrystallites. Wagner (1974) was able to show that the discharge channels in both HDPE and PP were located at the spherulitic boundaries. Phillips (1978) also studied the location of cavities relative to the crystalline morphology. They all concluded that spherulitic boundaries are the

weakest pathways for discharge propagation because of the higher concentration of voids and foreign materials accumulated in these regions. Spherulitic structure being the characteristic feature of morphology in semicrystalline polymers, such as in PE and PP, attracted more attention in terms of understanding the influence of this morphological feature on dielectric strength. Kolesov (1980) studied the effect of spherulite size on breakdown strength under impulse voltage conditions. The spherulitic size of specimens was modified by appropriate heat treatments. It was found that the electric strength of the specimens was decreased as the spherulite size increased until the mean spherulitic diameter became equal to the specimen thickness. He concluded that, as the spherulite size decreases the density of the polymer within the boundary region increases, thus resulting in improvement of electrical properties. Nitta and Funayama (1978) demonstrated a linear relationship between the treeing inception voltage and spherulitic radius. Ceres and Schultz (1984) pointed out the importance of morphological parameters such as lamellar thickness and degree of crystallinity. For this purpose, while keeping these parameters constant, they followed the effect of spherulite size. In another set of experiments, this time, by keeping the spherulite size constant they altered the degree of crystallinity. Their results showed a trend similar to that observed by Kolesov, i.e. dielectric

strength decreased with increasing spherulite size. For the case of degree of crystallinity, lower crystallinities resulted in lower electric strengths. They also tried to control the molecular nature of the spherulitic boundaries by applying different rates of crystallization. However, their results showed that the samples with more foreign interspherulitic material had a longer electric life. This contradictory result confirms the complicated nature of dielectric properties. Yahagi (1980) tried to investigate the relationship between drawn and annealed samples of PE and dielectric properties such as electrical conductivity, thermally stimulated conductivity and dielectric breakdown strength. He interpreted his data in terms of mechanical drawing and isothermal crystallization of a bulk polymer from its melt providing increased numbers of trap sites for electrons due to a change in morphology on a lamellar level. Preferential orientation of vinyl unsaturation induced by mechanical drawing was found to affect the dielectric properties, too.

All the above morphological investigations show that dielectric properties of crystalline polymeric materials are closely related to the morphology of the polymer. Therefore, the thermal histories of crystallization and annealing together with mechanical post-treatments of semi-crystalline polymers need to be carefully controlled in

order to achieve the desired insulation performance from a polymeric dielectric.

2.3.3 Accelerated Aging

Most of the technical interest in aging of electrical insulation is concerned with accelerating the aging to determine in a relatively short time whether the material will have a satisfactory life. Two methods of examination are commonly used. In constant stress life testing, the time of breakdown for identically prepared samples is measured. On the other hand, in dynamic tests, the electrical field at the time of breakdown is recorded as a function of aging time (Trinth and Vincent 1980).

Based on studies of films and actual cables a life equation for extruded dielectric cables has been proposed. The so-called "life equation" in its simplest form correlates the stress with time at constant temperature (Howard 1951).

$$t_c = A\, E_c^{-n} \qquad (2.3.1)$$

where t_c is the time of testing, E_c is a constant stress and n is an exponent.

This empirical correlation is widely used to predict life expectation through accelerated tests by exposing the dielectric to constant high stress and

measuring the time to failure. A logarithmic plot of the above equation produces a linear correlation which can be extrapolated to the operational stress.

When stress is increased in discrete steps the life equation can be written as (Starr and Endicott 1961).

$$t_1/t_2 = (E_1/E_2)^{-n} \qquad (2.3.2)$$

where E_1 and E_2 represent different stresses, t_1 and t_2 represent corresponding times.

The above equations are often optimistic and failure rates are considerably higher than predicted (McKean 1976).

Because of the statistical nature of accelerated aging tests, statistical analysis of the data is necessary for comparing insulation performance. The Weibull probability distribution function has gained wide acceptance in the statistical breakdown of solid dielectrics (Weibull 1951, Bahder et.al. 1973). The use of this distribution is rationalized on the basis of a postulated breakdown mechanism which depends on a random chain of "weak links" between the electrodes (Epstein and Brooks 1948). The cumulative Weibull distribution function is given by;

$$p = 1-[\exp-(t-\gamma/\alpha)^{\beta}] \qquad (2.3.3)$$

where α is the scale parameter, β is the shape parameter, is the location parameter and t is a random variable which is usually the time to breakdown or the electric field strength required for breakdown where the electric field increases linearly with time. p indicates the proportion of specimens initially tested which will fail by time t. The scale parameter α represents the time required for $(1-e^{-1})$, or 63.2 percent, of the tested units to fail. The shape parameter (β) is a measure of dispersion of the failure times from $t=\alpha$. The parameter γ indicates the time from voltage application in which failure of any unit is not possible. Therefore equation (2.3.3) is applicable for $t \geq \gamma$.

$$\text{For } 0 \leq t \leq \gamma \qquad p = 0 \qquad (2.3.4)$$

2.4. Polymers Used in High Voltage Cable Applications

Traditional oil impregnated paper insulation has been replaced by polymeric insulation because of improved technology and the economy of the latter technique. Besides the difficult and expensive production of oil impregnated cable insulation, the affinity of this insulation for water makes it prone to water treeing. On the other hand, most polymers have very limited affinity for water, especially at room temperature. Apart from economical and developed technological reasons, various electrical properties of

polymers such as dielectric constant and low dielectric loss values make them attractive for cable insulation applications.

While plasticized polyvinylchloride (PVC) and ethylene-propylene rubber (EPR) are mainly used for low voltage applications, PE and XLPE comprise the major volume of polymer consumption in high voltage applications rated 5 kV and above (Kiss et al. 1979).

2.4.1 Polyethylene

PE produced by free radical addition polymerization of ethylene at high pressures, 1000 to 3000 atmospheres, is known as low density polyethylene, LDPE, and has a density in the range of 0.91-0.94 g/cm^3. Variation in density is due to change in crystallinity caused by the nature of the branches obtained during the polymerization process. The branches are of two distinct types, long and short chain branching.

Long chain branching arises from intermolecular chain transfer reactions. In this type of reaction a propagating active chain front is terminated and transferred to the backbone of an already terminated chain. The size of the branch depends on the molecular weight of the transferred chain, the position of the newly created active center and the chain length of the newly growing chain.

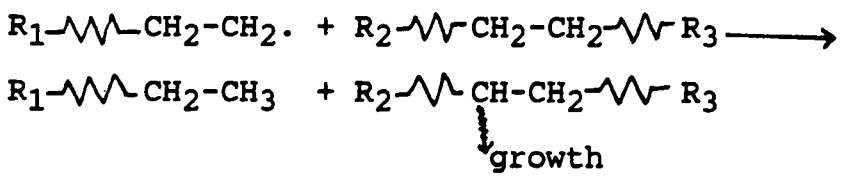

This type of branching leads to branches which are as long as the main polymer chain and they have an observable effect on the solution and melt viscosities.

The second branching mechanism produces short-chain branching by intramolecular chain transfer. "Back-biting" of a growing active front creates a transient six-membered ring that results in butyl branches (Roedal 1953).

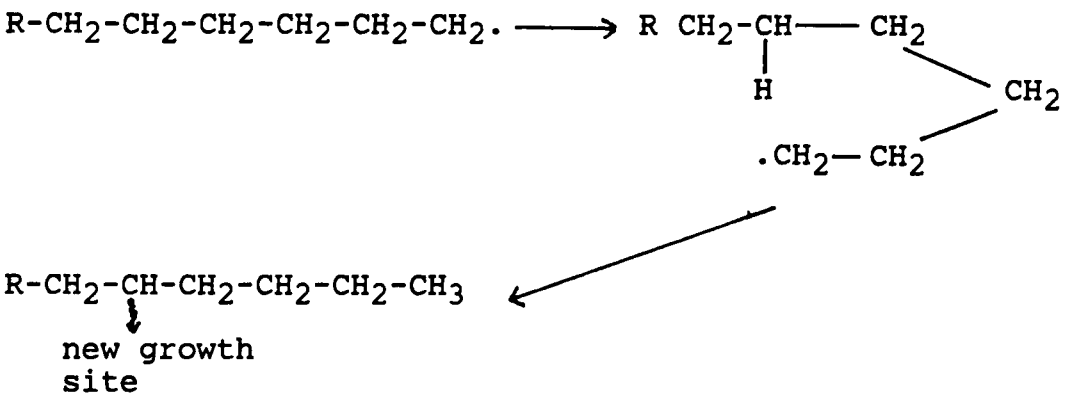

A mechanism accounting for the ethyl branches assumes an intermolecular transfer reaction on the butyl branches as follows,

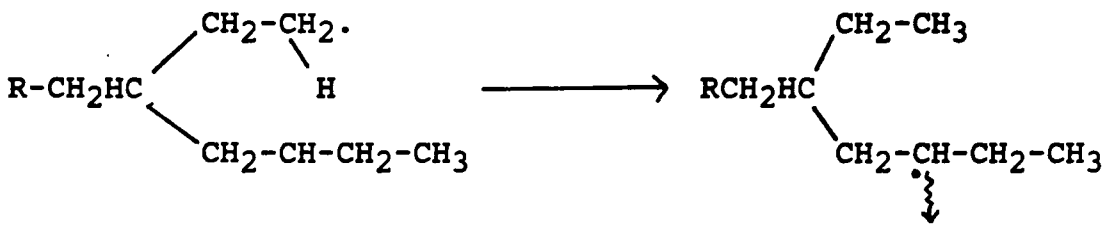

Typical number average molecular weights for LDPE range from 20,000 to 50,000. The range of molecular size is very wide with a heterogeneity index between 20 and 50 (Sillars 1973). LDPE is generally 50-60 % crystalline with melting points in the range 110-115 ^{o}C. The non-polar nature of PE, not having electrical losses at high frequencies, makes this polymer a favorable insulation especially for higher frequency communication and radar fields where low dielectric loss has overriding importance.

High density polyethylene, HDPE, can be produced in several ways including radical polymerization of ethylene at low pressures, polymerization with supported metal oxide catalysts and coordination or Zeigler-Natta polymerization of ethylene (Lenz 1967). The latter techniques have been commercialized extensively and are used for HDPE production in large volumes.

HDPE, consisting of linear chains containing less than one side chain per 200 carbon atoms in the main chain, is 70-90 % crystalline. Density is in the range of 0.95 - 0.97 gm/cm^3 and the melting point is above 127 ^{o}C, typically

about 135 ^{o}C. It is stiffer and stronger than LDPE, therefore its usage in electrical insulations is restricted. However its electrical properties are not sensibly different from those of LDPE (Sillars 1973).

In general, with their low water absorption characteristics, resistance to most solvents and good dielectric properties, polyethylenes are one of the most commonly used polymers in insulation. Application of LDPE is increased further by improving its mechanical and thermal properties. Its thermoplastic character is eliminated by crosslinking. With almost the same electrical properties, XLPE, has proved to be a better insulation for cable applications (Dougherty 1984, Dissado et al. 1984) because of its higher dielectric strength.

2.4.2. Crosslinked Polyethylene

The usual method of synthesizing PE networks is either to vulcanize the melt with peroxides or to introduce crosslinks by high energy irradiation in the solid state. Gamma or beta high energy radiation causes crosslinking via a combination of macroradicals created during irradiation (Charlesby 1952). While C-H bond scission results in crosslinking, C-C bond scission causes to molecular degradation of the crosslinking polymer (Charlesby and Pinner 1959, Rijke and Mandelkern 1971). When dicumyl peroxide (DCP) is used chain scission is reduced (Miller

1960, Barton and Lazar 1967, Karakelle 1986). While crosslinking with DCP in the melt produces more evenly distributed crosslinks, solid state irradiation crosslinking results in preferential crosslinking of the amorphous phase. Crosslinking by irradiation is restricted to thin samples because of the limited penetrability of the radiation (Kulkarni and Mashelkar 1981).

The chemistry of decomposition of DCP in different media has been studied (Loan 1963). DCP undergoes homolysis at a reasonable rate at elevated temperatures without significant decomposition in the temperature range of molten PE (Kharasch et al. 1951). Peroxide induced crosslinking has been viewed as a simple process that involves peroxide homolysis to yield cumyloxy radicals which abstract secondary hydrogens from PE molecules and create macroradicals. Combination of the macroradicals results in crosslinking, thus one peroxide molecule give rise to one crosslink consisting of a single C-C bond (Dannenberg et al. 1958, Miller 1960). On the other hand, Hulse et al. (1981) showed that disproportionation reactions compete with coupling reactions and decrease the efficiency of crosslinking.

The general scheme for thermal decomposition of DCP and the crosslinking mechanism is as follows:



Dicumyl peroxide Cumyloxy radicals

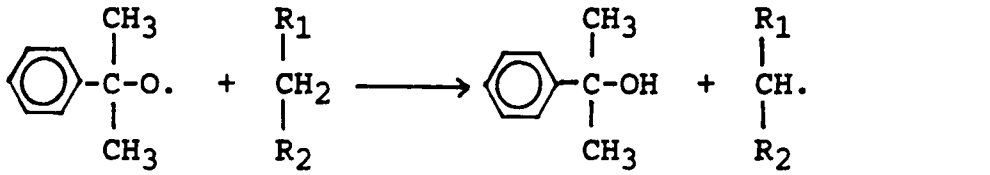

Cumyl Alcohol Polymer radical

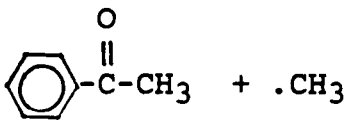

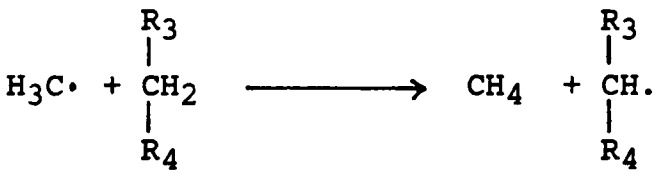

Methane Polymer radical

where R_1, R_2, R_3, R_4 are alkyl segments of a polymer chain. The crosslinking reaction is:



Chemical modification of PE chains during crosslinking is also possible by combination of polymer radicals with methyl and peroxy radicals.

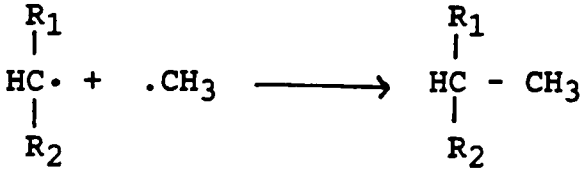

or

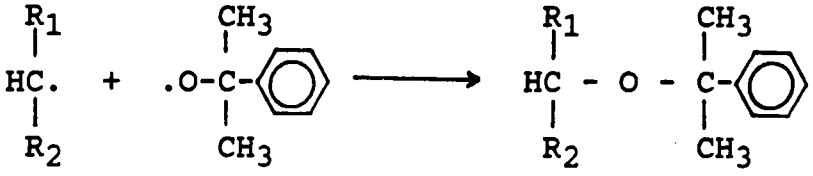

The major decomposition products from the dicumyl peroxide crosslinking reaction are, cumylalcohol, acetophenone, methane, methanol and α-methyl styrene. The significance of the decomposition products in practice is that acetophenone is widely recognized as an agent reducing water tree growth (Wagner and Wartusch 1977).

With the improvements in stress cracking, dimensional and thermal stability and with the preserved dielectric advantages of PE, XLPE has been a very widely used polymer for cable insulation both for medium and high voltage applications.

2.4.3. Manufacture of Cable Insulation

The first use of insulated wires was for telegraph purposes and dates back to the first half of the nineteenth century. For underground power conveyance insulated wires were first used in the 1880`s (Black 1983). After using cotton, gutta percha, vulcanized rubber and oil impregnated paper, with the introduction of PE, thermoplastic dielectrics started to replace the traditional insulations (Graneau 1979, Weedy 1980). The first 15 kV cable with extruded PE insulation went into service in 1955 and the first 138 kV cable in 1963 (Gravdes 1963). Since then XLPE with its dimensional and thermal stability has been preferred over PE especially in high voltage applications.

High voltage cables are designed in such a way that the insulation wall thickness will be wide enough to meet safety requirements. The requirement for XLPE is a minimum of 0.016 mil/V insulation thickness. Figure 1 shows a cross-section of a typical single core three-polymeric layer insulation cable. In Figure 1, (1) is the sheath, (2) and (4) are the inner and outer semiconductor layers, (3) is the polymeric insulator and (5) is the conductor. The semiconducting layer is generally carbon black doped PE or EVA copolymer (Nitta 1980). Depending on the purpose, XLPE is usually blended with anti-oxidants, voltage stabilizers etc.

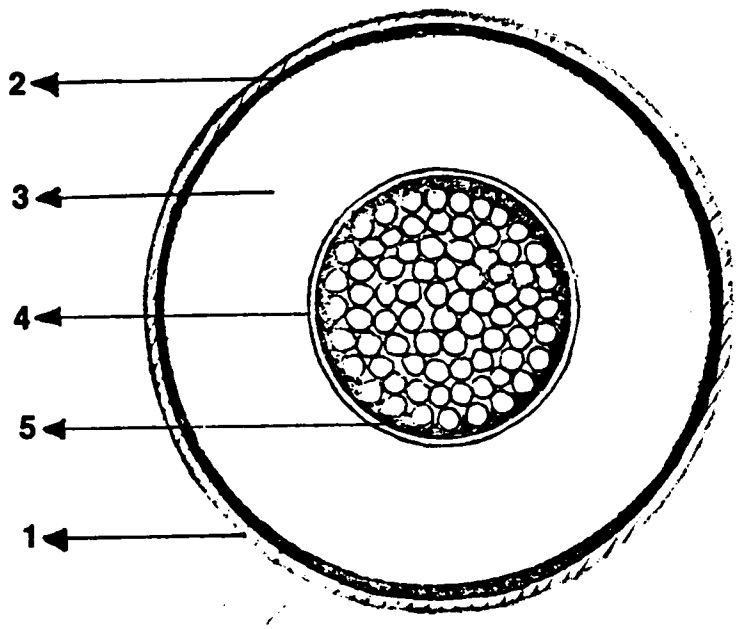

Figure 1 Cross-section of a typical single core three-polymeric layer cable insulation.

A typical manufacturing process of such a three-layer XLPE insulation cable consists of extrusion of these layers on the conductor sequentially with three extruders through cross-head dies. For the case of XLPE production, after extruding the PE-DCP blend and the semiconductor layers, the cable is passed through a long catenary vulcanizing pipe maintained at 200 ^{o}C for achieving the crosslinking reaction, then the cable is quenched. As a heat medium superheated pressurized steam is widely used. Dry curing, using a heated inert gas medium, is also practiced in order to eliminate the water uptake problem experienced in steam curing (Meyer and Chammel 1980).

Figure 2 is a schematic representation of an insulation cable extrusion process. In this figure, (1) is the uncoated conductor wire source, (2) inner layer semiconductor material extruder, (3) insulating material extruder, (4) heating zone (crosslinking zone), (5) cooling zone, (6) pressure seal, and (7) take up system.

2.5. Polymer Crystallization and Morphology

2.5.1. Polymer Crystallization

Many polymers can crystallize if certain requirements are met. The fundamental requirements for crystallization in polymers are nearly complete regularity of the chemical and the geometric structure (Meares 1965).

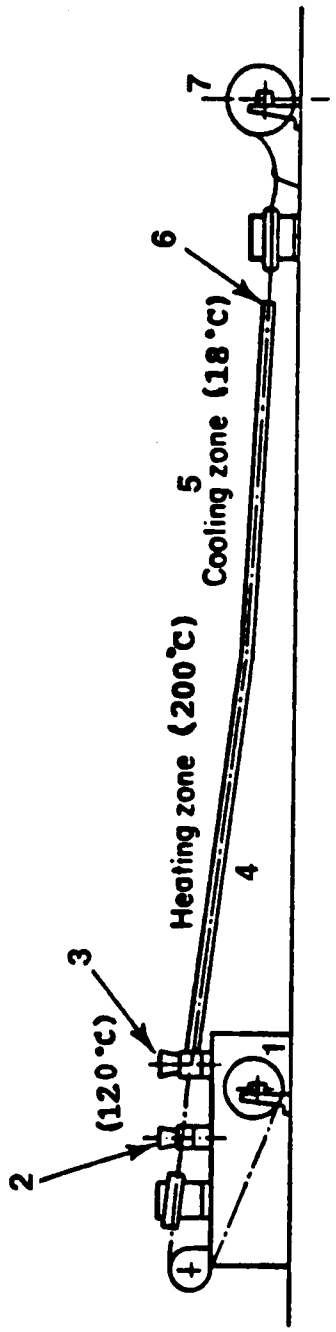

Figure 2 Manufacture of conventional XLPE cable using catenary continuous vulcanization process.

Chemical regularity of a polymer molecule is determined by the kind of atoms and atomic groups and their spatial distribution. While irregularly spaced bulky groups inhibit the chain segments from fitting into a crystal lattice, specific groups arranged along the chain in a regular manner establishing strong molecular bonds can facilitate crystallization. Regular spatial distribution of atoms has a major effect on polymer crystallization. While stereoregular polymers result in higher degrees of crystallization most atactic polymers cannot crystallize. For the case of geometric regularity, in general, linear chains crystallize more readily than their branched versions. Random distribution of cis- and trans- configurations along a polymer chain deforms the geometric regularity of the chain, thus preventing crystallization.

The simplest form of lattice generated by polymer molecules would have all the chains lined up parallel to one another. The structure would then be characterized by three features; (1) the conformation of the chain around the linear axis; (2) the pattern of packing of chains in a plane perpendicular to their length and; (3) the displacement parallel to the axis of each chain relative to its neighbor. Conformational continuity from one unit cell to the next presents a restriction which is not present in the unit cell of ordinary low molecular weight substances. The simplest side-by-side arrangement of all linear zig-zag chains in

register results to a rectangular parallelepiped as is the case for PE (Figure 3). In some cases there may be staggering of chains in order to provide a better fit for particular interchain bonding. In this case the parallelepiped is no longer rectangular.

Polymer chains with bulky substituents cannot attain the planar zig-zag form due to steric hindrance. Therefore, the isotactic chain twists along its axis to accommodate bulky substituents and creates a helical structure. The lattice structure then depends on the packing of helical chains and is usually hexagonal.

2.5.1.1. Chain Folding

Before the discovery of chain folding, the fringed micelle model (Bunn and Alcock 1945) (Figure 4) served the early development of polymer science. In this model, segments of chains cluster to form small crystals interconnected by the entangled segments of the chains which form amorphous regions. In other words, a single chain traverses a crystallite, moves through an neighboring amorphous region and then enters another crystallite. The fringed micelle is essentially a static model underestimating the mobility of chains in most polymer melts. Polymer molecules are capable of diffusing and arranging themselves into lower energy states by attaining favorable configurations during crystallization.

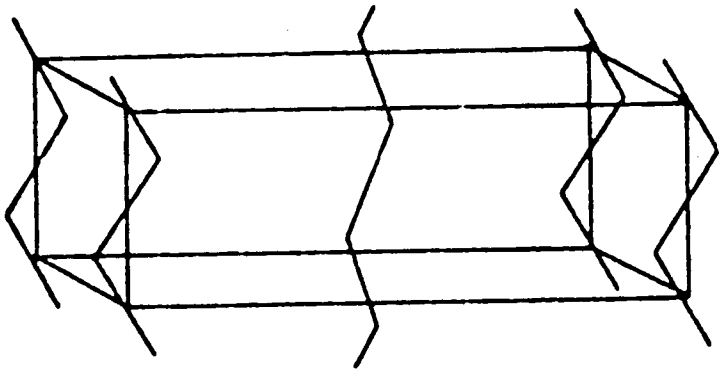

Figure 3 The simplest side-by-side arrangement of linear zig-zag chains.

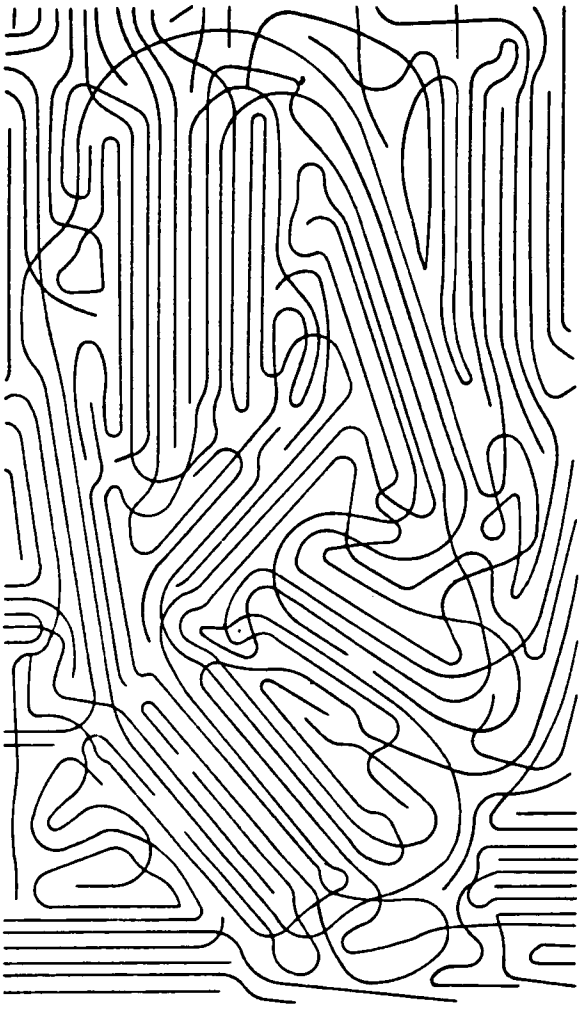

Figure 4 The fringed micelle model.

It was not until 1957 that Keller, Fisher and Till all reported chain folding in PE independently. Electron microscopy and electron diffraction of solution grown crystals led to the conclusion that long polymer molecules (10,000 A or more) could only be accommodated in the monolayer platelet single crystal (about 100 A thick) by some form of chain folding (Keller 1957). Chain folding can assume various forms in the crystal depending on the crystallization conditions and molecular characteristics of the polymer (Figure 5).

There has been considerable controversy regarding the precise details of the topography of solution grown crystals. The nature of the fold surface can be reduced to three basic models, regular adjacent reentry (Keller 1957), irregular adjacent reentry and switchboard or nonadjacent reentry models (Flory 1962).

2.5.1.2 Bulk Crystallization

The crystallization of polymers from the melt is not fundamentally different from crystallization from solution. The principal difference in bulk crystallization is the extent of contact between molecules in the coiled state. In dilute solution crystallization, polymer molecules are well separated and they can approach the growing surface as individual entities. In the melt, close interactions between molecules complicate the folding of an already

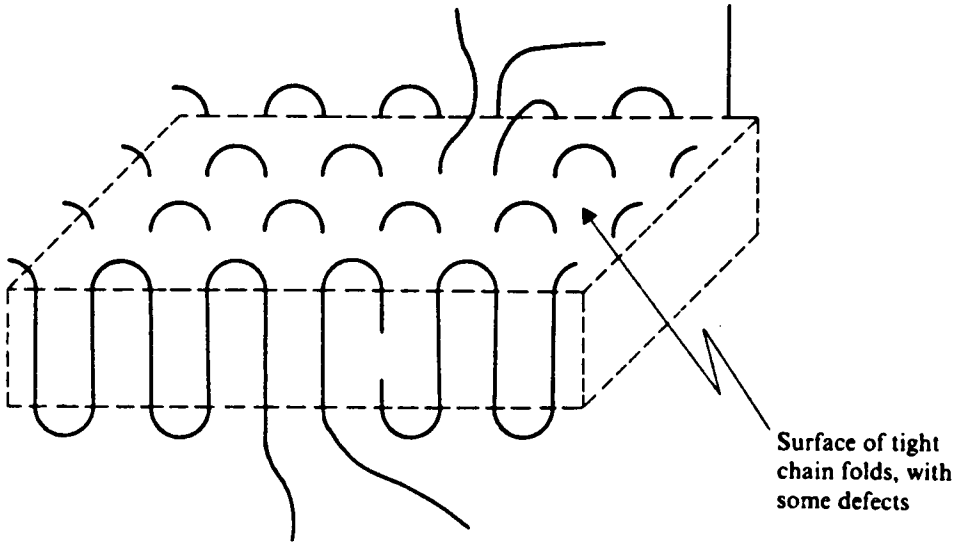

Figure 5 Chain folding in lamellar crystals.

existing molecule. Therefore, polymers crystallized from the melt can be less crystalline than single crystals prepared from solution. Analogous to multilayer growth obtained from concentrated solutions, melt crystallized polymers, being the limiting case, are polycrystalline aggregates in which the crystals are intimately tied together. The characteristic pattern of crystallization of polymers from the isotropic melt is spherulitic.

2.5.2 Polymer Morphology

The word morphology is used to describe the physical state and the characteristic features of the phases at various level of detail. When electron microscopes were not contributing to the field of research, X-ray crystallography was used to obtain indirect information on morphological features. Sharp X-ray reflections, being indicative of crystalline regions, and diffuse ones, being indicative of amorphous regions, made it possible to gain insight on the nature of semicrystalline materials. Calculations based on the widths of X-ray diffraction rings and line broadening resulted in crystallite size estimations of the order of a few tens of nanometers.

2.5.2.1 Lamellar Crystals

The discovery of the lamellar characteristic of spherulitic structures dates very closely to the discovery

of PE single crystals (Keller 1957, Bassett and Keller 1959). Lamellar PE crystals have been revealed in the electron microscopy study of thin samples. Figure 6 shows a schematic representation of spherulites, having lamellar structure and chain folding. Melt crystallized PE exhibited diffraction patterns, corresponding to a 300-500 ^{o}A periodic structure, which were more diffuse than single crystal patterns (Geil 1966, Blais and Manley 1967) suggesting even more disorder.

Developments in understanding lamellar morphologies came later than morphological studies of spherulites. This is simply due to their much finer structures requiring much higher resolution than the conventional optical methods used for spherulitic morphology studies. Understanding of lamellar morphologies was achieved after the acceptance of chain folding in single crystal lamellar studies from high resolution electron microscopy.

2.5.2.2 Spherulites

Spherulites were first revealed by Bunn and Alcock (1945) in thin films of branched PE. Spherulites are approximately spherically symmetric, birefringent polycrystalline entities which are crystallized from the melt in the absence of significant stress or flow. The microstructure of melt crystallized polymers is ordinarily composed of thin ribbons of folded chain lamellae radiating

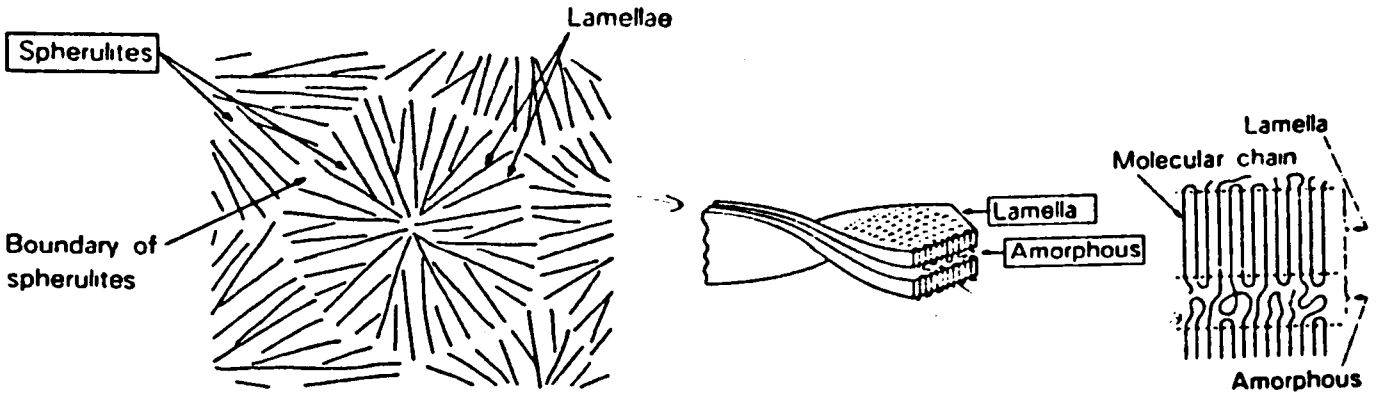

Figure 6 Schematic representation of spherulites having lamellar structure and chain folding.

from centers dispersed throughout the matrix. Those nucleating centers may be single crystal-like entities precipitated from the homogeneous polymer melt or could also be heterogeneous or foreign materials. Wunderlich and Sullivan (1962) demonstrated the morphological link between simple, lozenge, single crystals and b-axis oriented ribbons in spherulites by increasing the concentration of the crystallization solution. They showed that solution grown dendrites become thicker and thicker and become richer in branches and eventually take on spherulitic symmetry with increase in solution concentration. As the ribbon-like lamellae grow out from the nucleus they branch to satisfy the necessary space filling requirement and the remaining polymer may crystallize at a later stage in a more disordered fashion (Fava 1971).

Spherulites are characterized by a black Maltese cross lying parallel to the extinction directions of the polarizer and analyzer when viewed between cross-polars in an optical microscope. When the sample is rotated in its own plane the Maltase cross remains stationary implying that all radii are crystallographically equivalent. The concentric extinction banding observed in spherulites is thought to be caused by cooperative periodic twisting of the lamellar ribbons as they grow out from the center. The Maltese cross is always observed in spherulitic polymers whereas the banding does not occur in all cases.

Precisely how a spherulite develops depends on thermal gradients, nucleation and growth phenomena related to the nucleating agents, as well as the structural characteristics of polymer chains. A common progression of spherulitic growth is depicted in Figure 7 (Bassett 1981).

2.5.2.3. Degree of Crystallinity

The degree of crystallinity of a polymer is one the useful and practical concepts used to describe the degree of order reached after a polymer is crystallized. With degree of crystallinity measurement one can assign a weight or volume fraction of crystalline material to any semicrystalline polymer sample. Although it is a useful parameter in industrial processes, crystallinity does not describe the structure of the crystallites. This is mainly because of the diversity of factors which determine the polymer morphology.

Since semicrystalline polymers are two phase systems, the degree of crystallinity can be formalized as:

$$X = (P_a - P)/(P_a - P_c) \qquad (2.5.1)$$

where P_a and P_c denote partial properties of the amorphous and crystalline phases and P is the overall property of semicrystalline polymer.

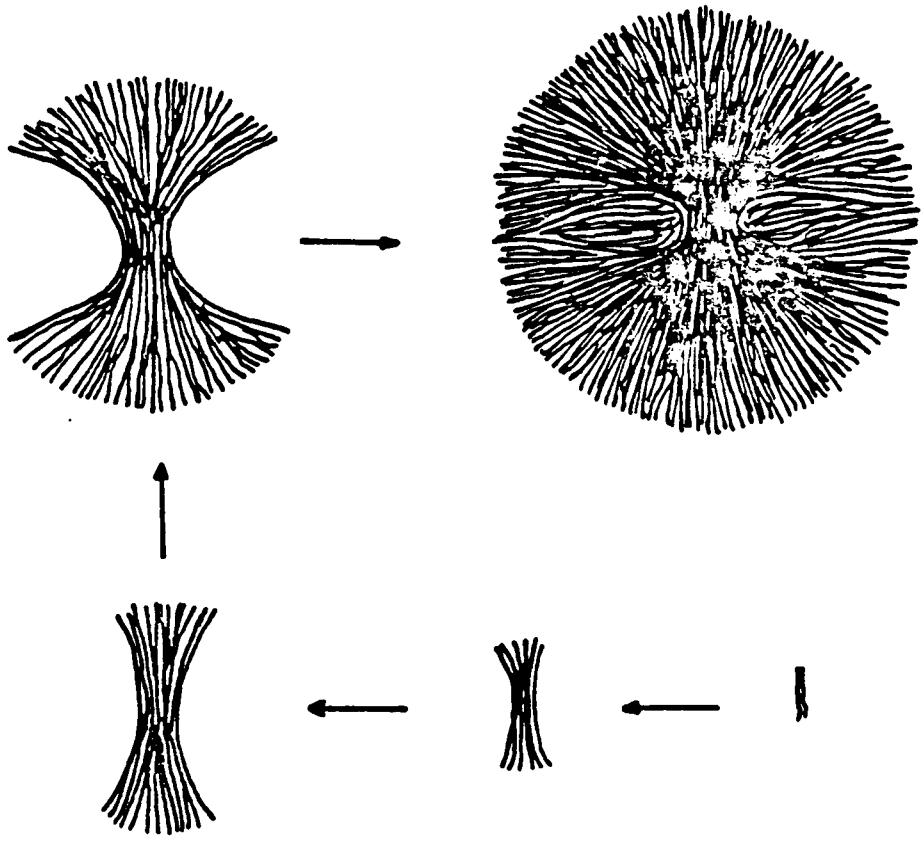

Figure 7 Schematic representation of spherulitic growth (from Bassett 1981).

Consequently any measuring probe which senses P, e.g. specific volume, specific heat, scattering intensity, resistivity, IR absorption, birefringence etc., enables one to assess the degree of crystallinity.

2.6. Thermal-Morphological Relationships

2.6.1. Melting

Melting is the transformation of a crystalline material into the liquid state.

Thermodynamically the crystalline state can be characterized by the free energy

$$G_c = H_c - TS_c \qquad (2.6.1)$$

The polymer chain conformation in the crystalline state is such that it gives an overall minimum energy. On the other hand, the melt is a state of higher enthalpy with no long range order and accordingly with much higher entropy. Analogous to Equation 2.6.1 the free energy of the melt is

$$G_l = H_l - TS_l \qquad (2.6.2)$$

At melting $G_c = G_l$ thus from Equations (2.6.1) and (2.6.2)

$$T_m = (H_l - H_c)/(S_l - S_c) \qquad (2.6.3)$$

$$\text{or} \qquad T_m = \Delta H/\Delta S \qquad (2.6.4)$$

As a result, the melting point of a polymer is a function of the enthalpy and the entropy changes in the process, which in turn are determined by the flexibility and the cohesive energy densities of the chains.

The melting of polymer crystals, unlike the narrow melting point of simpler crystals, occurs over a range of temperatures. A typical DSC melting curve for a semicrystalline polymer is shown in Figure 8. The maximum of this curve is taken as being the melting temperature, T_m. T_{on} is the onset of melting and return to the base line temperature ,T_{rb}, indicates the temperature at which the last traces of the thickest crystals disappear. The melting range and the melting point of a polymer are governed by many factors, such as molecular weight and molecular weight distribution (Chiang and Flory 1961, Harland et al. 1972), chemical and geometric structure of macromolecular chains, and crystallization conditions. These factors determine the lamellar thickness, lamellar thickness distribution, surface free energies, imperfections of the crystal lattice etc., all of which influence the melting behavior of the polymer. Extensive studies of the lamellar thickness and melting temperature dependence on crystallization temperature and degree of supercooling (Kawai and Keller 1965) in polymer single crystals show that, in general, higher

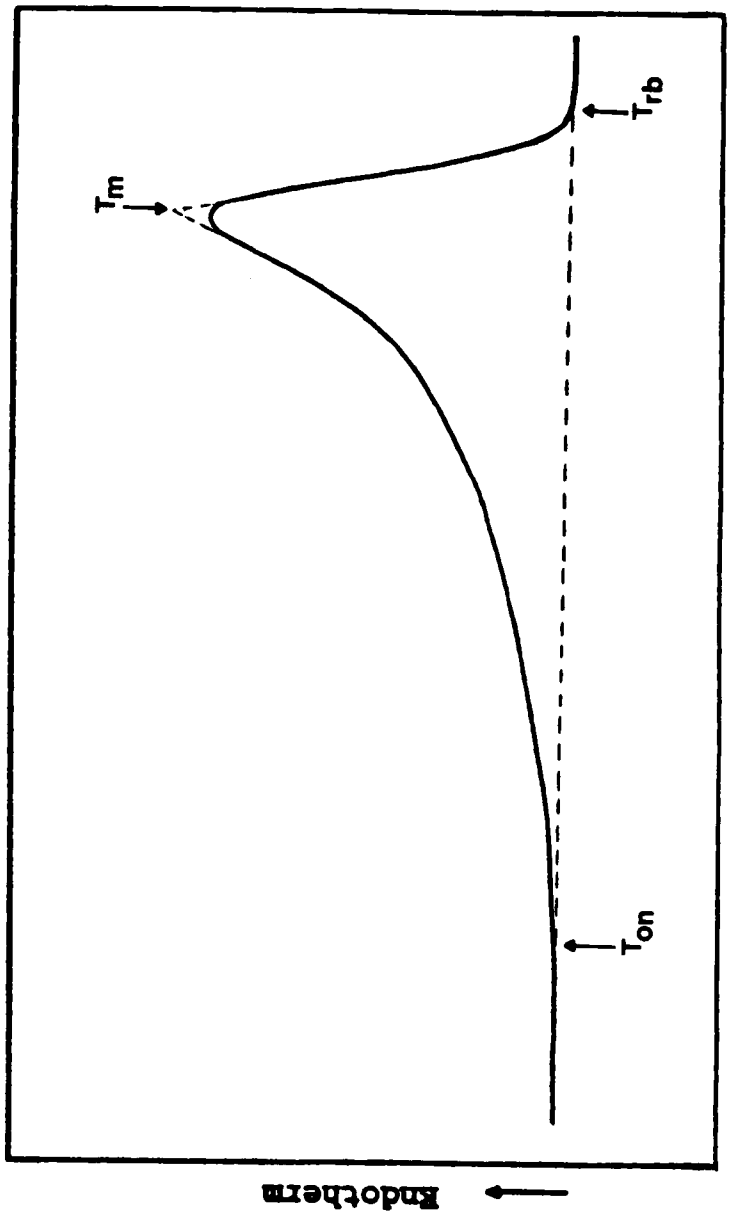

Figure 8 A typical DSC melting curve for a semicrystalline polymer.

crystallization temperatures are associated with higher melting points (Fischer and Hinrichsen 1966). In solution crystallization, the concentration and the solvent used were also found to affect the lamellar thickness and the melting temperature.

The melting point, T_m, of a polymer crystal can be related to its thickness and surface free energy thermodynamically as follows;

$$T_m = T_m^o \left[1-(2\sigma_e/\Delta H_f l)\right] \qquad (2.6.5)$$

where T_m^o is the equilibrium melting point, σ_e is the fold surface free energy, ΔH_f is the heat of fusion and l is the lamellar thickness (Hoffman and Weeks 1962).

The equilibrium melting point, T_m^o, is the melting temperature of an infinitely large perfect crystal of the polymer in question. Polymers crystallized by the usual procedures tend to have a T_m well below T_m^o. ΔH_f and T_m^o are usually considered as constants in the above equation.

2.6.2. Annealing

The term annealing implies heat treatment without large scale melting. When a polymer is held at or above its crystallization temperature but below its melting point annealing generally occurs, although it can also occur at a temperature below its crystallization temperature. The

annealing process activates molecular mobility and promotes great stability by the elimination of defects and frozen-in stresses thus bringing the system closer towards thermodynamic equilibrium. Much of the understanding of polymer annealing is based on studies of single crystals. Statton and Geil (1960) first discovered the irreversible increase on annealing in the long period of solution grown single crystals of PE. An early suggestion involving a mass transport mechanism in PE along the molecular chain via point defect movement was made by Reneker (1962). Dreyfuss and Keller (1970) proposed a simpler mechanism which involved rearrangement of portions of the molecule only without coordinated displacement of the molecule as a whole. Figure 9 shows the preferred doubling of the initial fold length. This is known as lamellar thickening. The fundamental cause of thickening is that thinner lamellae are metastable because of their comparably higher surface energy and they become more stable upon decreasing the number of folds through thickening. Elimination of defects also contributes to a reduction of high energy centers.

The time dependence of the increase in fold length was expressed by Fischer and Schmidt (1962) through the equation

$$l = l_o + B(t) \log[(t/t_o) + 1] \qquad (2.6.2)$$

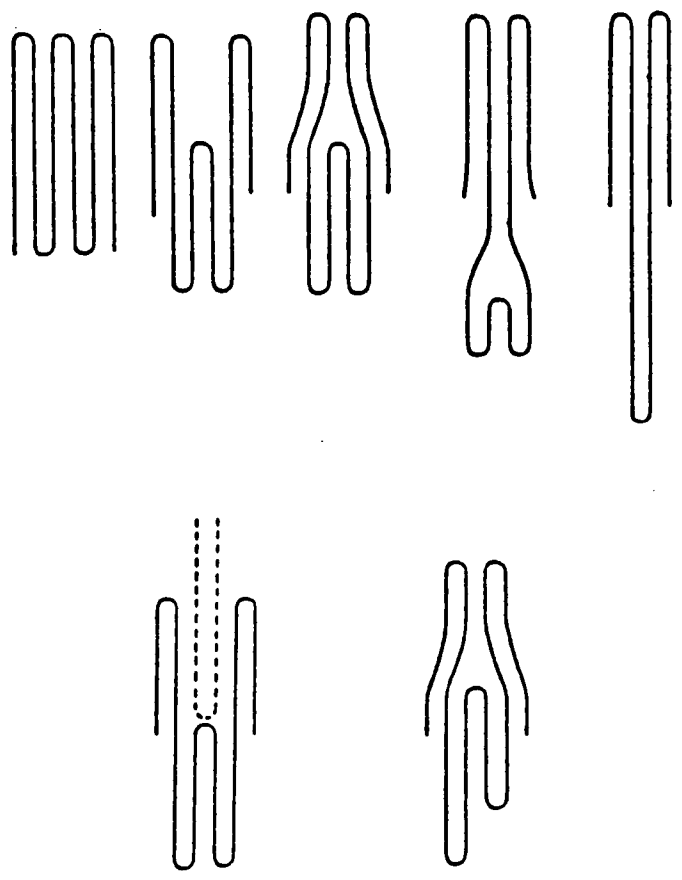

Figure 9 A schematic representation of lamellar thickening (Dreyfuss and Keller 1970).

where l_o is the lamellar thickness at $t=t_o$ and B(t) is proportionality constant.

Petermann et al. (1976), from their TEM observations of the annealing process of PE lamellar crystals, suggested that two major events take place during annealing. One process involves the melting of those regions of the crystals in which the melting point is lower than the annealing temperature. Molten crystals recrystallize and result in crystal growth. The alternative process is solid-state crystal growth by the migration of the amorphous region between crystallites. Wunderlich (1976) proposed that annealing can be experimentally separated into at least three different temperature regions (1) low temperature region; changes in defect concentration and stress without chain fold increase (2) intermediate temperature region; chain fold increase and change in crystal size without melting and (3) high temperature region; recrystallization.

These three temperature regions of annealing proposed for solution grown crystals of PE have not been defined accurately for melt crystallized samples. The early work on melt crystallized PE by Geil (1962) dealt with the increase in the X-ray long period and density as a function of annealing temperature and time. A logarithmic time dependence of X-ray long period was observed. Electron microscopic studies of annealed bulk crystallized PE have shown that during thickening no gross change in structure

and orientation of the crystals occurs. Quenched non-spherulitic samples were still non-spherulitic after annealing and had random lamellar orientation. Spherulitic samples remained spherulitic with the same diameter and ring spacing on annealing (Geil 1963). On the other hand, Petermann and Schultz (1978) studied the microstructure and annealing behavior of cold-drawn isotactic PP and they found that upon low temperature annealing of the drawn PP a fringed micelle structure was developed while high temperature annealing resulted in two-phase microstructure with folded chain crystallites and distinct low density amorphous domains.

3. EXPERIMENTATION

3.1. Materials

3.1.1. High Voltage Cables

Low density polyethylene (LDPE) and crosslinked low density polyethylene (XLPE) are used largely in power distribution and transmission cables rated 5 kV and above. While LDPE resins are used in distribution cable insulations for lower voltage applications, XLPE is used in transmission cable insulation for higher voltage applications. This is mainly because of the better thermal and mechanical stability of XLPE.

Data summarizing the various kinds of transmission and distribution cables used throughout in this study are summarized in Tables 1 and 2 along with their designations respectively. Cables were supplied from the indicated major cable producing companies, i.e. Pirelli and Phelps Dodge and cable testing institutes, EPRI and Waltz Mill.

Cables A1 and A2 were extruded at 127 ^{o}C and cured at 260 ^{o}C. A thin stream of polyethylene glycol, PEG, (Union Carbide UCON LB3000) was used as the heat transfer medium in the curing process. The thin layer of PEG was heated by a 50 feet long pipe which was electrically heated from the

Table 1 Specifications of HV transmission cables

Cable Designation	Curing Medium	Insulator Thickness(mm)	Conductor Diameter(mm)	Supplier	Comments
A1	PEG	11-14	28	Pirelli	Freshly cut on (f.c.o.) 6'/81
A2	PEG	20-21	28	Pirelli	f.c.o. 6'/81
B1	Steam	16-18	20	Pirelli	f.c.o. 10'/78
B2	Steam	16-18	20	Pirelli	f.c.o. 6'/78
B3	Steam	16-18	38	Pirelli	f.c.o. 10'78
B4	Steam	21-22	38	Pirelli	f.c.o. 10'/79
C1	Dry	20-21	35	Pirelli	Prepared under RP 7887 of EPRI
E1	Steam	23-24	28	Phelps Dodge	Prepared for EPRI
E2	Steam	23-24	28	Phelps Dodge	Failed version of E1

Table 2 Specifications of HV distribution cables

Cable Designation	Thickness(mm) Insulator	Conductor	Supplier	Type	Comments
D1	4.4-4.8	8.0	Phelps Dodge	LDPE	Control A, original
D2	4.4-4.8	8.0	Phelps Dodge	LDPE	Control A, aged
D3	4.3-4.5	7.8	Phelps Dodge	LDPE	Navajo C, original
D4	4.3-4.5	7.8	Phelps Dodge	LDPE	Navajo C, aged
D5	6.0-6.2	10.2	IREQ	LDPE	Florida P & L, aged
D6	4.5-4.6	8.0	IREQ	LDPE	Florida P & L, aged
D7	6.2-6.5	7.1	IREQ	LDPE	Memphis, aged
D8	4.6-5.0	17.0	IREQ	XLPE	San Diego, original
D9	4.2-5.0	25.5	IREQ	XLPE	San Diego, SD-XL-FA-1, aged
D10	6.0-6.2	8.0	IREQ	XLPE	Memphis M2-12, aged
D11	6.8-7.1	7.5	IREQ	XLPE	Memphis M2-23, aged
D12	6.8-6.9	9.7	IREQ	XLPE	Florida F1-342-1, aged

outside. Extrusion rate was 2 ft/min for A1 and 1.55 ft/min for A2 and cured cable was quenched in water at room temperature. Steam cured cables, B1, B2, B3, E1 and E2 were all extruded with a rate of 4-5 ft/min at 120-130 ^{o}C and cured in steam at 275-290 ^{o}C and 240-270 psi. Quenching was achieved in water at room temperature. Dry cured cable C1 was extruded at 143 ^{o}C with an extrusion speed of 1.22-1.52 m/min. Hot nitrogen gas at 260 ^{o}C in a 51.8 meter long curing pipe was used as curing medium. Cured cable was precooled in nitrogen gas at 65-71 ^{o}C then was quenched in water in a 85 meter long quenching pipe.

The aging history of the field aged steam cured cable E2 at the Waltz Mill aging facilities is given in Table 3. The cable was subjected to wet and dry media alternately on a weekly rotation basis. The cyclic loading mode constituted eight hours under load and sixteen hours under no load. Maximum conductor temperature was achieved in the eight hour heating period, then in the sixteen hour period the cable was cooled down. This time period was generally not sufficient for ambient temperature to be reached.

All thin walled distribution cables were extruded at 120-130 ^{o}C and were cured in steam. The field aging treatments for some of the distribution cables were as follows; Cable D2 was aged over 31 months at 85 V/mil and 60 Hz. Cable D9 was aged over 10 ± 1 years. It's breaking

Table 3 Thermoelectrical history of field aged cable E2 at the Waltz Mill aging facility

Test Period	Φ-G Voltage		Conductor Temp.(°C)	Max. Jacket Temp.(°C)		Loading Mode	Test Period		Remarks
	%	KV		Main Run	Loop		Start	Finish	
0	-	80	25	25	25	continuous	8- 6-79	8- 7-79	24-hour test at 80 KV
1	120	96	90	77	76	cyclic	9-19-79	10- 3-79	
2	120	96	90	76	60	cyclic	10- 3-79	10-30-79	
3	140	112	90	63	60	cyclic	11- 1-79	12-21-79	
4	140	112	100	67	66	continuous	1- 2-80	2-16-80	
5	140	112	100	72	74	cyclic	3- 4-80	4- 9-80	
6	140	112	110	79	79	continuous	4-17-80	5-29-80	
7	140	112	110	80	82	cyclic	8-11-80	9- 4-80	Changed pothead internals on alternate bay long riser
8	140	112	120	82	81	continuous	4- 1-81	4-29-81	
9	140	112	120	82	82	cyclic	5- 7-81	6-25-81	
10	150	110	110	82	81	continuous	7-15-81	8-18-81	Efforts to eliminate discharge problems in shield interrupt dry bay
11	150	110	110	80	65	cyclic	1-29-82	2-26-82	Cable Failed

strength was 80 V/mil. Cable D10 was aged over 6 years at 30 V/mil and its breaking strength was 324 V/mil. D11 is the same as D10 except it operated at 55 V/mil. D12 was aged over 6 years at 48 v/mil and its breaking strength was 193 V/mil.

3.1.2. Crosslinked Polyethylene Preparation

In addition to investigating the physical and thermal properties of the different cables, crosslinked polyethylenes with different extractable levels were studied. The material used in all XLPE preparations was Union Carbide HFDE-4201. This polymer was a LDPE mixed with two percent by weight dicumyl peroxide (DCP Luperox 500) as crosslinking agent together with an antioxidant.

It is already known that the amount and the molecular weight of the extractable material depends on the amount of the curing agent added to the base resin, assuming that fully cured conditions are achieved (Kao 1983, Karakelle 1986). It is known also from the statistical nature of the crosslinking reaction that the longer chains readily participate in the crosslinking reaction. Here, the molecular weight distribution (MWD) of the base material was changed in order to alter the amount of extractables.

The MWD of the original base material, LDPE containing two percent DCP, was changed by adding certain amounts of the sol fraction obtained from the extraction of

cured specimens of the initial resin. For this purpose, first DCP free original base material was prepared by extracting the DCP with methanol. The extraction was carried out by dissolving ten grams of base material in 400 ml of p-xylene at its reflux temperature and precipitating the hot solution in 1200 ml of dry ice-cooled methanol while stirring rapidly. The white precipitate was filtered and washed with excess methanol while keeping the precipitation solution and the methanol cold by frequent additions of dry ice. Methanol soluble DCP was taken into the filtrate and then it was discarded. Solvent-free, methanol-free powder was obtained by drying in a vacuum oven at 80 ^{o}C for two days.

Homogeneous mixtures of the original LDPE and the additional low molecular weight fraction were achieved by dissolving them in hot xylene in known proportions. A fine powder of the new resin with altered MWD was obtained by precipitating the hot polymer solution in cold methanol as described earlier. After obtaining the dried fine powder, the new resin was blended with DCP of known percentage in a sufficient amount of methanol. The slurry was mixed with magnetic stirring and then the methanol was removed from the slurry by vacuum evaporation. Finally methanol-free powder was compression molded into three milimeter thick sheets. This was carried out in a hot press using a mold made of stainless steel plates with an aluminum separator template

having a four centimeter square hole. The molding was carried out at 120 ^{o}C and 1x10^{4} psi for ten minutes. After cooling the mold to room temperature, the molded sheet was cut into small pieces, remixed and remolded under the same conditions in order to assure a homogeneous distribution of DCP within the matrix. Curing of the molded LDPE film containing the DCP was carried out by raising the temperature of the hot press to 200 ^{o}C. The mold was kept at this temperature for five minutes in order to ensure that the DCP was at least 99.9 % decomposed. The crosslinked polymer film was then allowed to cool to room temperature under pressure.

Compression molded thin films for electric breakdown testing were prepared from Union Carbide HFDE-4201 polymer by successive reductions in thickness in the uncured state. Curing at 200 ^{o}C was then carried out at the final thickness of 1x10^{-2} inches. Films with dimensions 4"x 4"x 0.01" were then annealed for 30 minutes at 79, 85, 89, 93, 95, 100, or 107 ^{o}C. Failure testing of these samples was carried out by Cable Technology Laboratories.

3.2. Characterization of Cables

3.2.1. Extraction

Extraction studies were performed to determine the amount of uncrosslinked material, or sol, present in the

crosslinked PE networks. Estimates of the percent extractables were obtained by determining the weight loss of the crosslinked polymer and the weight of the extracted material. Ideally, the weight loss of the crosslinked polymer would be equal to the weight loss of extractables unless losses from the crosslinked network, or gel, occur due to physical rupture. Sol-gel measurements are widely used as an estimate of the degree of curing, thus, the crosslink density of network polymers.

Sol and gel fractions of the cables were determined as a function of radial position. Generally, radial slabs taken from each cable were sectioned tangentially (Figure 10) into eight equal sections with a cross-sectional area of 5x5 mm and a thickness of 1.5 - 3.0 mm depending on the insulation thickness of the cable. Whenever necessary, as judged by differences between adjacent samples from the eight-cut specimens, more detailed studies were carried out by sectioning the radial slab into as many as sixteen sections. Sectioning of cables was carefully carried out so as to eliminate the generation of dangling pieces of material that could easily break loose during extraction. After weighing each tangential slice, they were placed in perforated aluminum containers and immersed in boiling xylene, 138 ^{o}C, known to be more effective than soxhlet extraction (Kao 1983). The effective extraction temperature attained in a soxhlet extraction is

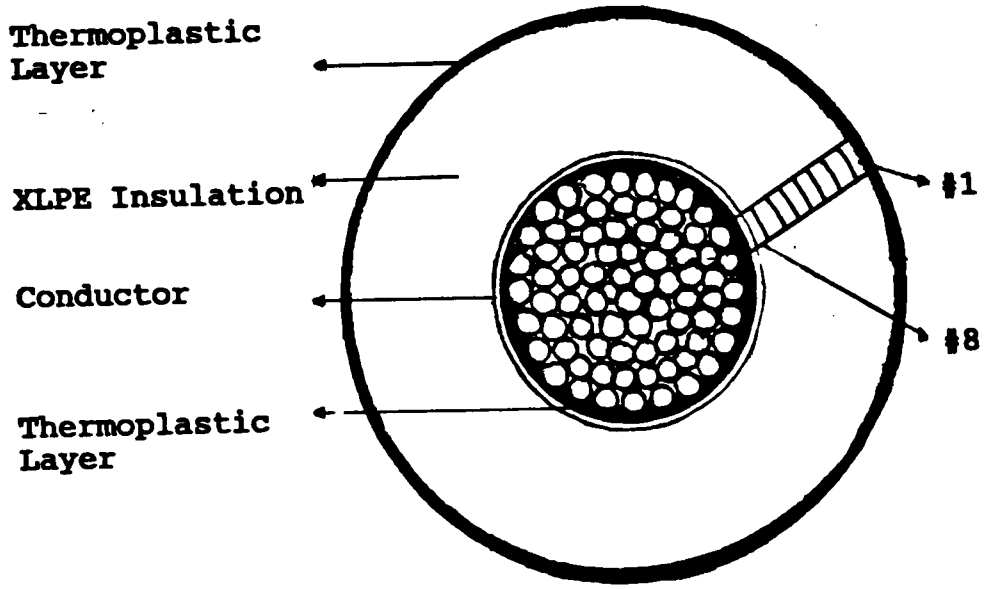

Figure 10 Radial sectioning of HV cable insulation.

much lower than the reflux temperature, thus prolonging the extraction time. Samples were refluxed in Erlenmeyer flasks for 24 hours under continuous stirring with a magnetic bar, then the solvent was replaced and the samples refluxed for an additional 24 hours for complete extraction of the sol material. It was found that almost 80 percent of the available sol was extracted in the first 24 hour extraction period. The second 24 hour extraction was sufficient for complete extraction of the remaining sol. Such a test was carried out by following the weight loss of the gel after extended extraction periods. After 48 hours of total extraction, the weight of gel was found to remain constant. After completion of extraction, gel samples were brought to constant weight by drying for 48 hours at 80 ^{o}C in a vacuum oven equipped with a liquid nitrogen trap. Sol material was recovered by precipitating the hot solution into cold methanol, the resultant precipitate being filtered and washed with excess methanol. The sol slurry was dried in a vacuum oven along with the gel samples. The gel and sol fractions were determined by following the weight loss of crosslinked polymer and calculated according to the following formula;

$$W_s = (W_{XLPE} - W_{gel})/(W_{XLPE}) \qquad (3.2.1)$$

$$W_g = 1 - W_s \qquad (3.2.2)$$

where W_{XLPE} is the weight of original unextracted XLPE, W_{gel} is the weight of the gel, W_s and W_g are the weight fractions of the sol and gel respectively.

3.2.2. Crosslink Density Determination

Crosslinked polymers, like linear ones, are diluted by solvents when the polymer-solvent interactions lead to an increased entropy of mixing. However, this mixing is limited by the degree of crosslinking of the network. The extent of swelling is inversely proportional to the density of crosslinks in the network and is highly dependent on solvent and temperature. As the network is swollen by the solvent, the network junctions, thus the chains, are forced apart to accommodate the increasing solvent fraction. Strained conformations result in retractive forces which tend to make the network return to more probable conformations. In the equilibrium state these two forces; entropy of dilution and retractive network forces are balanced.

Swelling experiments are normally carried out on samples of uniform shape and composition. Although early researchers (Proske 1941, Gravey 1941) noted that volumetric measurements of swelling were more accurate, many researchers today use gravimetric measurements (Munch et al. 1977, Sasaki et al. 1973, Pasthuma and Pennings 1976). As

their names imply in volumetric analysis the volume change of the swollen network is monitored, while in gravimetric analysis the weight change of the swollen network due to solvent intake is followed. Optical techniques developed to overcome the shortcomings of volumetric and gravimetric techniques have their own disadvantages (Chiklis and Grasshoff 1969, Buckley et al. 1962). Non-uniform swelling and light transmission through such samples are problems.

In this study the ASTM D 2765-68 (1971) gravimetric swelling analysis was optimized for extraction and swelling ratio calculations. In this technique, crosslinked PE is swollen in xylene at 110 ^{o}C for 24 hours. Since complete extraction of the sol cannot be achieved at 110 ^{o}C in 24 hours, this technique was modified by first extracting the sol completely at the reflux temperature and then the swelling experiment was conducted at 110 ^{o}C for 24 hours in order to assure gel solvent equilibrium. One of the drawbacks encountered in this technique was solvent adsorption on the swollen sample surfaces when the samples were removed from the solvent. Extra caution was paid in eliminating the solvent adsorption by blowing hot air momentarily on the surfaces before placing the swollen samples in stoppered weighing bottles. Also, keeping the surface to volume ratio a minimum helps to minimize surface effects.

Swelling tests were conducted for four different radial sections of each cable. The volume of each radial cube was close to 0.035 cm^3 for cable A1 and close to 0.190 cm^3 for cables C1 and E1. All the weight measurements were carried out using a Mettler microbalance with $1x10^{-6}$mg sensitivity. After measuring the weight of the swollen gel in the stoppered weighing bottle, the sample was freed from solvent in a vacuum oven at 80 ^oC using a liquid nitrogen trap and then reweighed. The drying process was continued to constant weight. The degree of swelling was calculated using the following formula:

$$\text{Swelling Ratio} = \frac{V_g + V_x}{V_g} \qquad (3.2.3)$$

In terms of the measured weights and densities the above formula becomes

$$\text{Swelling Ratio} = \frac{m_g / d_g + m_x/d_x}{m_g/d_g} \quad \text{or} \quad (3.2.4)$$

$$= 1 + \frac{(m_x)(d_g)}{(m_g)(d_x)} \qquad (3.2.5)$$

where V_g is the volume of the swollen gel, V_x is the volume of absorbed xylene, m_g is the weight of the gel, m_x is the

weight of absorbed xylene, d_g is the density of the gel and d_x is the density of xylene.

The average molecular weight between crosslinks is related to the equilibrium swelling through the Flory-Rehner (1943) formula

$$M_c=-d\ v_1\ v_2^{1/3} / [\ X\ v_2^2 / 2 + \ln(1-v_2) + v_2\ ] \qquad (3.2.6)$$

where v_2 is the volume fraction of the polymer in the swollen gel which is in equilibrium with pure solvent, v_1 is the molar volume of solvent, d is the density of the polymer and X is the polymer solvent interaction parameter and was taken as 0.33 (Tung, 1957). Crosslink density, d_c is defined as $d_c = 1/M_c$ where M_c is the molecular weight between crosslinks.

3.2.3. Molecular Weight Determination

In the crosslinking of PE using peroxides, the longer chains readily participate in the crosslinking for statistical reasons. In a recent study, Karakelle (1986) showed that the molecular weight of the original PE is 3.5 times that of the sol fraction obtained from its 2 % DCP cured XLPE and 8.2 times that of the 6.8 % DCP cured XLPE. Thus a knowledge of the molecular weight (MW) and molecular weight distribution (MWD) helps in the understanding of the efficiency of the crosslinking process. MW and MWD of

extractables from different cables and from the different radial sections of a cable were determined by Gel Permeation Chromatography (GPC) and intrinsic viscosity measurements. Intrinsic viscosity studies were carried out with an Ubbelohde Viscometer, Cannon 0B A71, in a glycerol constant bath temperature maintained at 75 ^{o}C. Polymer solutions were prepared in p-xylene with concentrations in the range 0.08-0.09 g/lt. After filtering the hot solution through medium sintered glass filter, the final concentration of the solution was determined. This was carried out by finding the amount of polymer in the sampled polymer solution by evaporating the solvent in a vacuum oven. For each concentration an average of three samplings was taken. After measuring the viscosity of the starting solution, the remaining concentrations were obtained by successive dilutions of the initial concentration using known additions of solvent. Specific viscosities, η_{sp}, were determined from the measured relative viscosities, η_{rel}. Intrinsic viscosities, $[\eta]$, were found from the plots of η_{sp} / c versus concentration, c. According to the Huggins equation

$$\lim_{c \to 0} \eta_{sp}/C = [\eta] + k'[\eta]^2 c \qquad (3.2.7)$$

The intrinsic viscosity was evaluated from the intercept at zero concentration obtained by a linear extrapolation. By using the Mark-Howink equation

$$[\eta] = K M^{\alpha} \qquad (3.2.8)$$

intrinsic viscosities were converted to molecular weights. K and α are the constants and for the branched PE-p-xylene system at 75 ^{o}C were determined by Harris (1952) as 1.35×10^{-4} and 0.63, respectively. Viscosity measurements for the extractable fractions from radial sections of cables A1, C1 and E1 were also determined.

The MWD of the extractables from cables A1 and E2 were determined in Union Carbide Laboratories using a GPC at 75 ^{o}C in xylene.

3.2.4. Infrared Spectroscopic Studies

Fourier Transformed Infrared Spectroscopy (FTIR) has the advantage of superior signal to noise ratio over dispersive infrared spectroscopy (IR) for measurements taken at equal resolution and for equal measurement time, with the same detector and optical throughput. With its long term durable frequency accuracy, applications such as quality control and long term aging and weathering over long periods are possible. Subtle differences between two or more samples are easily carried out by digital subtraction of their spectra.

In this work, FTIR was utilized to detect possible molecular changes occurring during aging. For this purpose,

quantitative comparison of the spectra from aged and unaged cables was carried out. Molecular changes along the radial direction were also monitored for the aged cable, E2. 100 micron thick radial sections were prepared using a microtome and then mounted on aluminum sample holders. Digilab FTS-20E FTIR equipment was used, data from 50 scans with 8 wavenumber sensitivity being recorded on a floppy disk and then processed using a BIO-RAD Digilab Division microprocessor interfaced with the FTIR. Thickness corrections were carried out by calculating the exact thickness of each microtomed slice from the fringes appearing at low wavenumbers (500-600 cm^{-1}). These fringes are normally obtained when the polymer film has perfectly smooth and parallel faces. The following formula was used to find the film thickness;

$$t = 1 / 2 \eta [n / (v_2 - v_1)] \qquad (3.2.9)$$

where, η is the refractive index of the polymer film, n is the number of fringes and ,v_1 and v_2 are the wavenumbers including n amount of fringes.

Thus, the relative film thickness, t_R, of a polymer film with a thickness of t_1 compared to a polymer film with a thickness of t_2 is found from the following formula;

$$t_R = t_1 / t_2 = n_1 / n_2 \left[(v_2-v_1) / (v_2-v_1) \right] \quad (3.2.10)$$

3.3 Thermal Studies

3.3.1 Annealing

Annealing takes place when a polymer is held at a temperature below it melting point. In a sense, it is a heat treatment lacking large-scale melting. During annealing, structural rearrangements, elimination of stresses and defects result in greater stability and perfection of micro structure.

When high voltage insulation cables are energized, due to power losses, joule heating is generated within the conductor. This heat is transferred to the insulator and the temperature of the insulator increases. During day load periods this temperature easily reaches 90 ^{o}C or even higher temperatures, thus defining the effective annealing range of the insulation material. Besides analyzing field aged cables, virgin cables were annealed isothermally in the laboratory and in variable temperature fields.

A typical annealing experiment was performed by placing a specimen in a preadjusted constant temperature bath. Annealing temperature was followed with a direct temperature read-out digital thermometer having its thermocouple in contact with the sample. Samples were placed in glass tubes having a 5 mm diameter and 0.2 mm wall

thickness for better heat transfer. Radial samples from cables A1, C1 and E1 were annealed in the same bath for the same time to permit better comparison. After keeping the samples in the bath for the desired period, they were allowed to cool to ambient. DSC analysis of annealed radial specimens was carried out using eight equal radial positions, #1 being the outer and #8 being the inner radial sections. Since sample position #8 of cable A1 was found to reflect insufficient curing this section was mainly used in the thermal analysis of the cables annealed under the same conditions.

Besides performing isothermal annealing of the cables, successive annealings of cable E1 were performed at temperatures of 95, 100, 103 and 107 ^{o}C. In one set of successive annealings a specimen was first annealed at 107 ^{o}C than at 103, 100 and 95 ^{o}C successively. In the other set of annealings, this sequence was reversed and the first annealing was carried out at 95 ^{o}C and then 100, 103 and 107 ^{o}C annealings followed. The shortest dwelling time at each temperature was 30 minutes and the longest was 120 minutes. With the understanding developed in correlating each generated peak with its annealing temperature, the field aged cable, E2, was radially analyzed to deduce its thermal history. For this reason, 32 radial sections were analyzed using DSC. Different heating rates such as 10, 20, 40 degree per minute, were used for the innermost layers in

order to check for any possible instrumental annealing during analysis.

In another set of annealing experiments, the effect of rate of cooling from the annealing temperature on the separation and the magnitude of the peaks was studied. For this purpose, the inner layer of Cable A1 was annealed at 97 or 107 ^{o}C for 30 minutes and cooled through quenching in liquid nitrogen or at 0.2 degree per minute.

For melt crystallization studies, samples were held in the melt at 135 ^{o}C for 15 minutes and then crystallized. After keeping the samples for the desired isothermal crystallization time they were taken out and allowed to cool to room temperature.

3.3.2. DSC Analysis

Differential Scanning Calorimetry, is based on the principle that the heat flow into or out of a sample relative to a reference material can be measured as a function of time or temperature while keeping the sample and reference at the same temperature. The sample and reference are heated separately by individually controlled elements with a programmed heating rate (Figure 11). The power to these heaters is adjusted continuously in response to any temperature differences arising during analysis. As a sample undergoes a transition, the sample heaters must supply additional energy to the material in order to keep the

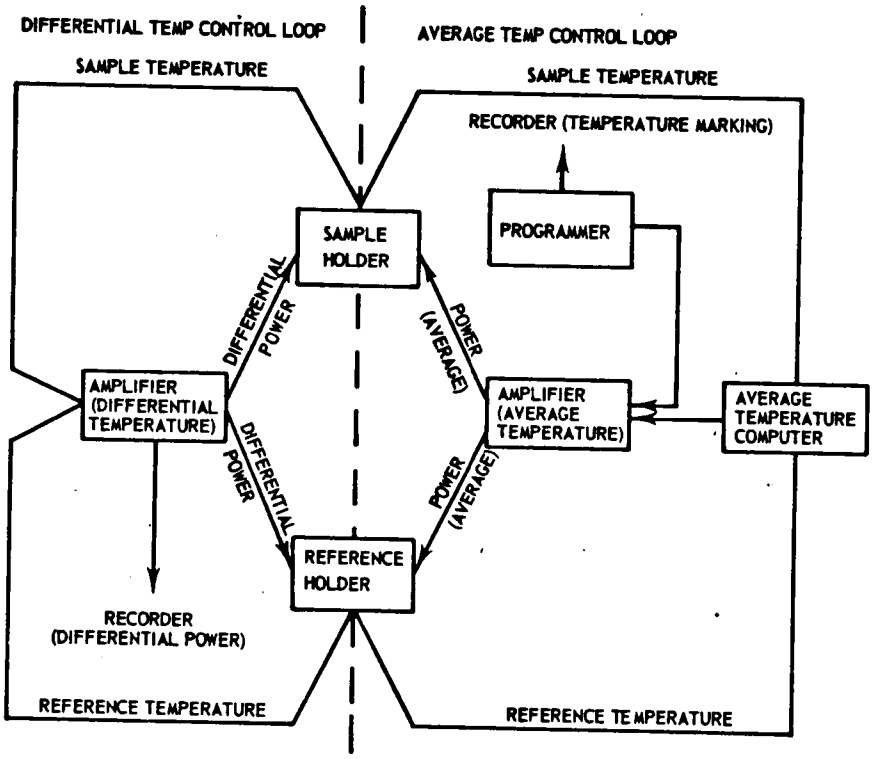

Figure 11 Schematic representation of a typical DSC system.

sample and reference temperatures the same. Power required to achieve this condition is recorded as the ordinate of the recorder with the programmed linear temperature, or the time scale, as the abscissa.

For thermal analyses, Perkin Elmer DSC-2 and Perkin Elmer DSC-7 models were utilized. The two models basically are the same in terms of their calorimetric capabilities. The DSC-7 has additional data processing and storage capabilities with its supplement Tac-7 interphase, PE 7500 computer, and graphic plotter.

The DSC was calibrated with standard substances, i.e. Indium (T_m=156.60 ^oC and ΔH=28.45 J/g) and Tin (T_m= 231.88 ^oC and ΔH=60.46 J/g) for its temperature axis (abscissa) and energy axis (ordinate). A Mettler microbalance with a $\mp$0.001 mg sensitivity was used throughout. Samples always were cut to a similar shape, and the sample weights were kept in the range 2.8 to 3.1 mg in order to minimize sample factors affecting the DSC data.

Finding the degree of crystallinity using DSC is based on heat of fusion measurements. The theory of the method derives from the pioneering work of Dole et al. (1966) who illustrated the broad utility of calorimetry in characterizing polymer morphology and thermal behavior. A two phase structural model is employed with the assumption that amorphous and crystalline phases have different heat capacities at any particular temperature and they are

additive (Peterlin and Meinel 1966, Mandelkern et al. 1968). The heat capacity of the amorphous regions can be extrapolated from or is identical to that of its melt state.

Degree of crystallinity is given by the following simple equation

$$X = (\Delta H_f / \Delta H_f^{\circ}) \times 100 \qquad (3.3.1)$$

where, ΔH_f is the measured heat of fusion of the polymer and ΔH_f is the heat of fusion of 100% crystalline polymer.

For a typical DSC measurement ΔH_f is calculated with the following formula:

$$\Delta H_f = \frac{\Delta H_{f,c} \times m_c \times c_s \times r_s \times A_s}{A_c \times C_c \times r_c \times m_s} \qquad (3.3.2)$$

where $\Delta Hf,c$ is the enthalpy of fusion of the calibrant in J/g , m_c is the weight of the calibrant in gram, A_c is the peak area, C_s and C_c are the chart speeds used for calibration and sample runs, respectively, r_s and r_c are the sensitivity (range) settings, m_s is the weight of the sample in grams and A_s is the peak area of the sample thermogram.

3.4 Thermo-Optical Studies

Crystallization from polymer melts can be measured by monitoring various physical properties of the material which are sensitive to crystallization. Among them the intensity of transmitted light as a measurable quantity was proposed by Stein et.al.(1967). This method is based on the ability of polymer crystals to rotate the plane of polarization of light. The polarizing plates, referred to as polarizer and analyzer used in the cross-polarized condition (Figure 12), have the property that only a specific component of polarization of the incident beam on them can penetrate. If the polarization directions of the two plates are set 90° to each other, no light will pass through. The light that passes through the polarizer has no component in the polarization component of the analyzer. A polymer crystal located between polarizer and analyzer reorients the polarization created by the polarizer, thus resulting in a passage of some of the light through the analyzer. To a good approximation the intensity of the transmitted light is a measure of the degree of crystallinity.

3.4.1. Instrumentation

This technique was utilized to study the in-situ annealing of cable samples. Figure 13 shows a schematic

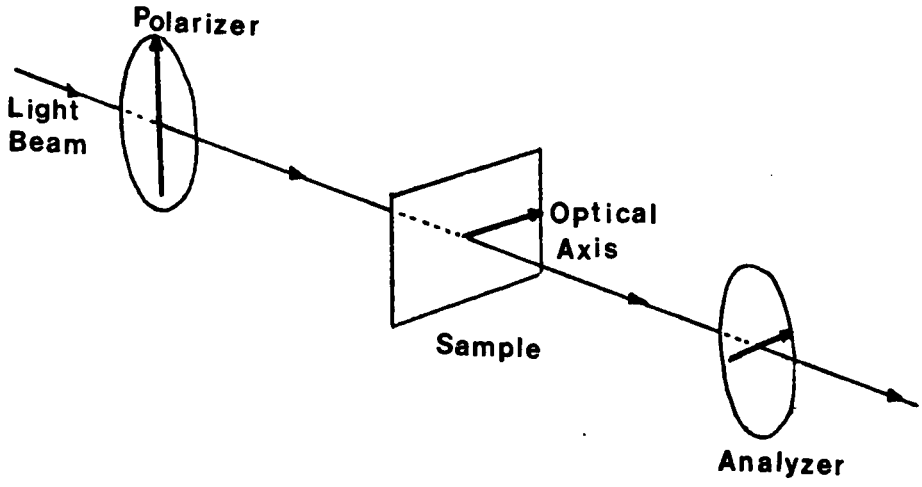

Figure 12 A uniaxial crystal between cross-polars.

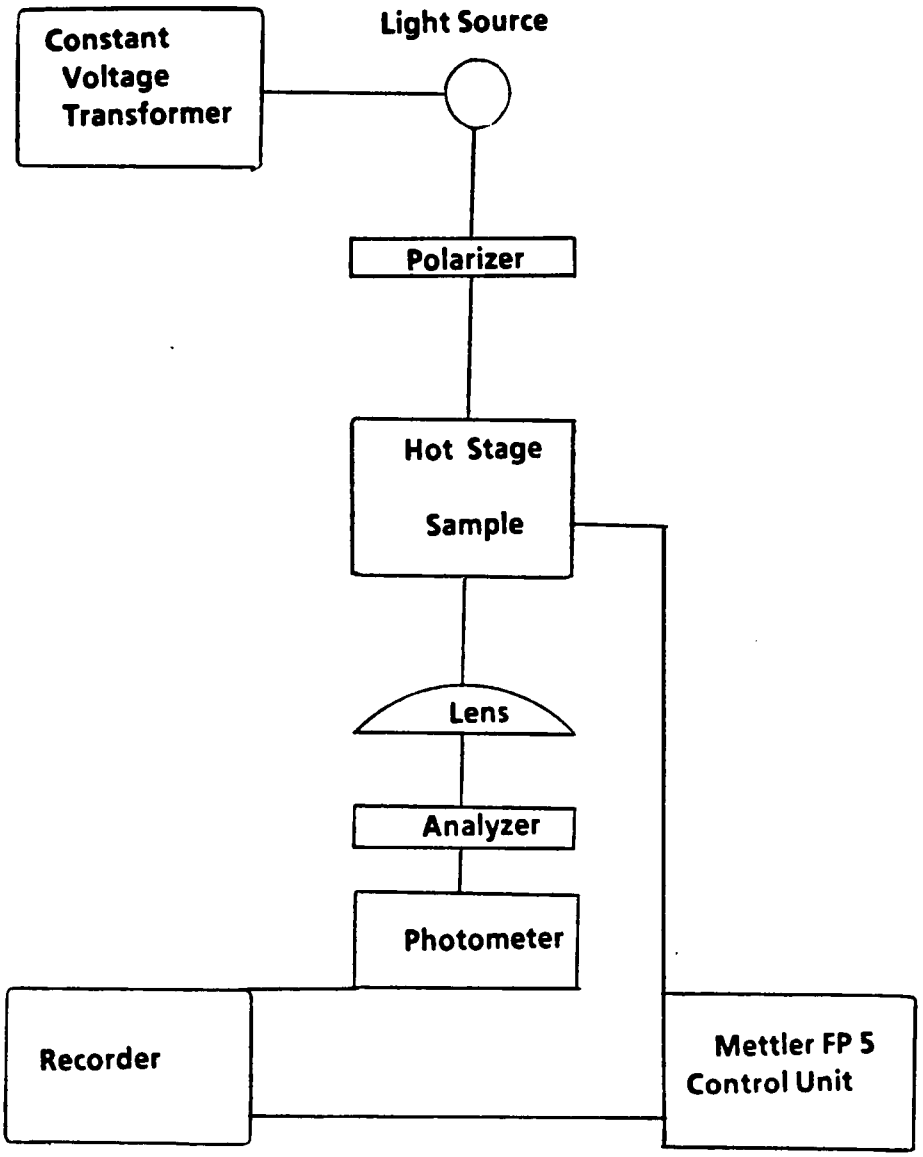

Figure 13 Thermo-optical light transmission microscope set-up.

diagram of the set-up established for this study. A Reichert Neovar Pol polarizing microscope was used, controlled heating of the hot stage being achieved through a Mettler FP 5 control unit. Controlled cooling of the hot stage was achieved by purging dry nitrogen gas through liquid nitrogen and conducting the cooled gas through the hot stage. A UDT 161 Radiometer/Photometer having a sensitivity in the range from 10^{3} to $10^{-3}\mu W$ was utilized in the direction of the transmitted light intensity. Analog output was fed to an Omni Scribe chart recorder. The microscope was attached to a constant voltage transformer in order to minimize the fluctuations in the light source.

3.4.2. In-Situ Annealing Studies

A typical annealing study was carried out, first, by calibrating the photometer to zero intensity in the melt state of the specimen. The sample was quenched to room temperature and then brought to the desired annealing temperature with 10 ^{o}C/min heating and kept there for the selected annealing time. Finally, the specimen was cooled down to room temperature. In order to permit correlation with DSC studies, annealed samples were run at 10 ^{o}C/min to obtain intensity versus temperature plots equivalent to DSC thermograms.

3.5. X-Ray Studies

3.5.1. Wide Angle X-Ray Studies

X-ray diffraction patterns from crystallizable polymers indicate that long range order exists. The degree of this long range order is often expressed as the degree of crystallinity of the polymer.

The method of measuring the degree of crystallinity by X-ray diffraction techniques is based on the fact that the total coherent scattering from N atoms is the same irrespective of the state of aggregation. The degree of crystallinity, X_c, is equal to the ratio of the integrated crystalline scattering to the total scattering, both crystalline and amorphous, and is given by (Alexander 1979);

$$X_c = \frac{\int_0^\infty s^2 I_c(s)\, ds}{\int_0^\infty s^2 I(s)\, ds} \qquad (3.5.1)$$

where, s is the magnitude of the reciprocal lattice vector and is given by $s=(2\sin\theta)/\lambda$, θ is one-half the angle of deviation of the diffracted rays from the incident X-rays, λ is the wavelength of the X-ray beam, $I(s)$ is the total

intensity of coherent X-ray scatter from the specimen, and $I_c(s)$ is the intensity of coherent X-ray scatter from the crystalline region.

Differentiation between crystalline and amorphous scattering in coherent scattering is possible by resolving the peak areas representative of each phase. This method is carried out over a range that includes the intense crystalline peaks and underlying amorphous peak. The diffraction pattern of PE can be resolved as three peaks. The two sharp peaks with (hkl) values (110) and (200) are representative of crystalline regions. The broad diffraction peak resulting from the amorphous regions is concealed under the crystalline peaks and is revealed as a shoulder on the low angle side of the (110) peak. The method resolving the peaks for a PE pattern is based on the symmetrical character of the peaks. The three peaks are corrected for atomic scattering factors, absorption, temperature and diffraction angle (Nichols 1954). The percentage of crystallinity is then expressed by the relation,

$$\% \text{ Crystallinity} = \frac{I_{110} + 1.43\, I_{200}}{0.69\, I_a + I_{110} + 1.43\, I_{200}} \times 100 \qquad (3.5.2)$$

where, I_a, I_{110}, I_{200} are the intensities, i.e. areas of the amorphous, (110) and (200) crystalline peaks, respectively and 0.69 and 1.43 are the correction factors.

A Rigaku Geigerflex D/Max X-ray Diffractometer was used in the transmission mode for obtaining the intensity versus 2θ scans for the virgin and annealed transmission cables for crystallinity calculations. The equipment was controlled using a panel equipped with microprocessors. A typical continuous scan was obtained with a scanning speed of 4 degree per minute in the scanning 2θ range of 10-40 °. The cathode voltage of the Cu tube was set at 35 kV and filament current at 40 mA. Data were recorded by an analog chart recorder coupled with the microprocessor operation unit.

In situ analysis of annealing was also studied by utilizing WAXS. For this purpose a high temperature X-ray cell (Figure 14) equipped with a constant temperature circulation bath, Haake F2, and additional electrical heating was used. Constant temperature bath oil was circulated through the inlets and outlets of the cell (1,2). Electrical heating was achieved with cartridge heaters (3) controlled by Omega 49 thermoregulators (4,5,6) and was applied to achieve rapid initial heating rates in order to prevent preannealing at temperatures lower than the desired annealing temperature. Similarly a second circulating bath was used for rapid cooling rates. A

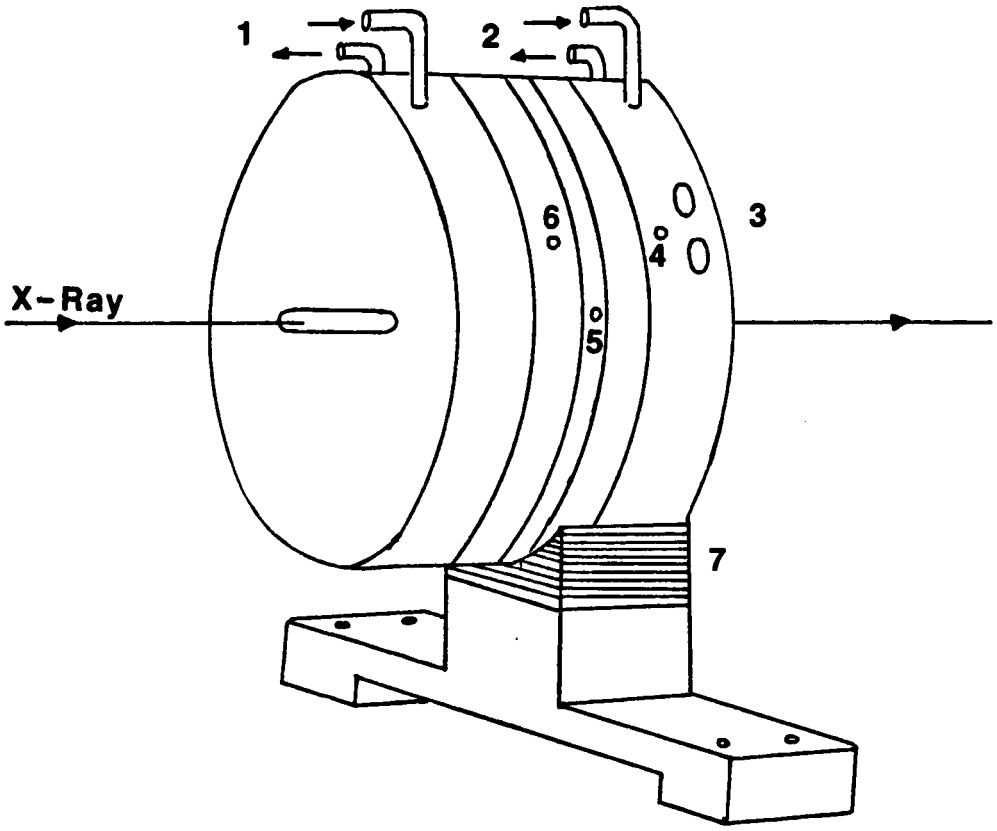

Figure 14 High temperature X-ray cell.

fiberglass block (7) was used as a separator between the diffractometer and the high temperature cell to prevent heat losses. Also, a plastic foam cover was used for isolating the cell from the atmosphere. The sample was kept between a pair of beryllium windows (8). This high temperature cell was mounted in the Rigaku X-ray Diffractometer system in the transmission mode.

Analogous to the light transmission studies, intensity versus 2θ plots were obtained while annealing the cable samples at a selected temperature. Also, percent crystallinities attained at some high temperatures were obtained by recording intensity versus 2θ plots analogous to the ambient study.

3.5.2. Small Angle X-Ray Studies

Small Angle X-Ray Scattering (SAXS) is used to study microscopic levels of structures represented by fluctuations in electron densities.

The NCSASR ten-meter SAXS apparatus at Oak Ridge National Laboratory (Figure 15), utilizes a 12 kW Rigaku-Denki rotating anode X-Ray generator. Monochromatization of the incident X-ray beam is achieved with a pyrolytic graphite single crystal to obtain copper Kα radiation with a wavelength of 0.154 nm. Beam collimation is accomplished through a pair of one mm^2 pinholes separated by 1.6 meters. A two dimensional position sensitive detector (2DPSD) with

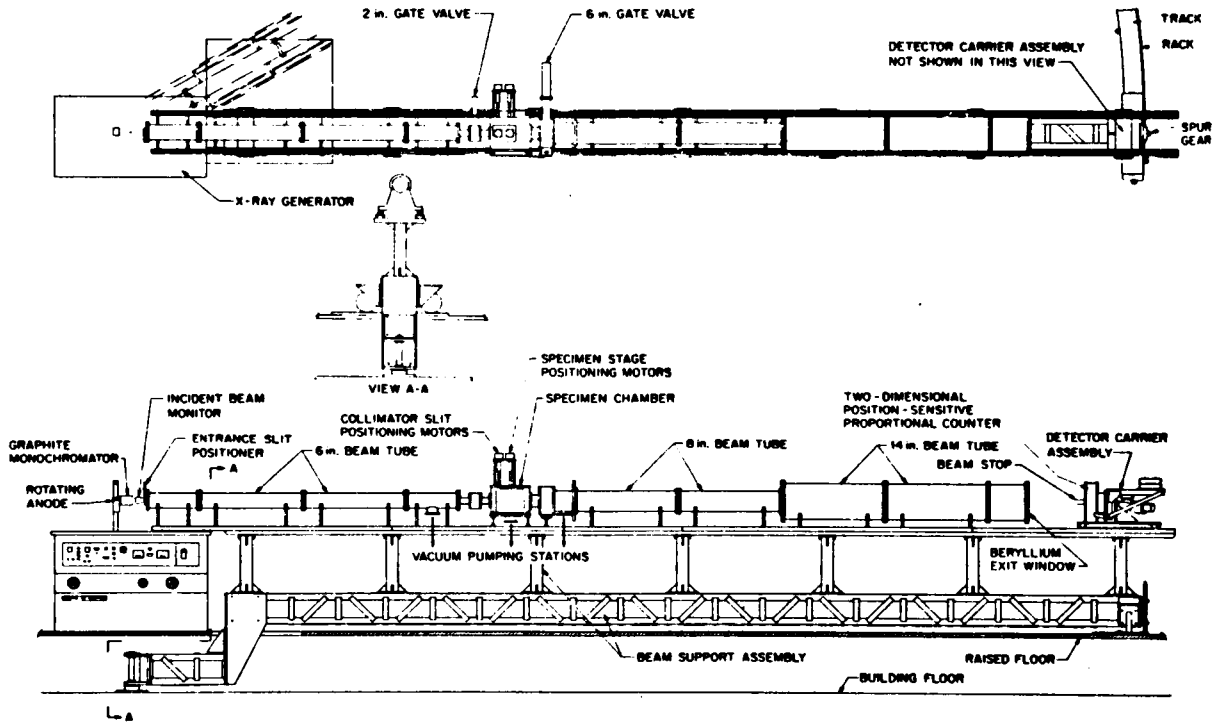

Figure 15 Schematic drawings of the ORNL ten meter SAXS spectrometer.

64 x 64 grid elements in a 20.7 x 20.7 cm area is used to measure the scattered intensity. The distance between sample holder and 2DPSD is variable in increments of one meter, from about one meter to about five meters, depending on the angular range of interest.

Scattered intensity is recorded by a Modcomp computer. The intensity data is corrected by subtracting background radiation and scattering and then normalized for detector sensitivity and transmission coefficient of the sample. Linearly averaged scattering intensity versus scattering angle plots by circumferential or angle averaging routines are also available in the data analysis software.

The sample chamber is evacuated to 3×10^{-5} torr and a sample holder disk that can hold up to ten samples is manipulated by the SAXS foreground program which automates the hardware. Before recording the scattering intensity contours of each sample, transmission coefficients of each sample are measured. The transmission coefficient is calculated using the following formula

$$T_m = \frac{I_{gc+s} - 0.7\ I_s}{I_{gc} - 0.7\ I_e} \qquad (3.5.3)$$

where T_m is the transmission coefficient of the sample, I_{gc} is the scattered intensity by glassy carbon, I_{gc+s} is

the scattered intensity by the glassy carbon and the sample I_s is the scattered intensity of the sample alone, I_e is the scattered intensity without any glassy carbon and sample, and 0.7 is the transmission coefficient of glassy carbon itself. The purpose of using glassy carbon is to profusely scatter the radiation away from the beamstop and increase the useful scattering intensity.

Average long periods of more populous crystals was found from the maximum of radial average intensity versus scattering vector plots. Scattering vector is given by the equation

$$K = (4\pi / \lambda)\ \theta \qquad (3.3.4)$$

where θ is the scattering angle λ is the wavelength of the X-ray source ($\lambda = 2d\theta$ for small scattering angles), and d is the characteristic dimension (for lamellar stacks this is the long period). By substituting for θ in Equation 3.5.4

$$d = 2\pi / K_{max} \qquad (3.3.5)$$

where K_{max} is the value of K at the maximum intensity.

3.6 Morphology Studies

Study of the bulk morphology of melt crystallized polymers has been made possible by introducing new techniques of sample preparation. Among these techniques, thin film preparation by microtomy has drawbacks such as poor contrast or deformation of true structures. Electron beam damage is best avoided by using the technique known as replication. In this technique, the topography of the internal or external surfaces of the bulk material is transferred to a thin film which can be studied in a transmission electron microscope (TEM). Major steps involved in this technique can be summarized as microtoming, etching, thin-film deposition (or carbon replication), isolation of thin replica film and finally TEM observation.

3.6.1 Microtoming

Although replicating fracture surfaces can be used to reveal the fine morphological details, this technique is susceptible to mechanical damage during fracture. Smooth surfaces obtained from microtoming are advantageous from the points of controlled replicate film deposition and its removal.

A modified American Optical Rotary Microtome Model 820 was used for preparing smooth surfaces. Cold stage

modification was used for minimizing mechanical damage during sectioning. With frequent addition of liquid nitrogen to the reservoirs attached to the sample holder and knife holder, temperatures around -45 ^{o}C were maintained during sectioning (Figure 16).

Mirror-like surfaces of the samples were produced by sectioning with glass blades prepared from 1 x ¼ x 12 " glass strips with the aid of special pliers. Figure 17 shows the geometry followed in blade cutting. Glass blades were carefully observed for the quality of their cutting edge in the optical microscope before use.

Both axial and radially cut slabs with 0.5 x 0.5 cm cross sections were microtomed. The 0.5 cm thick pieces having the microtomed smooth surface were cut and removed from the slab with a razor blade and finally etched chemically.

3.6.2. Etching

The etching technique used to reveal morphological entities is a method based on the greater chemical reactivity or solubility of less perfectly crystallized material and of amorphous parts of samples. By properly adjusting the etching conditions one can reveal the morphological details of a crystalline polymer sample by progressive removal of the amorphous or poorly crystallized material.

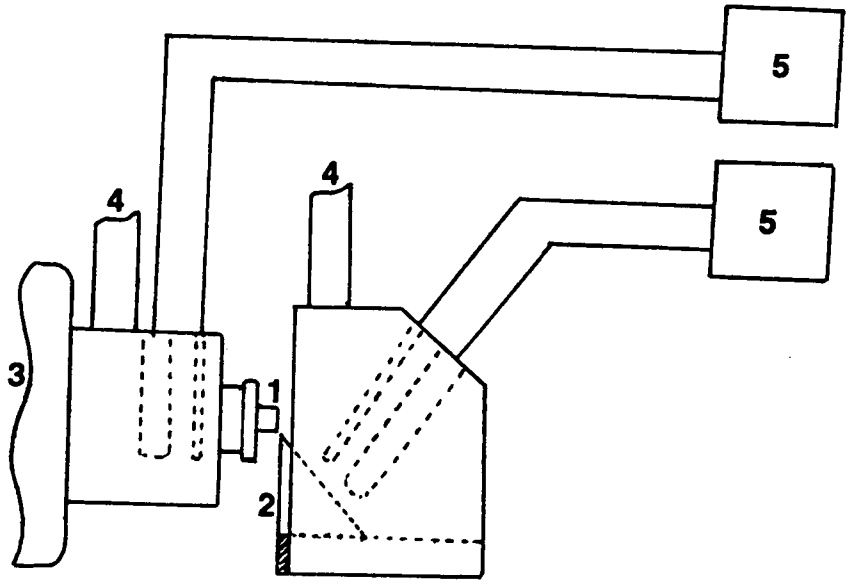

Figure 16 Schematic representation of the rotary microtome with cold stage modification.

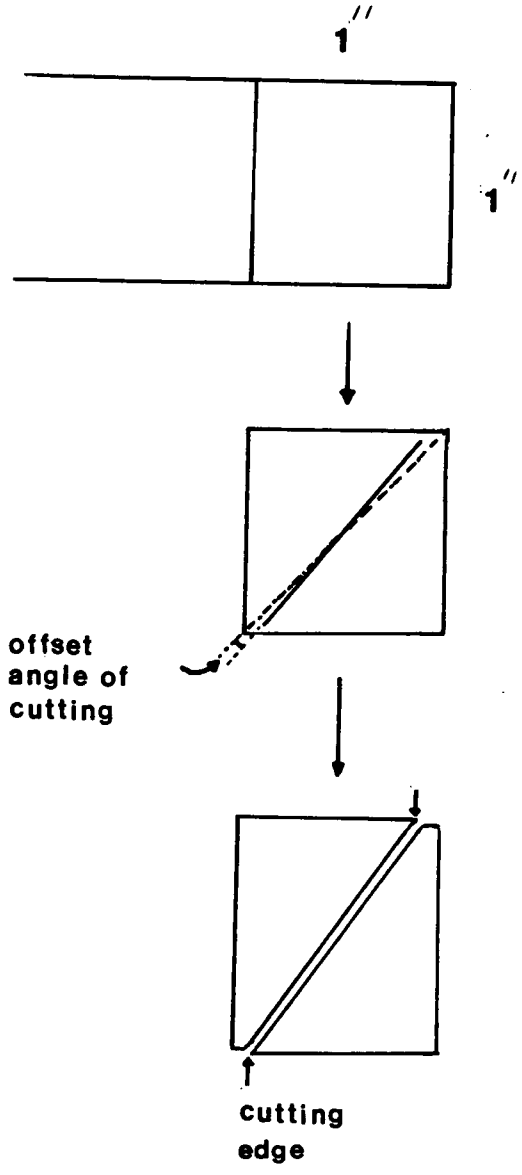

Figure 17 Schematic of glass blade preparation.

A permanganic etchant developed by Olley et al. (1979) for crystalline polyolefins and optimized for cross-linked PE systems (Naylor and Phillips 1983, Phillips and Gohil 1986) by adjusting the concentration and etching times was used.

Permanganic acid etchant was prepared by slow addition of potassium permanganate, $KMnO_4$, to concentrated sulfuric acid in a conical flask with rapid magnetic agitation. A dark green colored solution was obtained after dissolving the permanganate. The concentration of permanganic acid used ranged from 0.2 % to 0.8 % (w/w) potassium permanganate in the concentrated acid.

Cable samples prepared by microtoming were placed in 10 ml of the reagent in test tubes and the test tubes placed in an ultrasonic bath for etching. All etchings were carried out at room temperature with the help of water cooling coils which were necessary to limit the warming of the sonic bath water by the ultrasonic vibrations. A typical etching procedure for XLPE cables was etching twice for 30 minutes with 2 % (w/v) permanganic reagent. After etching, the acid etchant was decanted into running water and the samples transferred to tubes containing dilute sulfuric acid prepared from 2 parts of concentrated H_2SO_4 and 7 parts distilled water. This acid solution had been precooled to almost to its freezing point before using in order to prevent the heat of dilution of the permanganic acid melting

fine surface microstructures. After a 1.5 minute treatment in the dilute acid, samples were transferred to a 30 % solution of hydrogen peroxide in H_2O and kept for 1.5 minutes. Then the samples were washed in the tubes containing distilled water for 1.5 minutes and, finally, they were transferred to acetone for removing the water from the fine surface topography. After 1.5 minutes of acetone treatment, samples were mounted on glass slides and dried in a vacuum oven for two hours. Extra caution was taken to prevent any contamination from the atmosphere before coating the samples in a carbon vacuum evaporator.

3.6.3. Replication

A Danton DV 515 Vacuum evaporator was used for carbon coating and chromium shadowing. A film of carbon of the order of 200 A forms a replica of the specimen surface. Carbon replication was carried out for the etched specimen surface by evaporating carbon. A special fixture was used having a fixed 1/8" diameter carbon rod with a flat end, and a spring loaded moving arm holding the carbon with a section reduced to 0.04" diameter. The sample to carbon source distance was adjusted to 10 cm with a proper modification to prevent overheating of the sample surface during coating. A vacuum of about 1.5×10^{-5} torr was attained before carbon coating. The carbon rod was first degassed at red heat with a power setting of 20-30 amperes for 5 to 10 seconds.

Evaporation of carbon starts at 34-36 amperes and with a careful power adjustment evaporation was continued with visible sparkling. Samples were then shadowed with chromium from an angle of about 20°. Removal of the replica was achieved by deposition of a supporting polyacrylic acid (PAA) layer on the replica. Adequate deposition of the PAA was obtained by dropwise addition of 0.2% (w/w) PAA solution following each drying of the previous PAA deposition. The PAA holding the carbon replica was removed with the help of sharp tipped tweezers and then floated on distilled water with the PAA layer facing downwards. This way water soluble PAA was removed from the replica leaving the carbon-chromium replica floating on the water. Finally, the replicas were transferred to 400 mesh 3 mm diameter electron microscope grids for TEM work. A schematic representation of the replication process is given in Figure 18.

3.6.4. Microscopy

JEOL TEM 200 CX Scanning-Transmission Electron Microscope (STEM) and Phillips 300 TEM were used to study the prepared carbon replicas. The operating voltage was kept at 80 kV in all experiments.

AMR 900 Scanning Electron Microscope was used to study the surface topography of some cable samples.

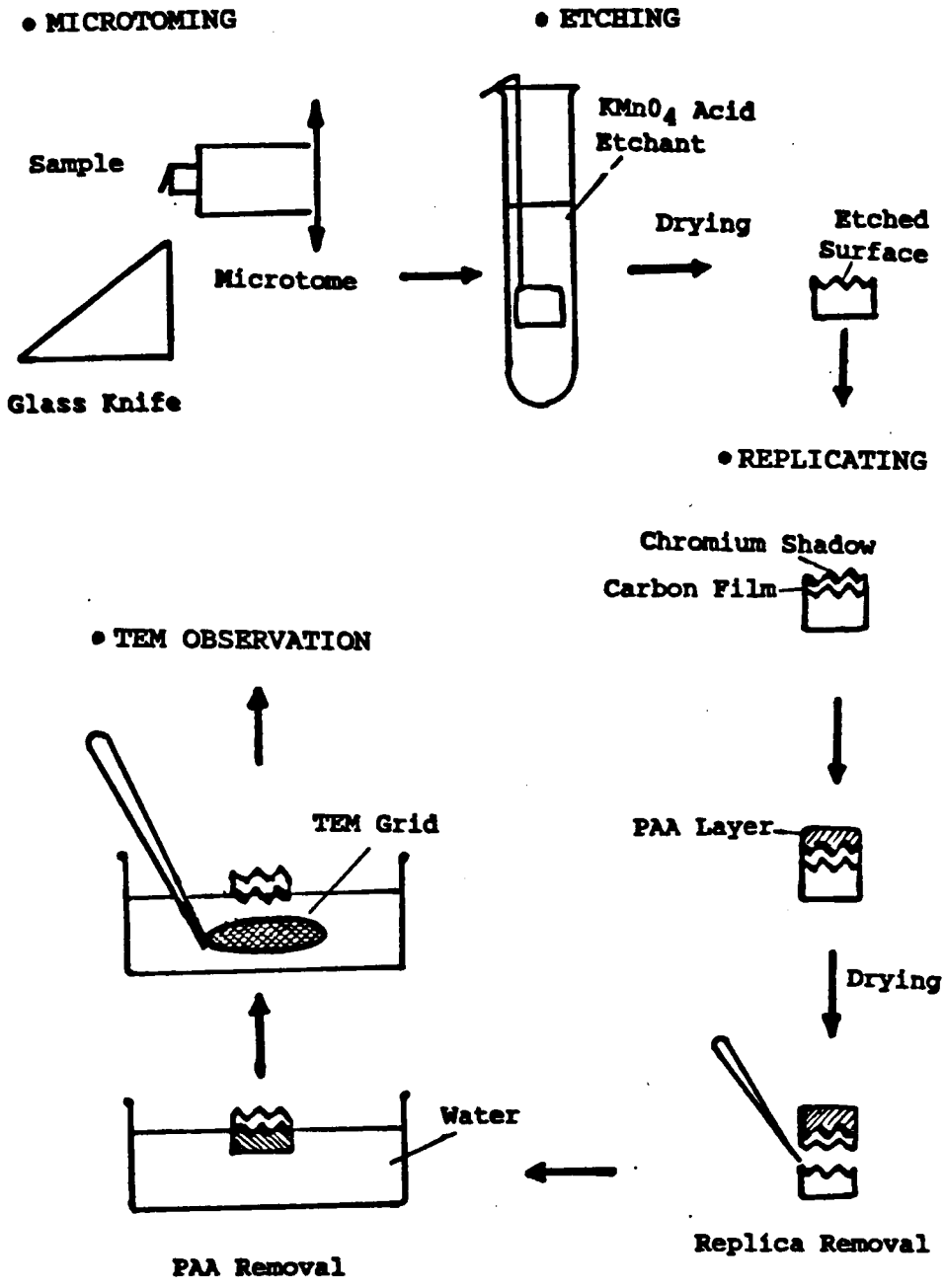

Figure 18 Diagram of the steps involved in morphological study using TEM.

A Reichert Neovar Pol polarizing optical microscope with a magnification range from 40 to 630 was used to study birefringent morphological patterns.

4. RESULTS

4.1 Crosslinking of LDPE

The MWD of the original Union Carbide HFDE 4201 LDPE was altered by adding certain amounts of low molecular weight polymer obtained from the extraction of its crosslinked sample. Fully cured LDPE with 2 % DCP results in about 17 % extractables with a Mv of 10,280. Uncrosslinked LDPE has Mv=32,000. After adding certain amounts of extractables and DCP to the uncrosslinked resin, as was explained in section 3.1.2, a cured blend resulted in different levels of extractables and swelling ratios depending on the amount of extractables and DCP added. Additional extractables were added by taking the weight of the original resin as a basis and adding DCP on the basis of the total amount of the blend. The total amounts of extractables available in crosslinked samples were calculated using the following formula,

$$\text{Calculated Percent Extractables} = \frac{W_B \times F_{os} + W_B \times F_{es}}{W_B + W_B \times F_{es}} \qquad (4.1.1)$$

where W_B is the amount of original LDPE, F_{os} is the fraction of sol available from crosslinked LDPE having 2 % DCP, and F_{es} is the fraction of sol added on the basis of original LDPE.

Equation 4.2.1 in its very simplified form can be given for original XLPE with extractables F_{os} = 17 % as,

$$\text{Calculated Percent Extractables} = \frac{0.17 + F_{es}}{1 + F_{es}} \times 100 \qquad (4.1.2)$$

Figure 19 shows a 1:1 relationship between experimental and calculated percent extractables for the crosslinked polyethylenes obtained from the original base material, and for the material with 20 % and 40 % additional extractables present, all containing 2 % DCP as crosslinking agent. Percent extractables versus swelling ratio for XLPE's cured with 2 % DCP is shown in Figure 20. It is clear from Figure 20 that as the percent extractables increases so does the swelling ratio, indicating that, depending on the MWD of the material, different crosslink densities can be obtained for the same DCP loading.

4.2 Original Cables

4.2.1. Extraction Studies

Extraction studies were carried out to determine the amount of uncrosslinked material present in XLPE cables as a function of radial position. Percent extractables determined from the weight loss of the samples after extraction in refluxing xylene as a function of radial

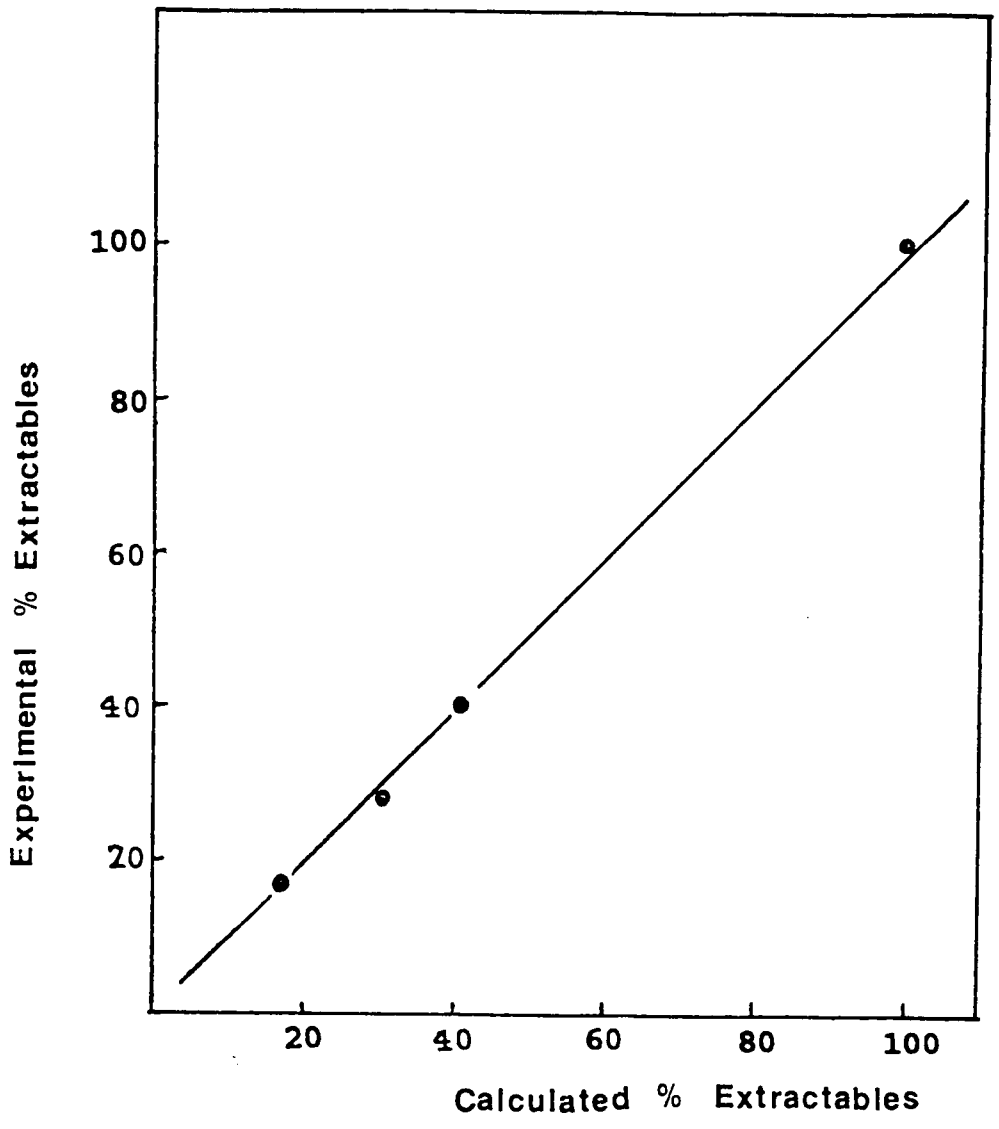

Figure 19 Experimental percent extractables versus calculated percent extractables for XLPEs prepared from the blends of 2 % DCP and LDPEs with different MWD.

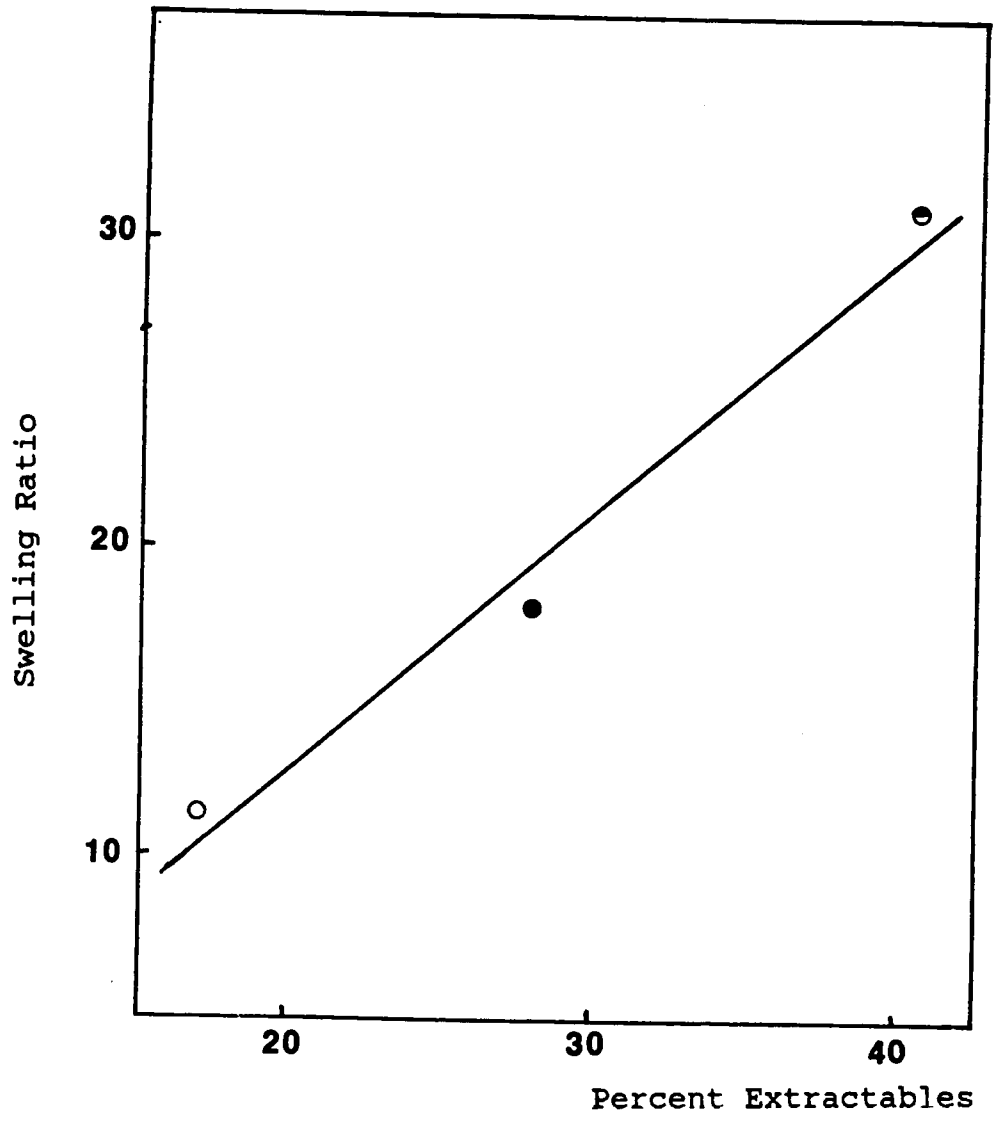

Figure 20 Swelling ratio versus percent extractables for XLPEs prepared from the blends of 2 % DCP with (O) LDPE (Union Carbide HFDE 4201), (●) LDPE + 20 % sol and (⊖) LDPE + 40 % sol.

position for cable A1 are presented in Figure 21. Since cable A1 has a variation in insulator thickness, extraction analyses were carried out for three different regions labelled M, L and R. Region M is the narrowest radial section and L and R are the regions 120° away from region M. As may be seen in Figure 21, all three regions show the same trend with scatter in the percent extractables of 0.2 to 0.9 %. For these three regions, the first five outermost sections have almost the same percent of extractables, averaging 15.5 %, while the remaining three eighths of radial section comprising the innermost layers, show an increase in percent extractables reaching 28 %. In Figure 22 data for radial section R, being representative of Cable A1, is plotted along with the percent extractables data of cable A2 for comparison. 230 kV Cable A2 was also cured in polyethylene glycol medium but has a thicker insulation wall than cable A1 (Table 1, p 62). A similar trend in percent extractable variation with radial position was observed for cable A2 having different levels of extractables for the corresponding radial sections. In general, cable A2 had comparably lower extractable values than cable A1. While the four outermost sections have extractable levels of about 14 %, the level increases in the inner sections and reaches 23 % at the innermost section.

Figure 23 presents the percent of extractables versus radial position for the steam cured cables made by

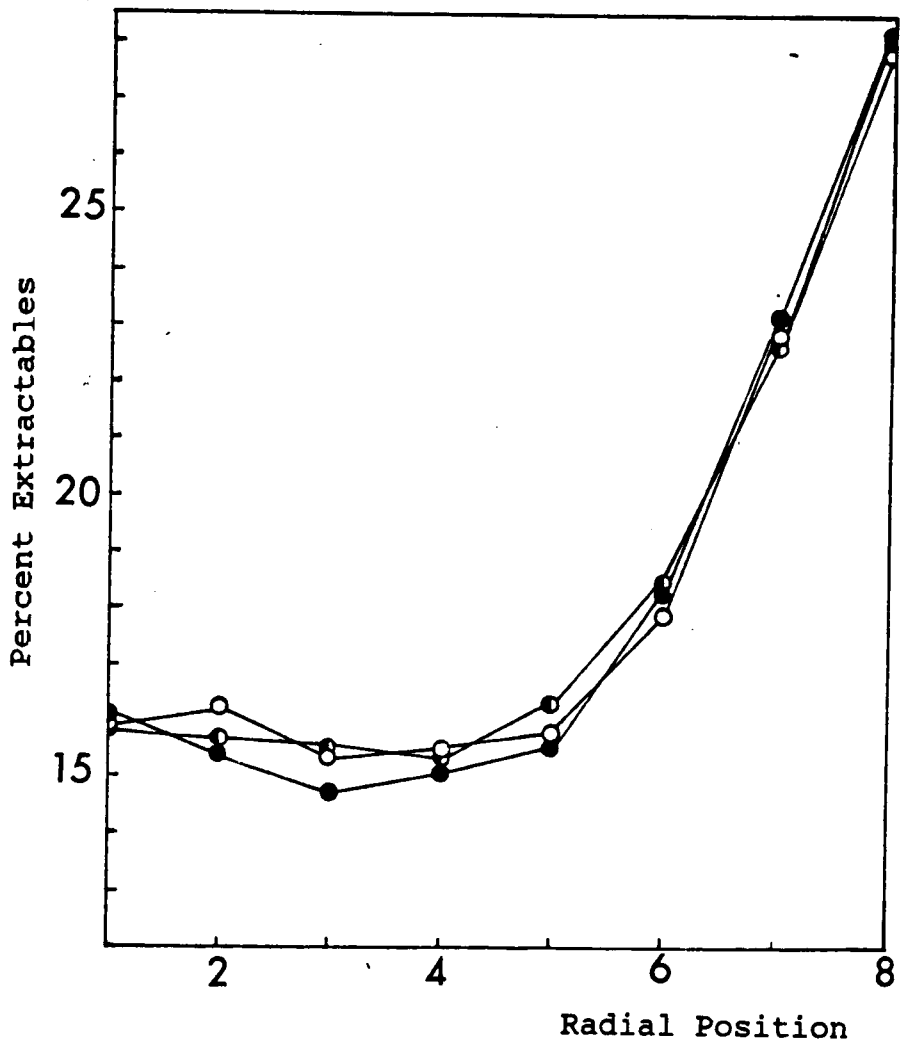

Figure 21 Percent extractables versus radial position for the radial directions (O) M, (◑) L and (●) R of cable A1.

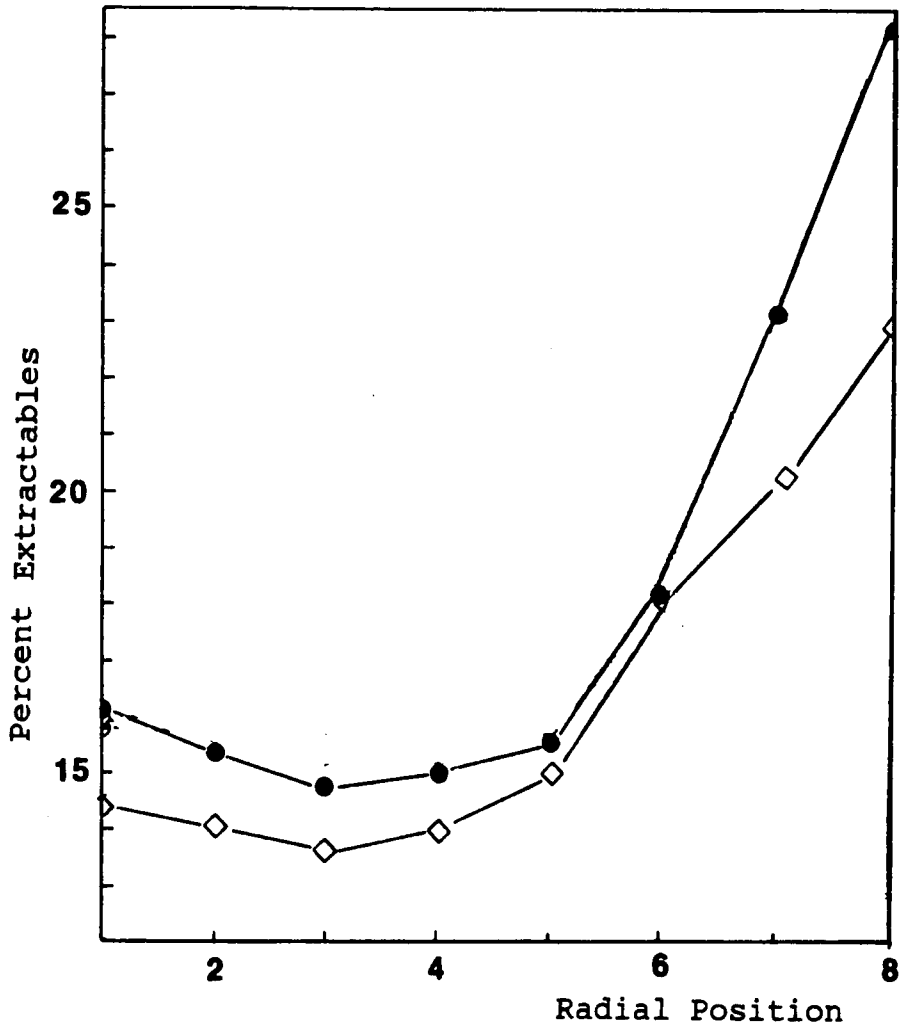

Figure 22 Percent extractables versus radial position for PEG cured cables (●) A1 and (◇) A2.

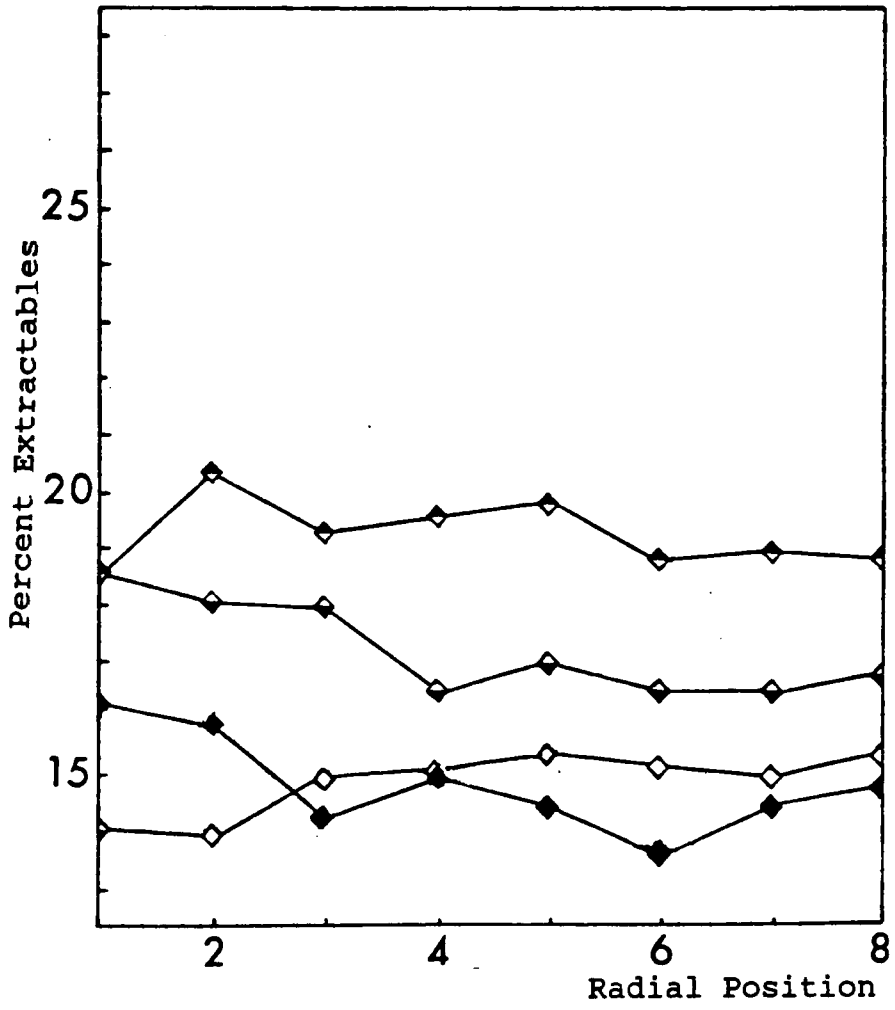

Figure 23 Percent extractables versus radial position for steam cured cables (◇) B1, (◈) B2, (◆) B3 and (◈) B4.

Pirelli. All of the steam cured cables, except cable B4, have a 650 mil insulation wall thickness. As can be seen from Figure 23 all the cables have a uniform distribution of percent extractables throughout their radial direction. Cables B1 and B2, having identical insulator and wall thicknesses, have different levels of extractables throughout their radial sections. While cable B2 has about 20 % extractables, the value is about 15 % for cable B1. Cables B3 and B4 with different insulation thicknesses and with the same conductor thickness showed a relatively different level of extractables. Cable B4 was found to have about 17.5 % extractables while B3 had about 15 %. Percent extractables as a function of radial position for dry cured cable C1 and steam cured cable E1 are presented in Figure 24 along with the data for cable A1. Cable C1 had extractable levels comparable with those of cable E1, the level of extractables remaining almost constant throughout the radial direction.

The radial distributions of extractable materials for the XLPE distribution cable (D8) was determined in a similar manner except that the radial direction was divided into four equal sections. In general, the amount of extractables recorded for this distribution cable was found to be higher than for the transmission cables. The average amount of extractables for original distribution cable D8 was found to be 21.9 %.

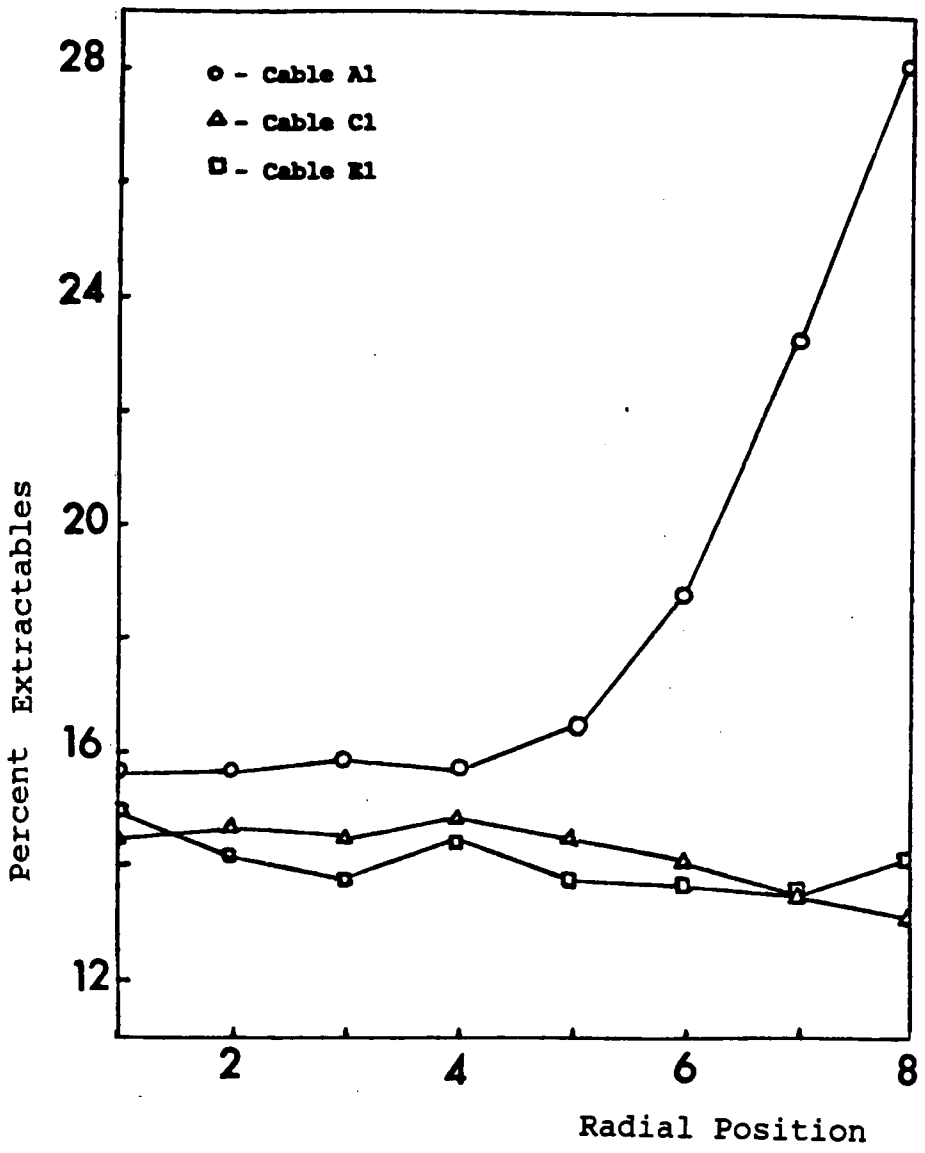

Figure 24 Percent extractables versus radial position for cables (O) A1, (Δ) C1 and (□) E1.

4.2.2. Crosslink Density Determination

Crosslink density determination of the radial sections of the cables was achieved by utilizing equilibrium swelling in xylene at 110 ^{o}C. After establishing equilibrium, swelling ratios were determined using the formula given in section 3.2.2. Figure 25 presents the swelling ratios versus radial position for cables A1, C1, E1 and A2. In swelling experiments radial sections were divided into four equal sections. Thus, each section in the swelling experiments corresponds to two of the sections used in percent extractables analysis. As can be seen from Figure 25, the change in swelling ratio as a function of radial position follows the trend observed for percent extractables. Figure 26 shows the relationship between percent extractables and swelling ratio. Except for the data scatter observed around 15.5 % extractables, a linear relationship was observed. The crosslink densities of the radial sections were calculated from the equilibrium swelling data using the Flory-Rehner formula given in section 3.2.2. Table 4 presents the calculated crosslink densities and molecular weights between crosslinks (M_c) for cables A1, C1, and E1. The crosslink density of the innermost layer of Cable A1 was found to be about half that of the crosslink density of the outermost layer. An almost constant crosslink density distribution was observed for

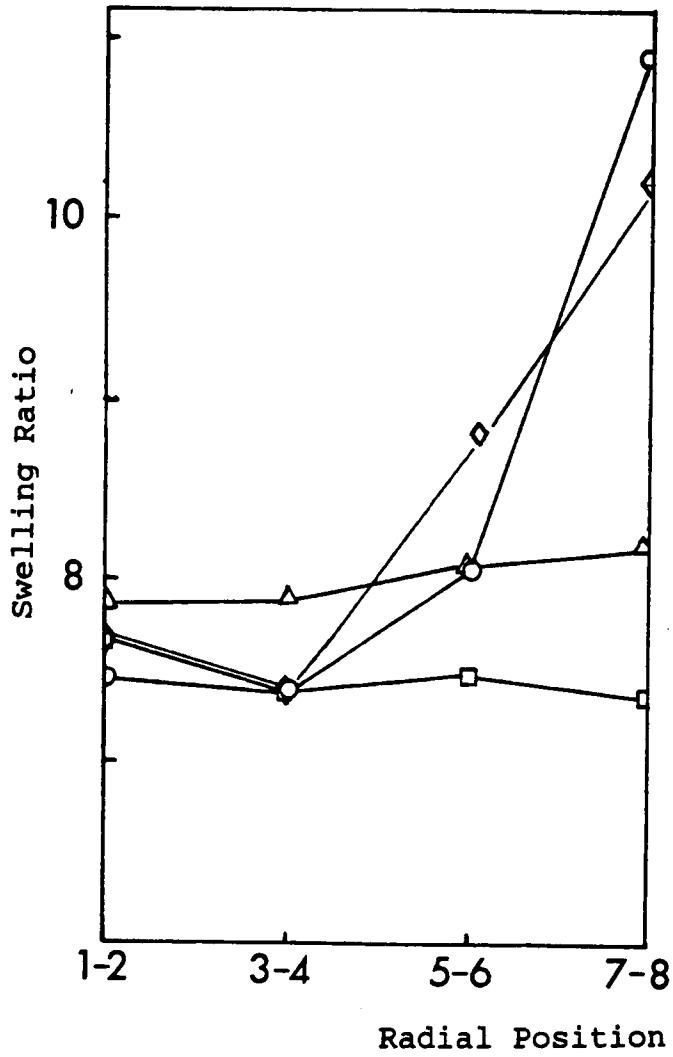

Figure 25 Swelling ratio versus radial position for cables (O) A1, (◇) A2, (△) C1 and (□) E1.

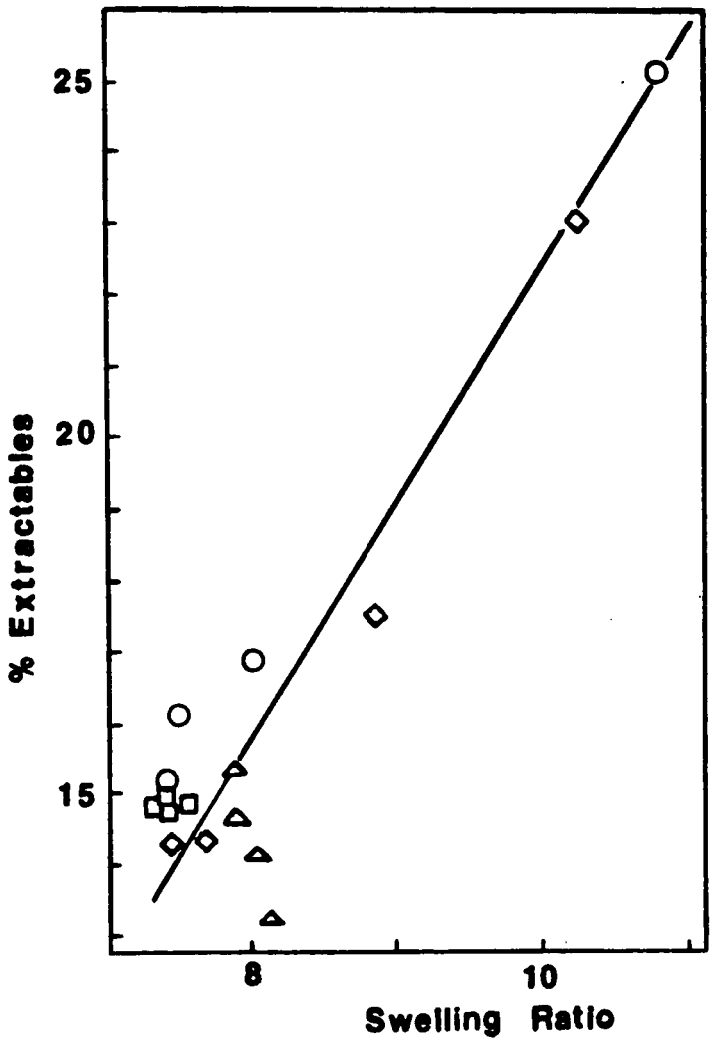

Figure 26 Percent extractables versus swelling ratio for cables (O) A1, (◇) A2, (△) C1 and (□) E1.

Table 4 Crosslink density and molecular weight between crosslinks data for cables A1, C1 and E1.

Radial Position	Cable A1		Cable C1		Cable E1	
	M_c	$d_c x 10^5$	M_c	$d_c x 10^5$	M_c	$d_c x 10^5$
1-2	8056	12.3	8284	12.1	8772	11.4
3-4	8169	12.2	9167	10.9	8284	12.1
5-6	9445	10.6	9736	10.3	7945	12.6
7-8	15213	6.6	10200	9.8	7812	12.8

cables C1 and E1. Cable C1 had a crosslink density between 9.8 and 12.1×10^{-5}. Cable E1 was found to have a more even distribution of crosslinks throughout its radial direction than the other cables (Table 4).

4.2.3. Molecular Weight Studies of Extractables

Viscosity average molecular weights, M_v, of the extractables obtained from cables A1, C1, and E1 were found from the intrinsic viscosity [η] of their solutions measured in xylene at 75 °C. These intrinsic viscosity values were converted to viscosity average molecular weights using the Mark-Howink equation (Equation 3.2.8). Table 5 presents the viscosity data obtained for cables A1, C1 and E1 and for the sol fraction obtained from the laboratory crosslinked PE. While extractables from the innermost and outermost layers of cable A1 were studied for their M_v's, average M_v values were obtained for cables C1 and E1 for the extractables obtained from their entire radial sections.

The molecular weight, MW, and molecular weight distribution, MWD, data of the extractables from cable A1 were obtained from a GPC study carried out in the Union Carbide Laboratories (Table 6). Polydispersity, M_w/M_n, for extractables obtained from the outer radial section of cable A1 was found to be lower than the value obtained for the innermost radial section. The trend observed for M_v values obtained from viscosity studies for the inner and outer

Table 5 Viscosity average molecular weight of extractables from cables A1, E1 and C1

	Cable A1-1	Cable A1-8	Cable E1	Cable C1	Sol from 2% XLPE
$[\eta]$ =	0.0398	0.0427	0.0377	0.0355	0.0474
$M_v x10^{-3}$=	8.316	9.298	7.630	6.936	10.974

Table 6 GPC results for extractables from different sections of cable A1

Cable	$M_n x10^{-3}$	$M_w x10^{-3}$	M_w/M_n
A1-1	7.99	26.2	3.28
A1-4	7.85	28.1	3.60
A1-8	8.53	31.7	3.72

layers of cable A1 was observed to be similar to the trend in the M_n values obtained from GPC. MW and MWD data for the mid-section of cable A1 were also obtained. As can be seen from Table 6 and Figure 27 the M_n value for the mid-section, cable A1-4, is slightly lower than the value obtained for the outer radial section.

The MWD of the Union Carbide HFDE 4201 low density PE is given in Figure 28. M_n for this material is 20,600 and the polydispersity is 6.4. The GPC data were obtained at 140 ^oC in trichlorobenzene. M_v of the extractables obtained from the crosslinked version of HFDE 4201 LDPE containing 2 % DCP was found to be 10,280.

4.2.4. Spectroscopic Studies

100 micron thick microtomed slices obtained from the outer and inner layers of the original cables were studied for their microstructural chemistry. Analyses of FTIR spectra were carried out in two regions, namely 2000-1500 cm^{-1} and 1000-800 cm^{-1}, in order to obtain information on the carbonyl and olefinic unsaturation groups, respectively. Figures 29 and 30 are the spectra showing these regions for the inner and outer layers of cables A1, C1, and E1.

Thickness corrected absorption values for carbonyl, -C=O, and three types of unsaturation, namely trans-vinylene ($R_1CH = CHR_2$), vinyl ($RCH = CH_2$) and

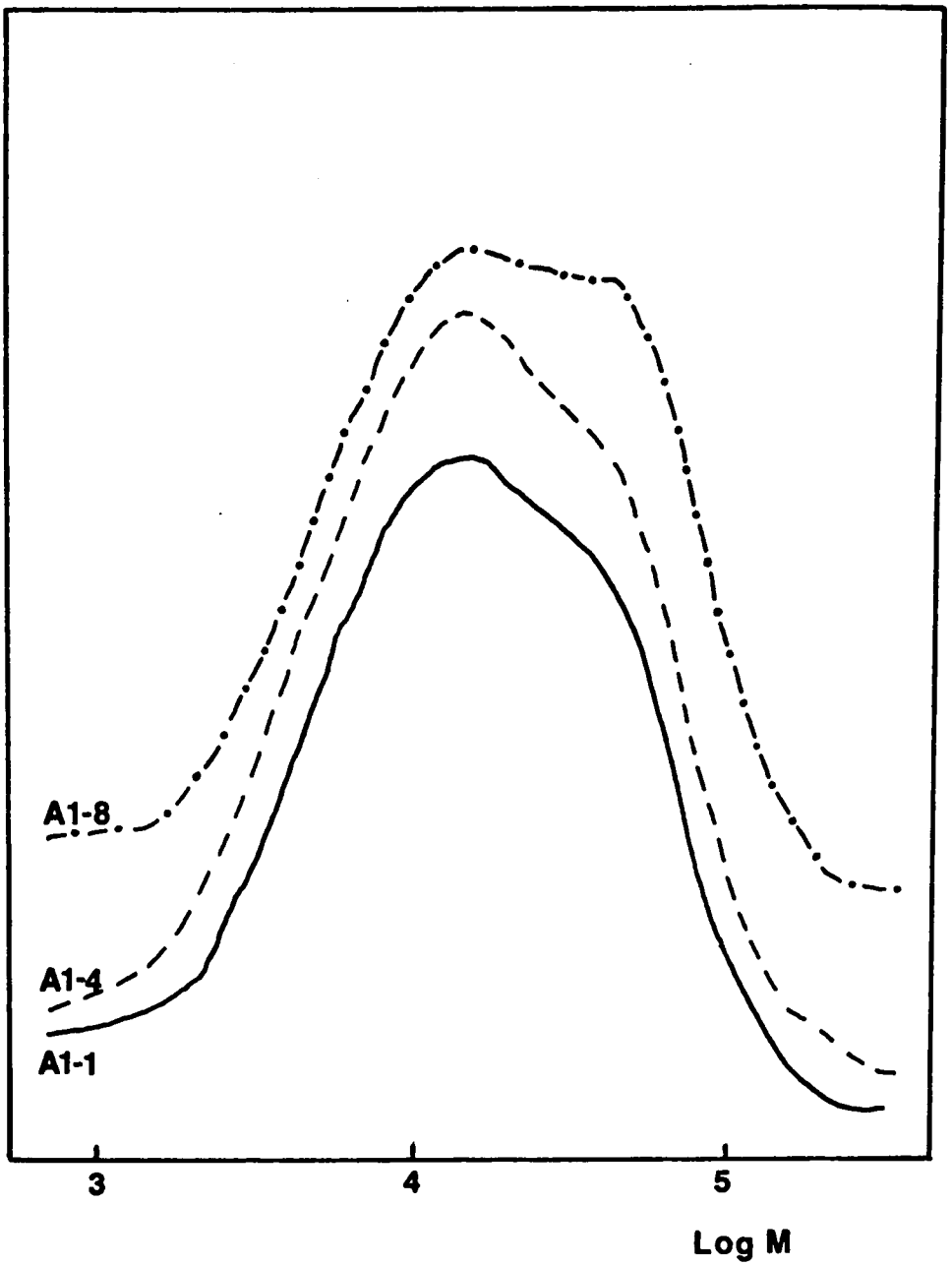

Figure 27 Molecular weight distributions for the extractables obtained from the indicated radial positions of cable A1.

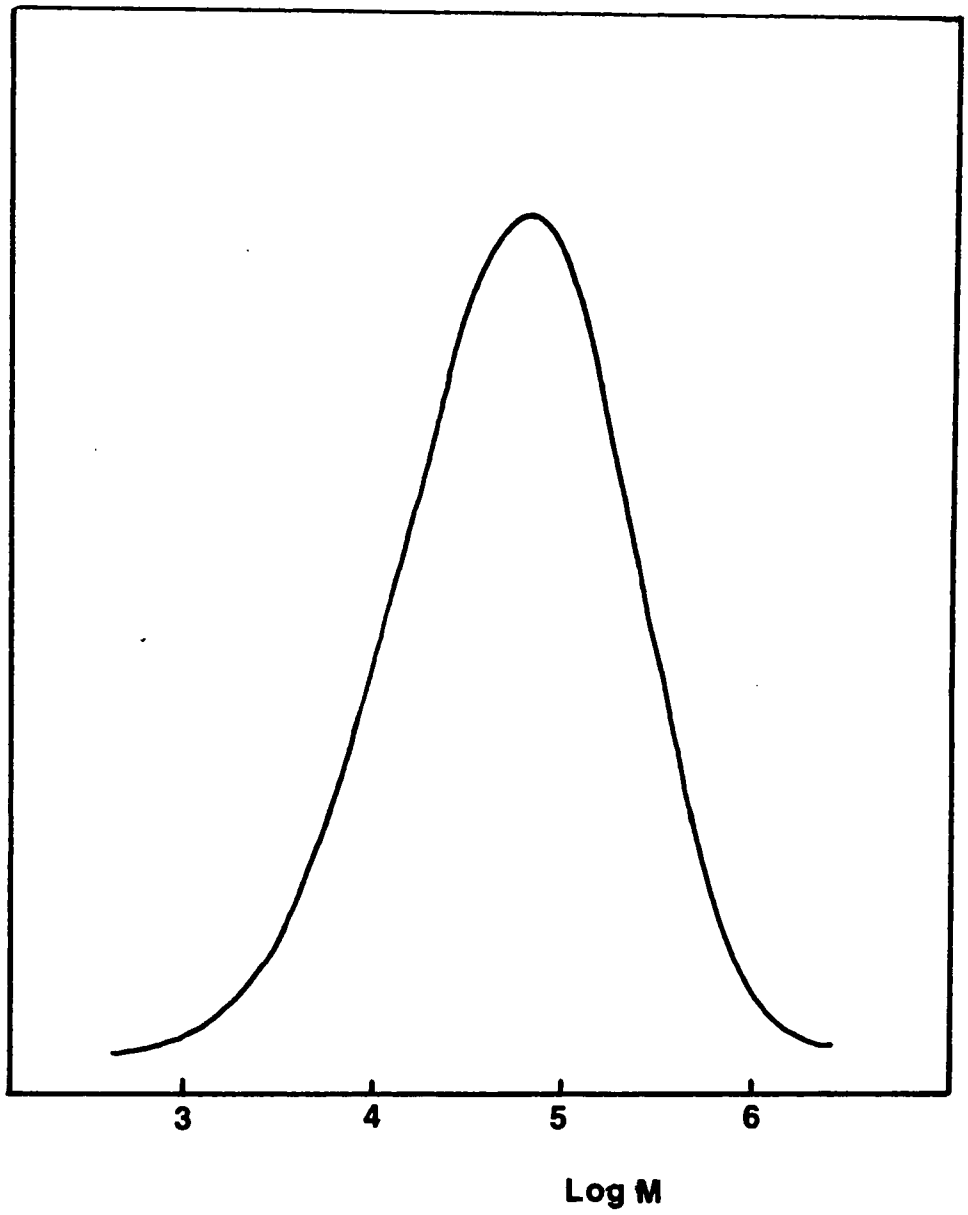

Figure 28 Molecular weight distributions for the uncrosslinked Union Carbide HFDE 4201 LDPE.

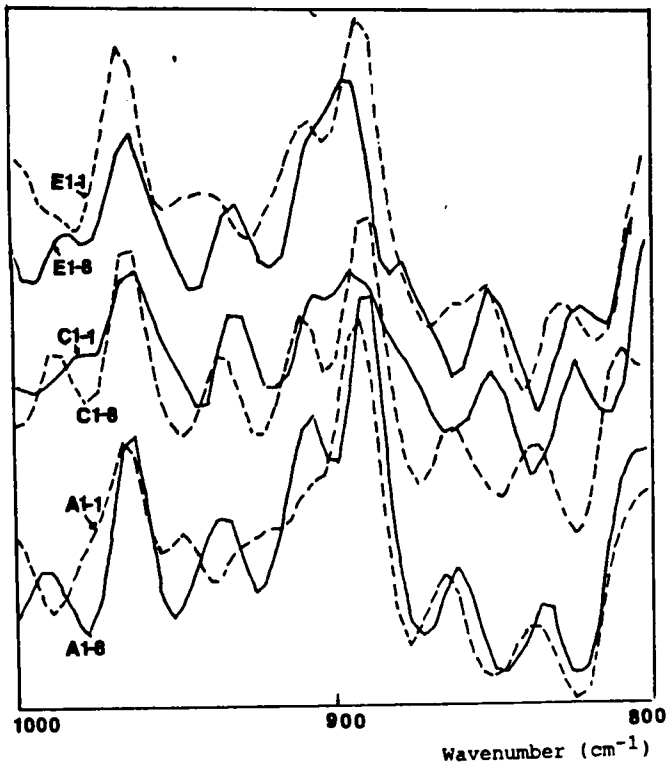

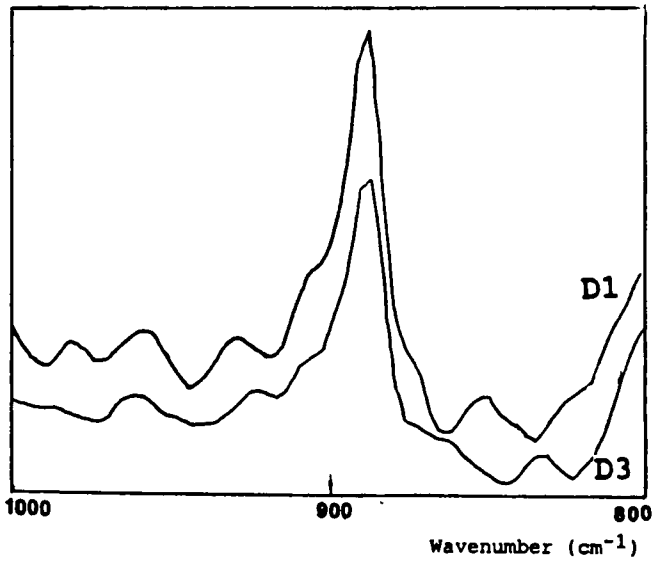

Figure 29 FTIR spectra of HV cables in the 800-1000 cm^{-1} region.

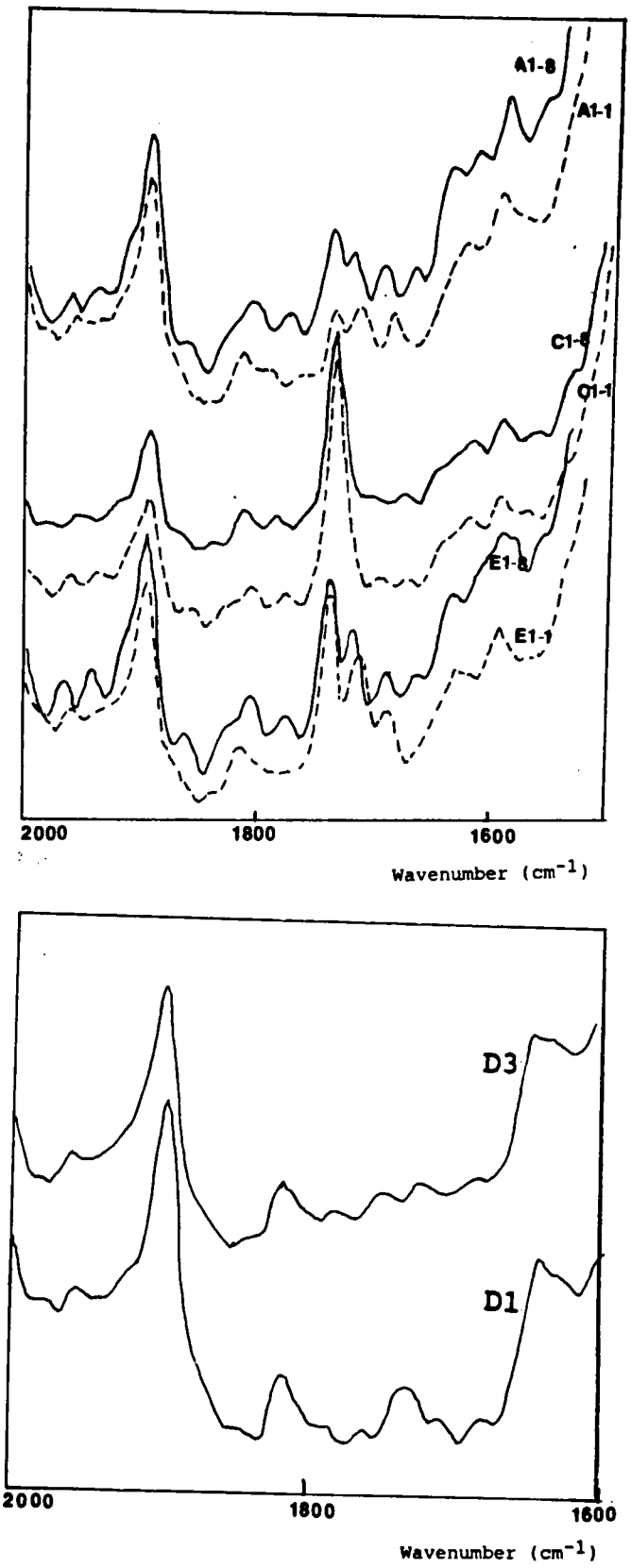

Figure 30 FTIR spectra of HV cables in the 1600-2000 cm^{-1} region.

vinylidene ($R_1R_2C = CH_2$) are given in Table 7. Carbonyl absorption for both layers of cable C1 was found to be comparably higher than in the other cables. Vinylidene absorption was found to be highest for radial sections of cable A1. The inner sections of cables C1 and E1 had relatively lower vinylidene absorptions than the other cables. Trans-vinylene and vinyl unsaturation were recorded in the range $1.25x10^{-2}$ to $1.99x10^{-2}$ a.u./mm for all the cables.

Similar analyses were carried out for the distribution cables. FTIR spectra from original LDPE distribution cables D1 and D3 along with those for the transmission cables are shown in Figures 29 and 30. As is given in Table 7, in general, carbonyl absorption levels for distribution cables, being in the range 0.7 to $1.13x10^{-2}$ a.u./mm, were found to be relatively lower than the values, $(0.95-9.61)x10^{-2}$ obtained for transmission cables. Similarly, lower levels of trans vinylene absorptions for distribution cables were obtained compared to transmission cables. On the other hand, slightly higher vinylene absorption for distribution cables, $(3.45-4.0)x10^{-2}$ a.u./mm, were obtained compared to $(1.63-3.12)x10^{-2}$ a.u./mm of transmission cables. Vinyl absorptions for both cables were found to be comparable. This evidence shows that the starting microstructure of LDPE insulation differs from that

Table 7 FTIR data of the indicated original distribution and transmission cables

Cable	ABSORBANCE (a.u./mm)x10^{-2}			
	Carbonyl	Trans Vinylene	Vinyl	Vinylidene
A1-1	0.95	1.70	1.30	3.17
A1-8	1.35	1.86	1.89	3.12
C1-1	7.59	1.90	1.40	2.70
C1-8	9.61	1.60	1.25	1.63
E1-1	2.59	1.97	1.34	2.85
E1-8	1.27	1.77	1.77	1.97
D1	0.70	0.63	1.60	4.90
D3	0.27	0.35	1.17	3.49

of XLPE insulation in terms of both unsaturation and carbonyl levels.

4.2.5. DSC Studies

Thermal analyses of cables were carried out using a Perkin-Elmer DSC-II and a Perkin-Elmer DSC-7 both having basically the same calorimetric capabilities. Unless otherwise stated the heating rate was kept at 10 deg/min.

Melting endotherms of radial sections taken from cables A1, C1 and E1 are shown in Figures 31-34. Cable A1 with variable insulation thickness was studied in two regions. These regions are the narrowest and the broadest regions of the insulation wall and they are 180 degree apart from each other. DSC endotherms for eight radial sections for the narrow (Figure 31) and for the broad regions (Figure 32) are analyzed for their melting temperatures, T_m, return to the base line temperatures, T_{rb}, and heat of fusion, ΔH_f values. Similar analyses were carried out for cables C1 (Figure 33) and E1 Figure 34. Figure 35 presents the data for the broad and narrow regions of cable A1 along with the values obtained for cables C1 and E1. Melting endotherms from the narrow and broad regions were found to be essentially the same. In general, the difference between the T_m s of the outermost and innermost layers of the two regions was found to be about three degrees. A similar comparison involving T_{rb} values shows about a two degree

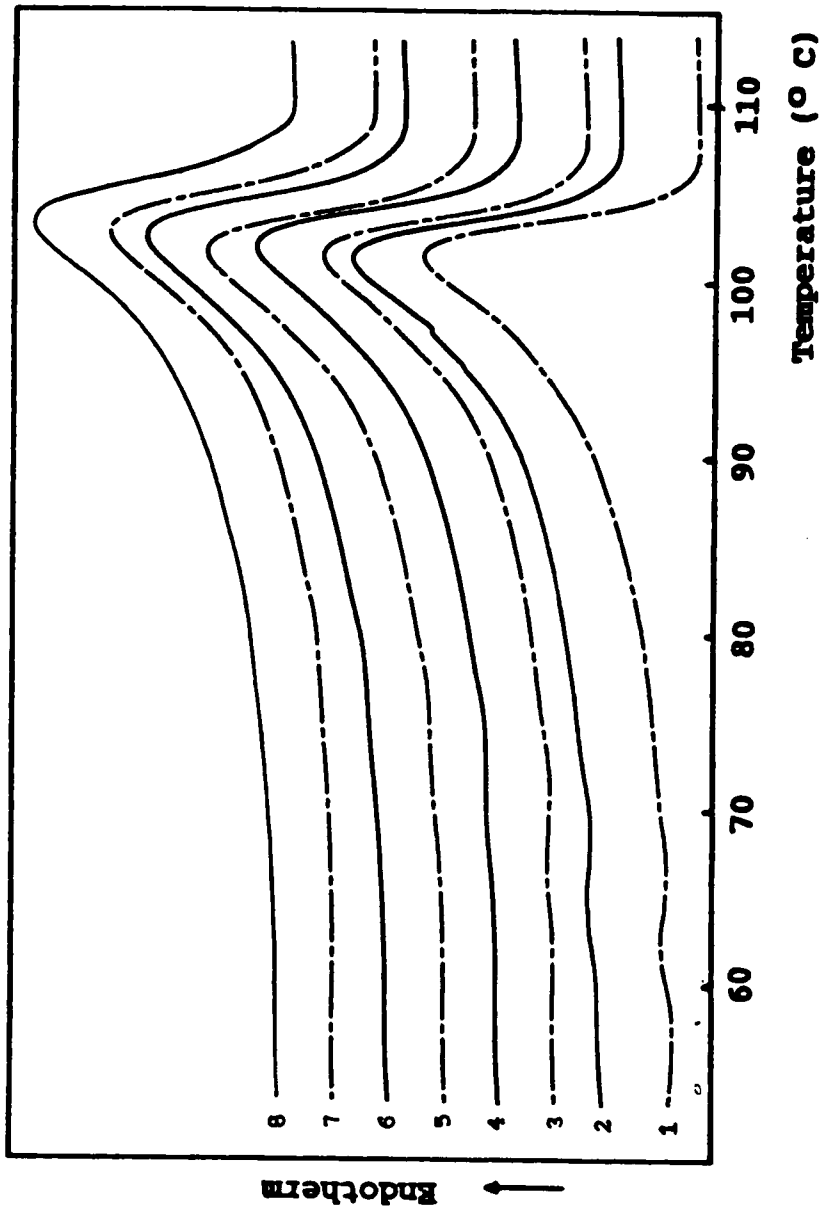

Figure 31 DSC thermograms obtained from the indicated radial positions of the narrow radial section of cable A1.

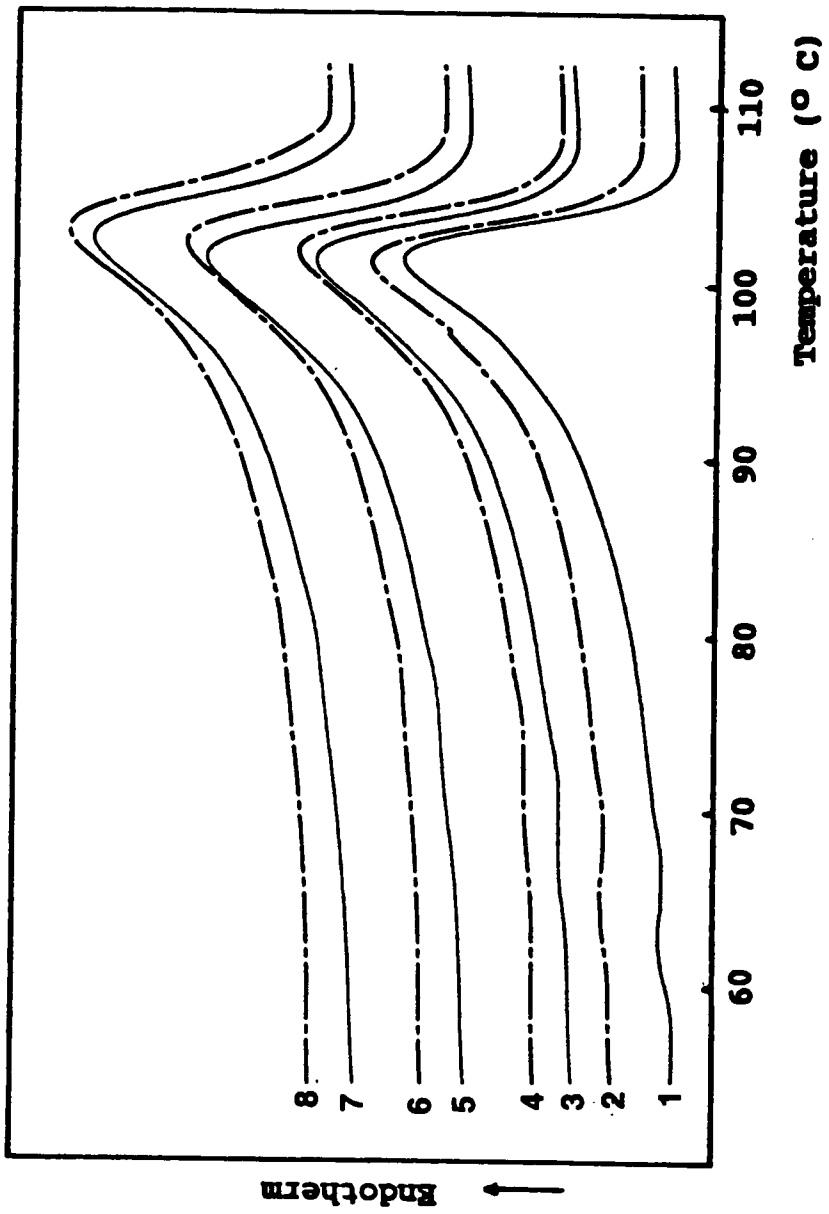

Figure 32 DSC thermograms obtained from the indicated radial positions of the wide radial section of cable A1.

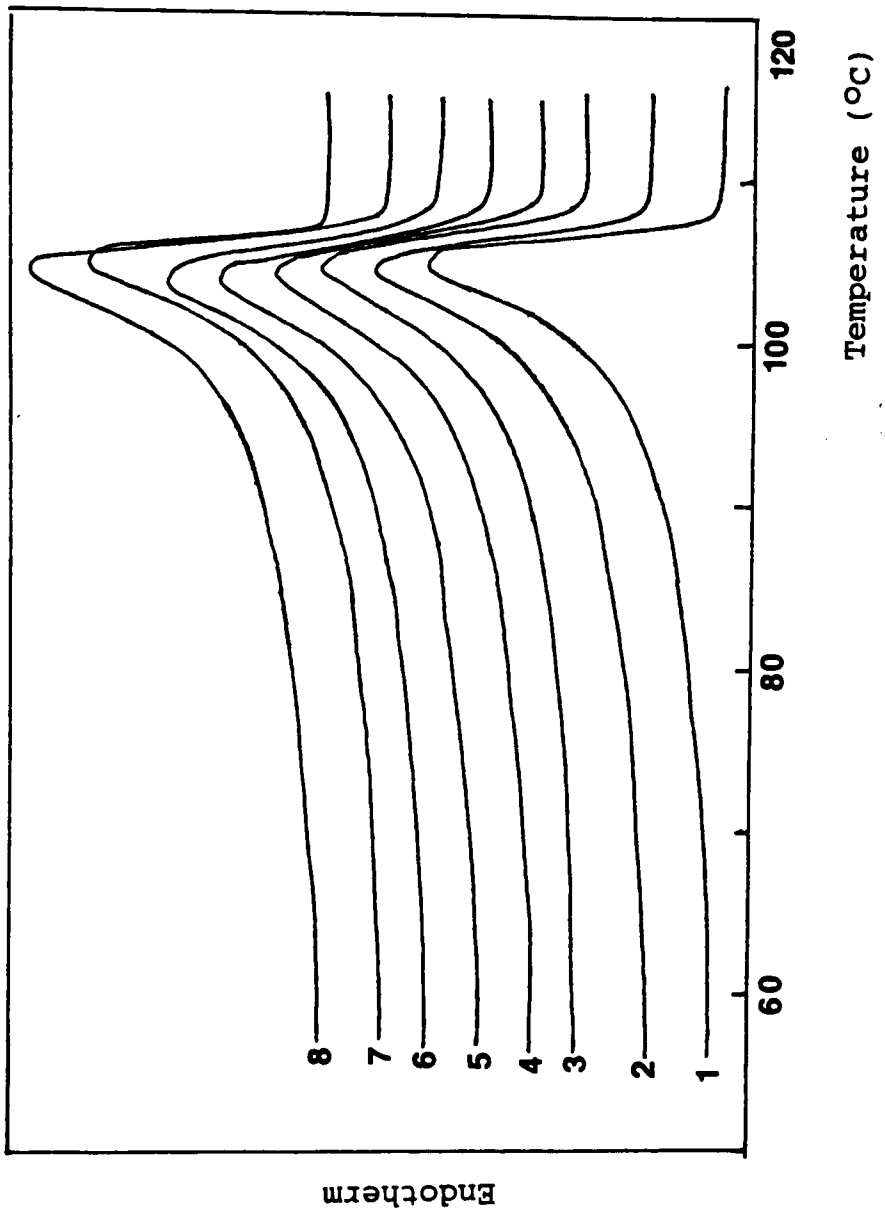

Figure 33 DSC thermograms obtained from the indicated radial positions of cable C1

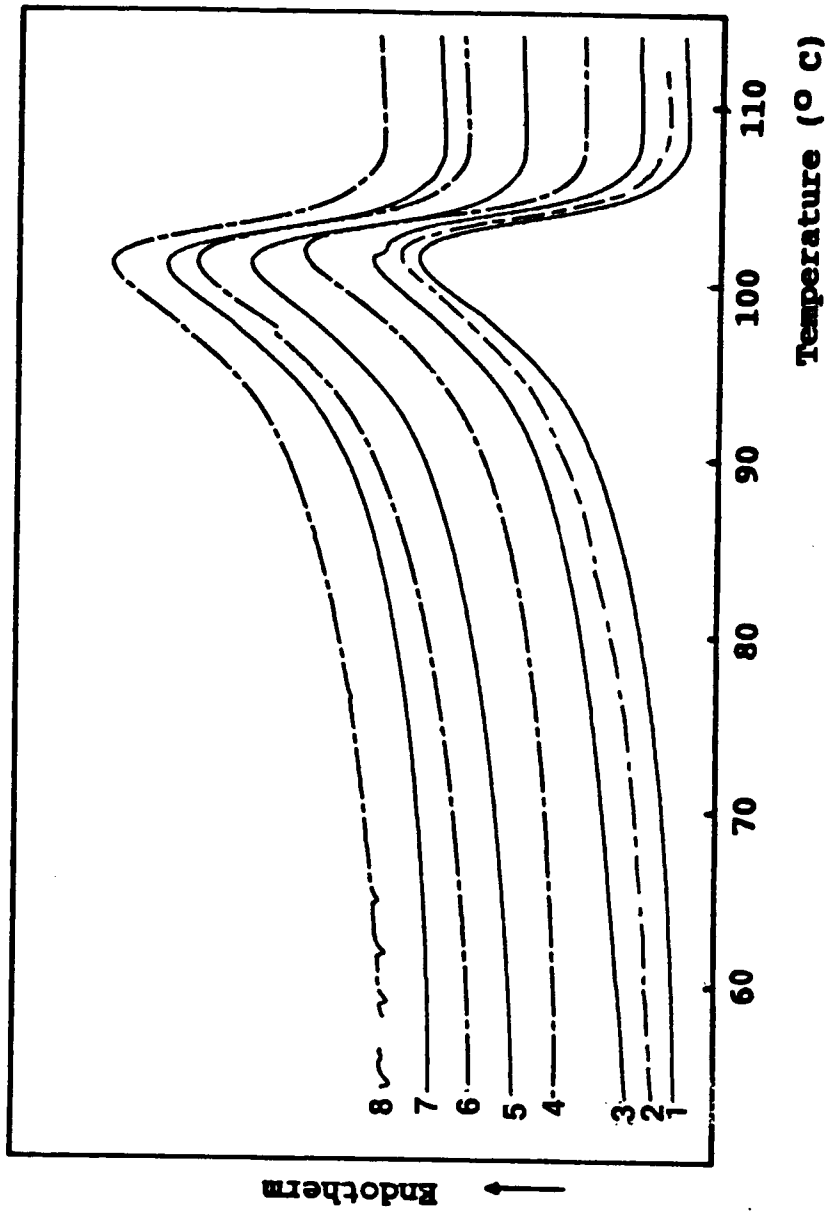

Figure 34 DSC thermograms obtained from the indicated radial positions of cable E1.

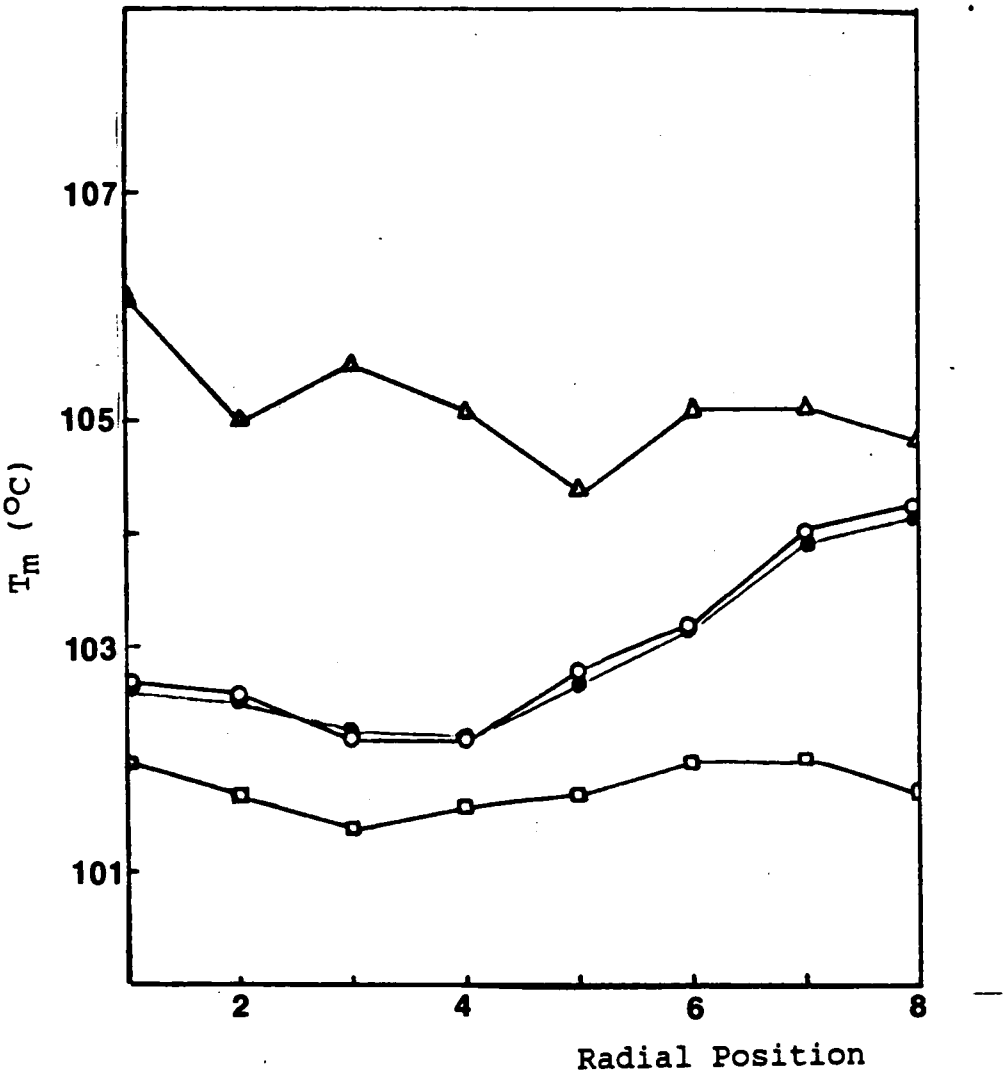

Figure 35 Melting temperature, T_m, versus radial position for cables A1 (O) narrow and (●) broad regions (Δ) C1 and (□) E1.

difference (Figure 36). The relationship between percent extractables and T_m and T_{rb} for cable A1 is plotted in Figure 37. It is clear from this figure that both T_m and T_{rb} are functions of percent extractables. Percent crystallinity as a function of radial position is given in Figure 38, for cables A1, C1 and E1. Percent crystallinities from DSC data were calculated by taking the ΔH_f of 100 % crystalline XLPE as 156 J/g. This value was found by, first measuring the percent crystallinity of a 2 % XLPE standard using WAXS and, secondly, the ΔH_f value of the same sample was found from the DSC measurement extrapolated to 100 % crystallinity by considering the related WAXS crystallinity. It is seen from Figure 38 that cable C1 was found to have an average crystallinity of 53.9 % while the average crystallinity values for cables A1 and E1 were found to be 49.5 % and 49.4 %, respectively.

Dry cured cable, C1, and steam cured cable, E1, did not show any major variation in T_m and T_{rb} throughout their radial direction (Figures 33-35). Cable C1 having about the same amount of extractables as Cable E1, showed higher T_m and T_{rb} values across the entire radial cross-section. The greatest difference in Tm was found to be 1.8 degrees. Comparison of cable C1 with cable A1 shows that the former with a 14 % extractable level has a comparable melting temperature to the inner section of the latter having 28 % extractables. In the case of T_{rb}, relatively

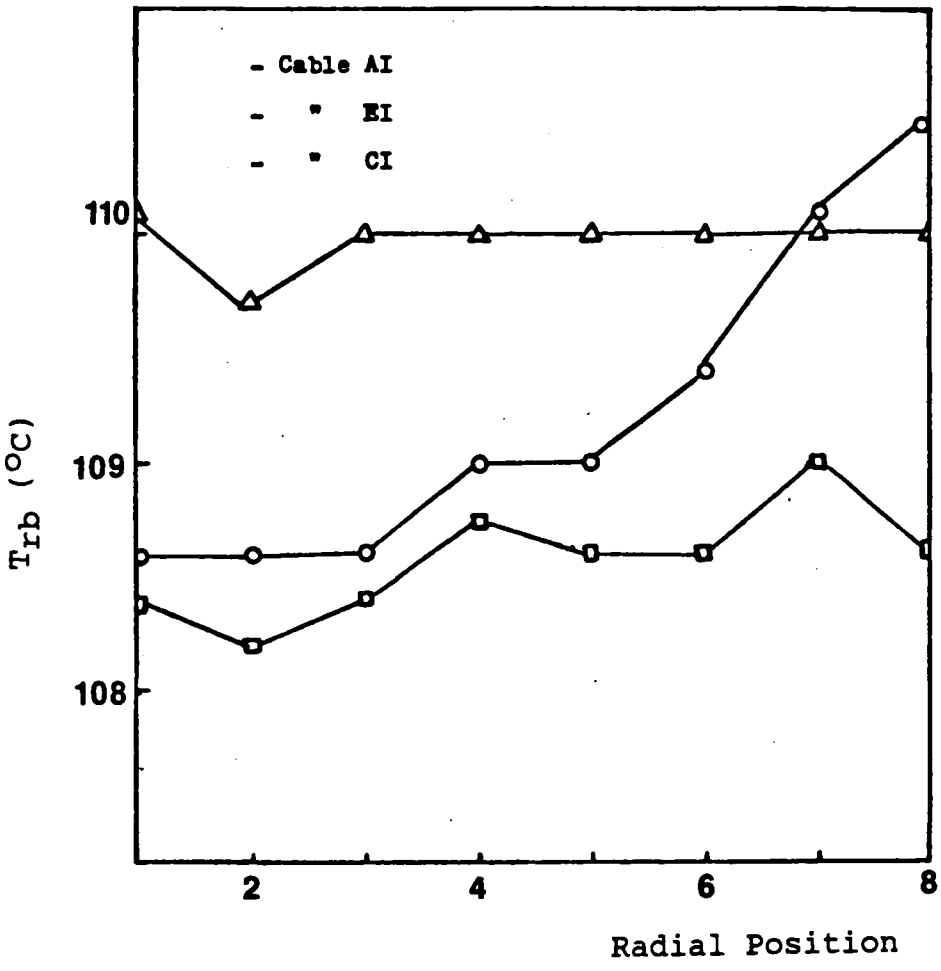

Figure 36 Return to the base line temperature, T_{rb}, versus radial position for cables (O) A1 narrow region, (Δ) C1 and (□) E1.

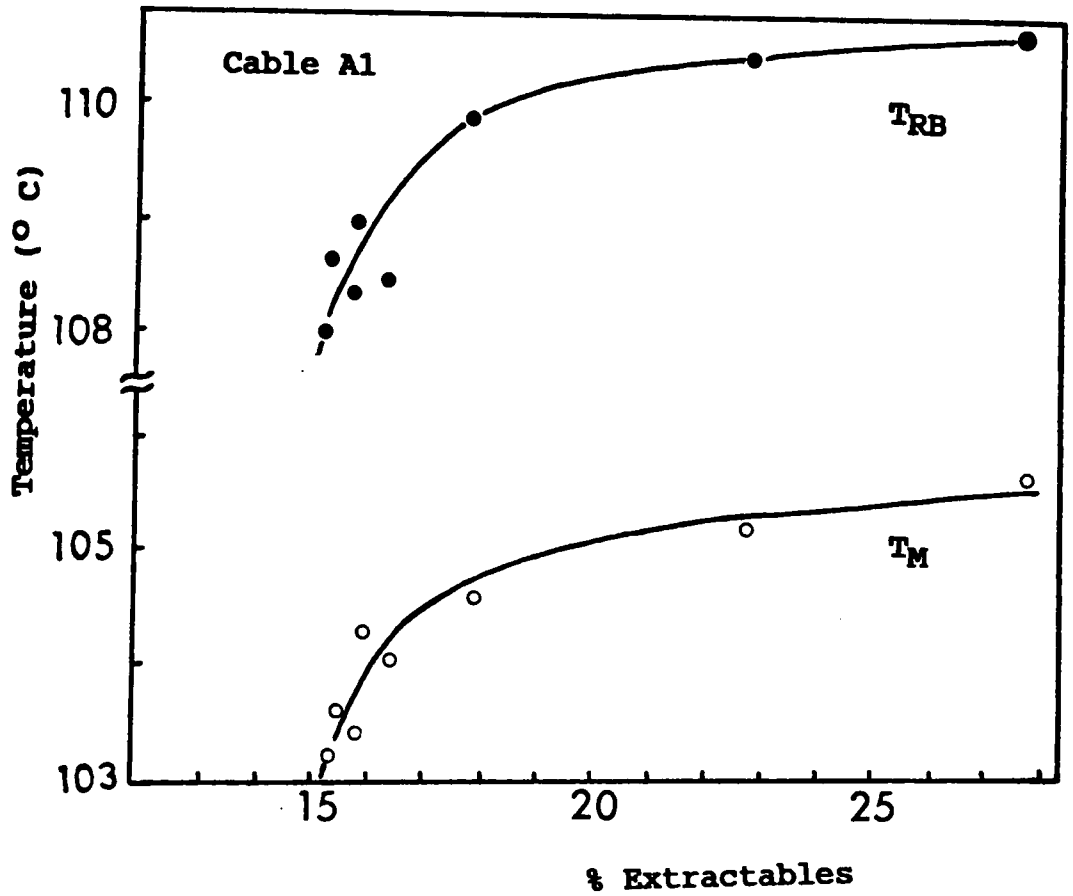

Figure 37 T_m and T_{rb} as a function of % extractables for cable A1.

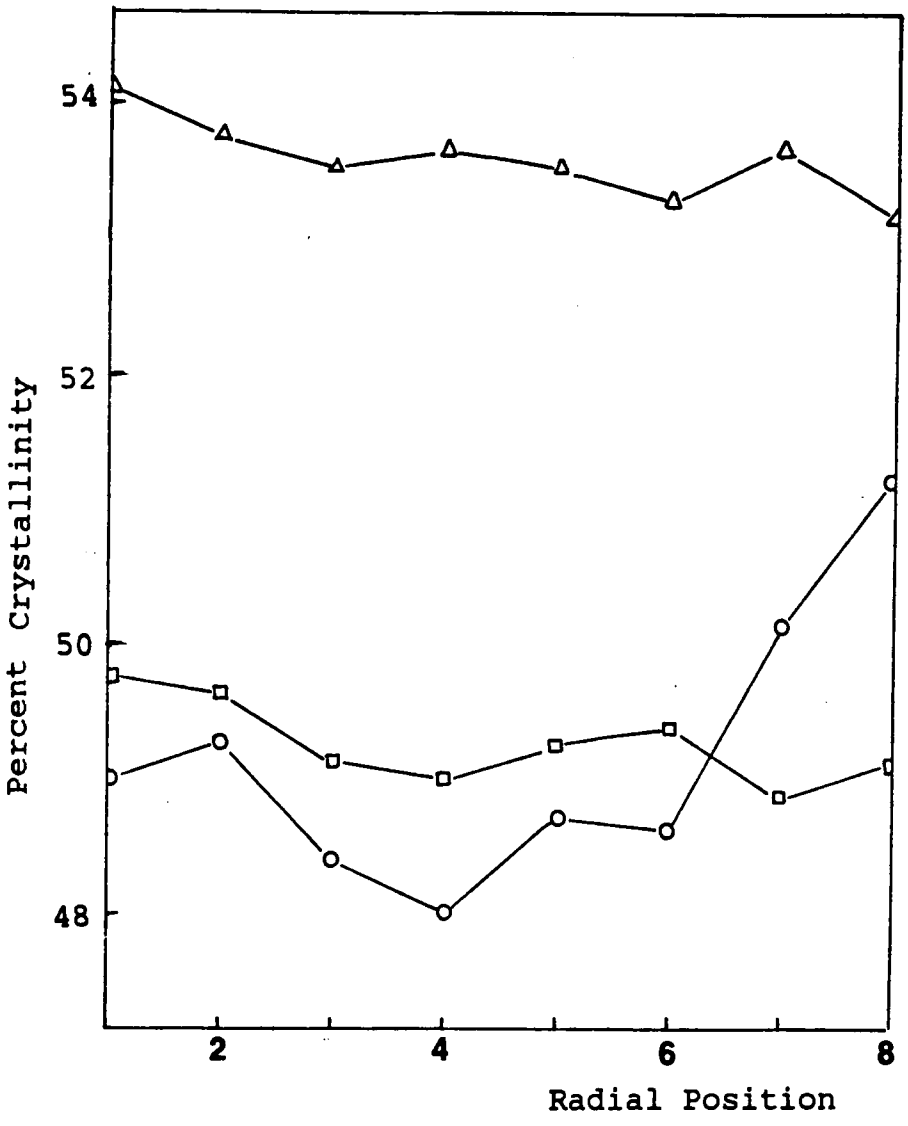

Figure 38 Percent crystallinity obtained from DSC as a function of radial position for cables (O) A1, (Δ) C1 and (□) E1.

lower temperatures were observed for the inner radial sections. Percent crystallinities for both cables C1 and E1 remained close to constant throughout their radial direction.

In addition to comparing the thermal data of the original cables (with different thermal processing histories) the cables were also analyzed after they had acquired the same thermal history. This was achieved through a multistep experimentation carried out in the DSC. After running each specimen at 10 deg/min for its original thermal information, the sample was kept at 130 ^{o}C for three minutes then cooled down to 40 ^{o}C using a 60 deg/min cooling rate. The specimen was then rerun at 10 deg/min in order to record the endotherm of the thermally treated sample. T_m and T_{rb} temperatures obtained for heat treated samples are compared with the ones obtained for the originals in Figure 39 for cables A1, C1 and E1. While the T_m s of each section of the cables did not show much variation, the T_{rb} s were found to have changed. A drop of 1.5 degrees was observed for cable E1 and the inner layers of cables A1 and C1. The outer layers of cables A1 and C1 did not show this drop in T_{rb}.

The effect of extractables on ΔH, T_m and T_{rb} was closely studied by recording the endotherms of the outermost and innermost layers of the original cable and their corresponding gel fractions all of which were crystallized on cooling from the melt, 135 ^{o}C, to room temperature prior

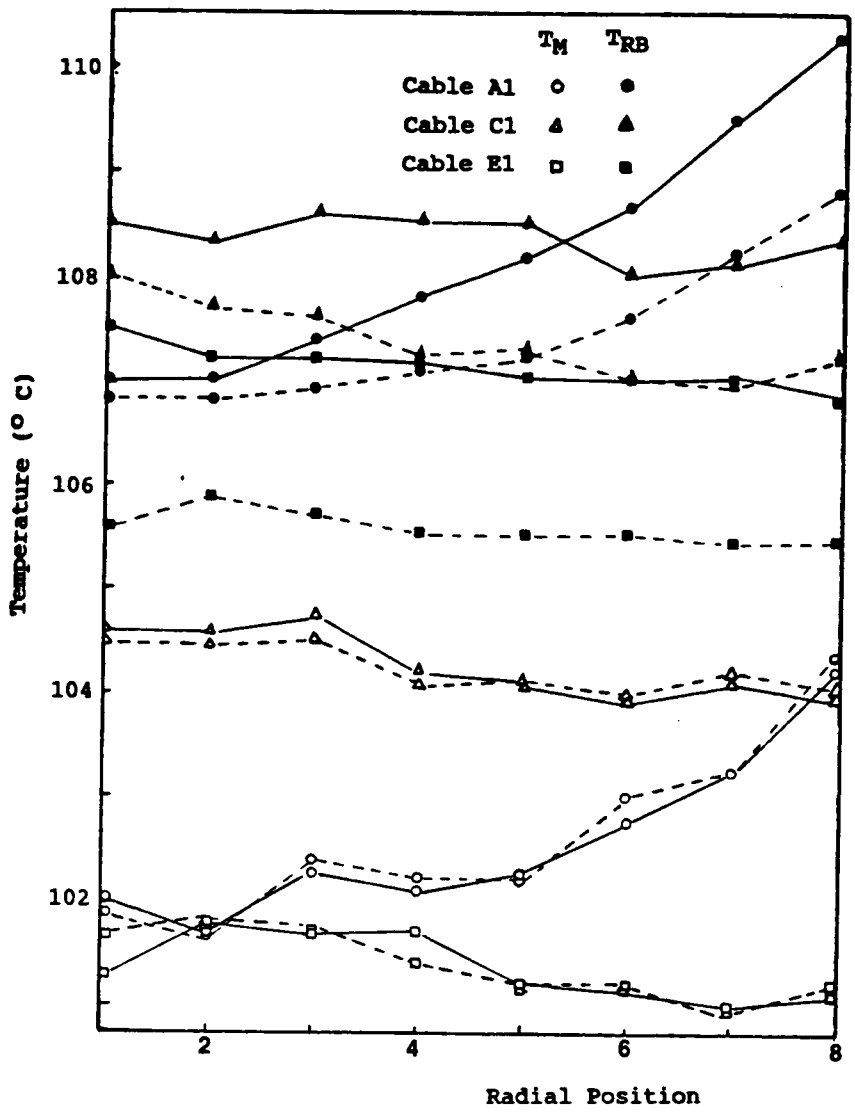

Figure 39 T_m and T_{rb} as a function of radial position for original (_____) and heat treated (----) cables A1, C1 and E1.

to their DSC analyses. After studying the DSC of the radial sections of the unextracted original cable, they were extracted, completely dried, crystallized and then analyzed in the DSC. Figure 40 shows DSC thermograms for the original and gel fractions of the outer and inner layers of cable A1. While the original cables had crystallinities of 48.8 % and 50.9 % the gel was found to have crystallinities of 62.2 % and 69.8 % for the outer and inner layers, respectively. The original cable had T_m s of 100.9 and 103.3 ^oC for its outer and inner layers, whereas the gel had T_m's of 100.8 and 100.6 ^oC for the outer and inner layers, respectively. Again, for T_{rb} s a similar trend was observed, results being 105.6 and 105.4 ^oC for the gel and 106.5 and 108.2 ^oC for the original cable, outer and inner layers, respectively. Table 8 summarizes all these values.

Melting endotherms obtained from radial sections of original LDPE and XLPE distribution cables are presented in Figures 41-42. This time, the insulation was divided into three or four equal sections radially. While for some cables each of those four sections were analyzed, for some only the inner and outer layers were investigated. T_m, T_{rb} and ΔH_f values are summarized in Table 9 and for LDPE and XLPE original distribution cables. In general, it is seen that, D8 XLPE distribution cable has lower T_m and T_{rb} than the LDPE cables. All the LDPE distribution cables have T_m s around 107.5 and T_{rb}'s around 110.5-111.9 ^oC.

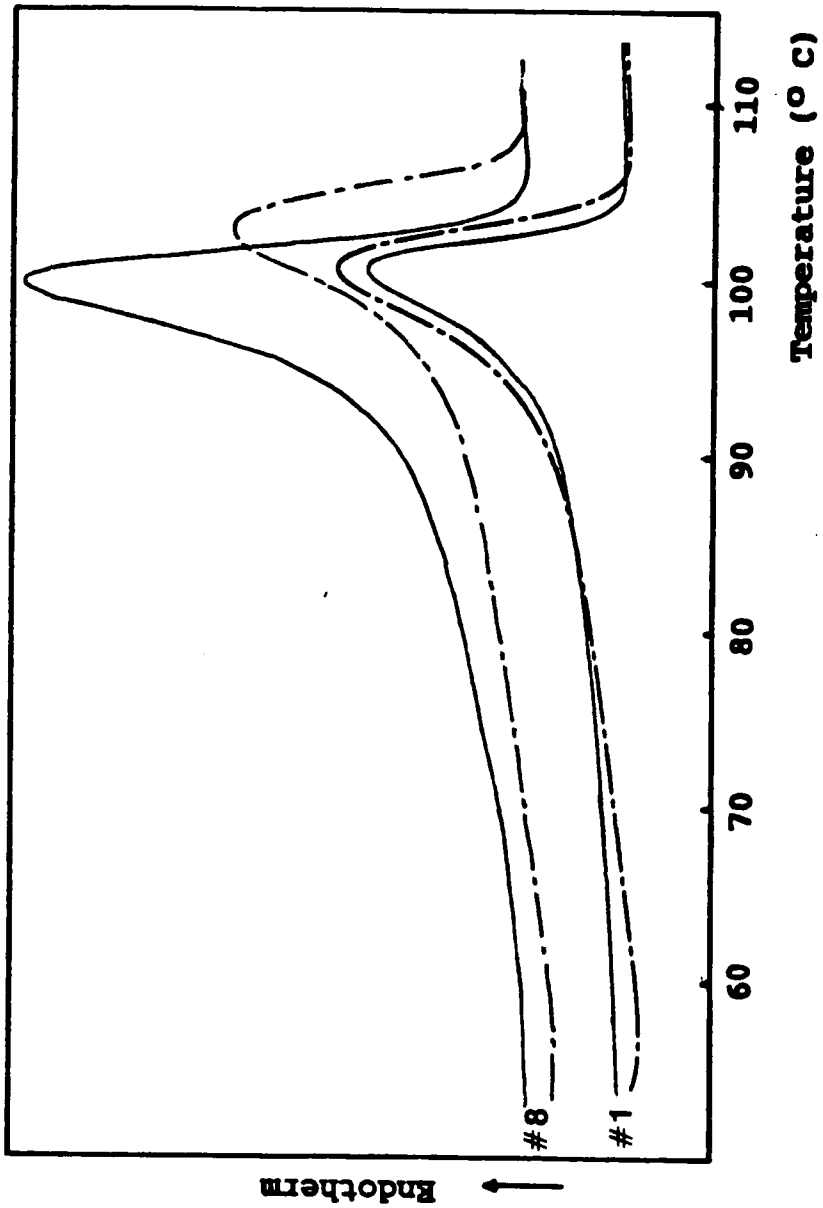

Figure 40 DSC thermograms obtained from the outer (#1) and inner (#8) radial sections of the unextracted (---) and (——) gel versions of cable A1.

Table 8 DSC data of the original and gel fractions of the inner and outer radial sections of cable A1

Cable	ΔH (J/g) Orig.	Gel	T_m (^oC) Orig.	Gel	T_{rb} (^oC) Orig.	Gel	Percent Crystallinity Orig.	Gel
A1-1	76.0	97.0	100.9	100.8	106.5	105.6	48.7	62.2
A1-8	79.4	109.1	103.3	100.6	108.2	105.4	50.9	69.8

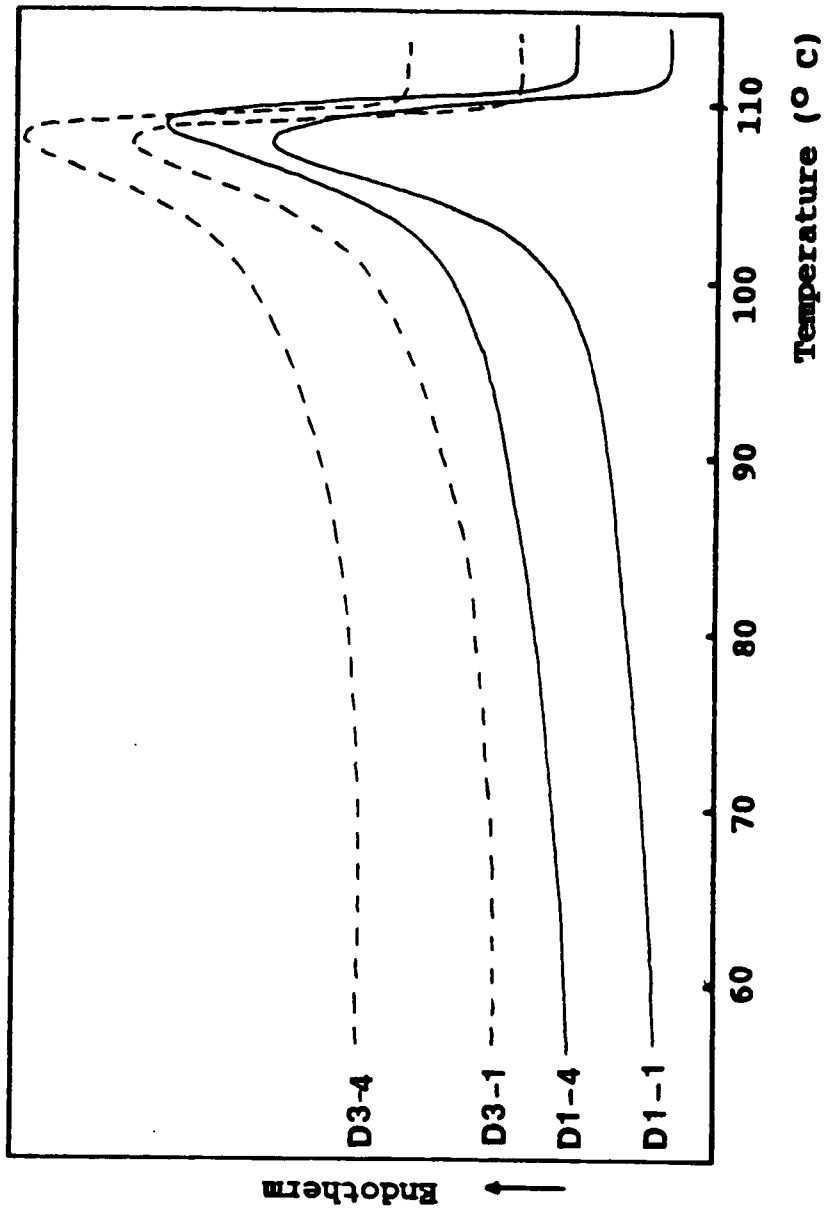

Figure 41 DSC thermograms obtained from the outermost (#1) and innermost (#4) layers of D1 and D3 LDPE distribution cables.

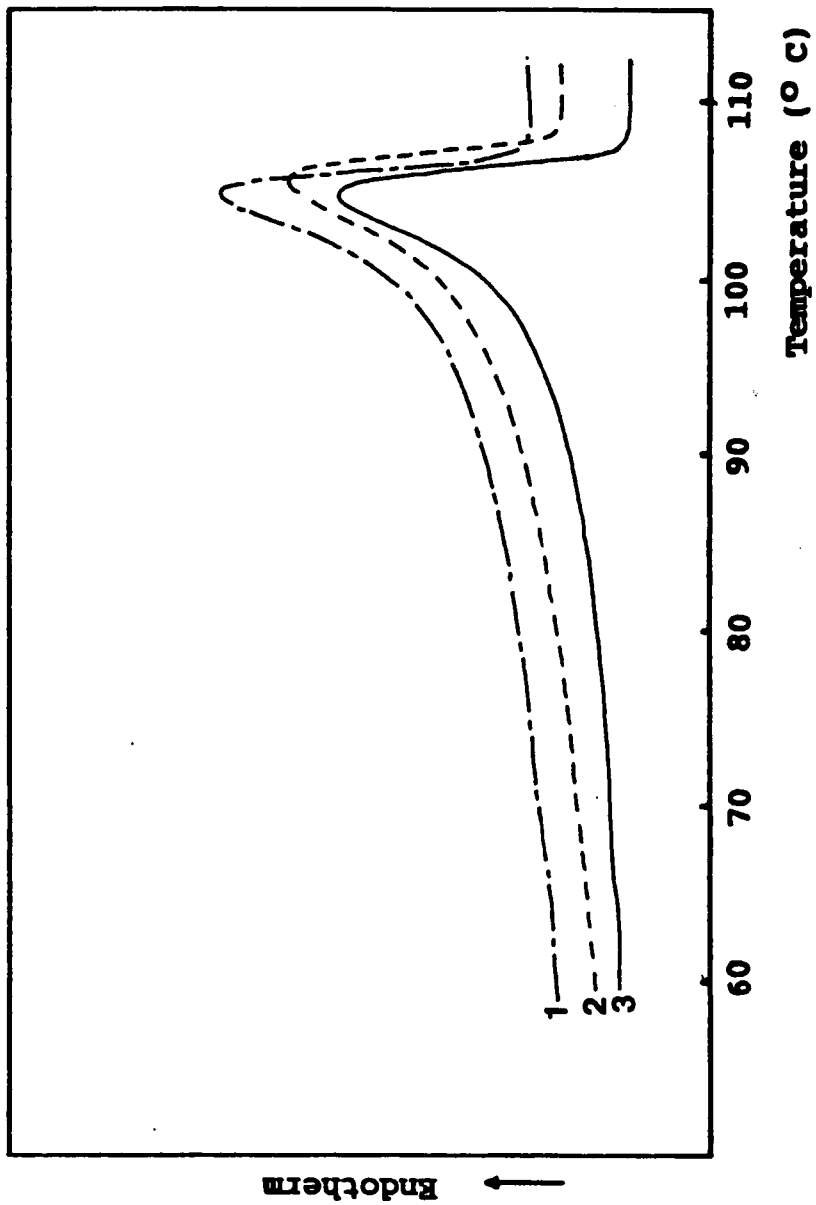

Figure 42 DSC thermograms obtained from the outermost (#1), the innermost (#3) and middle (#2) sections of D8 XLPE distribution cable.

Table 9 DSC results of the indicated original distribution cables

Cable	T_m (°C)	T_{rb} (°C)	ΔH (J/g)	Percent Crystallinity
D1-1	107.7	111.9	90.1	57.8
D1-4	108.8	111.6	94.9	60.8
D3-1	107.6	110.6	88.4	56.7
D3-4	107.8	110.6	88.7	56.8
D8-1	104.4	107.7	65.6	42.1
D8-4	105.1	108.4	65.9	42.0

D8 original distribution cable showed characteristic swirls throughout its insulation. The cloudiness due to the swirls was more pronounced in the mid section (about 1/3 of the whole radial section). A DSC thermogram obtained from an isolated cloudy swirl was found to show a T_m 0.2 ^oC lower than that obtained for the clear region.

4.2.6. X-Ray Studies

Wide angle X-Ray (WAXS) studies were carried out to find the radial distribution of crystallinity and the values of crystallinity at various annealing temperatures by the use of a high-temperature X-Ray cell. Small angle X-Ray (SAXS) studies were utilized to find crystal thickness, X-ray flat film patterns being obtained to study possible crystal orientation in the outer and inner layers.

Layers from cables A1, C1 and E1 gave concentric diffraction rings with even intensity distribution. Flat film pictures obtained for cable A1-1 and A1-8 in the radial direction are shown in Figures 43a-b. The nomenclature of the directions is given in Figure 44.

Intensity versus 2θ scans for the innermost layers of cables A1, C1 and E1 are given in Figure 45. The remaining radial sections were observed to have identical plots with different percent crystallinities. Values of crystallinities found using the peak resolution technique for cables A1, C1,

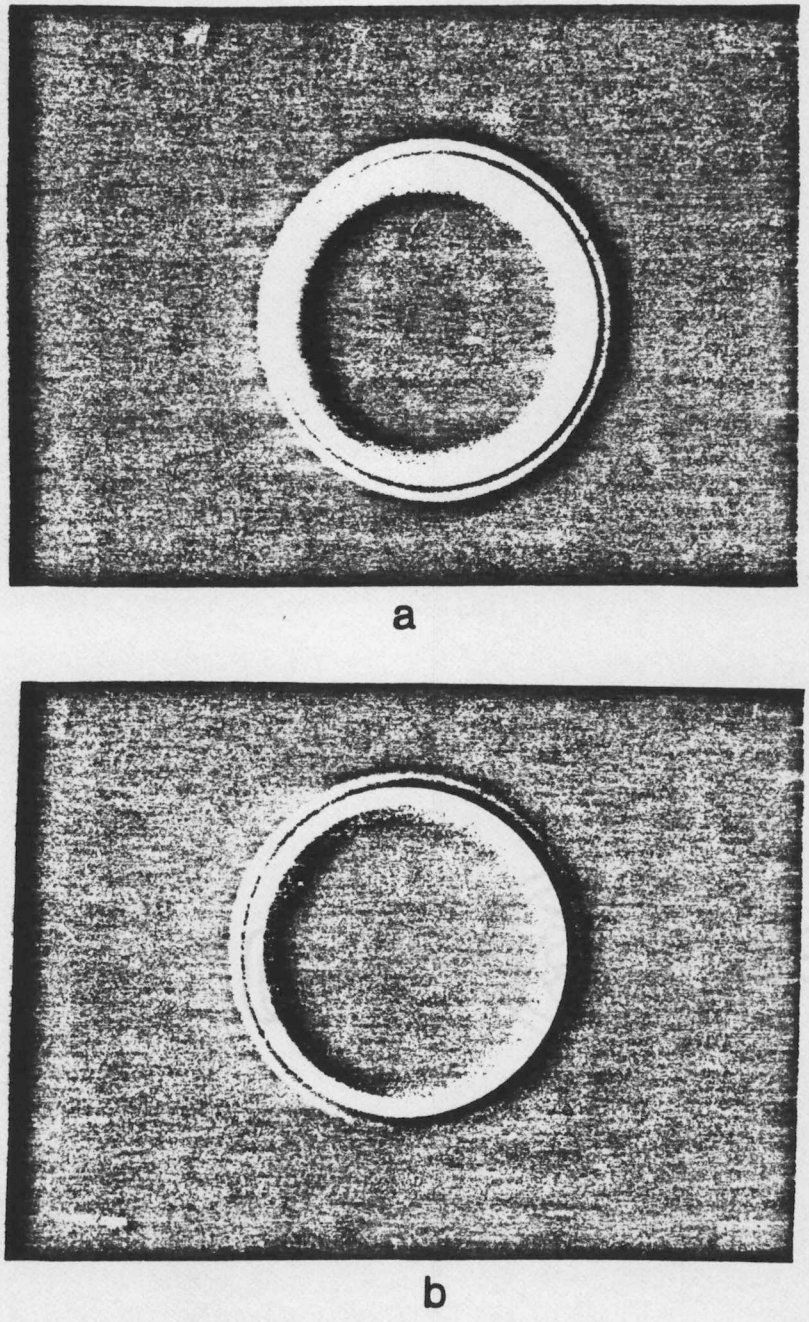

Figure 43 Wide angle X-ray diffraction patterns of (a) the outermost and (b) the innermost layers of cable A1 in the radial direction obtained using a flat plate camera.

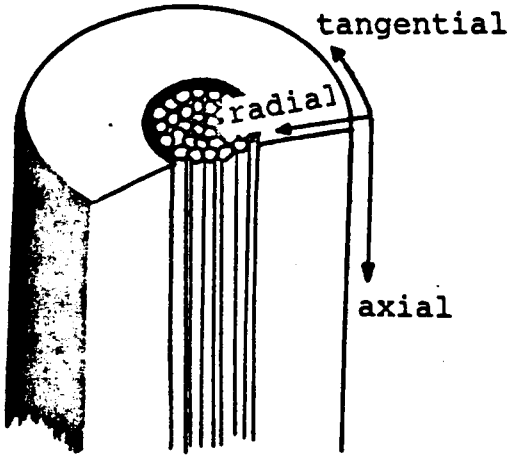

Figure 44 Representation of the direction nomenclature used in the cable analyses.

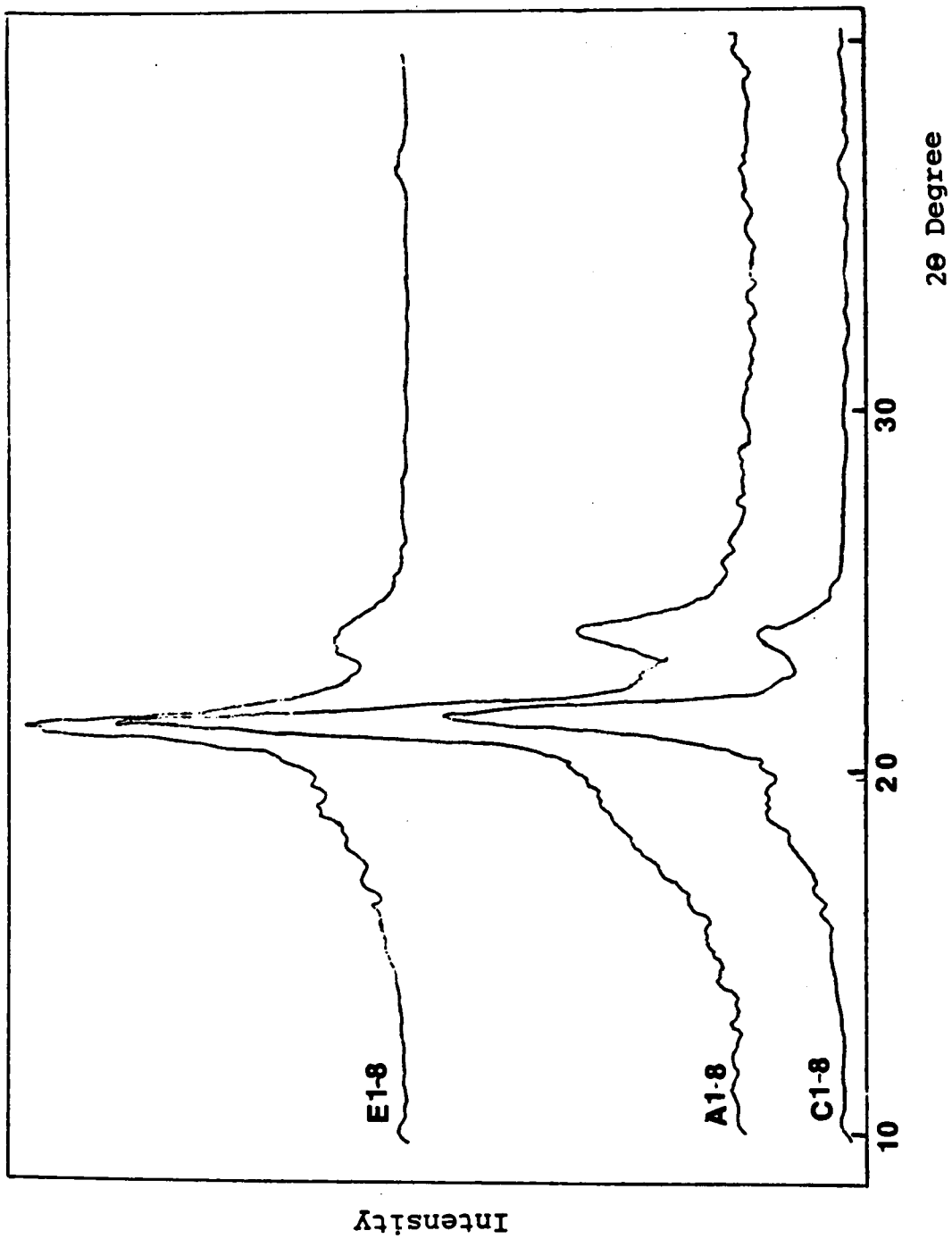

Figure 45 Intensity versus 2θ WAXS diffraction patterns obtained for the indicated cables.

E1 and distribution cables D1 and D8 are summarized in Table 10.

SAXS scattering intensity contours obtained for the inner and outer layers of cables A1, A1-8 gel, C1, C1 quenched, E1 and distribution cables D1 and D8 are shown in Figures 46-50. Cable C1 showed iso-intensity contours indicative of zero orientation at both the inner and outer layers (Figure 47). Breaks in the intensity contours at lower scattering angles for the outer layer of cable A1 and inner layer of cable E1 were observed indicating the start of microstructural orientation.This break is more pronounced for the inner and outer layers of cables A1 and E1, respectively. Circumferential average intensity versus scattering vector plots for the inner and outer radial sections of cables A1, C1, E1, D1 and D8 were obtained after subtracting the parasitic scatterings and normalizing for the detector sensitivity and transmission coefficient of the sample (Figure 51-54). Broad diffraction maxima typical of semicrystalline polymers with fluctuating crystalline and amorphous thicknesses were observed for both inner and outer layers of the cables. The breadth of the peaks for each cable section was similar. Major differences between cables were observed at small scattering angles corresponding to entities bigger than 200-300 ^{o}A.

Table 10 WAXS and SAXS results of the indicated original transmission and distribution cables

Cable	% Crystallinity	Long Period(^{o}A)	Lamellar Thickness(^{o}A)	$\sigma_e x10^3$ (J/m^2)
A1-1	47	193	90	79.8
A1-8	48	210	101	85.0
A1-8 Gel	52	157	81	
C1-1	51	192	98	94.1
C1-8	50	193	96	98.3
C1-1 Quenched	49	189		
E1-1	48	191	92	88.3
E1-8	47	201	94	92.8
D1	57	186	105	
D8	40	182	82	

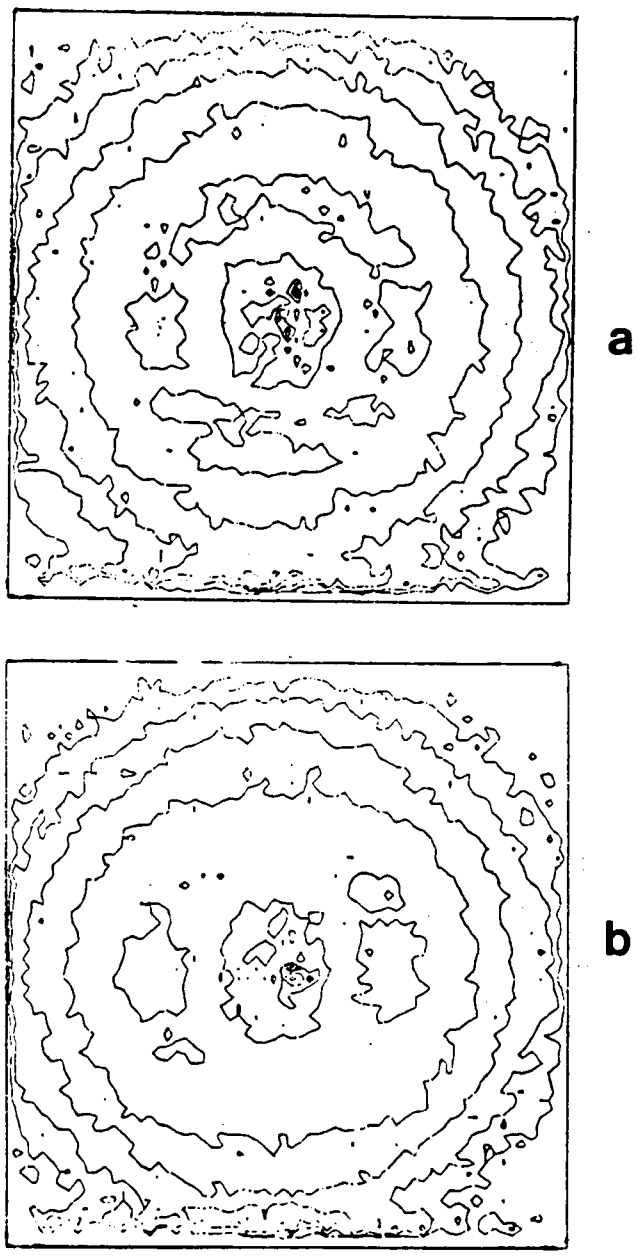

Figure 46 SAXS contours obtained from (a) outer layer (b) inner layer of cable A1.

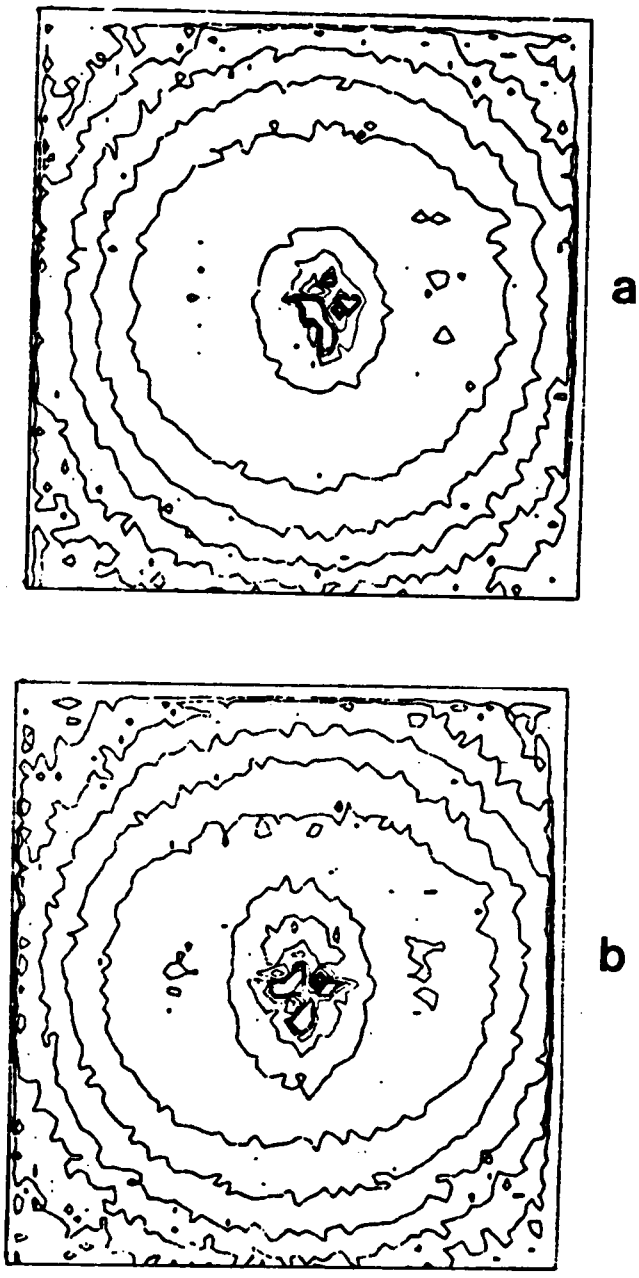

Figure 47 SAXS contours obtained from (a) outer layer (b) inner layer of cable C1.

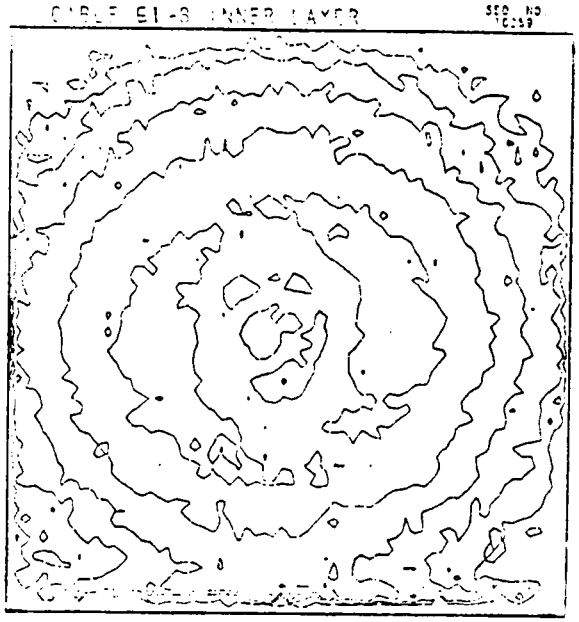

a

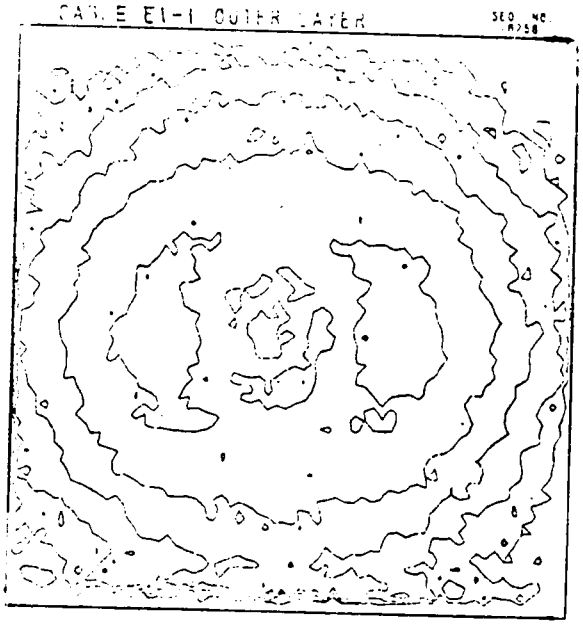

b

Figure 48 SAXS contours obtained from (a) outer layer (b) inner layer of cable E1.

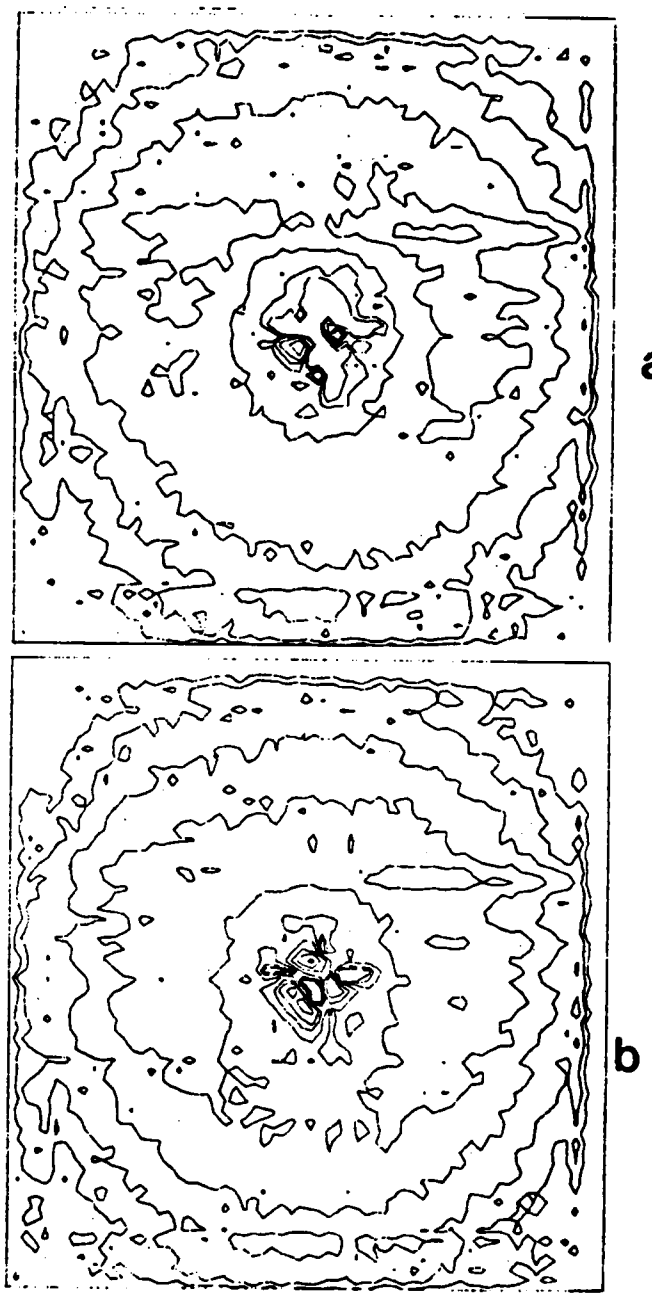

Figure 49 SAXS contours obtained from (a) gel fraction of inner layer of cable A1 (b) outer layer of cable C1 quenched from the melt.

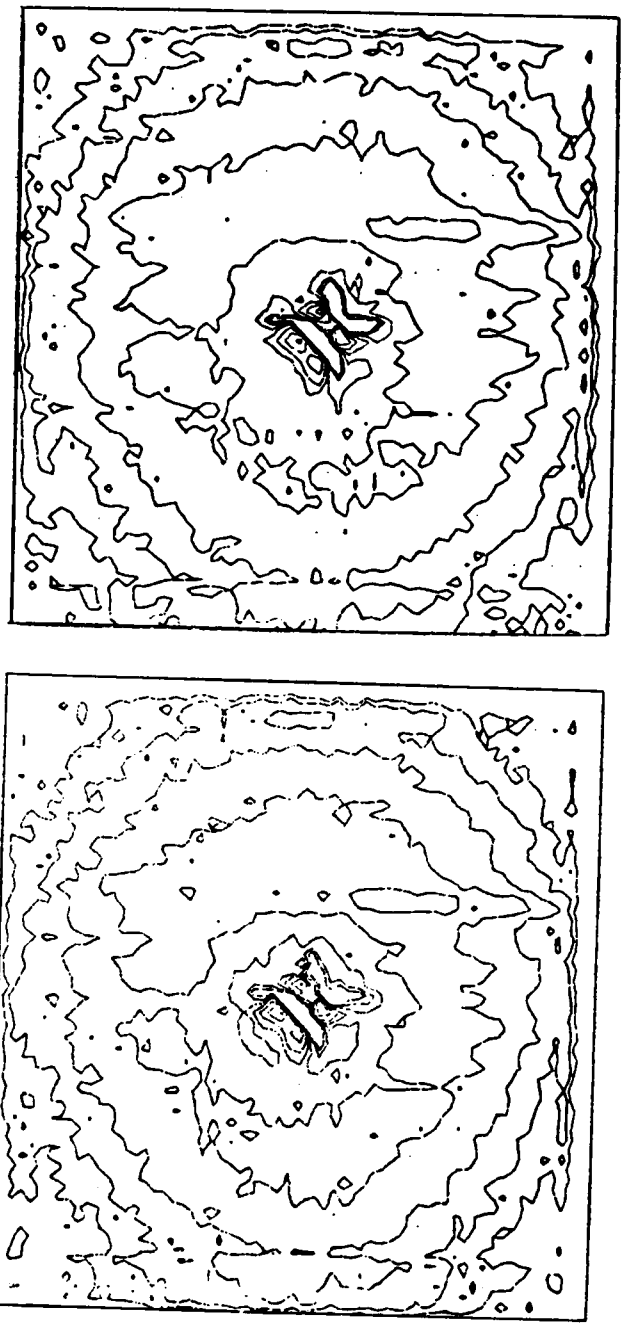

Figure 50 SAXS contours obtained for original distribution cables (a) D1 and (b) D8.

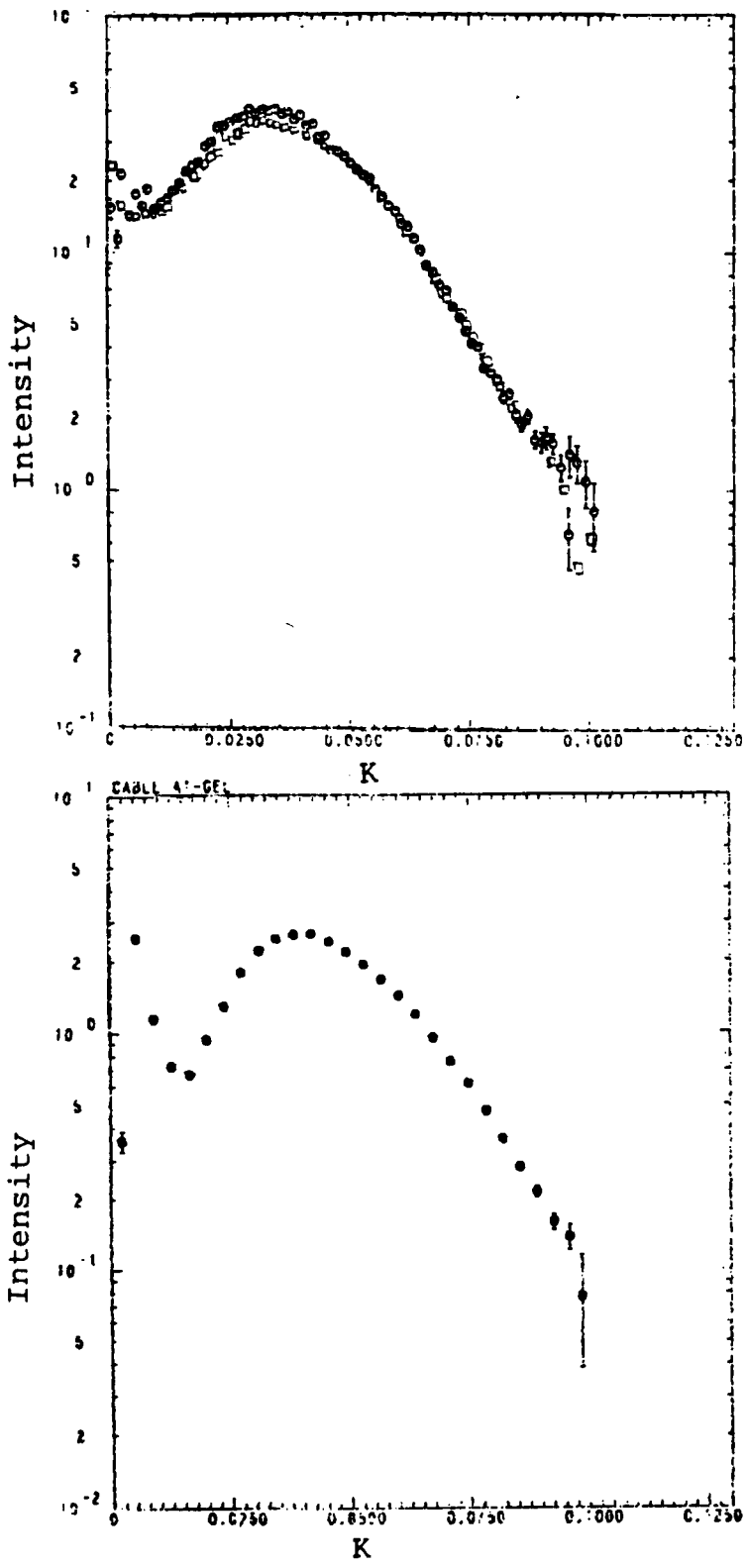

Figure 51 Circumferential average intensity versus scattering vector for the outer (O) and inner (□) layers of cable A1 and (●) A1-8 gel.

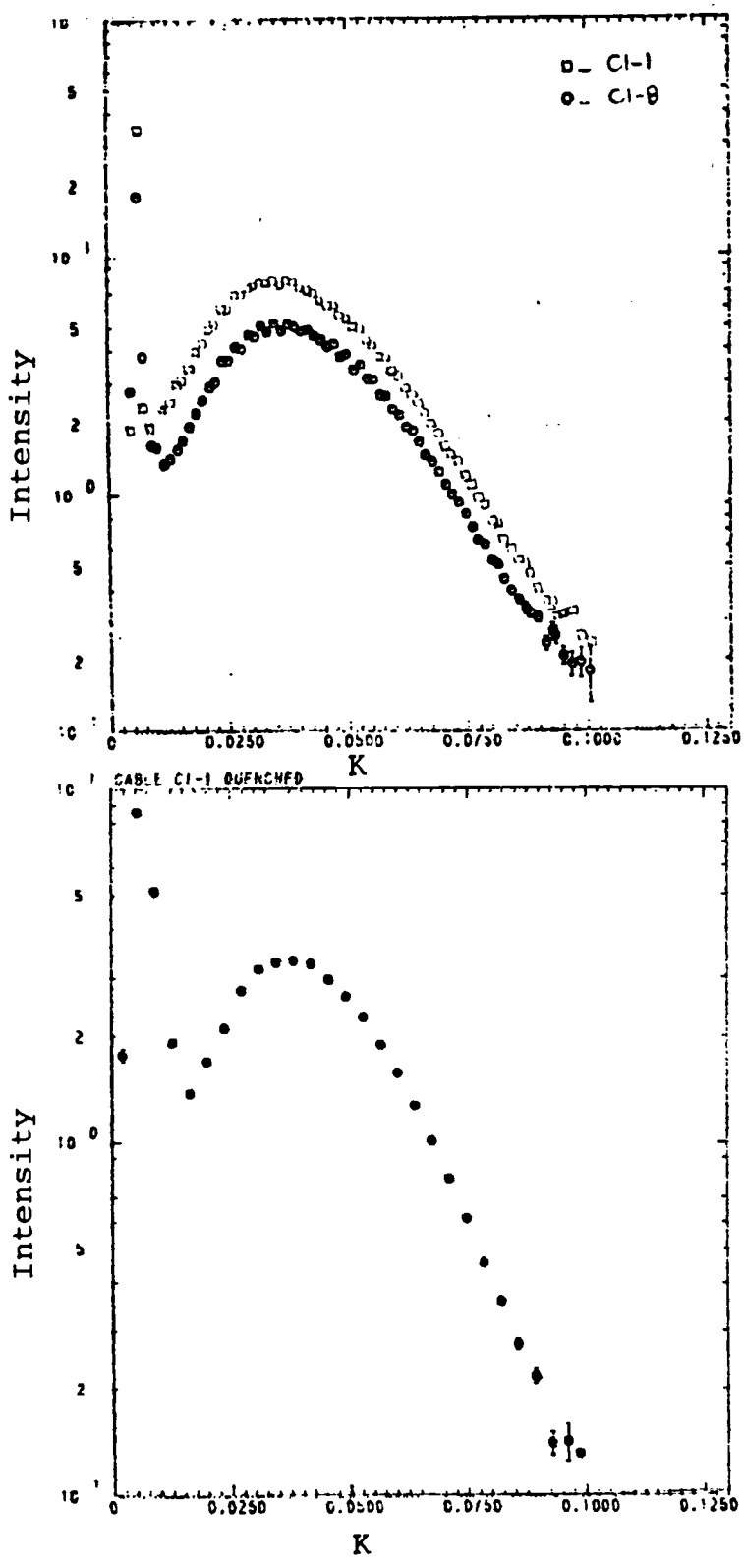

Figure 52 Circumferential average intensity versus scattering vector for the outer (O) and inner (□) layers of cable C1 and (●) C1-1 Quenched.

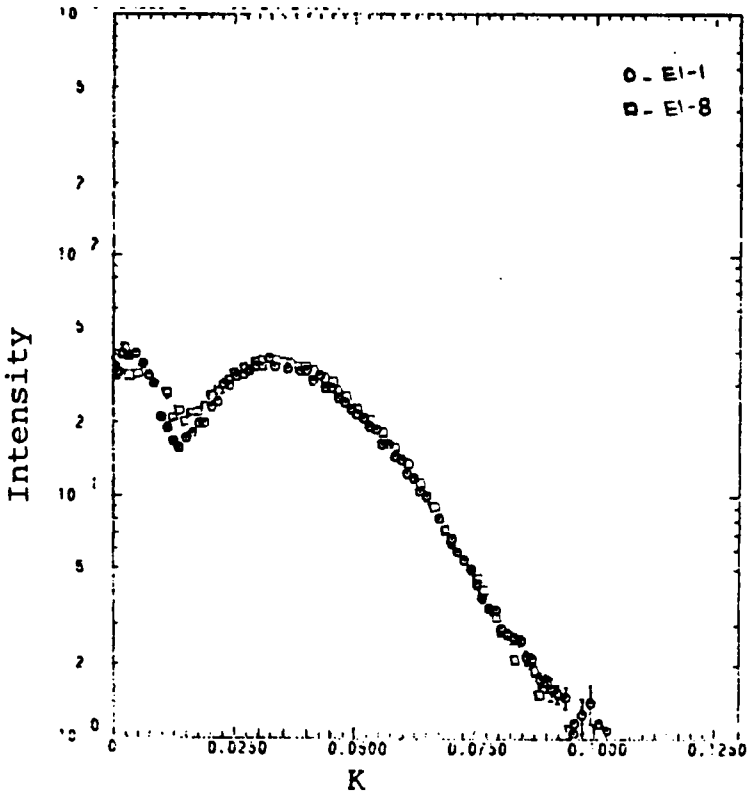

Figure 53 Circumferential average intensity versus scattering vector for the outer (O) and inner (□) layers of cable E1.

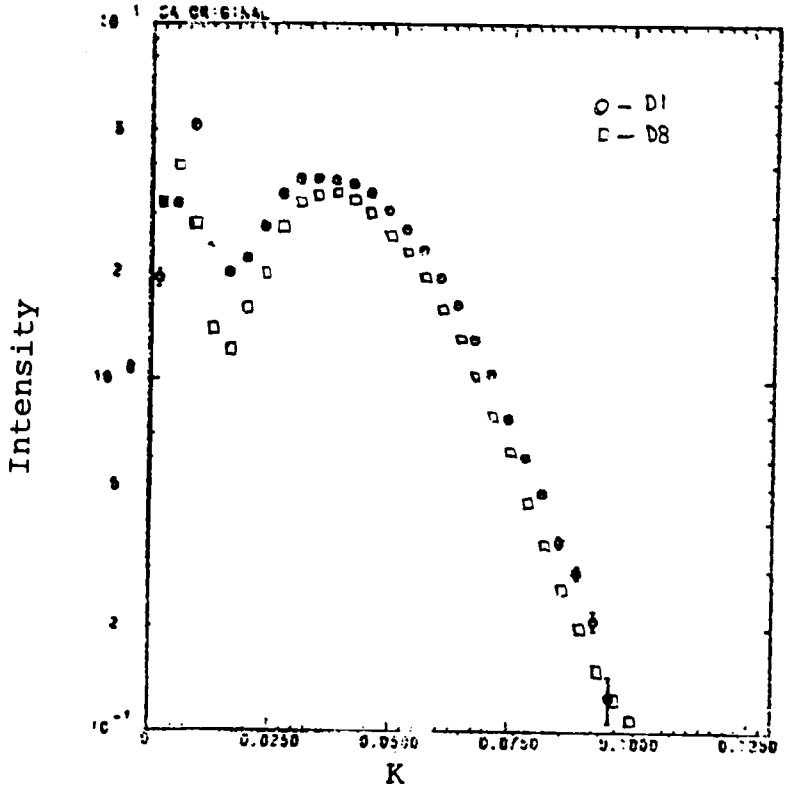

Figure 54 Circumferential average intensity versus scattering vector for distribution cables (O) D1 and (□) D8.

4.2.7. Optical and Electron Microscopy

Morphological details of XLPE and LDPE cables at gross and fine levels were studied by utilizing optical and electron microscopes.

Optical microscopy was utilized to analyze gross entities such as flow lines and blue line formations. The circular blue lines are less than one mm thick and they are found to be located generally at the stress transition regions. The lines were not present in cable E1 but were present in cables A1 and C1. Figure 55a taken from the cross section of cable A1 between cross-polars shows the location of the blue line relative to the positions of the heavily stressed inner layers and the lightly stressed outer layers. Concentric frozen-in stress fields are continuous along the axial direction (Figure 55b).

D8 original distribution cable was found to have cloudy structures visible between cross-polars. Figures 56a-c show pictures taken from 25 μm thick microtomed slices along the radial plane. No spesific morphological entities were found to be associated with these flow patterns. Figure 57 gives a closer look at the swirled area in Figure 56c marked as A. Typical spherulite birefringence was not observed. Figure 58 shows optical microscope pictures taken from the microtomed slices cut along the cable axis. This time, intricately swirled features were not observable.

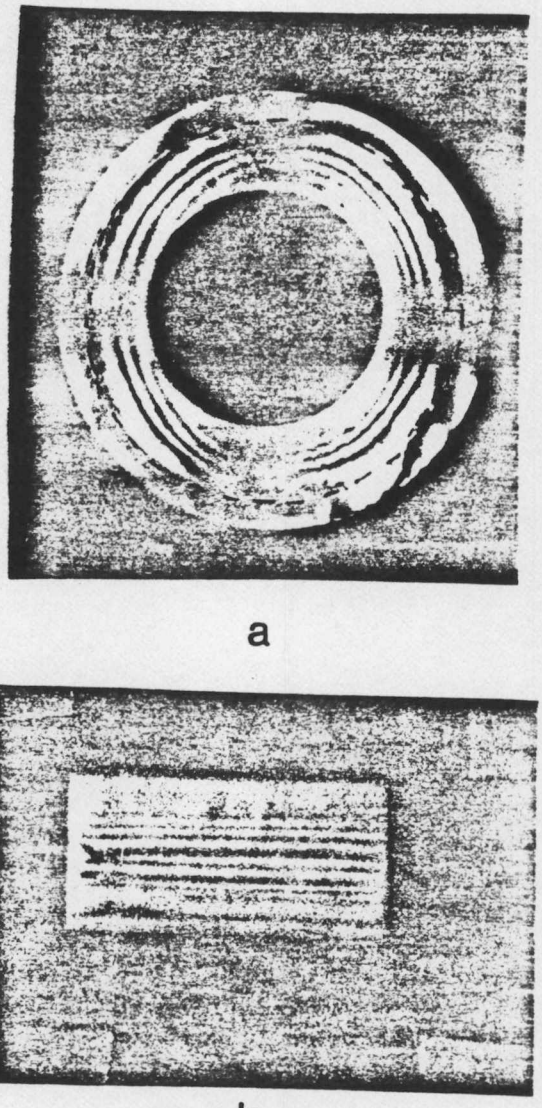

Figure 55 Optical microscope pictures of a microtomed slice of cable A1 taken between cross-polars showing (a) concentric frozen-in stress lines (b) similar lines along the axial direction. Dotted line in (a) corresponds to blue line.

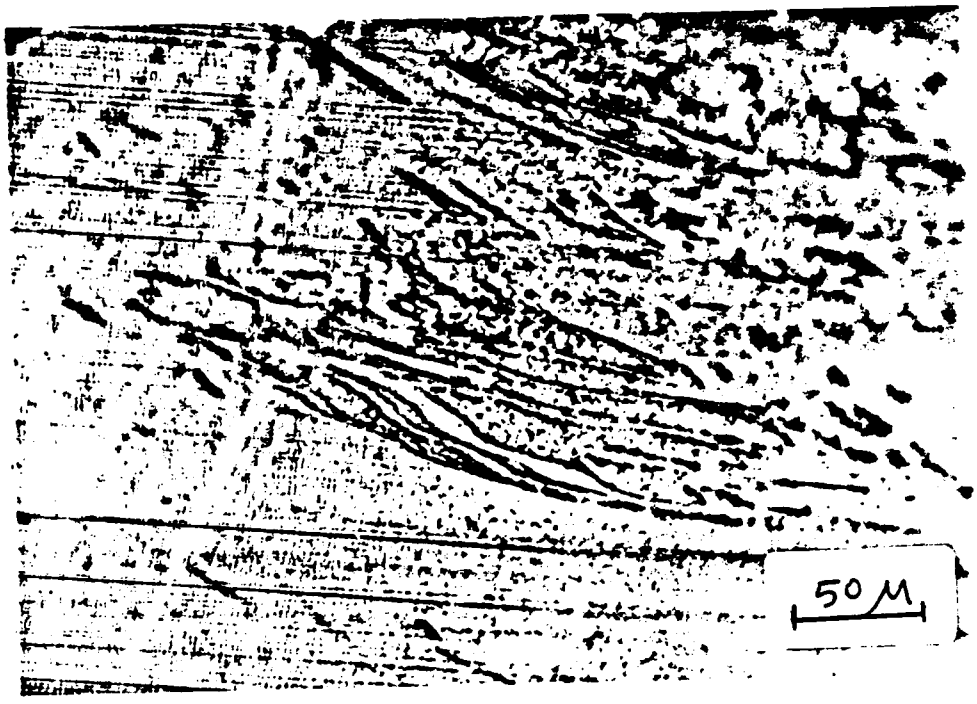

a

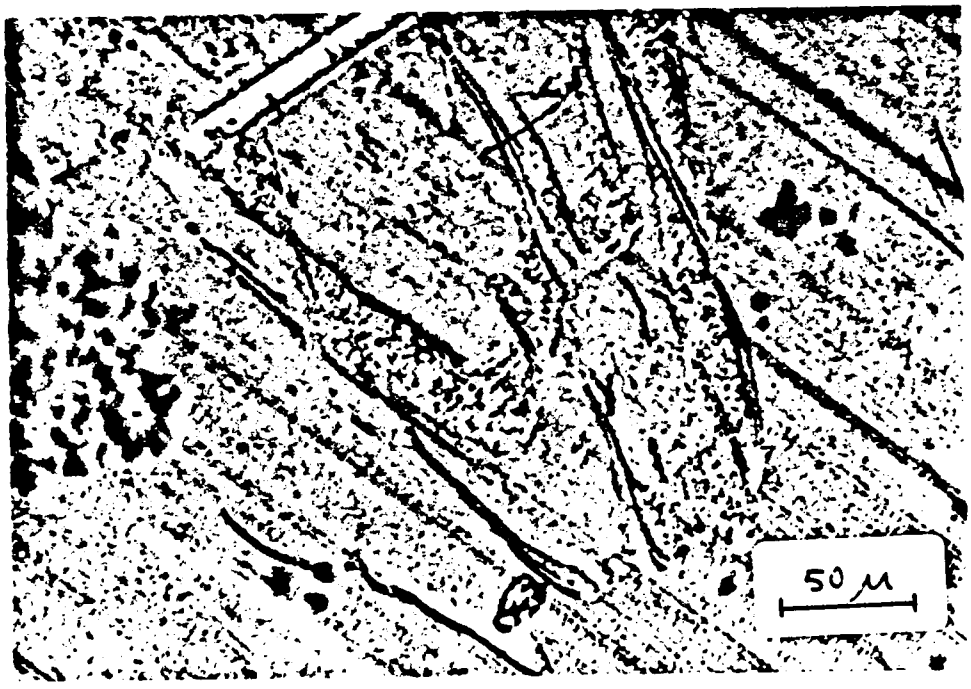

b

Figure 56 (a)(b)(c), optical microscope pictures of a microtomed slice of distribution cable D8 taken between cross-polars showing swirled features in the radial plane.



c

Figure 56 Continued



Figure 57 A higher magnification optical microscope picture of the area "A" in Figure 56-c.

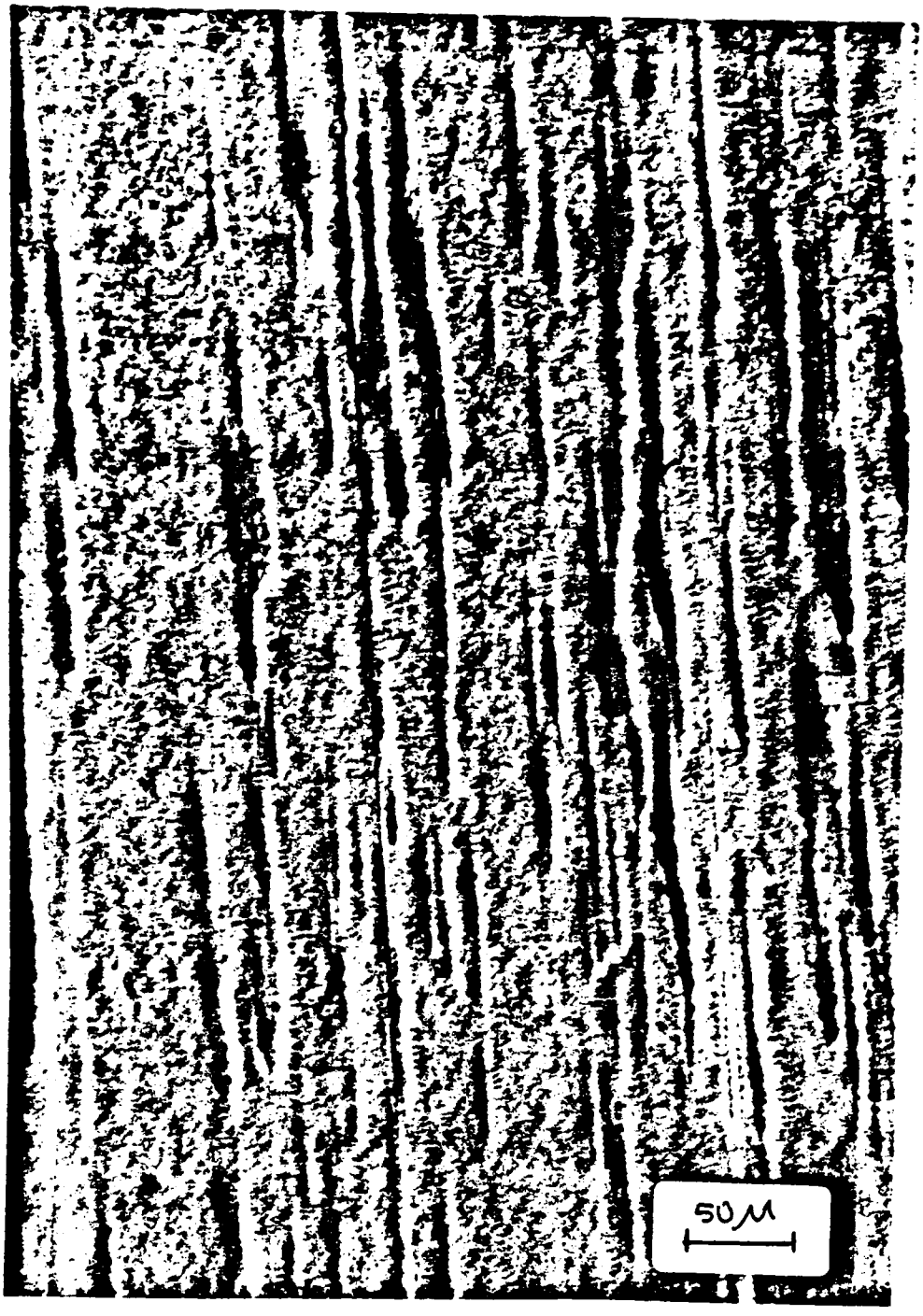

Figure 58 Optical microscope picture of a microtomed thin slice of distribution cable D8 in the axial plane.

Instead, 3-5 μm wide features all aligned in the axial direction were observed. Swirls were found to be present after heat treatment. Figure 59 is the SEM picture of the melt crystallized samples showing the topography related with the swirls.

Carbon replicas of etched surfaces were studied under TEM in order to reveal the fine morphological details. Figures 60a-b show TEM micrographs taken from 2 % XLPE crystallized at 92 ^{o}C for two hours. Sheaves were found to be the main morphological entities. The regions between the sheaves are lamellar organizations with random orientation. Sheaves are composed of 12-15 lamellae with a banding periodicity of two μm.

The inner layers of cable A1 were crystallized under similar conditions. Figure 61 shows sheaf structures spread between background lamellae. TEM micrograms obtained from the inner layers of original cable A1 showed sheaf-like bundles which are composed of 7-15 lamellae. Unlike the ones obtained during laboratory crystallization, these sheaves do not have any banding (Figures 62a-b). Volume filling entities between sheaves appear to be worm-like S and C shaped lamellae. Wide crystals can be seen spread throughout the areas between sheaves (Figure 63). For the case of steam cured cable, sheaves are detectable for the outer layer. Background lamellae are not as distinct as was observed in the inner layer of cable A1. Two-three μm sized sheaves

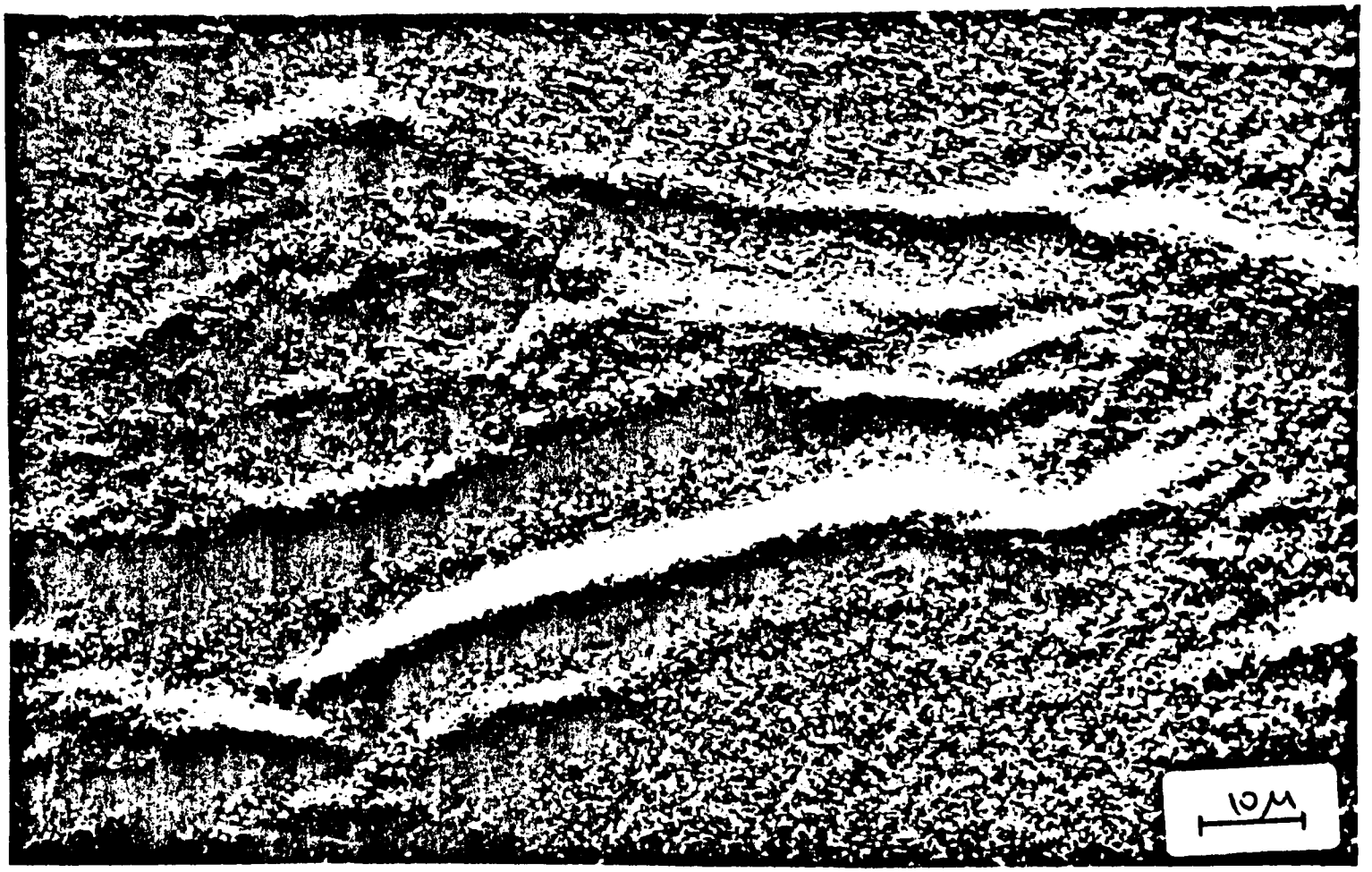

Figure 59 SEM picture showing the topography of the melt crystallized distribution cable D8.

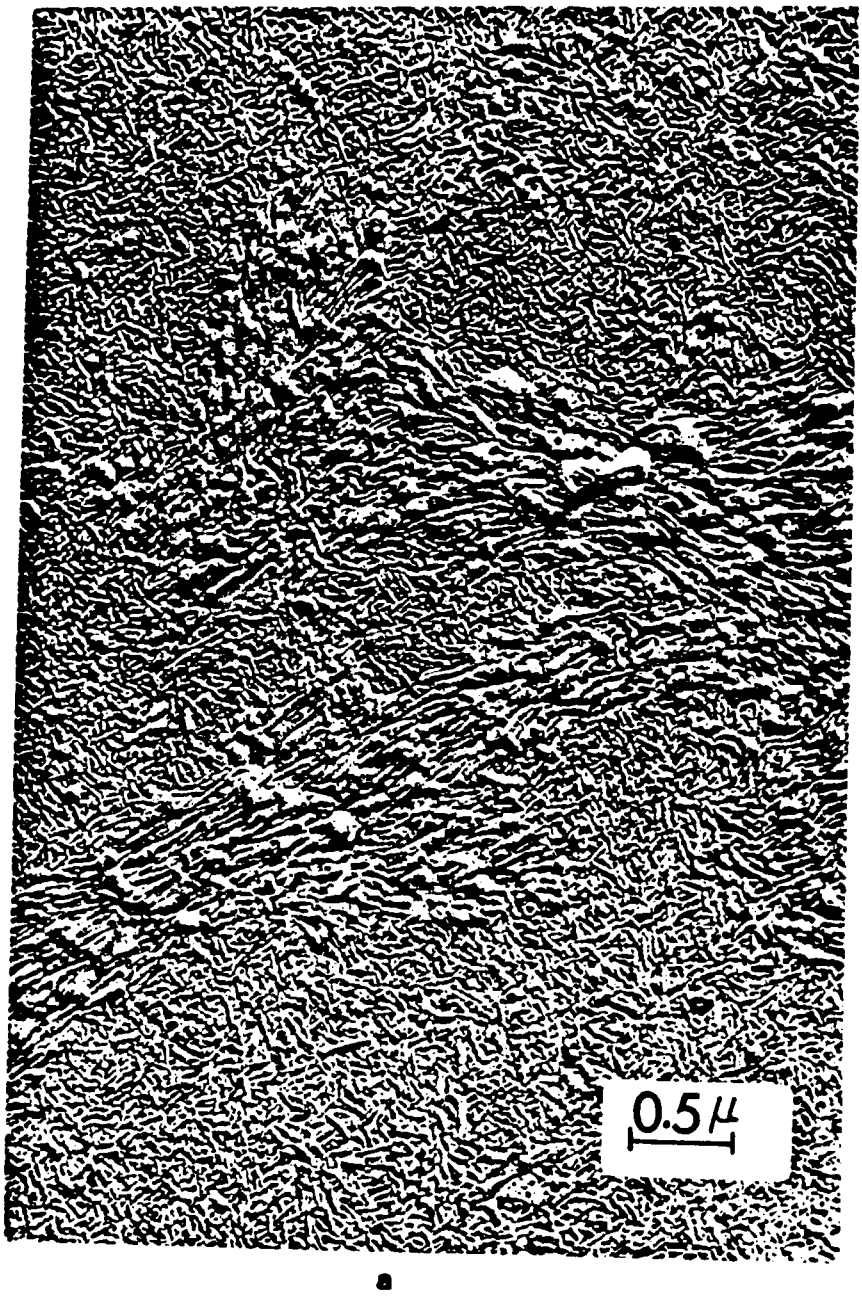

a

Figure 60 (a)(b) TEM pictures of 2 % XLPE crystallized at 92 °C for two hours.

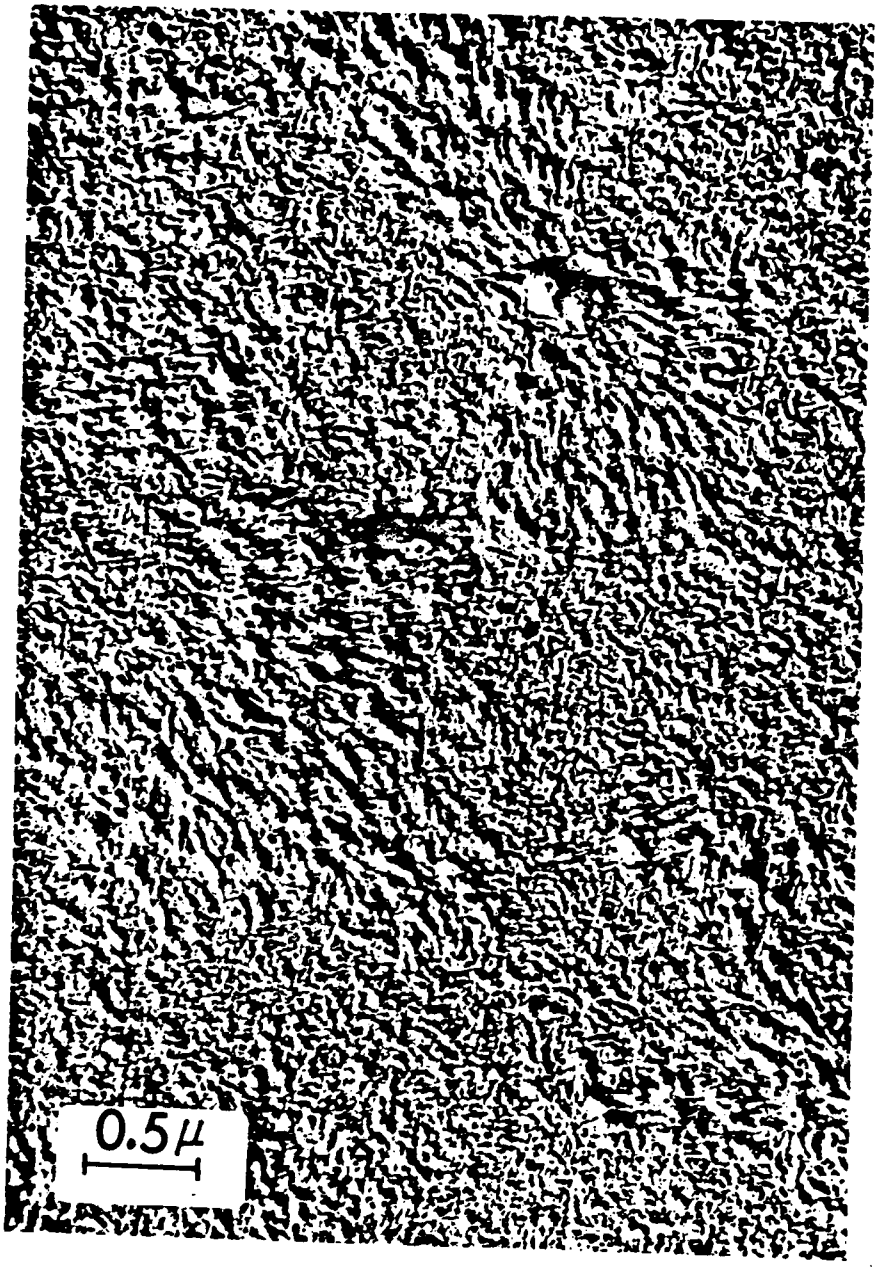

b

Figure 60 Continued

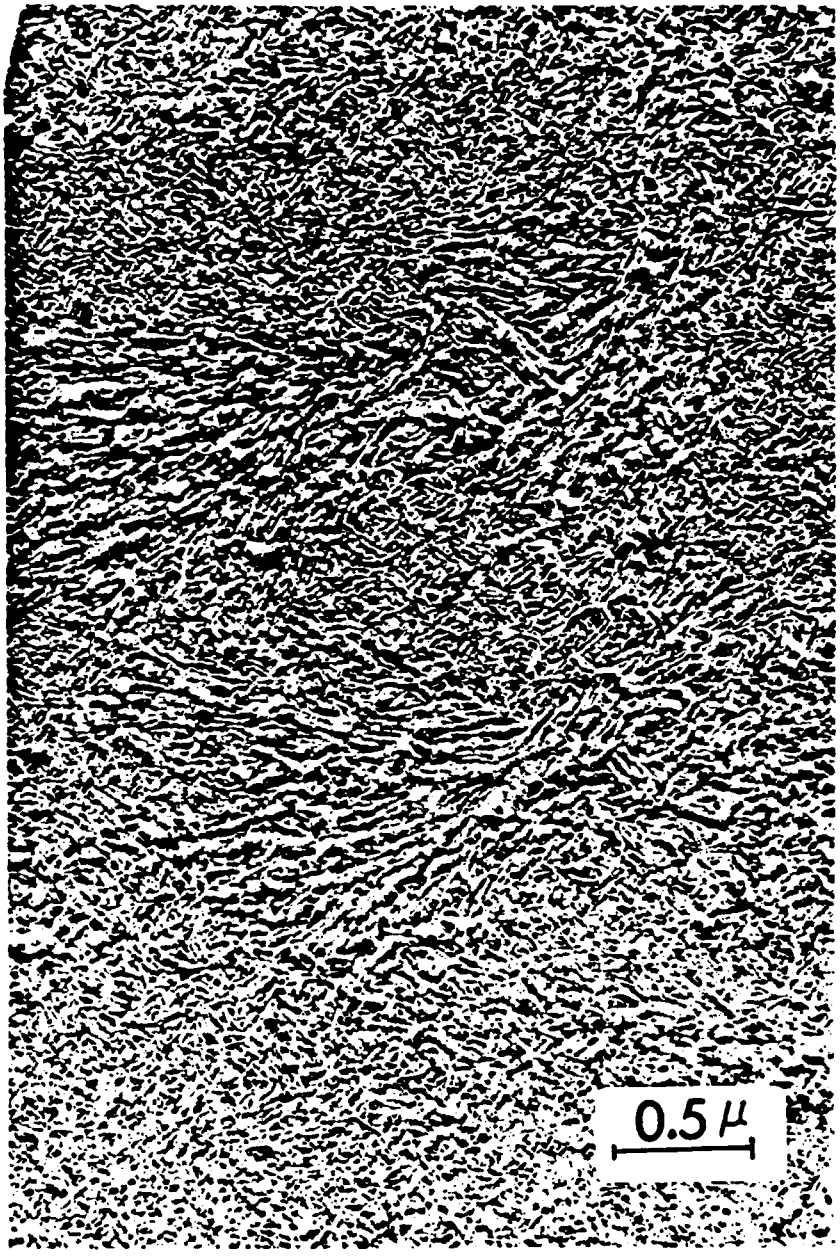

Figure 61 TEM picture of cable A1-8 crystallized at 92 °C for two hours.



a

Figure 62 (a)(b) TEM pictures of the inner radial section of original cable A1.



b

Figure 62 Continued



Figure 63 TEM picture showing worm-like lamellae with random orientation in the regions between sheaves for cable A1-8.

exist with random orientation (Figures 64a-b). The inner layer of cable E1 shows more detailed structure than the outer layer (Figures 65a-b). Sheaves this time are not completely isolated from the background, they are more or less interwoven, yet, sheaf centers are detectable. Micrographs from the inner section show spherical voids (Figure 65a-b) with a size distribution plotted in Figure 66.

The outer layer of dry cured cable C1 showed very well developed morphologies with banded sheaves and twisting lamellae (Figures 67a-b). S and C type lamellae are observable but not as extensively as they were observed in cable A1. Laboratory quenched samples of the outer layer of dry cured cable C1 did not show the characteristic banded sheaves observed in the cables in the as-processed condition (Figures 68a-b). The inner layers of this cable had smaller non-banded sheaves resembling those of the inner layer of steam cured cable (Figure 69). LDPE distribution cable D1 showed banded spherulitic structures (Figure 70) with a banding periodicity of 1-2 μm.

4.3. Thermally Aged Cables

4.3.1. DSC Studies

Iso-thermal annealing of cable specimens was carried out for various time intervals at temperatures of

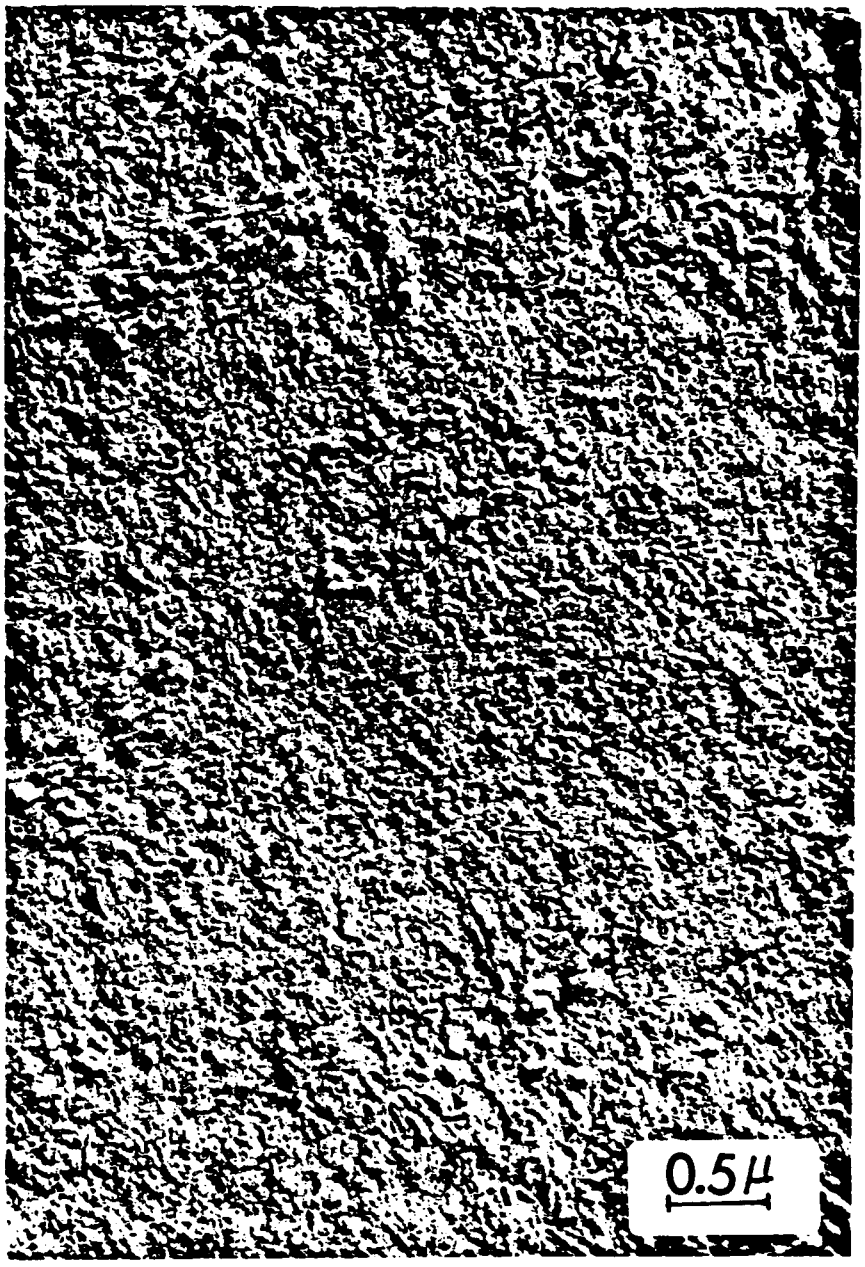

a

Figure 64 (a)(b) TEM pictures of the outer radial section of original cable E1.

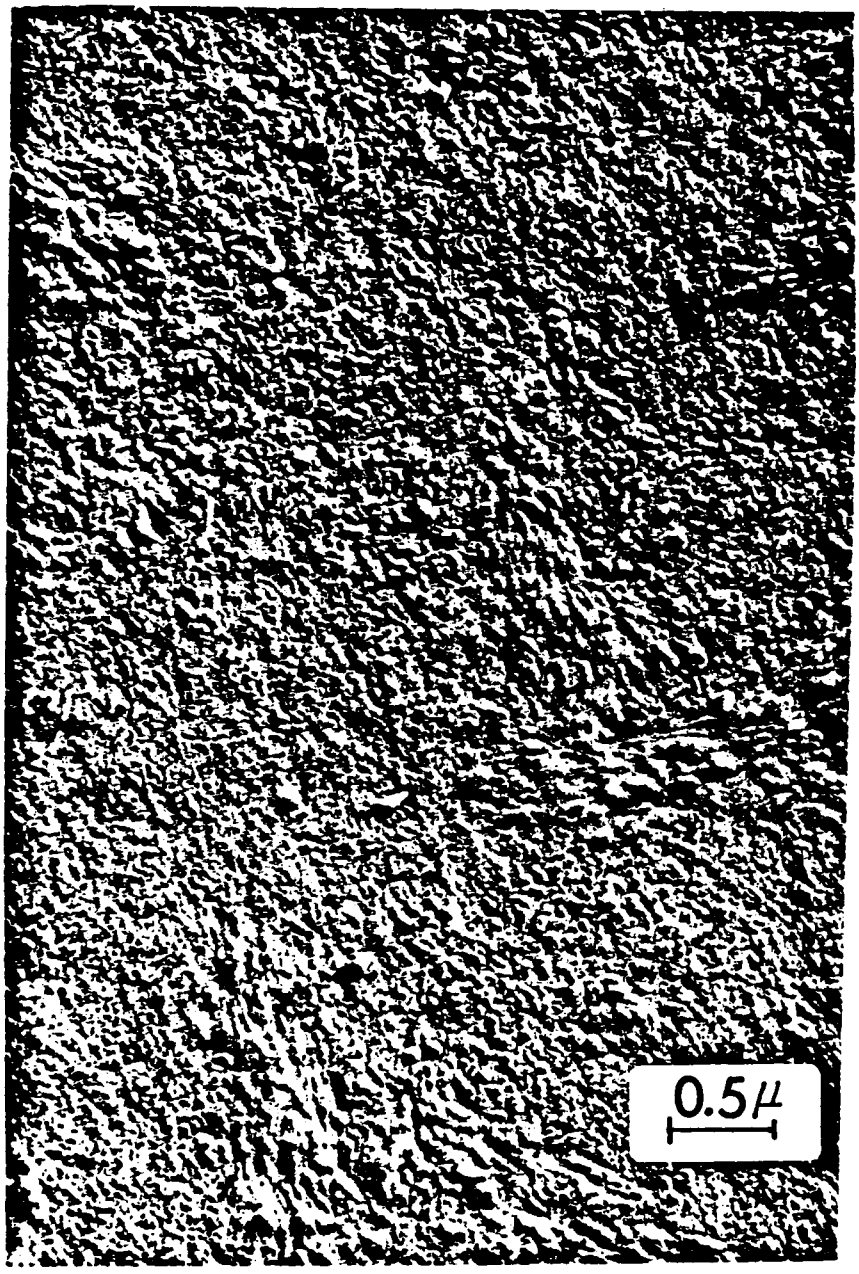

b

Figure 64 Continued



a

Figure 65 (a)(b) TEM pictures of the inner radial section of original cable E1.



b

Figure 65 Continued

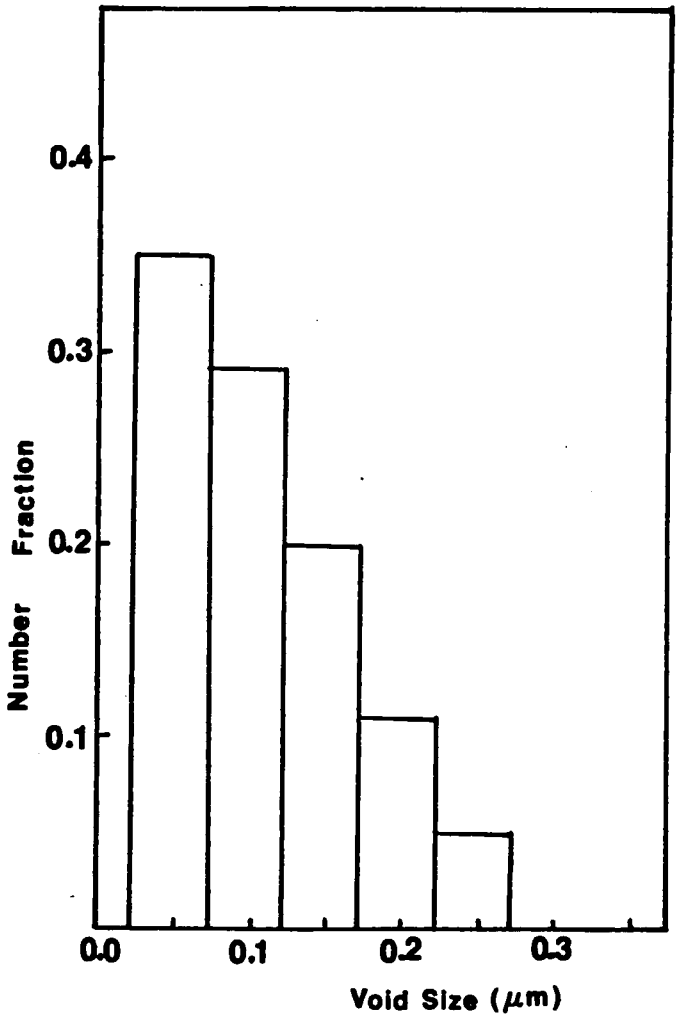

Figure 66 A histogram of the void size distribution of cable E1.

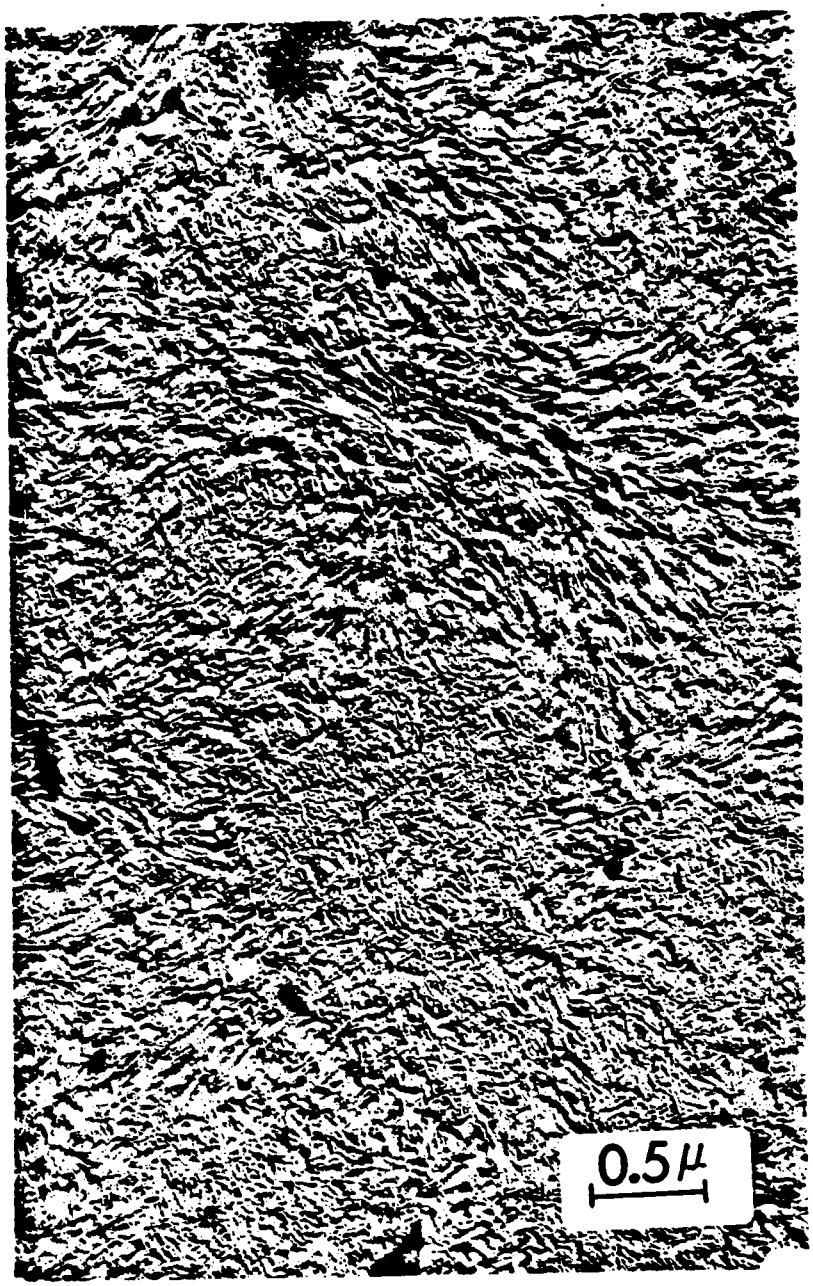

a

Figure 67 (a)(b) TEM pictures of the outer radial section of original cable C1.

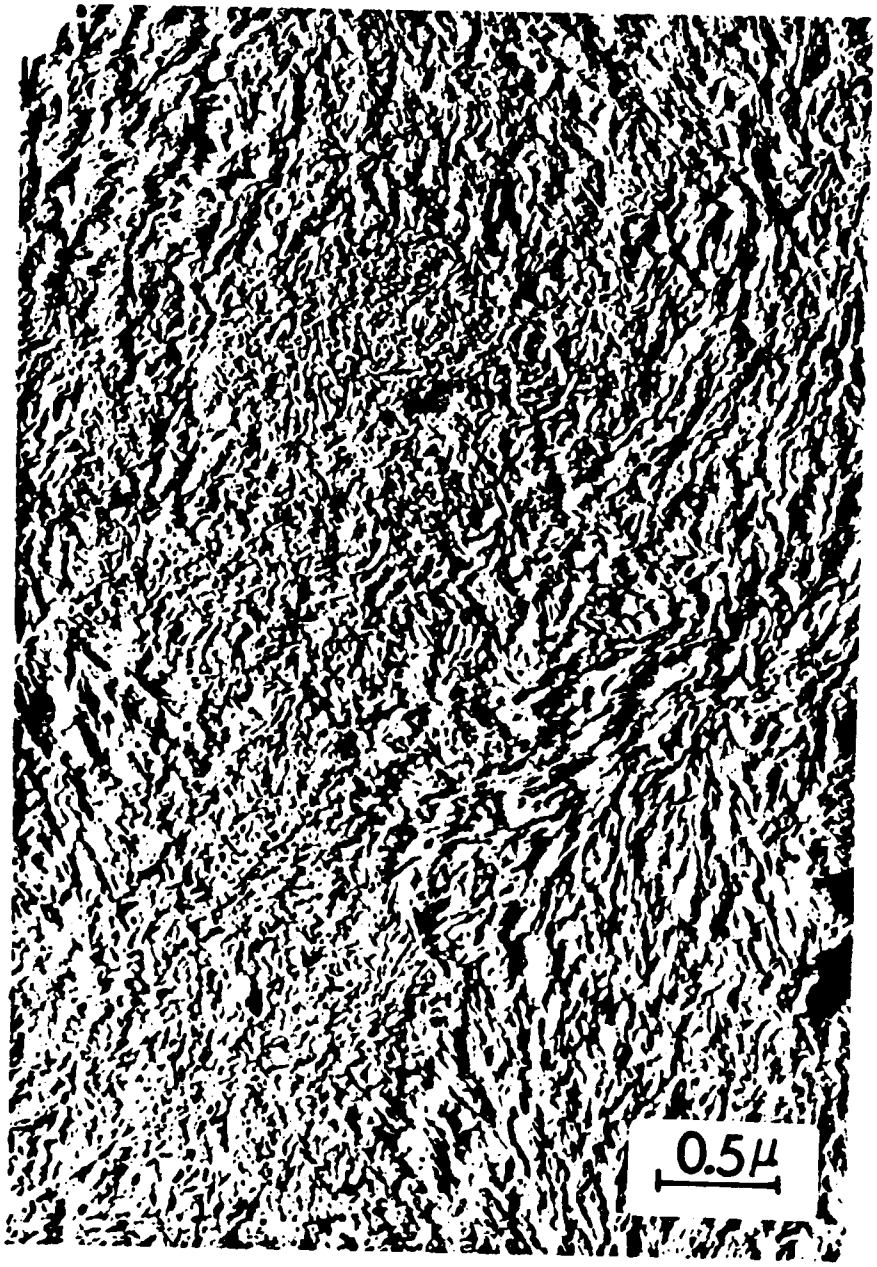

b

Figure 67 Continued

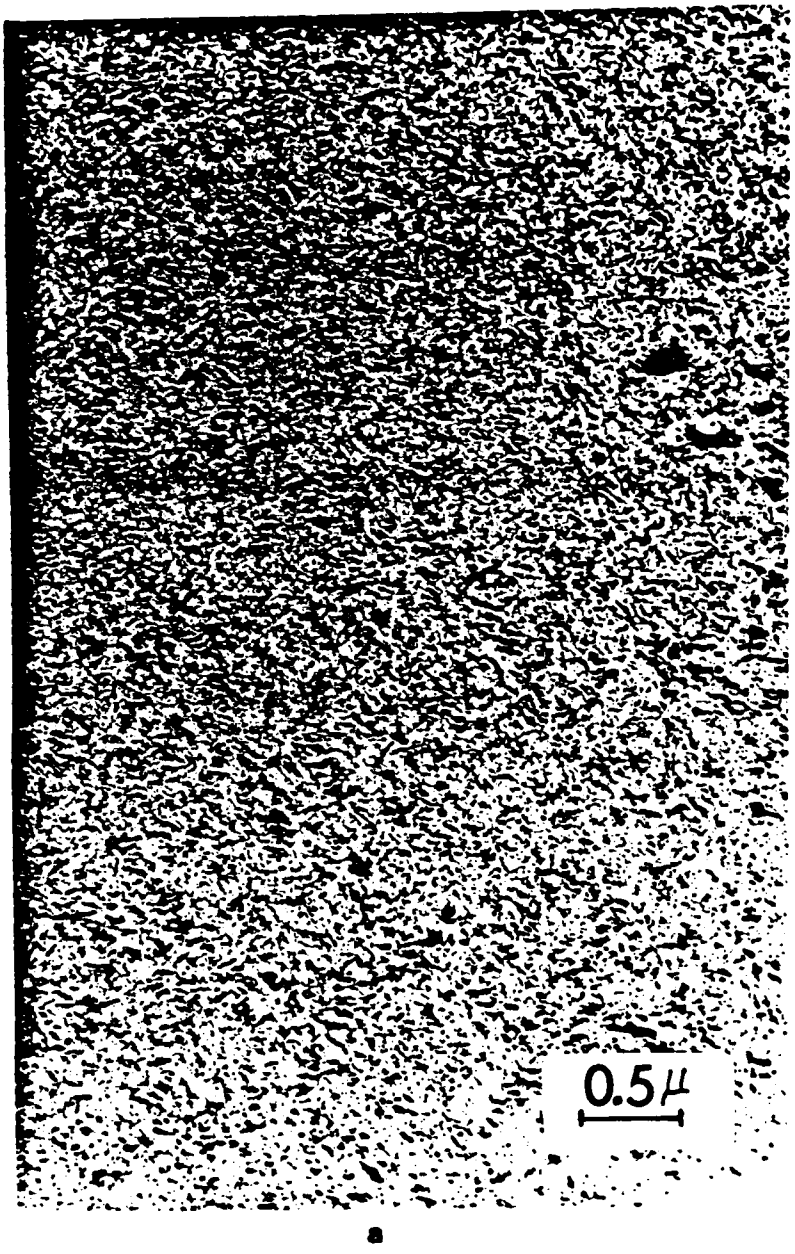

a

Figure 68 (a)(b) TEM pictures of the outer radial section of cable C1 after it was quenched from the melt.

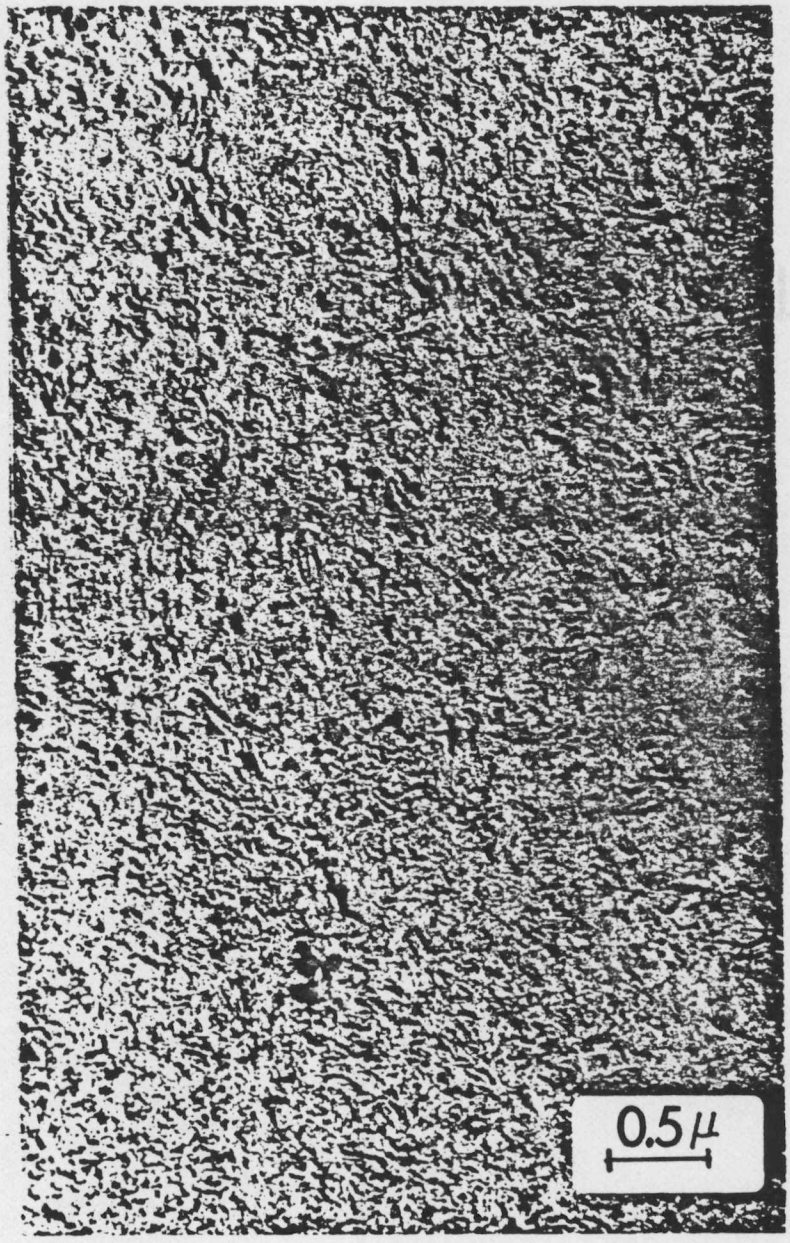

b

Figure 68 Continued



Figure 69 TEM picture of the inner radial section of original cable C1.

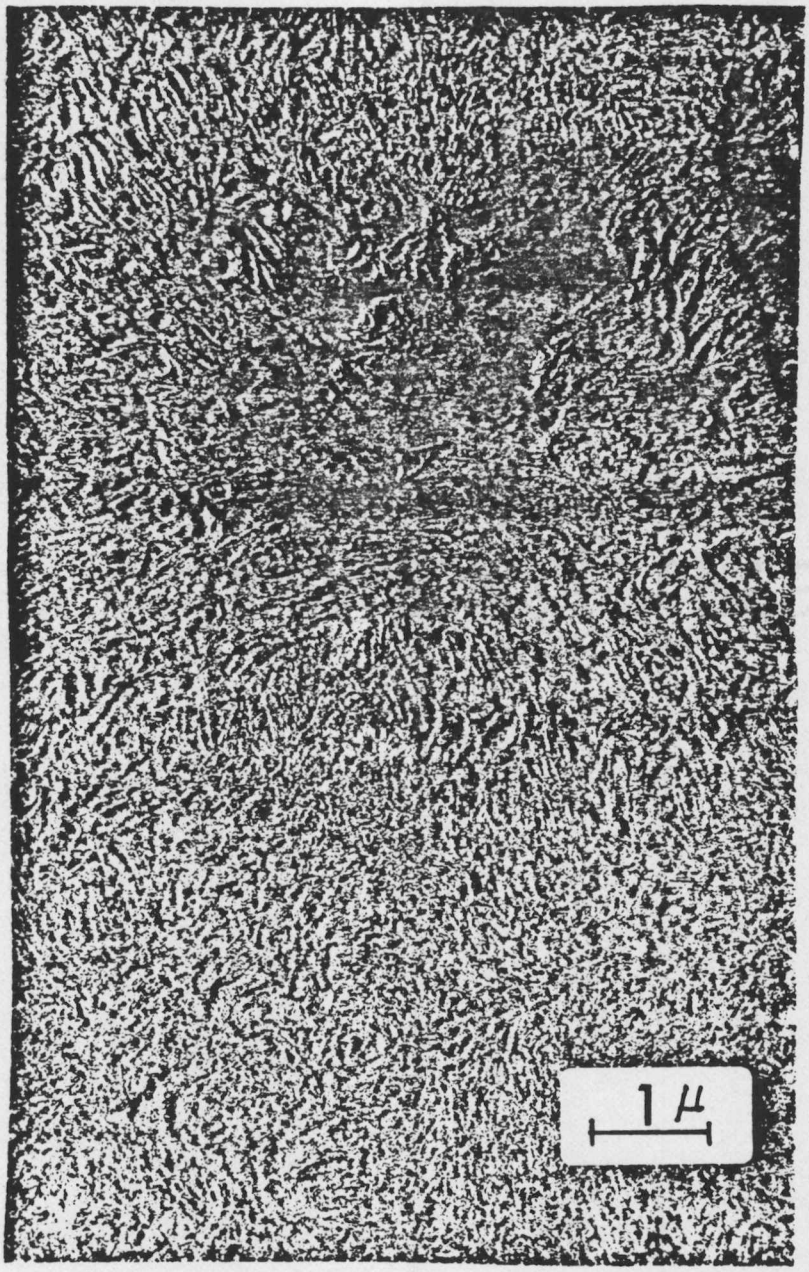

Figure 70 TEM picture of original distribution cable D1.

90, 92, 95, 97, 100, 103, 105 and 107 ^{o}C. In general, these annealing temperatures were separated into two major classes; above the melting point (103-107 ^{o}C) and below the melting point (90-100 ^{o}C) for all three major cables (A1, C1 and E1) having average melting points close to 103 ^{o}C. Comparative annealing behavior of each cable at these temperatures was established as well as a comparison of the behavior of the different radial sections of cable A1 having variable extractable contents. Figures 71-74 show the results of annealings carried out at 90, 92, 95 and 97 ^{o}C for the indicated periods of annealing times for the inner layer of cable A1. Comparative DSC thermograms obtained after two hour annealings are given in Figure 75. As can be seen from these figures, while the position of the major melting peak remains almost constant, a newly generated low temperature recrystallization peak advances to higher temperatures while increasing in magnitude. The major melting peak and the recrystallization peak are best resolved after 90 ^{o}C annealing.

A 1 to 1.5 % increase in overall crystallinity was observed for 90, 92 and 95 ^{o}C annealings while at 97 ^{o}C crystallinity was observed to remain unchanged compared to 50.5 % crystallinity of the corresponding section of the original cable after 24 hours of annealing. Peak position versus annealing time is given in Figure 76.

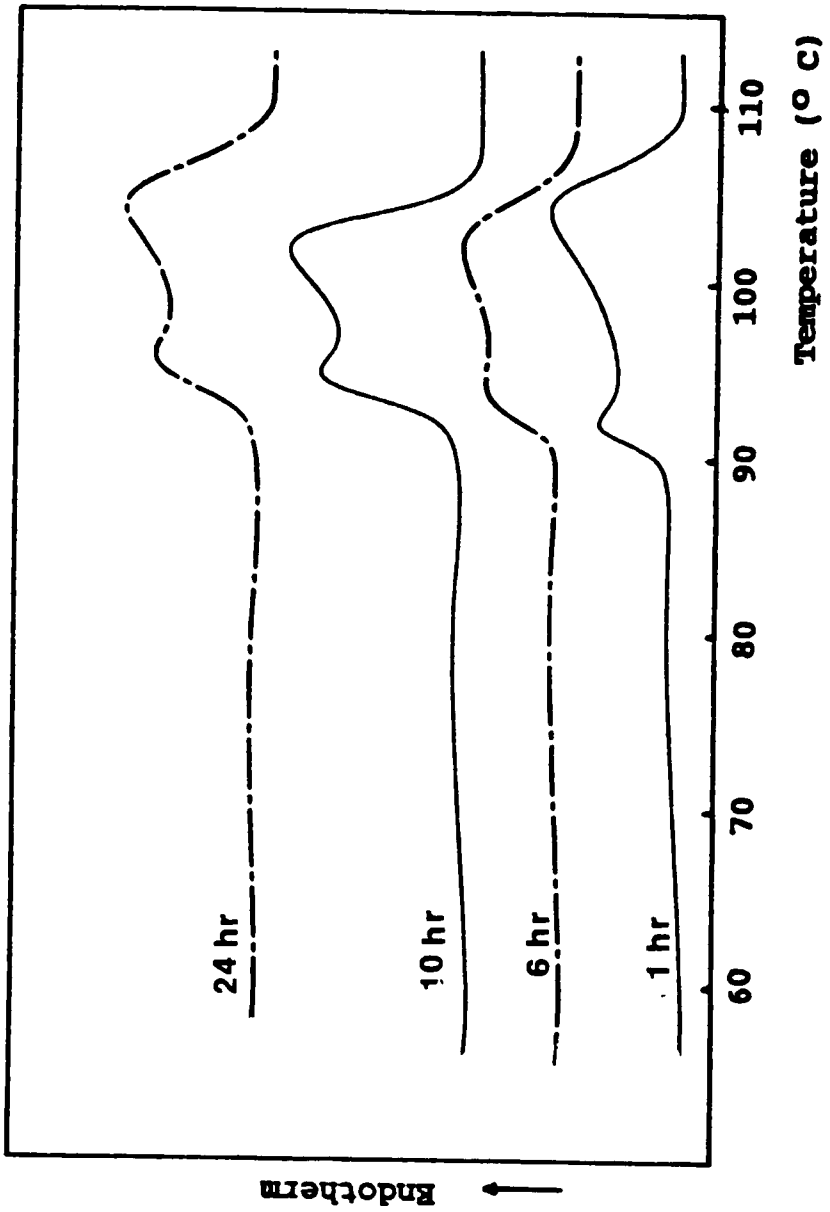

Figure 71 DSC thermograms obtained from the inner radial section of cable A1 annealed at 90 °C for the indicated periods of time.

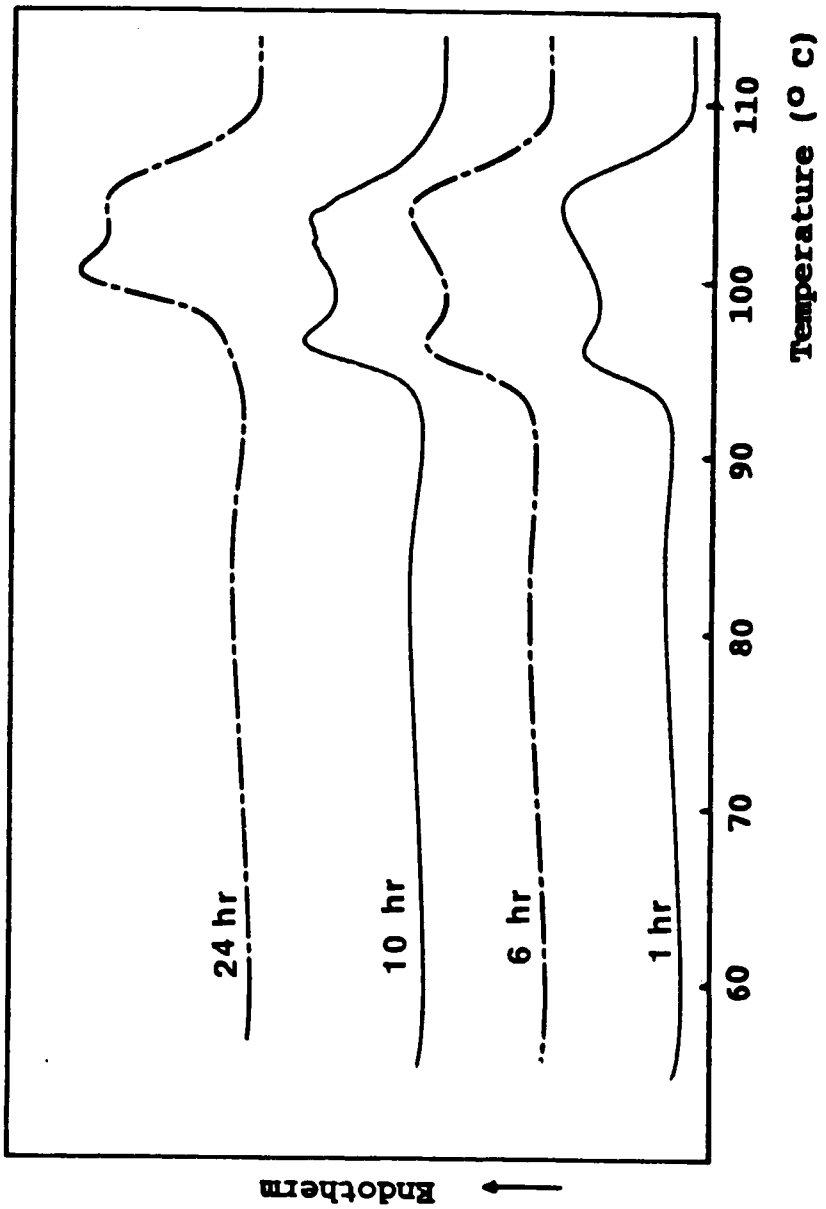

Figure 72 DSC thermograms obtained from the inner radial section of cable A1 annealed at 92 °C for the indicated periods of time.

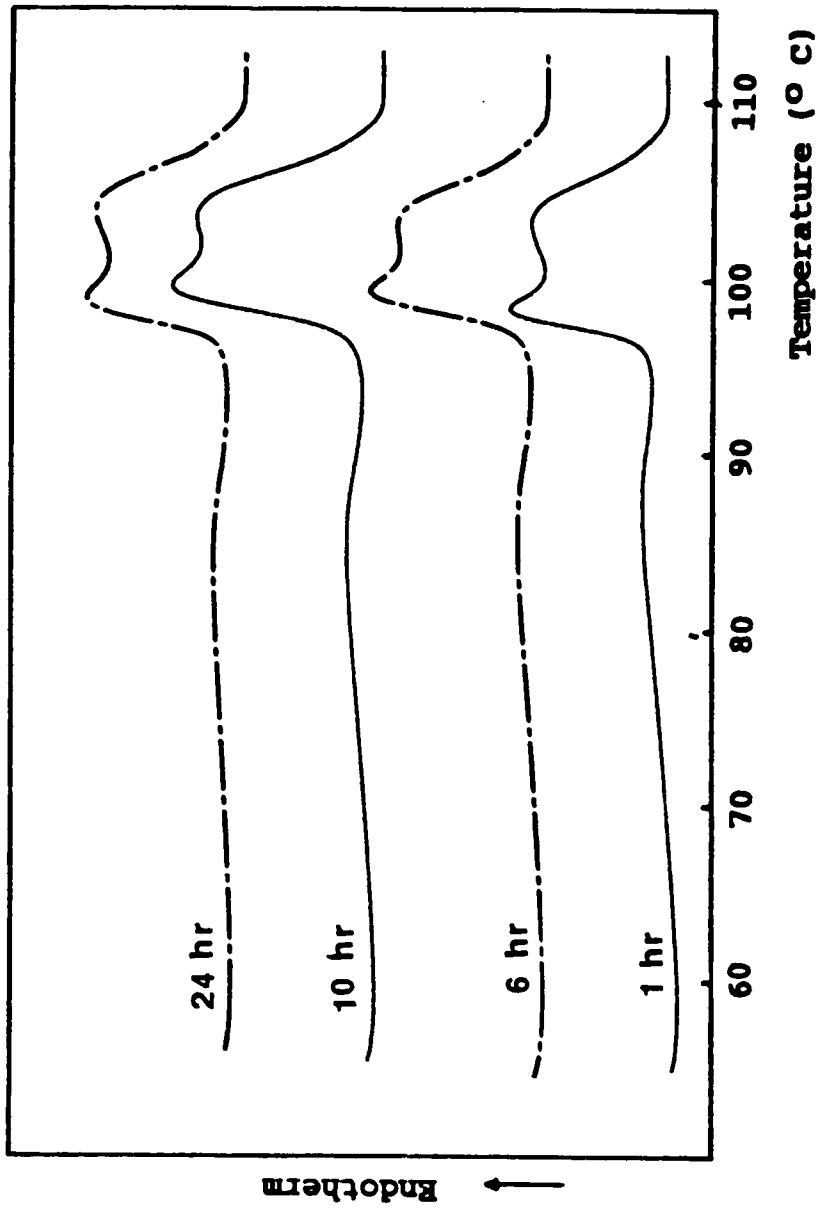

Figure 73 DSC thermograms obtained from the inner radial section of cable A1 annealed at 95 °C for the indicated periods of time.

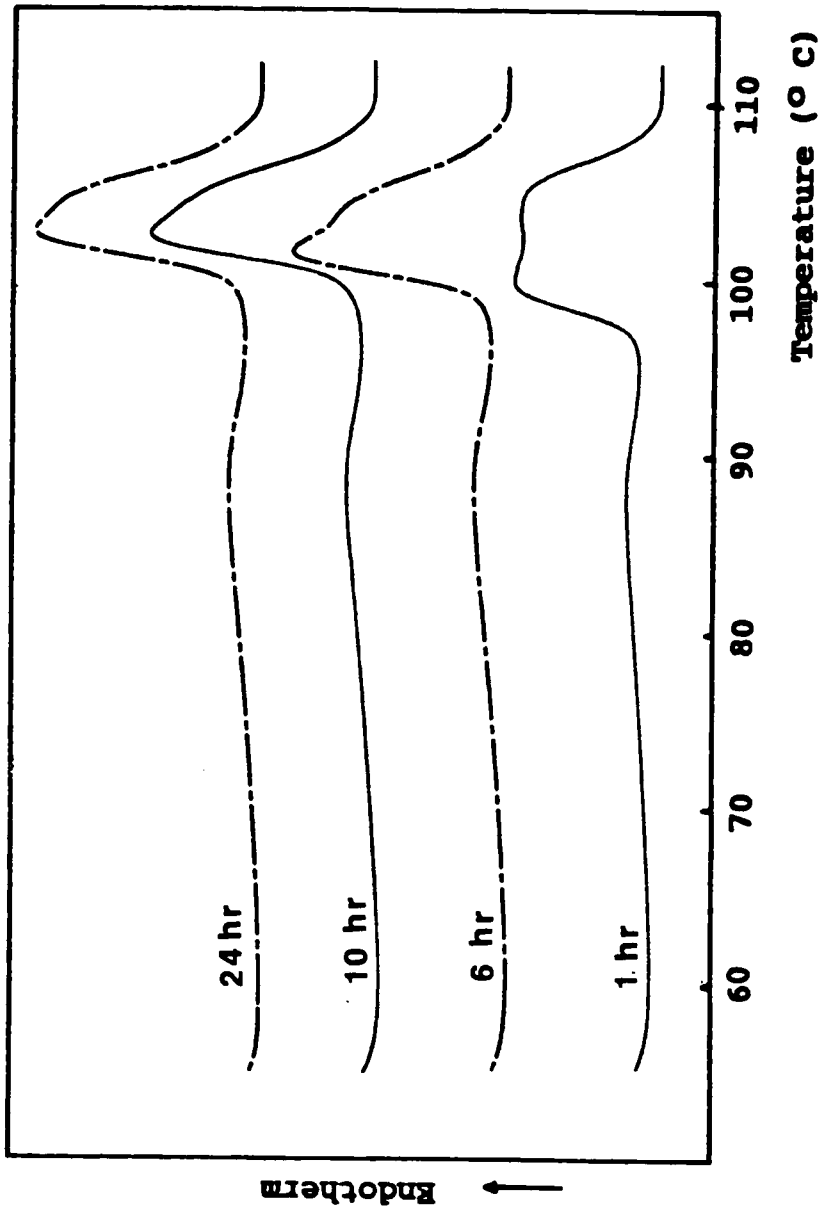

Figure 74 DSC thermograms obtained from the inner radial section of cable A1 annealed at 97 °C for the indicated periods of time.

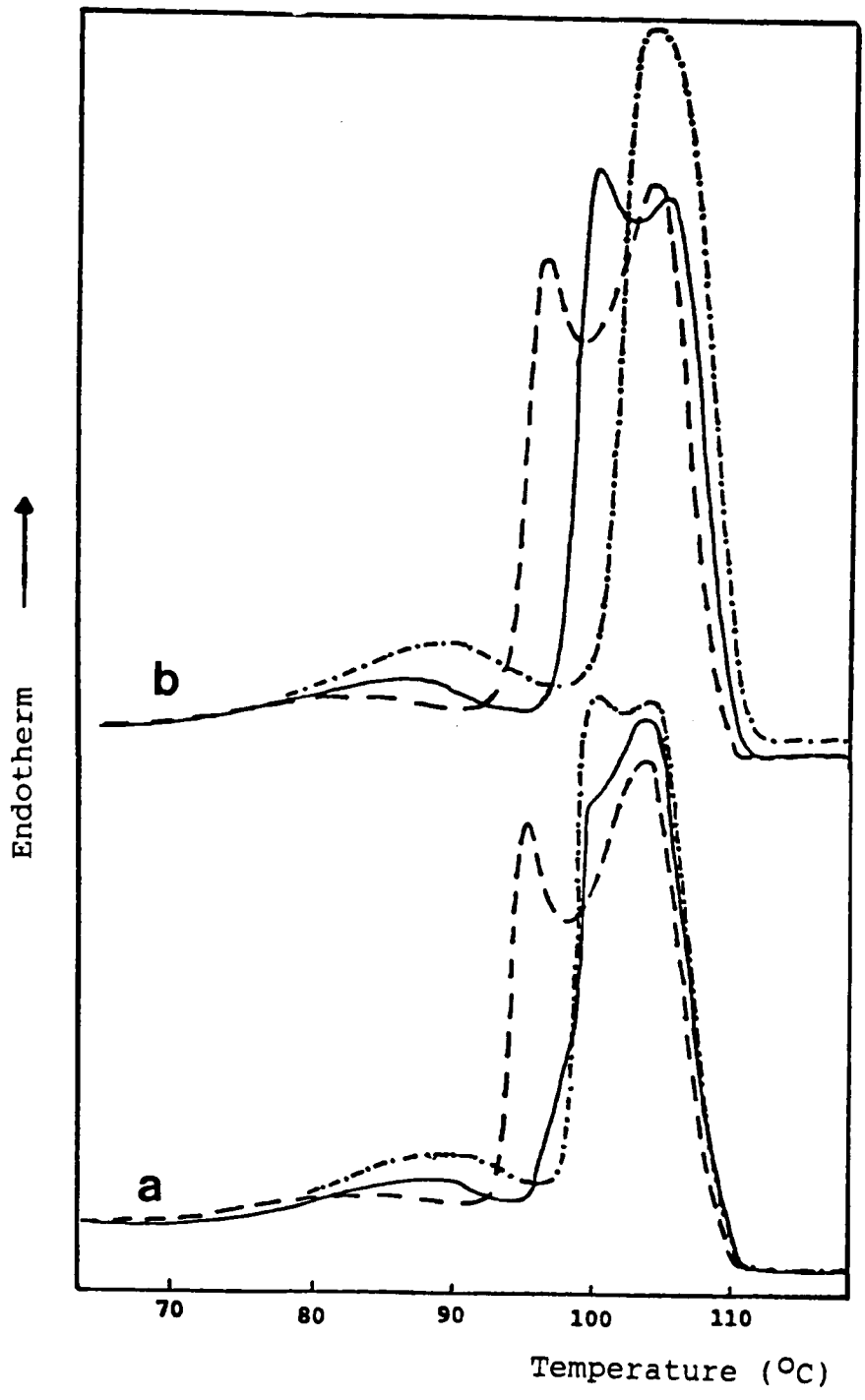

Figure 75 Comparative DSC thermograms obtained for cable A1 after annealing at (---) 92 °C, (____) 95 °C, (-·-·-) 97 °C for (a) two hours (b) ten hours.

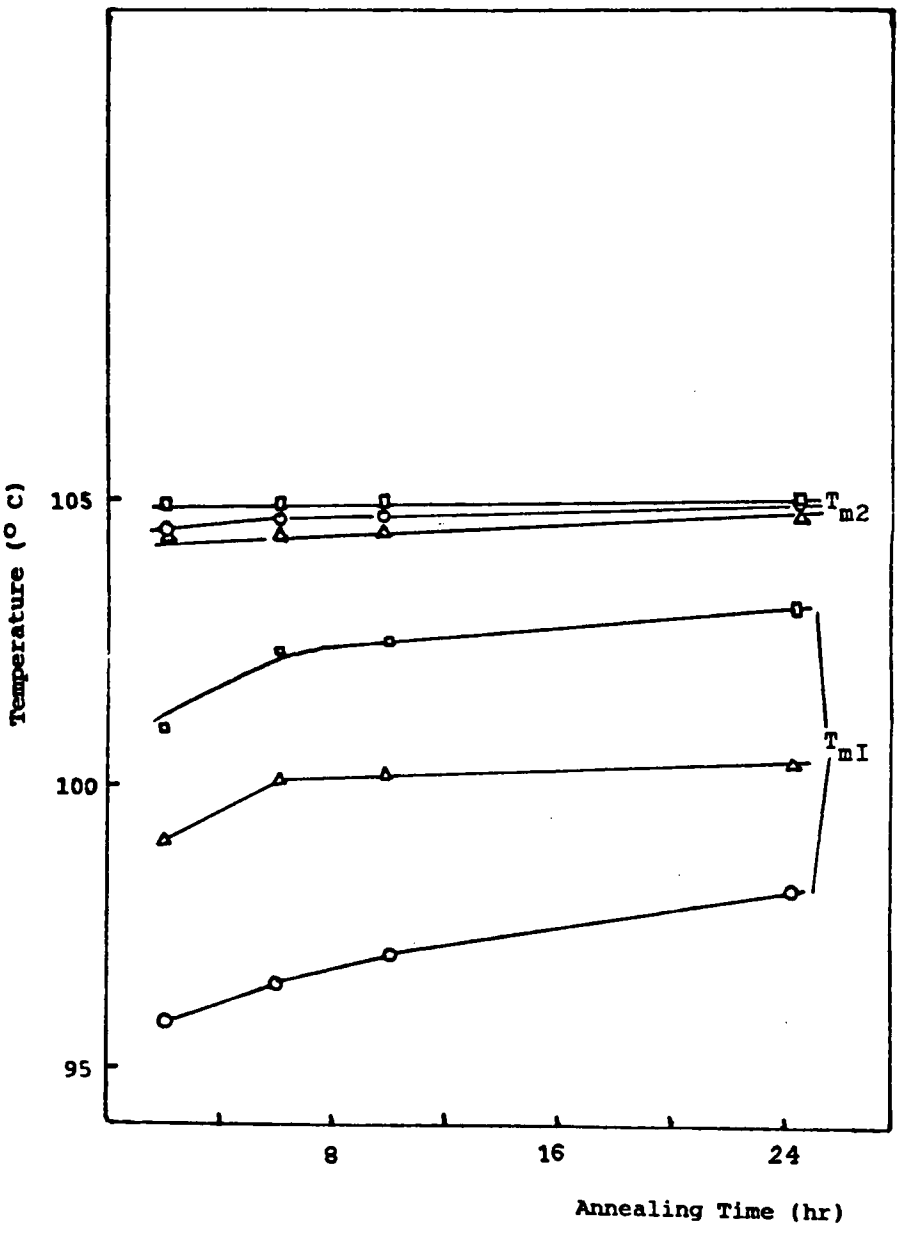

Figure 76 Melting peak temperatures as a function of annealing time for cable A1 annealed at (O) 92, (Δ) 95 and (□) 97 °C.

DSC thermograms obtained at annealing temperatures between T_m and T_{rb} are quite different in shape from the ones obtained below T_m. Comparative DSC curves obtained from high temperature annealings are given in Figure 77. Instead of the two overlapping peaks observed at lower annealing temperatures, two well separated peaks are generated. A broad peak appears at temperatures lower than the annealing temperature and a sharp narrow peak occurs above the annealing temperature.

As the annealing temperature drops from 107 ^{o}C to 100 ^{o}C, the breadth of the sharp peak increases and reaches a maximum at 100 ^{o}C annealing. The breadth of the high temperature peak, at half maximum, for 60 min annealings at 100, 103, 105 and 107 ^{o}C is given in Figure 78. For 107 ^{o}C annealings the position and the breadth of the high temperature peak was found to be stabilized after two days of annealing (Figure 79). The positions of the low and high temperature peaks obtained at high temperature annealings, 103, 105 and 107 ^{o}C, as a function of annealing time are given in Figure 80. The magnitude of the high temperature peak as a function of annealing time for 103, 105 and 107 ^{o}C annealings is given in Figure 81 along with similar data for Cable E1. Figure 82 presents the change in the magnitude of the high temperature peak at 107 ^{o}C for extended periods of annealing. The overall crystallinity was found not to

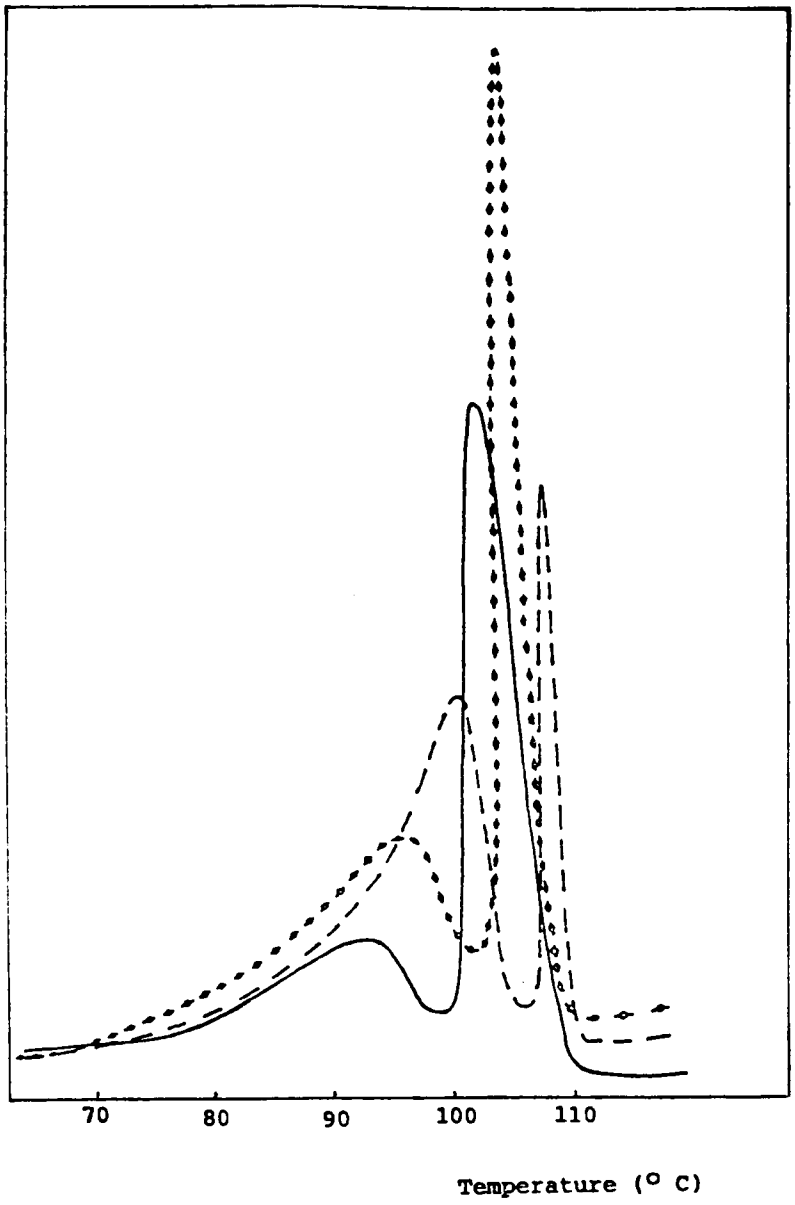

Figure 77 DSC thermograms obtained from the inner radial section of cable A1 annealed at (——) 100 °C, (•••) 103 °C and (– – –) 107 °C for one hour.

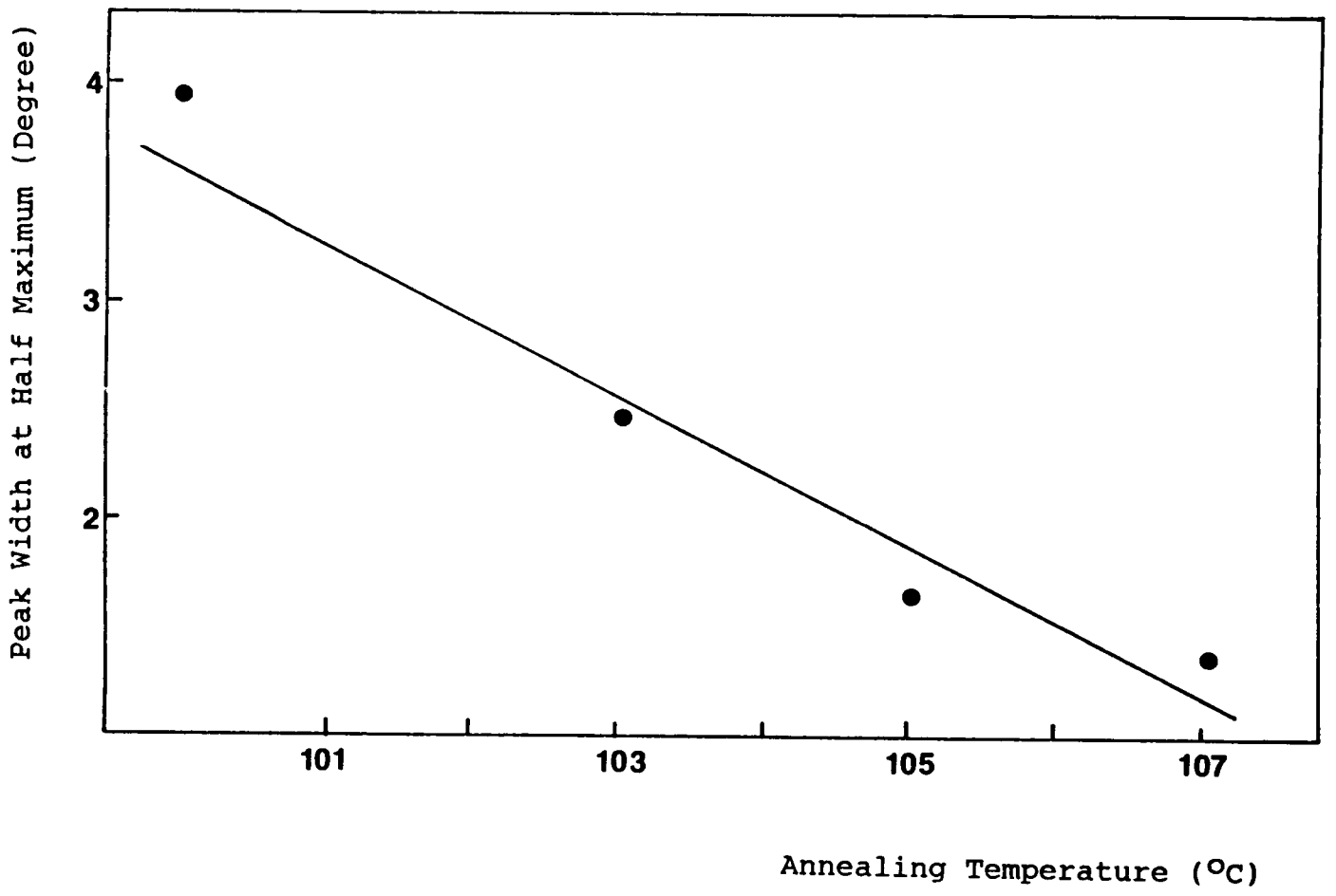

Figure 78 High temperature peak width at half maximum versus annealing temperature.

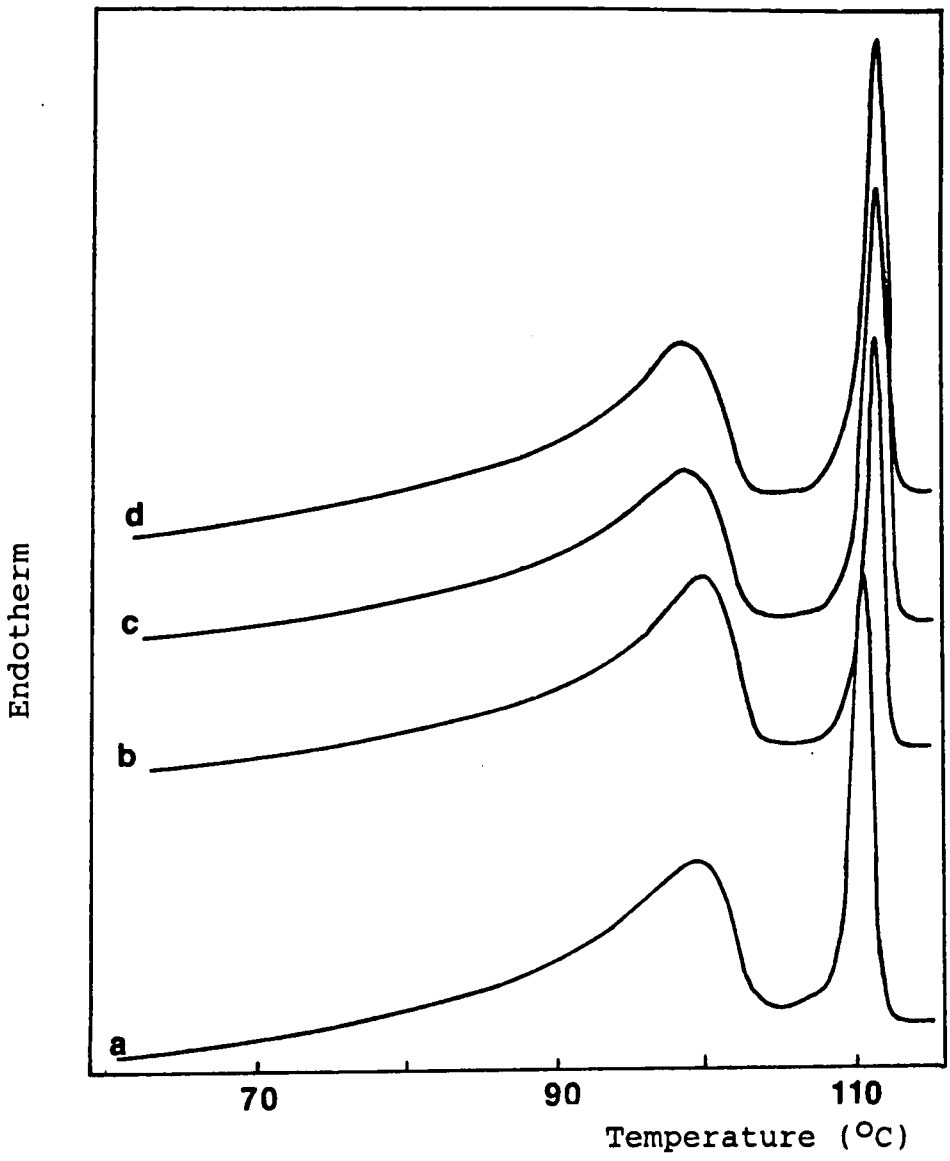

Figure 79 DSC thermograms obtained from the inner radial section of cable A1 after annealing at 107 °C for (a) 2, (b) 7, (c) 15 and (d) 21 days.

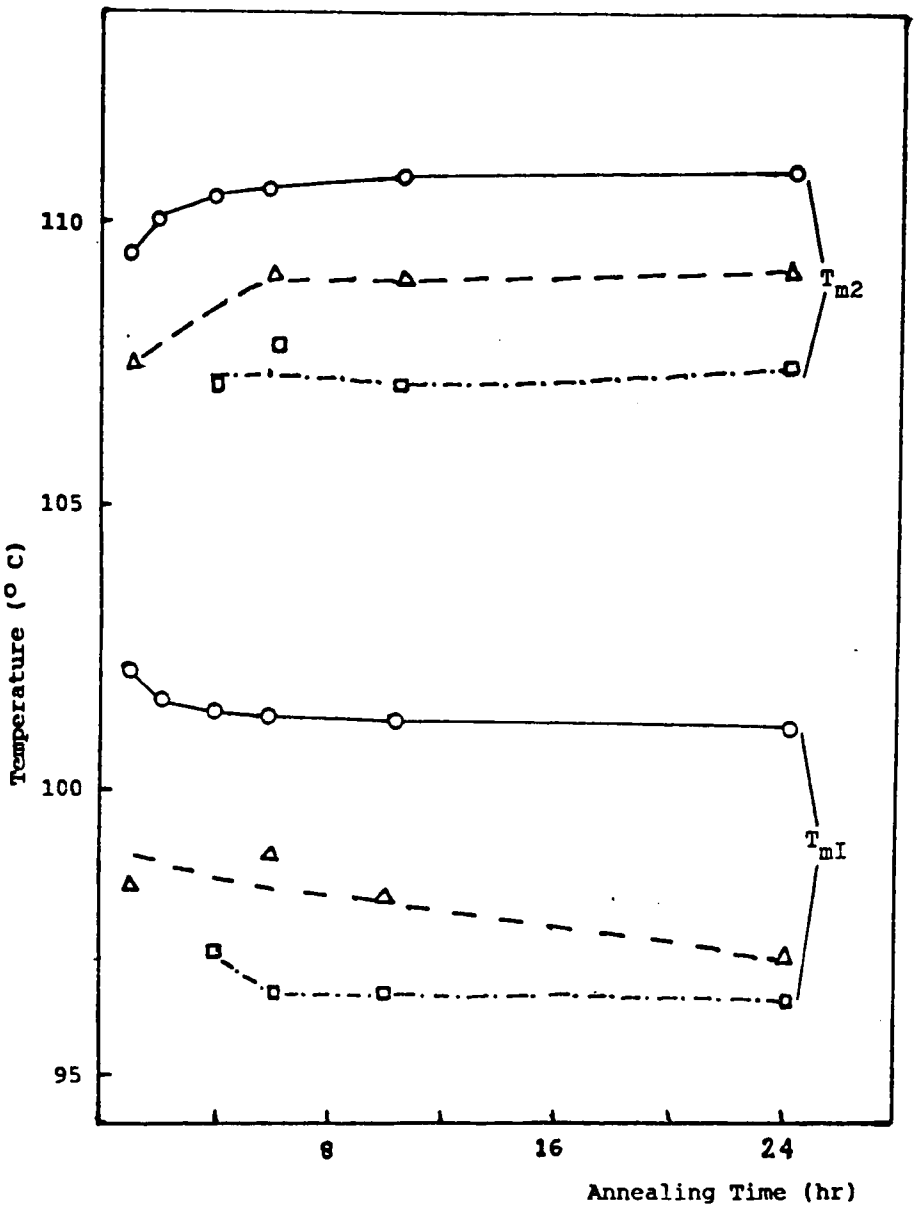

Figure 80 Melting peak temperatures as a function of annealing time for cable A1 annealed at (□) 103, (Δ) 105 and (○) 107 °C.

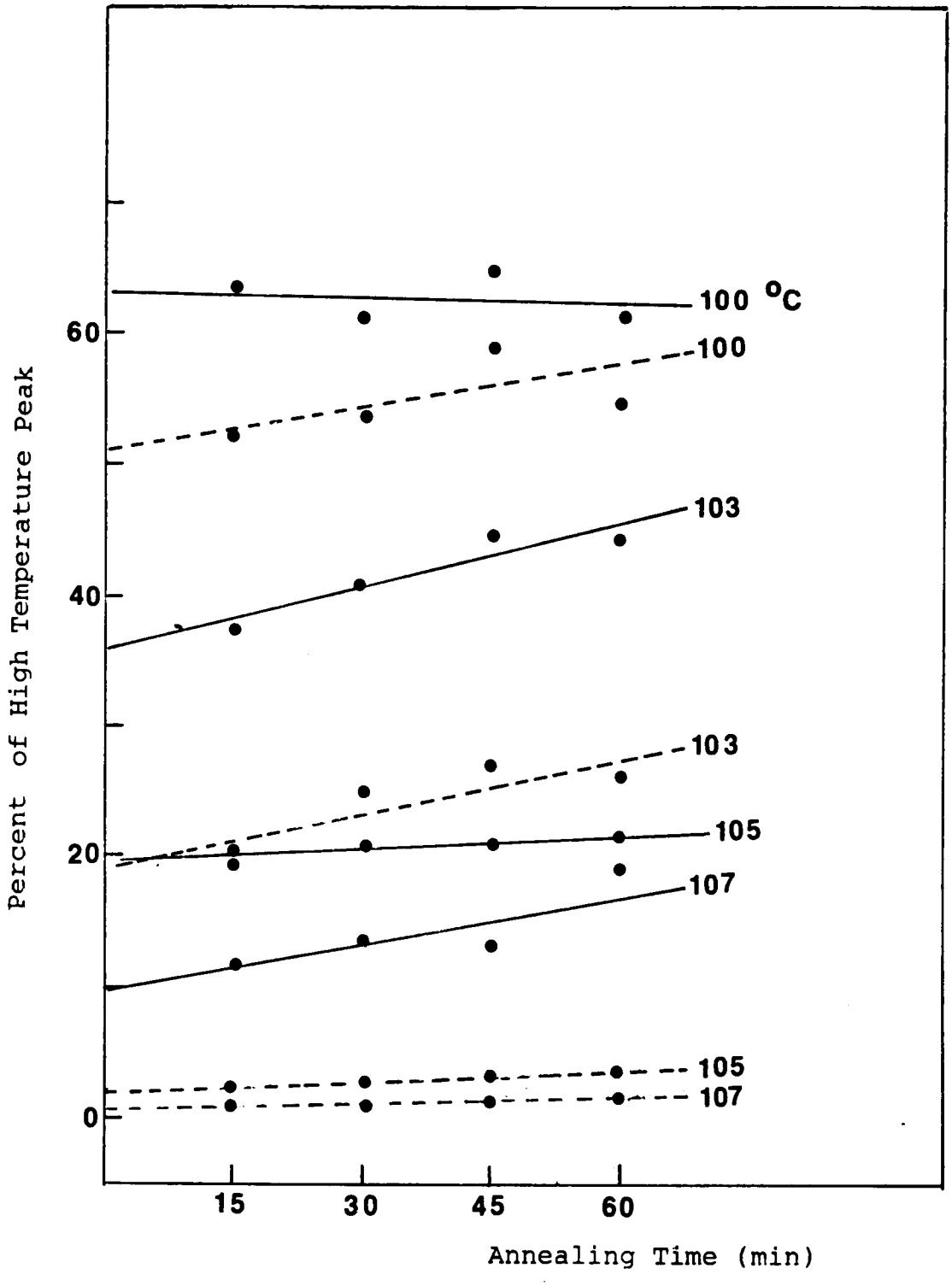

Figure 81 Percentage of high temperature peak as a function of annealing time for cables A1 (——) and E1 (---) at indicated temperatures.

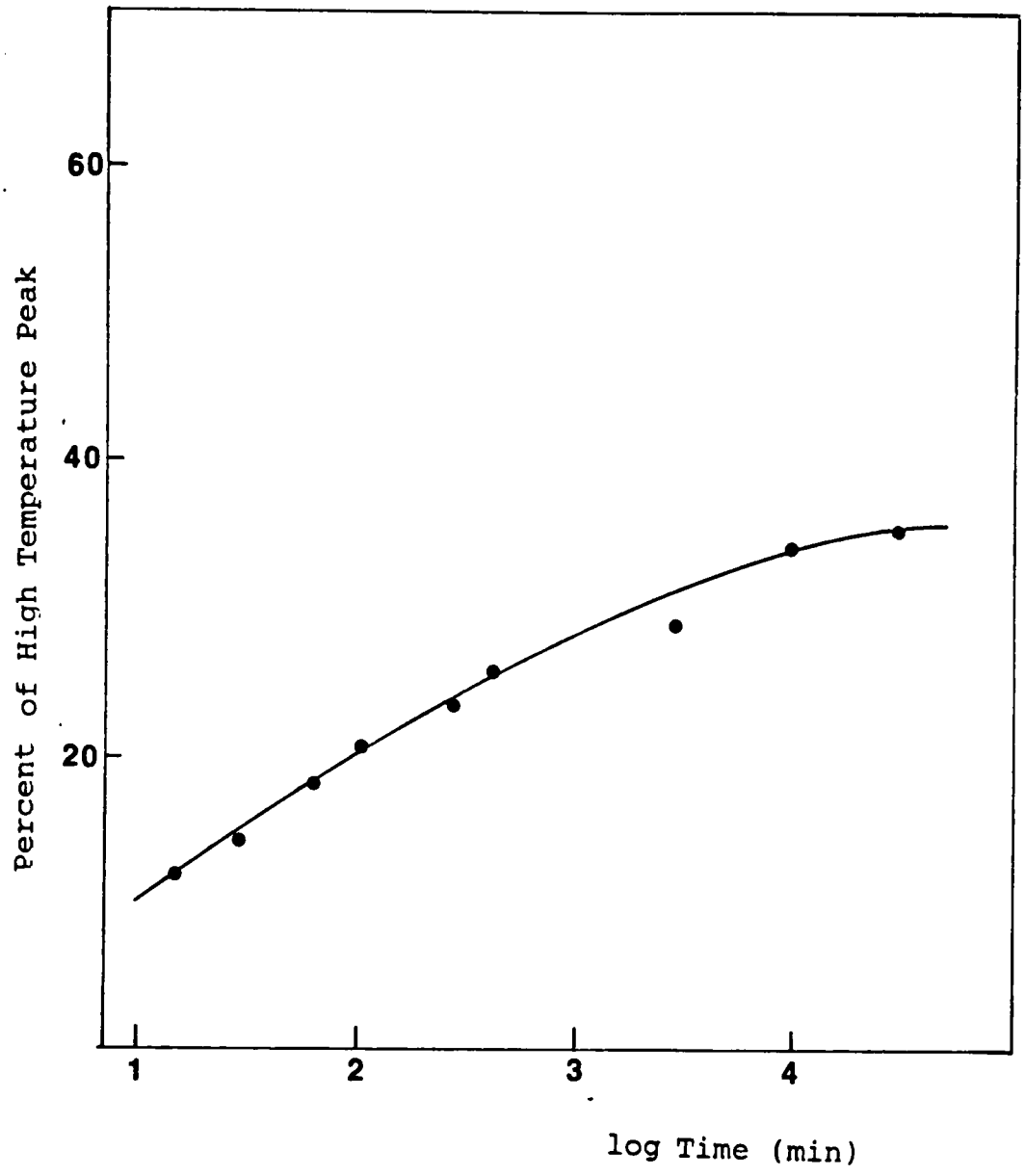

Figure 82 Percent of high temperature peak as a function of time for cable A1 annealed at 107 °C.

change compared to the corresponding section of the original cable (ca 50.5 %) after 100, 103, 105 and 107 ^{o}C annealings.

DSC analyses of the outermost layer of cable A1 annealed at 90, 92, 95 and 97 ^{o}C essentially resulted in similar DSC curves to those observed for the innermost layer. Figure 83 shows comparative curves for cable A1-1 and cable A1-8 at these temperatures after 60 minute annealings. The change in the peak temperatures as a function of annealing time is given in Figure 84 for the indicated annealing temperatures.

A similar comparison of the outer and inner layers of cable A1 was carried out for the higher annealing temperatures and comparative DSC curves are plotted in Figure 85 for 60 minute annealings at 100, 103 and 107 ^{o}C. The magnitude of the high temperature peak obtained from 107 ^{o}C annealing comprises 18 % of the total crystallinity of the inner layer, while it only accounts for 3-4 % of the total crystallinity of the outer layer. The positions of the high temperature peaks as a function of annealing time are plotted in Figure 86. The high temperature peak position appeared to be affected mainly by 100 ^{o}C annealing. For annealing at 107 ^{o}C the peak position did not change.

Similar annealing studies were carried out for periods of up to two hours for the gel fraction obtained from the inner layer of cable A1. Comparative DSC curves obtained from the inner section of the original cable A1 and

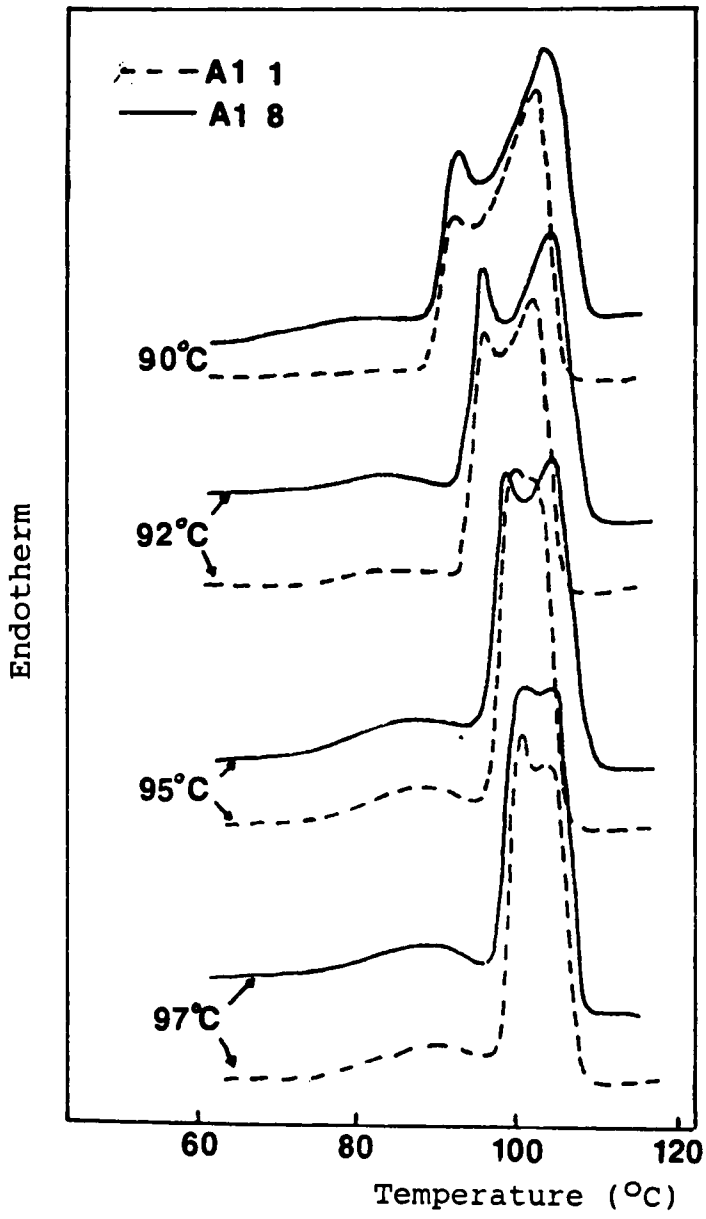

Figure 83 DSC thermograms of the outermost and innermost radial sections of cable A1 annealed at 90, 92, 95 and 97 °C for one hour.

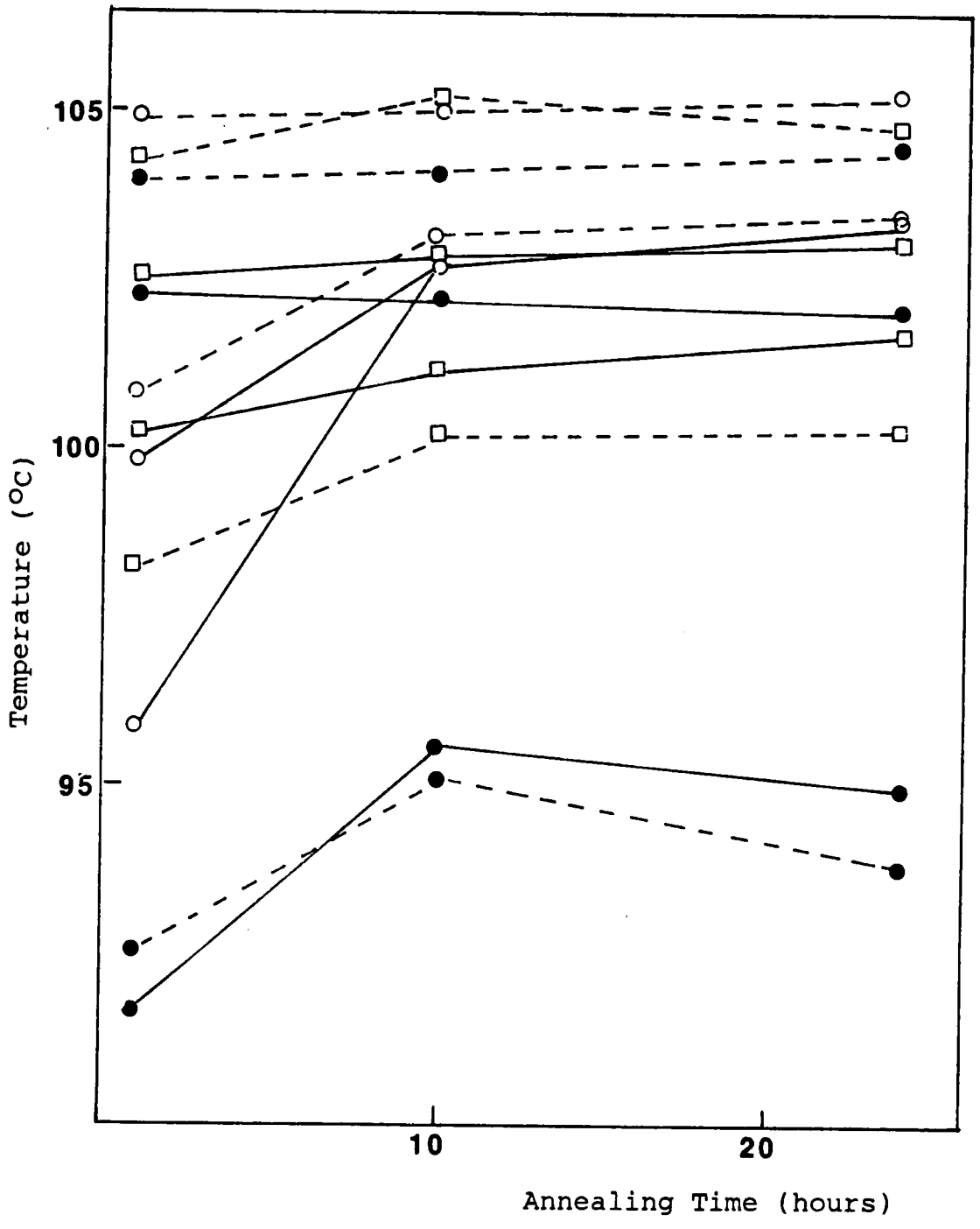

Figure 84 Melting temperatures as a function of annealing time for the outermost and innermost layers of cable A1 at (●) 90, (□) 95 and (○) 97°C.

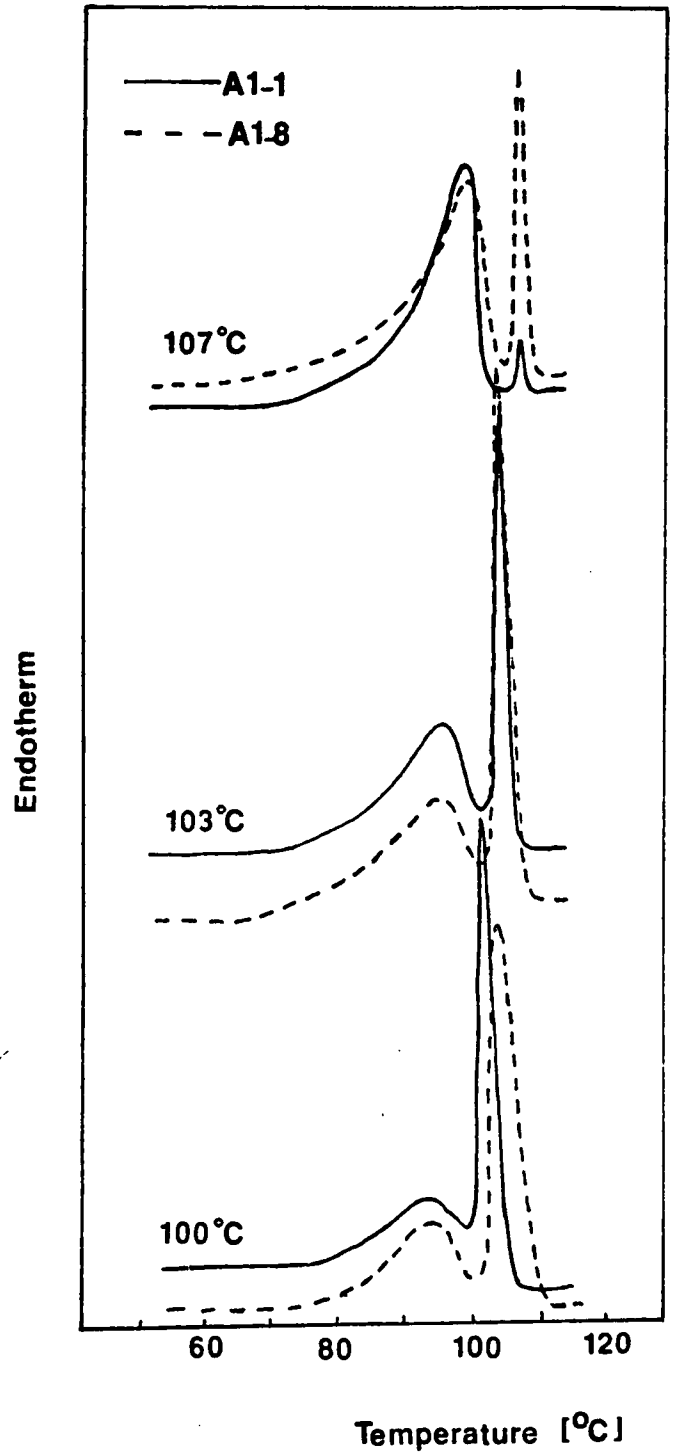

Figure 85 DSC thermograms of the outermost and innermost radial sections of cable A1 annealed at 100, 103 and 107 °C for one hour.

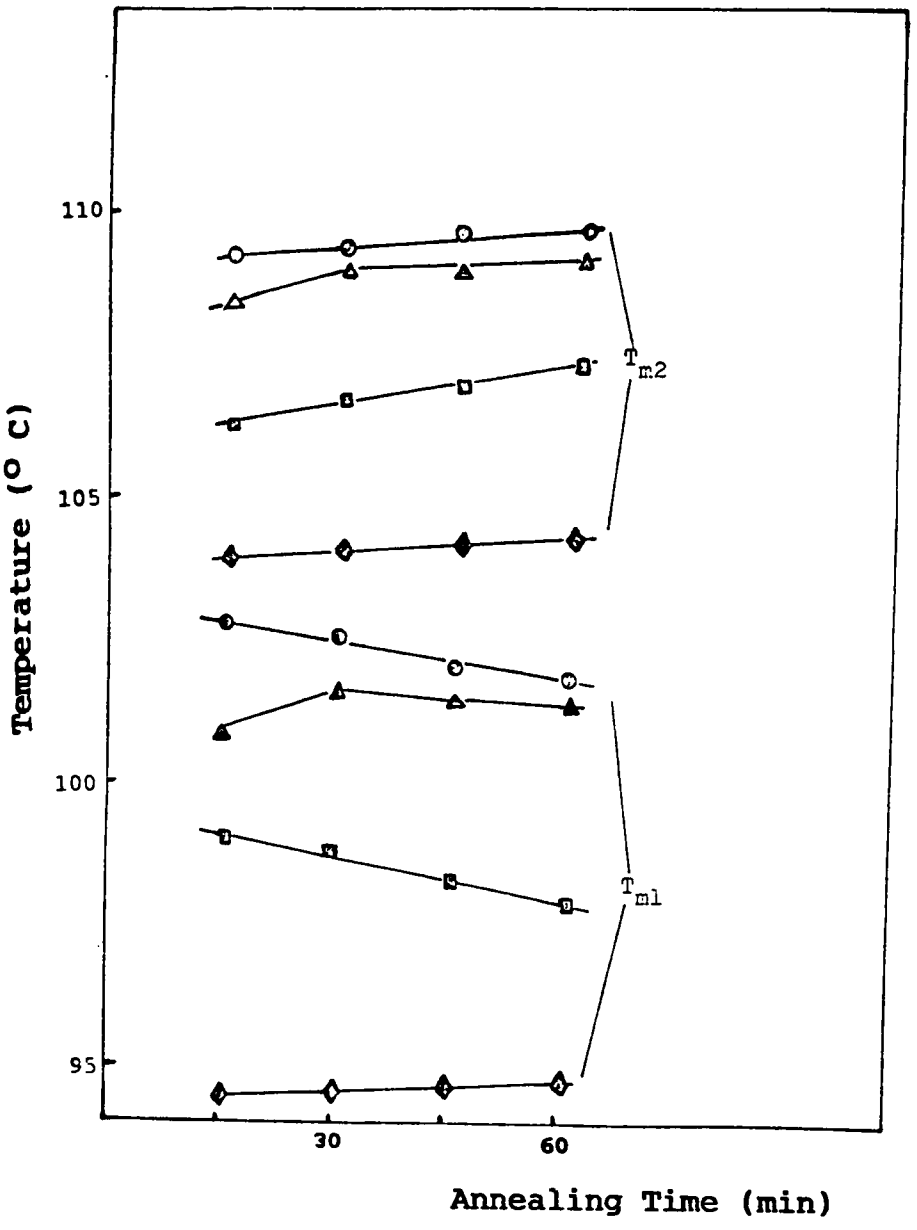

Figure 86 Melting temperatures as a function of annealing time for the outermost and innermost radial sections of cable A1 annealed at (♦) 100, (■) 103, (▲) 105 and (●) 107 °C for one hour.

from the gel fraction of this section are shown in Figures 87 and 88 for 60 minutes annealing at temperatures of 92, 95, 97, and 100,103 and 105 ^{o}C, respectively. Peak temperatures of the DSC thermograms obtained in low and high temperature annealings for cable A1-8 and A1-8G (gel of A1-8) are given in Figures 89 and 90. Merging of the two overlapping peaks was observed to be faster for the gel fraction. The major melting peak was found to decrease in magnitude with increasing annealing temperature.

Cable E1 having an amount of extractables comparable to the outer layer of cable A1 showed similar DSC curves. Comparative curves from the inner layers of these cables were presented in Figures 91 and 92 for 60 minute annealings at 90, 92, 95, 97 and 100, 103 and 107 ^{o}C, respectively. The magnitude of the high temperature peak of cable A1 obtained after 107 ^{o}C annealing is higher than the one obtained for cable E1. Comparisons of magnitudes and peak temperatures of the high temperature peak as a function of annealing time are given in Figure 93 and 94, respectively.

Annealing studies for Cable E1 at 90 ^{o}C were carried out for periods of up to two months, since it is the normal operating temperature of XLPE cables. Figure 95 shows DSC curves obtained after 8, 16, 24 and 60 days of annealing at 90 ^{o}C. The increase in crystallinity after 60 days of annealing was found to be close to 3.9 %. There was

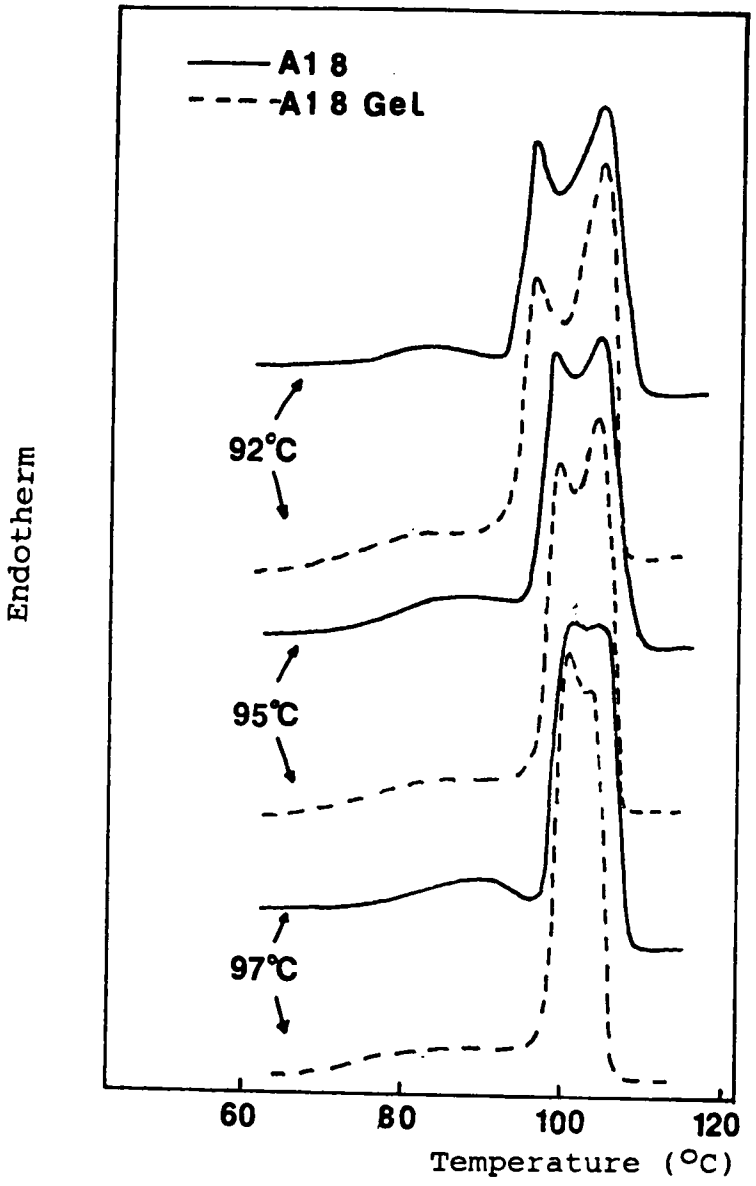

Figure 87 DSC thermograms of the innermost radial section of cable A1 and its gel fraction at the indicated annealing temperatures.

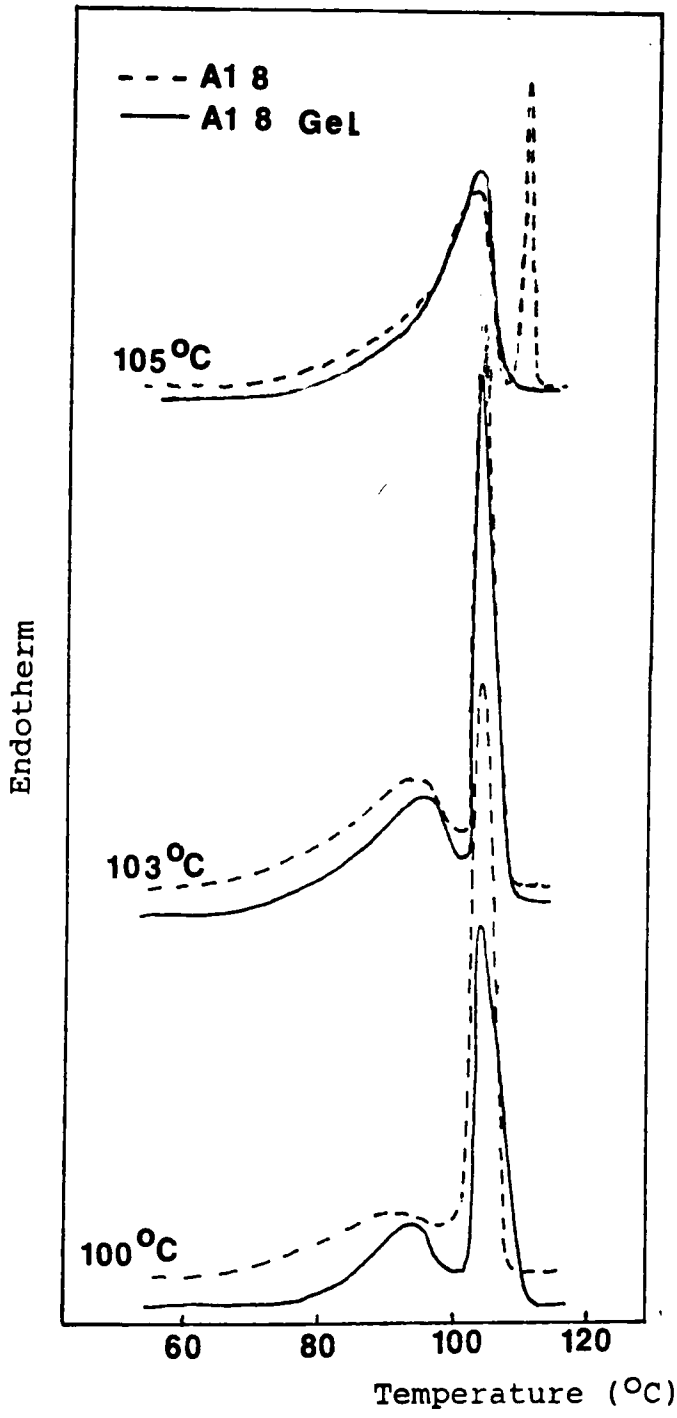

Figure 88 DSC thermograms of the innermost radial section of cable A1 and its gel fraction annealed at 100, 103 and 107 °C for one hour.

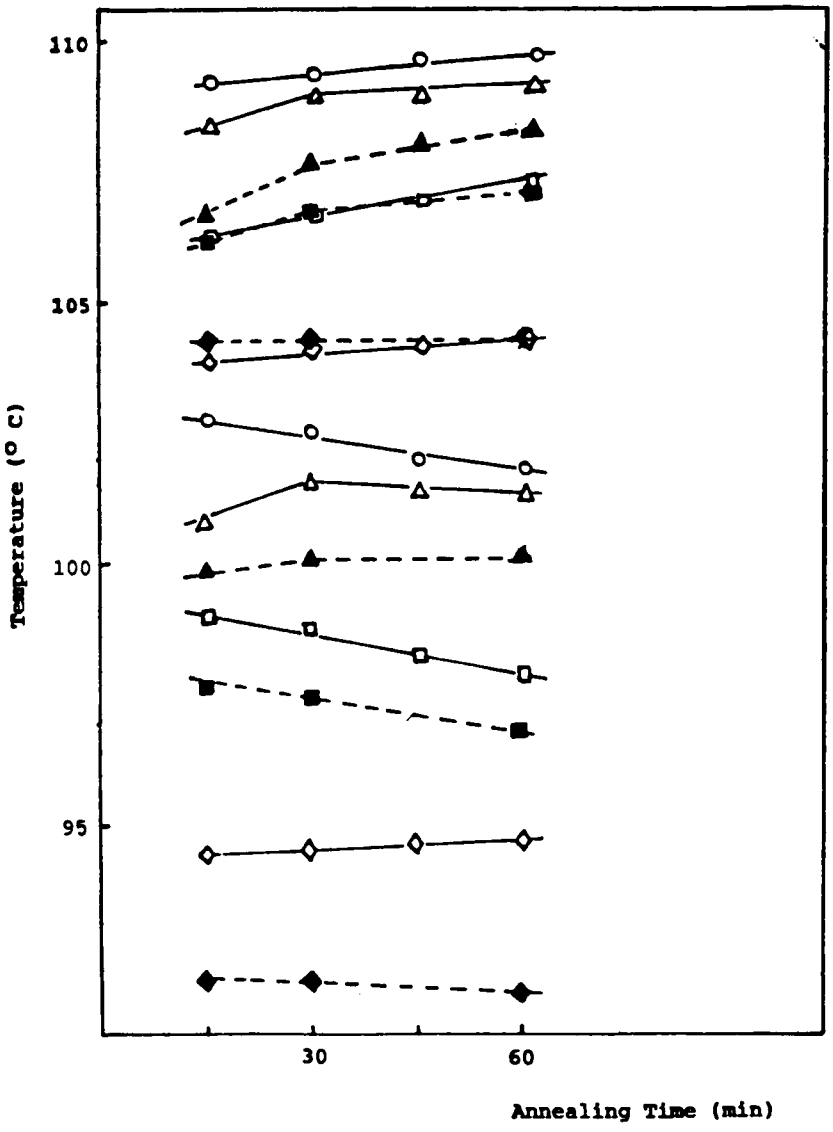

Figure 89 Melting peak temperatures as a function of annealing time for the innermost radial section of cable A1 (——) and its gel fraction (---) annealed at (●,■) 100, (▲,△) 103 and (●,○) 107 °C.

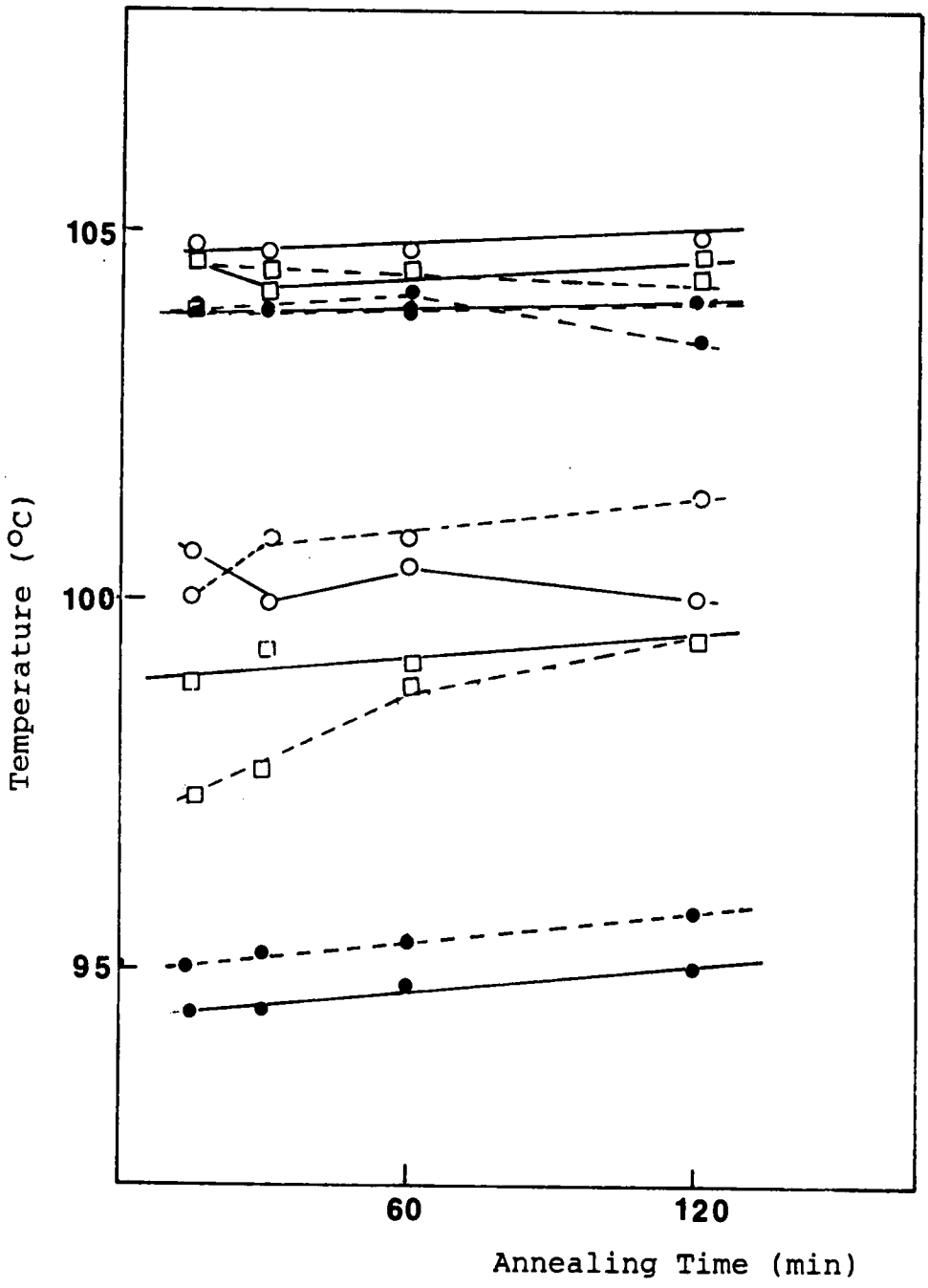

Figure 90 Melting peak temperatures as a function of annealing time for the innermost radial section of cable A1 (——) and its gel fraction (---) annealed at (●) 92, (□) 95 and (○) 97 °C.

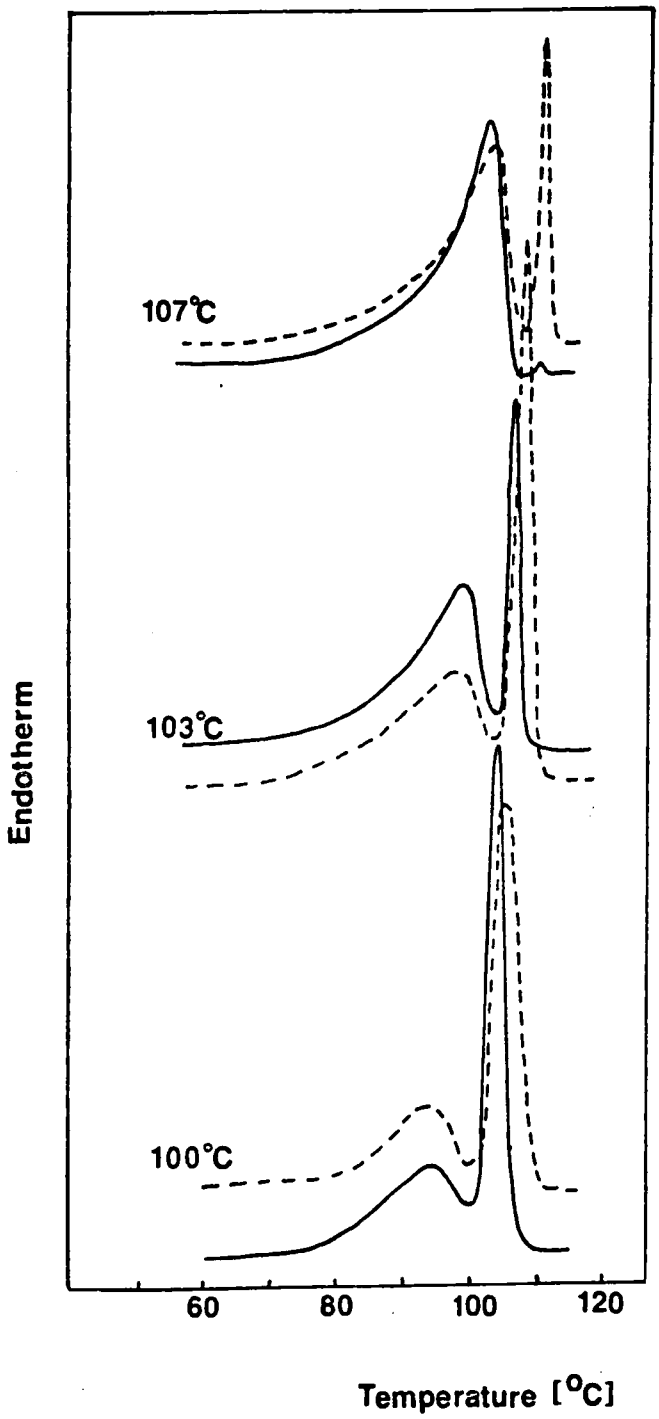

Figure 91 DSC thermograms of the innermost radial sections of cables A1 (---) and E1 (——) annealed at 100, 103 and 107 °C for one hour.

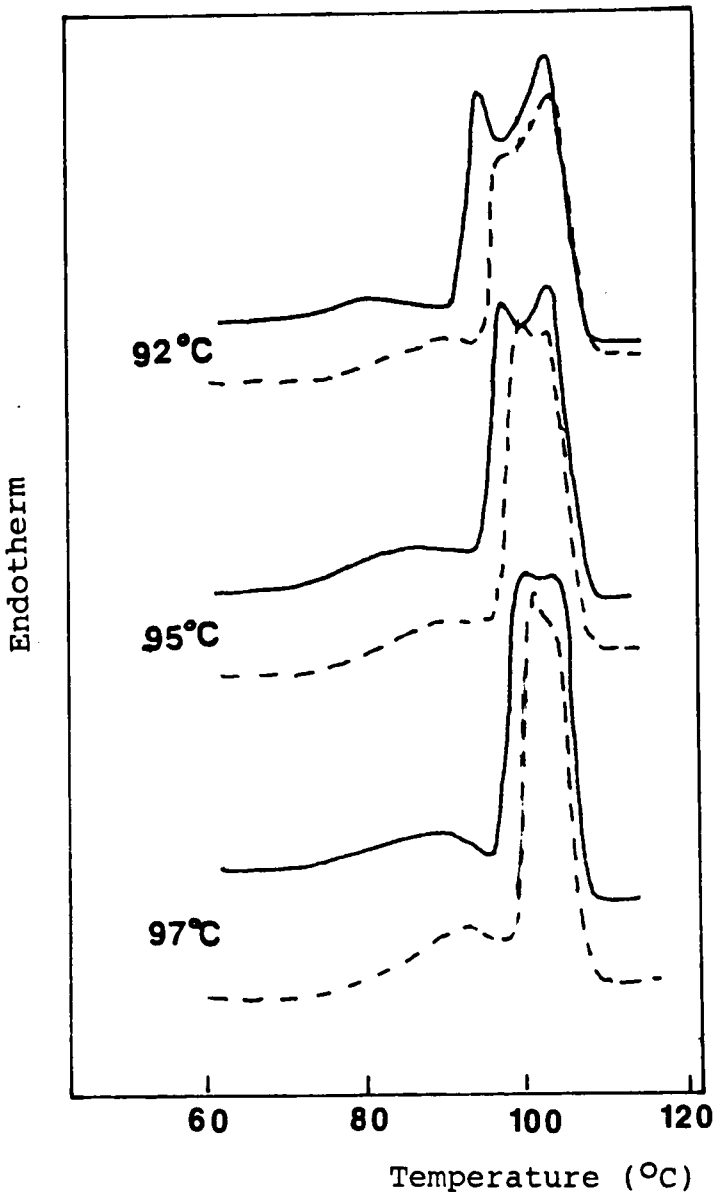

Figure 92 DSC thermograms of the innermost radial sections of cables A1 (---) and E1 (——) annealed at 92, 95 and 97 °C for one hour.

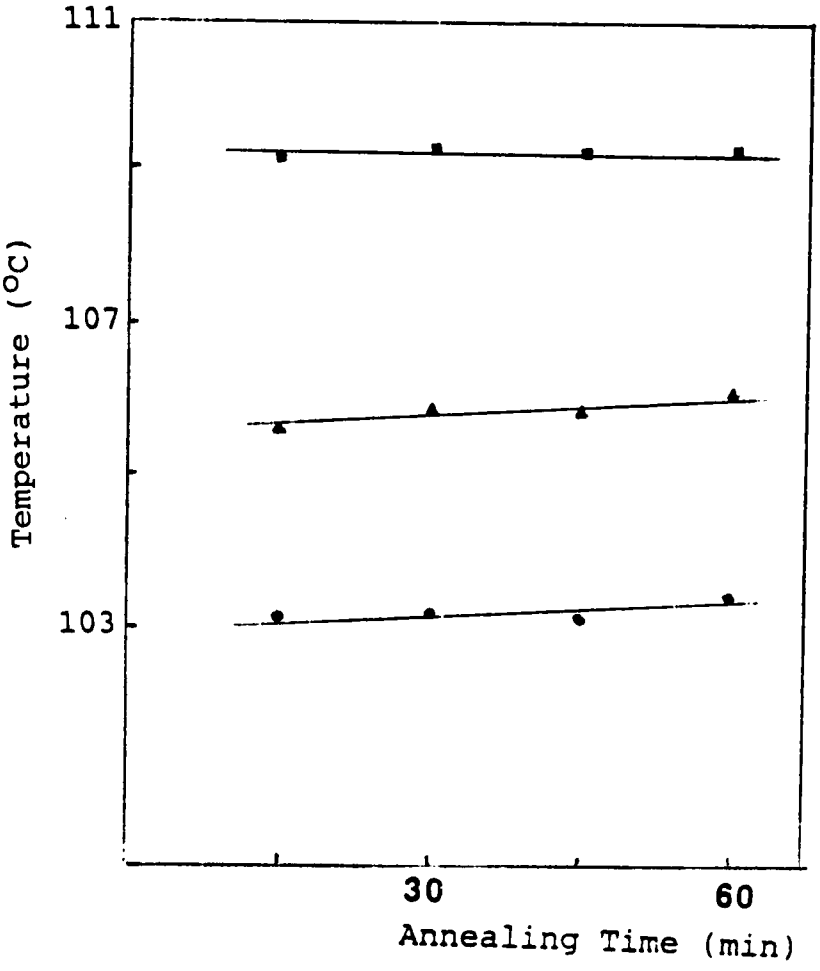

Figure 93 Melting peak temperatures as a function of annealing time for cable E1 annealed at (•) 100, (▲) 103 and (■) 107 °C.

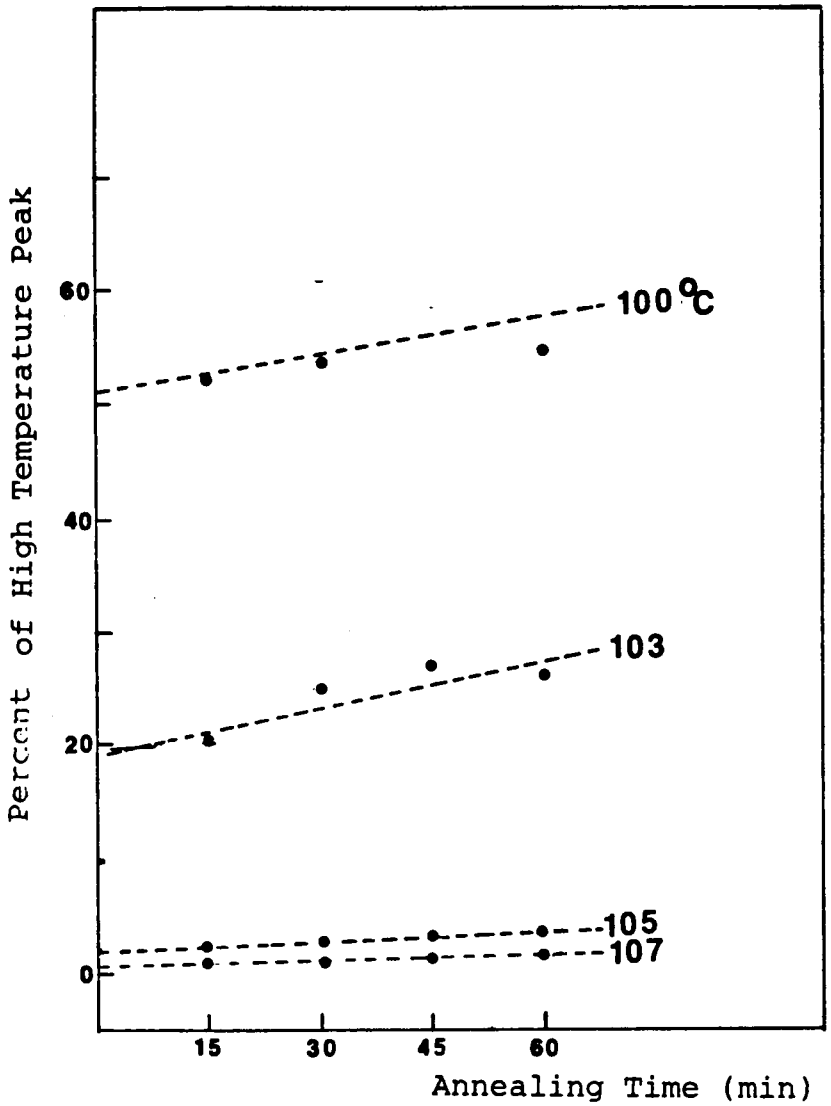

Figure 94 Percentage of high temperature peak as a function of annealing time for cable E1 at the indicated temperatures.

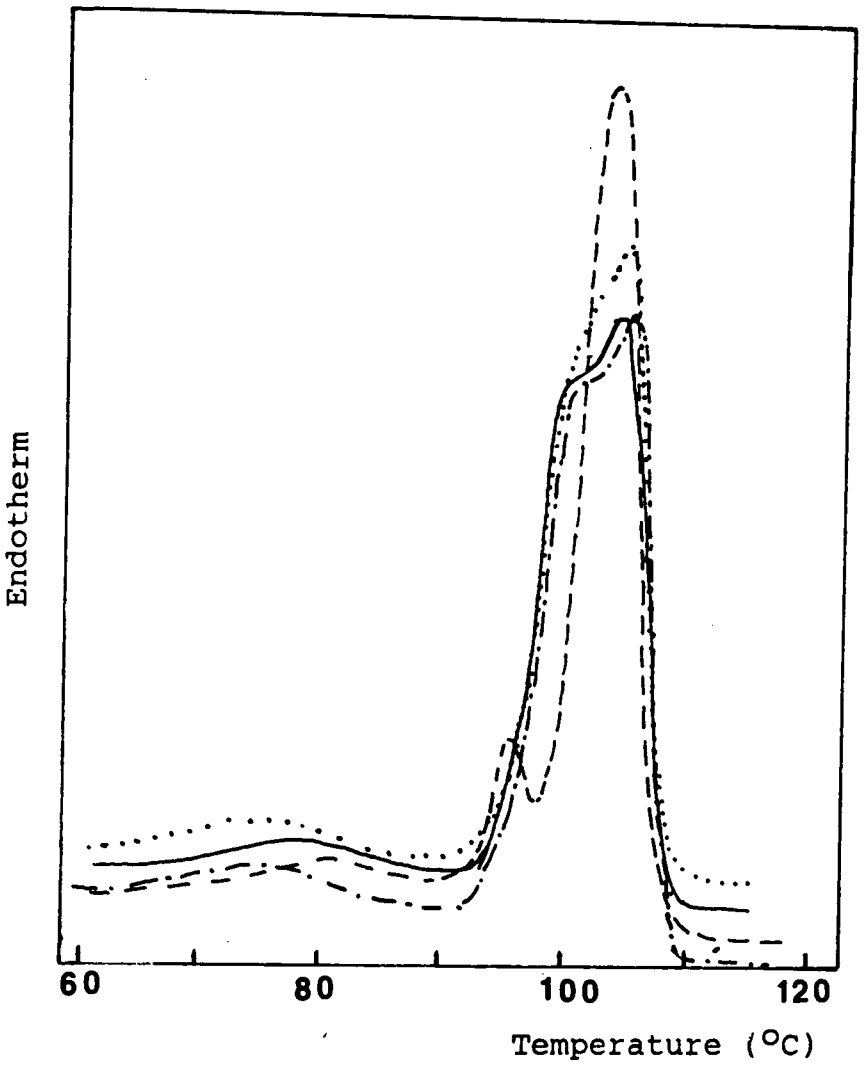

Figure 95 DSC thermograms of cable E1 after annealing at 90 °C for (- - -) 8 days, (— — —) 16 days, (-.-.-) 24 days and (·····) 60 days.

observed to be a three degree increase in major melting temperature, which became constant after 24 days of annealing. The crystallization peak generated around 95 ^{o}C merges with the major melting peak and increases in magnitude and temperature. 90 degree annealing was also carried out following isothermal treatment at 110 ^{o}C for periods of 8 and 24 hours (Figure 96). A major melting peak was found at 103.1 ^{o}C in each case which is comparable to the one obtained for 90 ^{o}C annealings. The overlapped recrystallization peak is higher in magnitude than for 90 ^{o}C annealing. Annealing at 110 ^{o}C for four days resulted in a quenched peak with a small hump around 113 ^{o}C (Figure 97).

Multistep isothermal annealing of Cable E1 was carried out, first at 107 ^{o}C and then at 100 ^{o}C using 60 minute periods at each temperature. As can be seen from Figure 98 two newly generated sharp peaks appeared around 104 and 110 ^{o}C from the annealings at 100 ^{o}C and 107 ^{o}C. More peaks developed when the samples were subjected to successive annealings at 107-103-100-95 ^{o}C. DSC curves obtained for 30 minute and 120 minute successive annealings at each of those temperatures are shown in Figure 99. As can be seen from this figure the position of each each newly generated peak was raised by 0.5 ^{o}C and the crystallinity change was found to be around two percent.

Comparative annealing studies for cable C1 were also carried out for the two basic temperature regions,

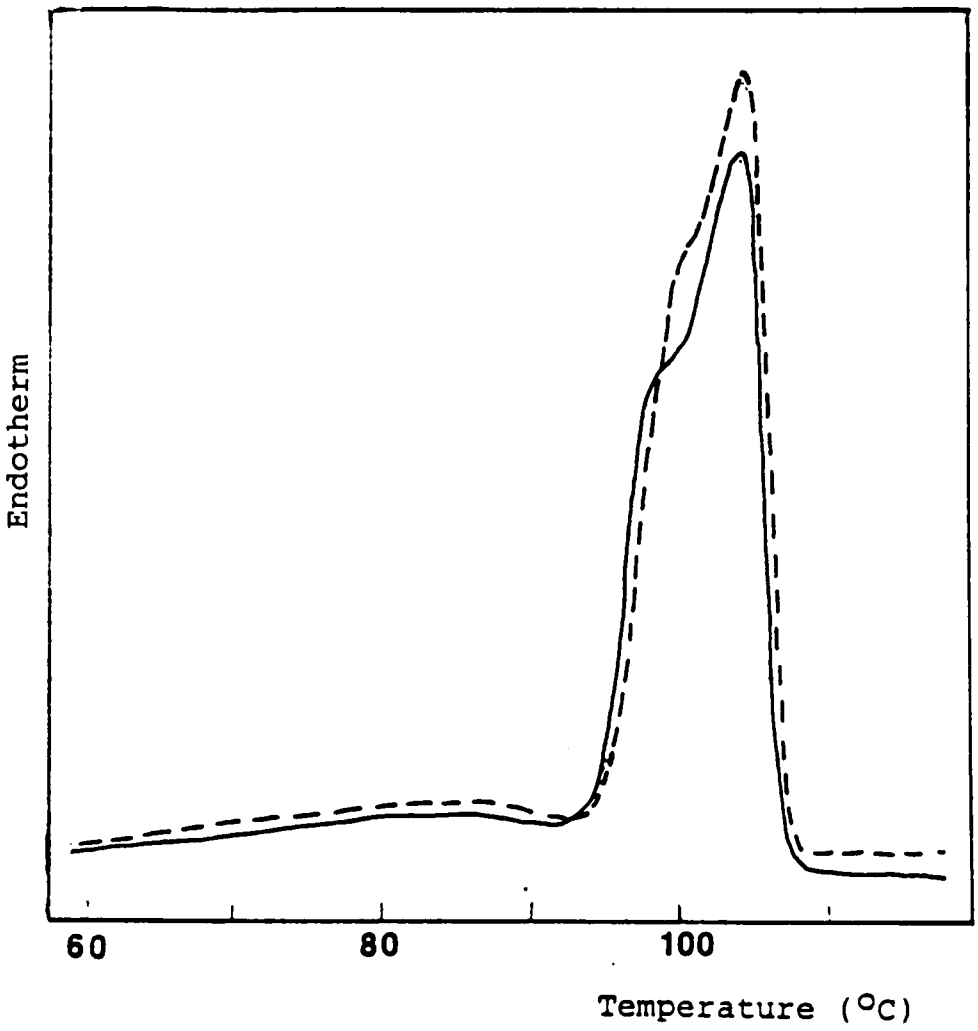

Figure 96 DSC thermograms of cable E1 annealed at 90 °C after holding at 110 °C for (——) four days and (- - - -) eight days.

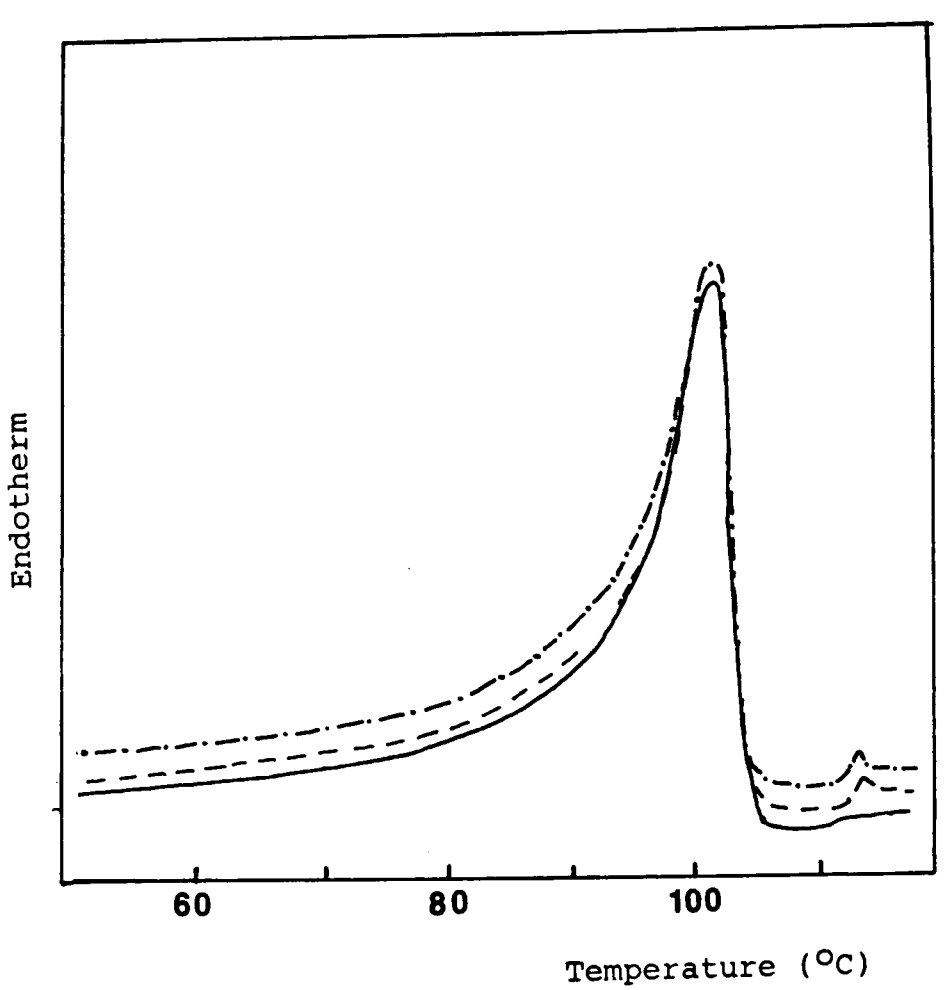

Figure 97 DSC thermograms of cable E1 cooled to ambient temperature after holding at 110 °C for (·····) one day, (– – –) four days and (——) eight days.

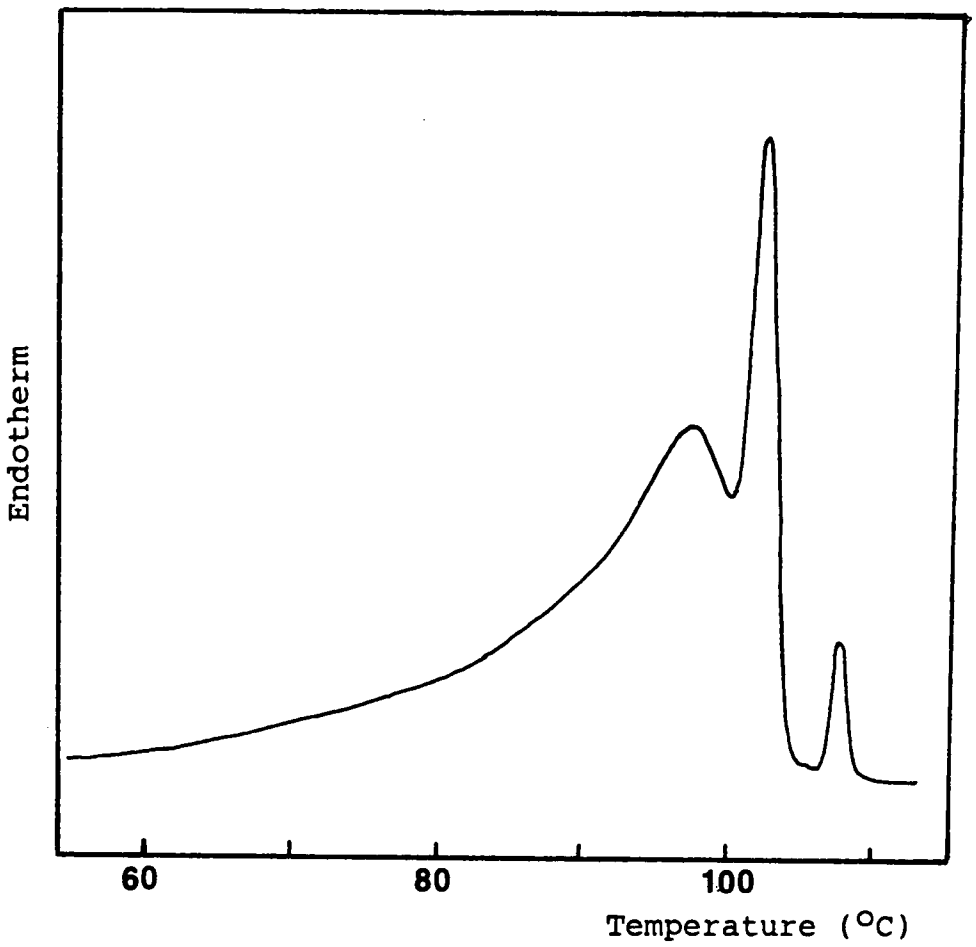

Figure 98 DSC thermograms of cable E1 annealed at 107 and 100 °C successively for 60 minutes at each temperature.

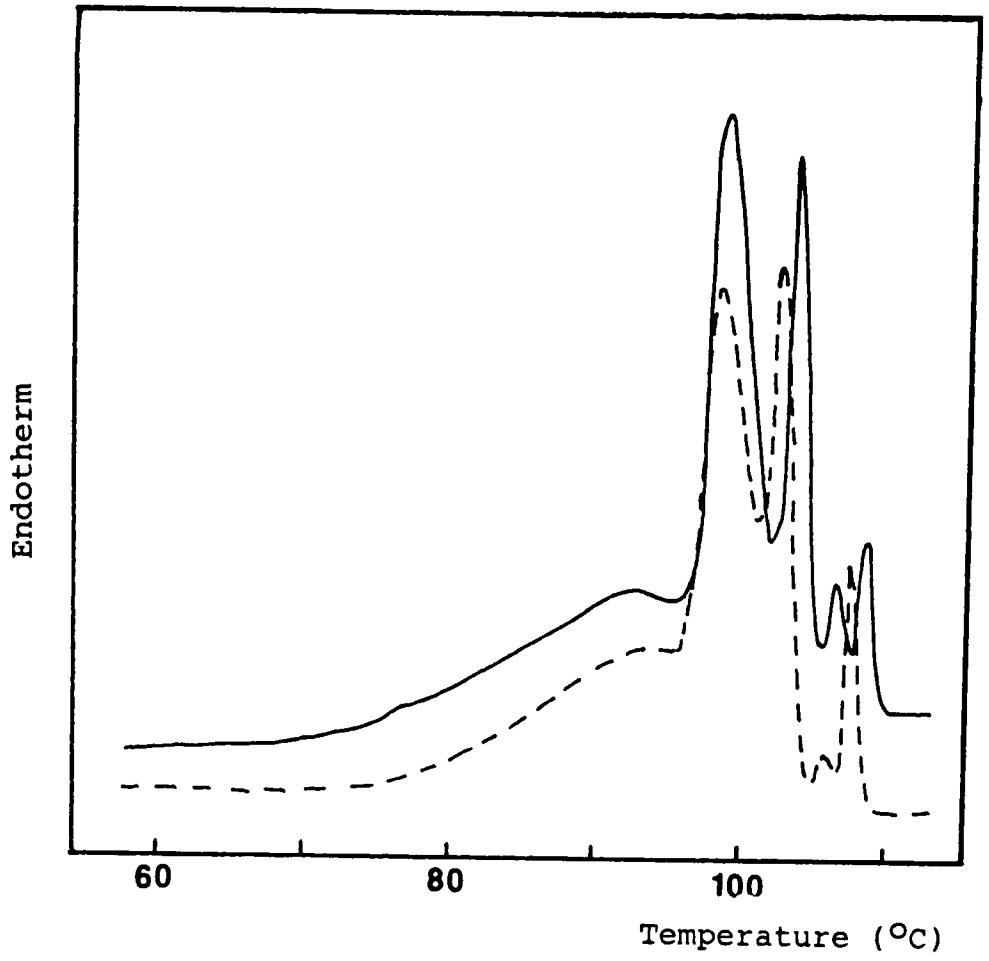

Figure 99 DSC thermogram of cable E1 annealed at 107, 103, 100 and 95 °C successively for (- - -) 30 min. and (———) 60 min. at each temperature.

namely 92, 95, 97 and 100, 103, 105, 107 ^{o}C regions. Figures 100 and 101 show the DSC curves obtained from the inner layers of cables A1 and C1 after annealing at the indicated temperatures for 120 minutes. Peak maxima and the magnitude of the high temperature peak as a function of annealing time are given in Figures 102 and 103. The magnitudes of the high temperature peaks of C1 and A1 were found to be comparable for 107 ^{o}C annealing. On the other hand, the magnitude of the high temperature peaks obtained from the 100, 103 and 105 ^{o}C annealings were all found to be higher for identical annealing periods.

In order to understand the annealing process at 107 ^{o}C and its impact on the behavior on the extractable materials, annealed samples were cooled to room temperature at different cooling rates. Figure 104 shows DSC thermograms obtained from samples quenched and slowly cooled (0.2 deg/min) from 107 ^{o}C after annealing for 30 minutes. Different rates of cooling after annealing were also applied following annealing at 97 ^{o}C. The results are given in Figure 105.

4.3.1 Thermo-Optical Studies

Transmitted light intensity versus time plots were recorded for 25 μm thick cable slices while annealing them in a hot stage mounted on the microscope. Figures 106-109 show the light transmission data obtained for annealings

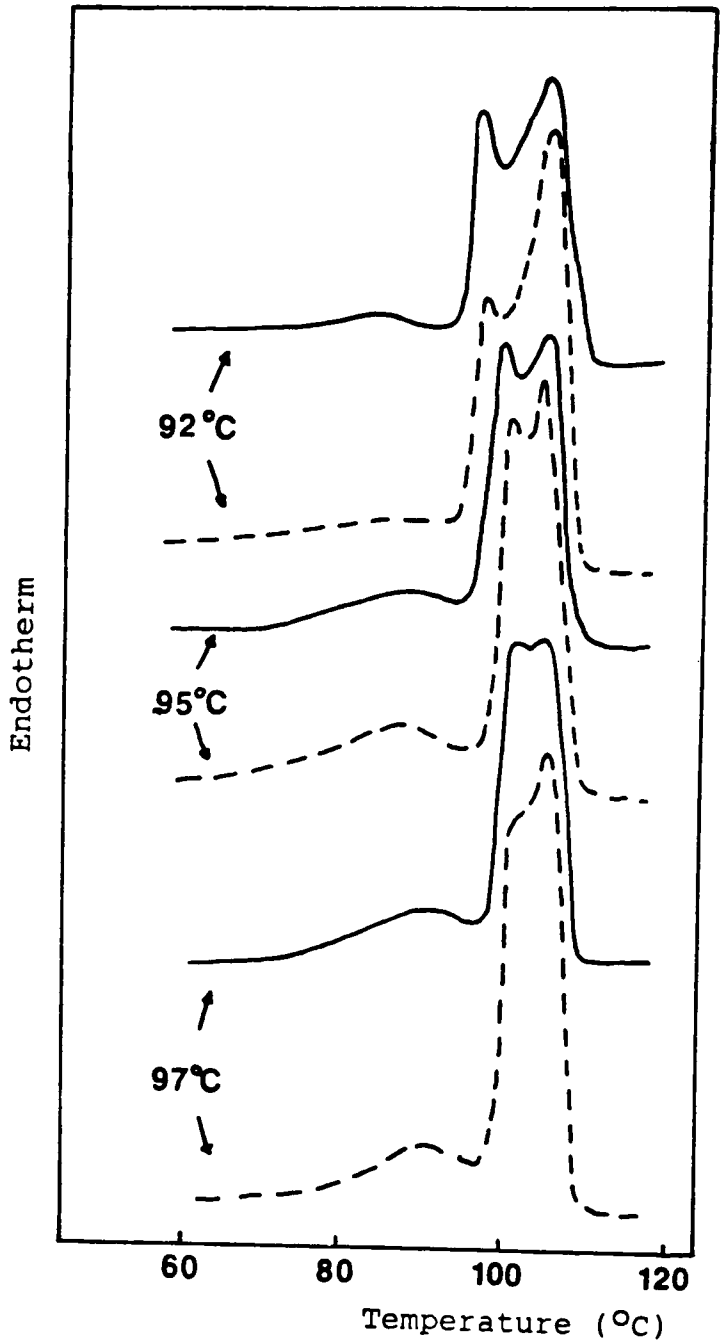

Figure 100 DSC thermograms of the innermost layers of cable A1 (———) and cable C1 (– – – –) annealed at 92, 95 and 97 °C for two hours.

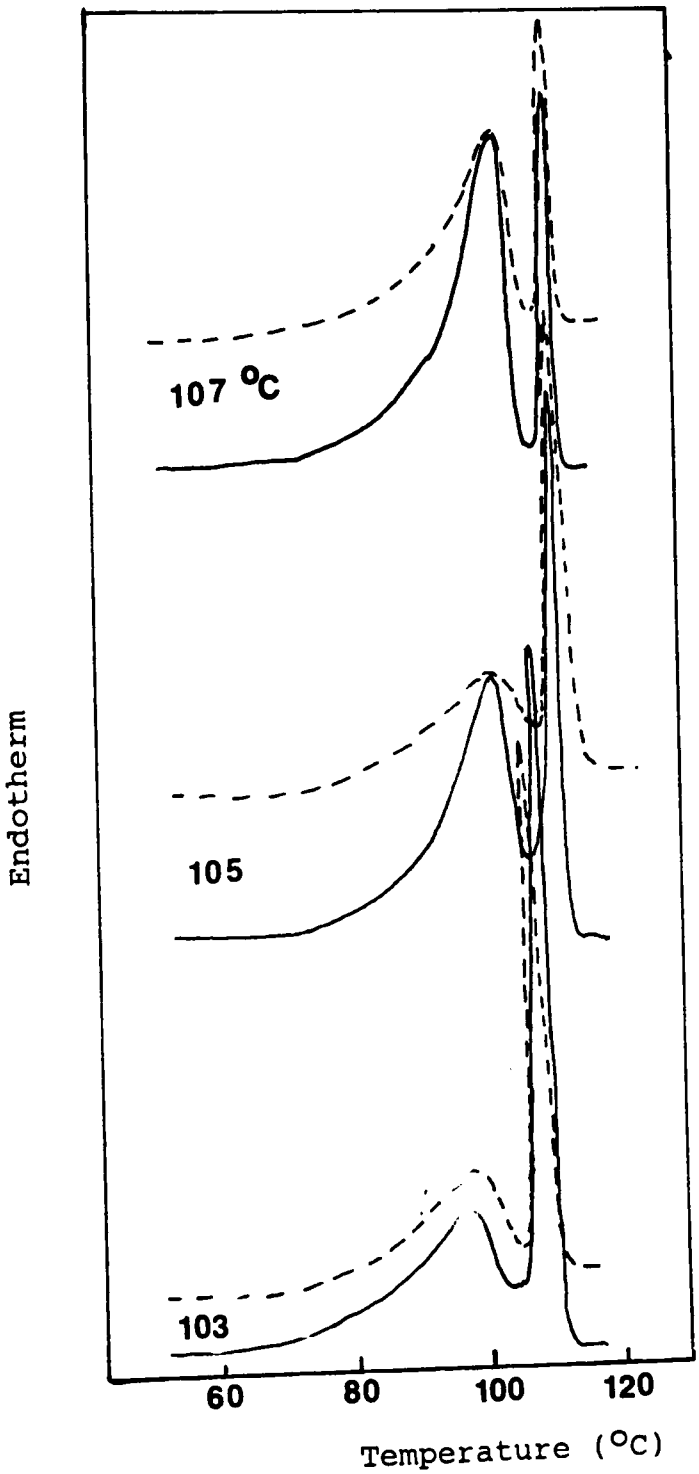

Figure 101 DSC thermograms of the innermost layers of cable A1 (——) and cable C1 (----) annealed at 100, 103 and 107 °C for one hour.

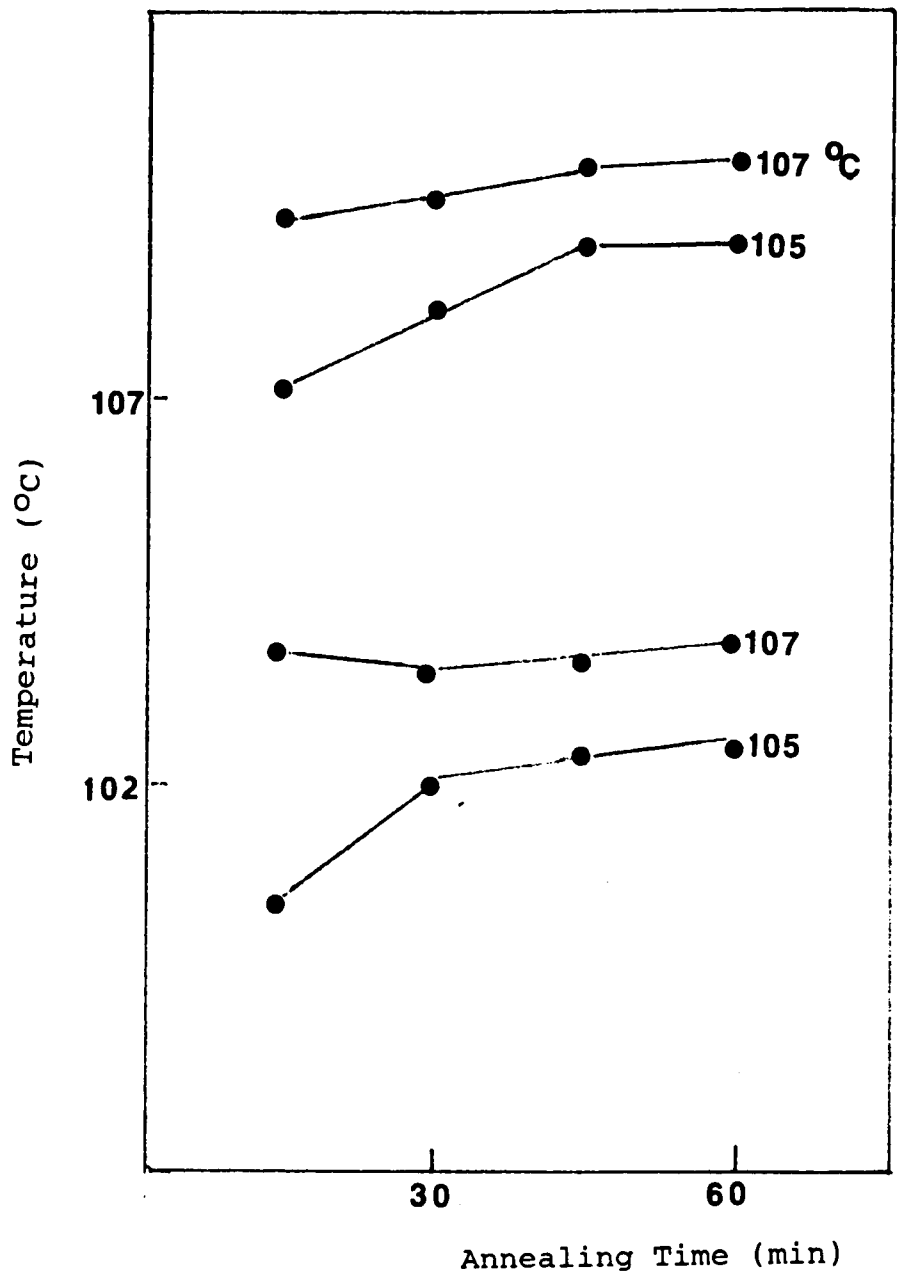

Figure 102 Melting peak temperature as a function of annealing time for the innermost radial section of cable C1 at the indicated annealing temperatures.

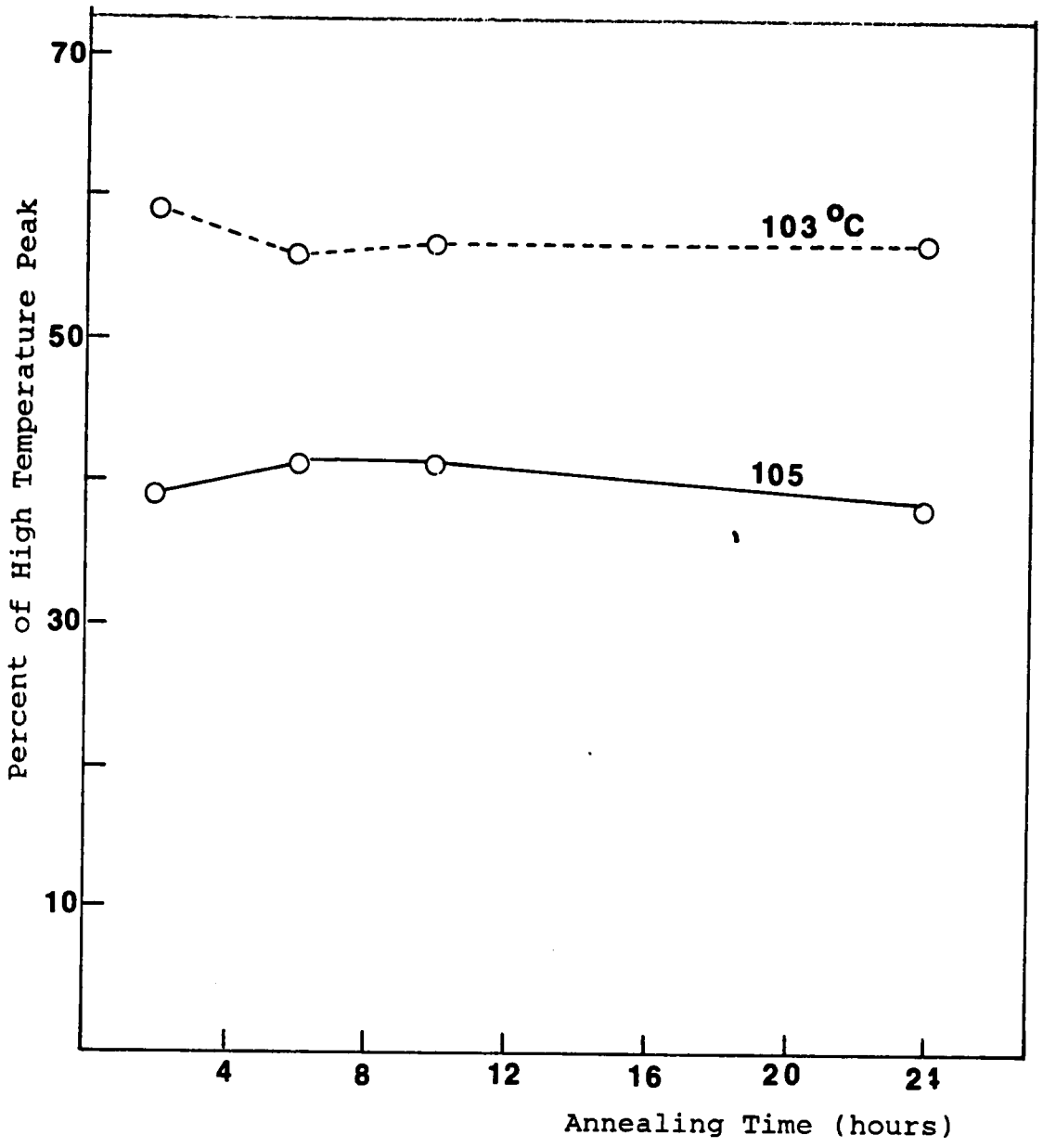

Figure 103 Percent of high temperature peak as a function of annealing time at the indicated temperatures for cable C1.

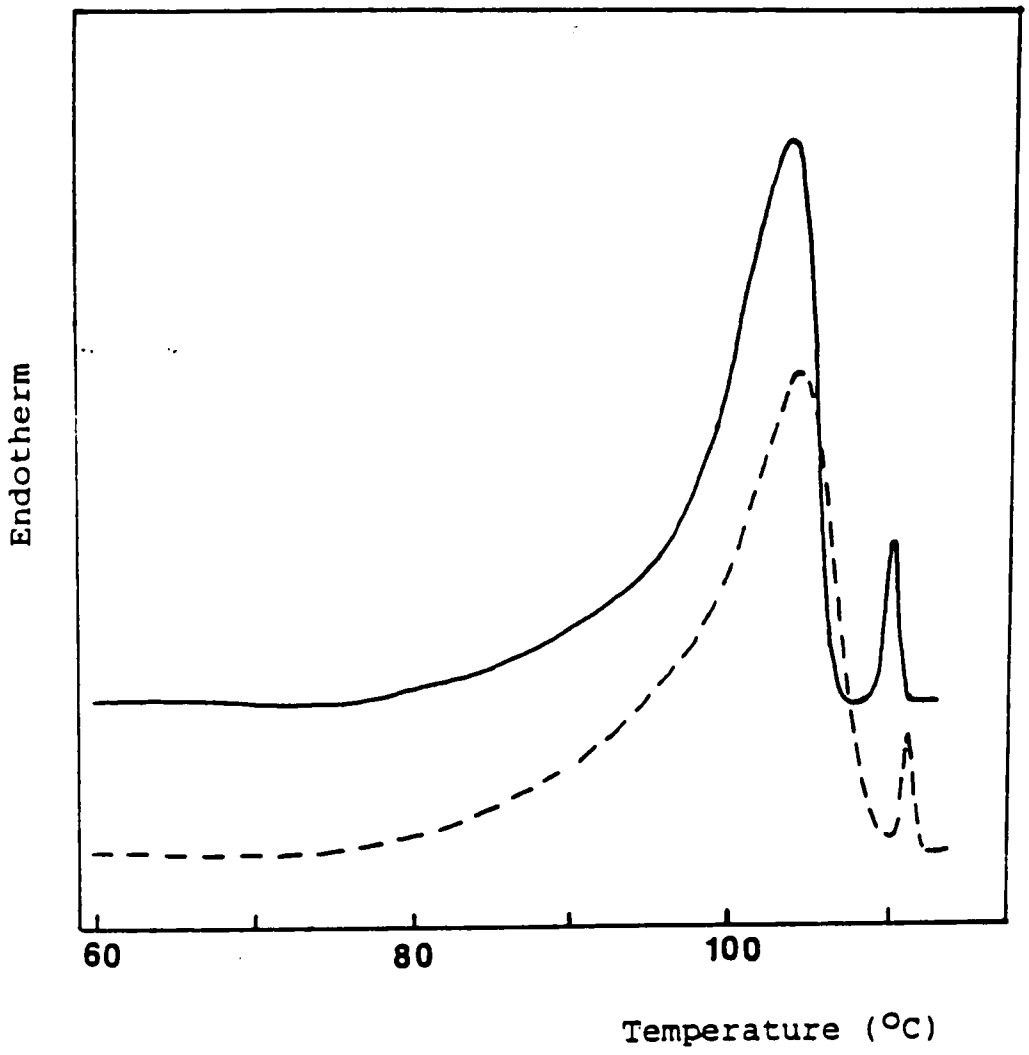

Figure 104 DSC thermograms of cable A1-8 cooled to ambient temperature at 0.2 deg./min (– – –) and quenched (———) after annealing at 107 °C for 30 minutes.

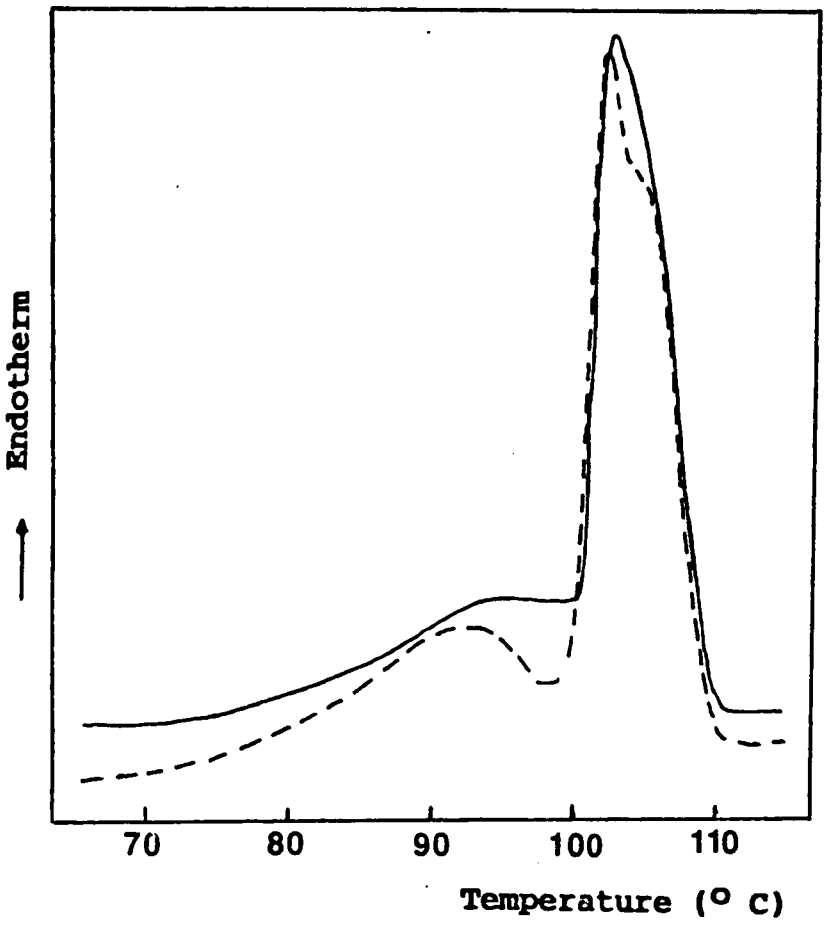

Figure 105 DSC thermograms of cable A1-8 cooled to ambient temperature at 0.2 deg./min (- - - -) and quenched (———) after annealing at 97 °C for 30 minutes.

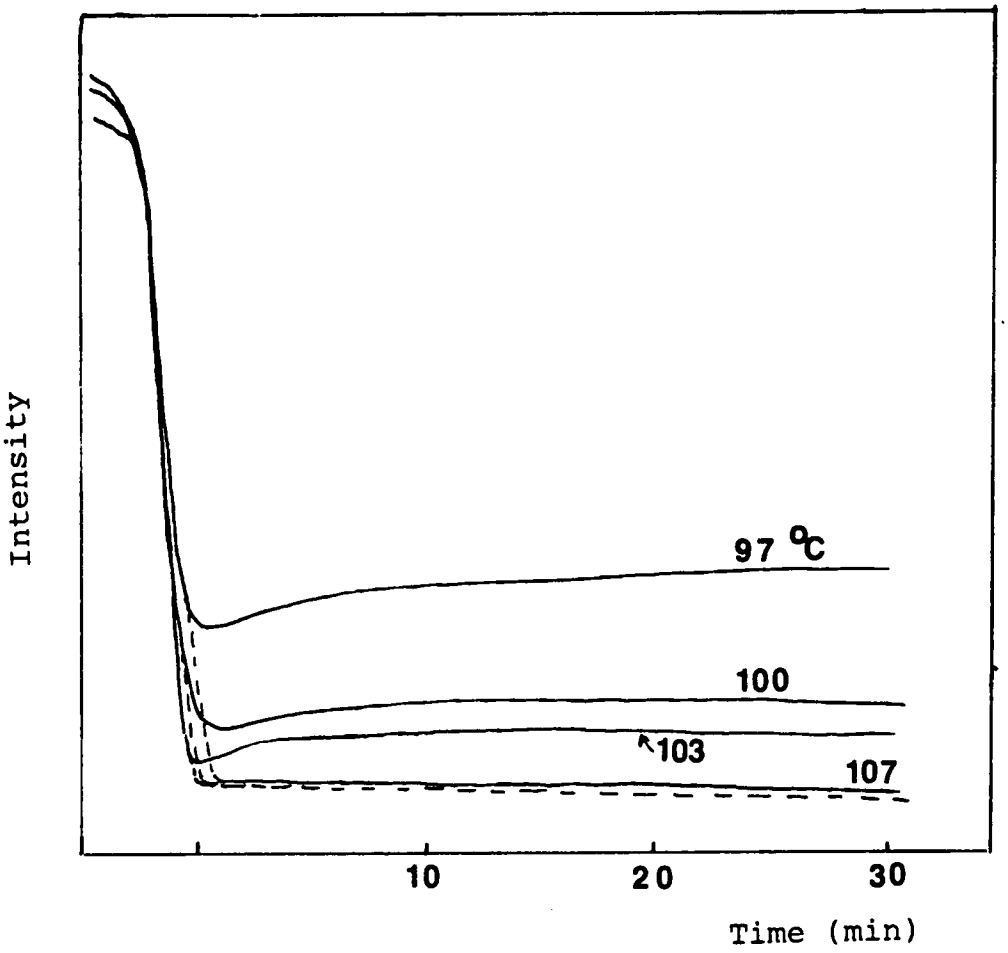

Figure 106 Light transmission intensity versus time plots of cable A1-8 annealed at the indicated temperatures.

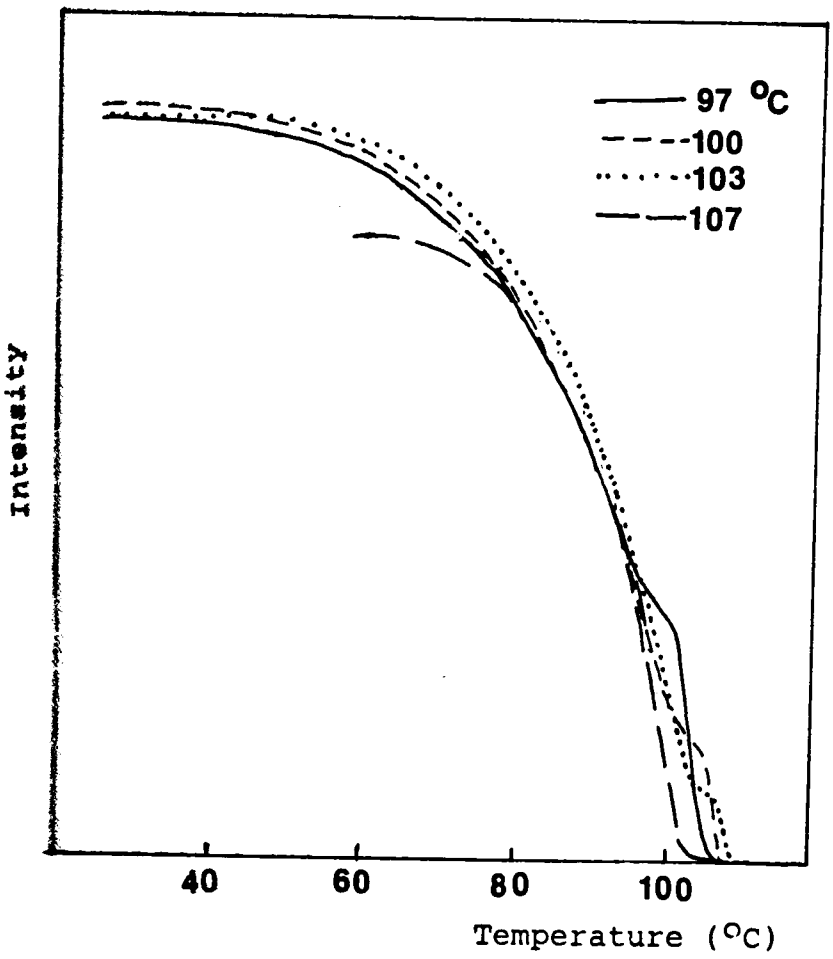

Figure 157 Light transmission intensity versus temperature plots of 10 deg/min heating of cable A1-8 annealed at the indicated temperatures.

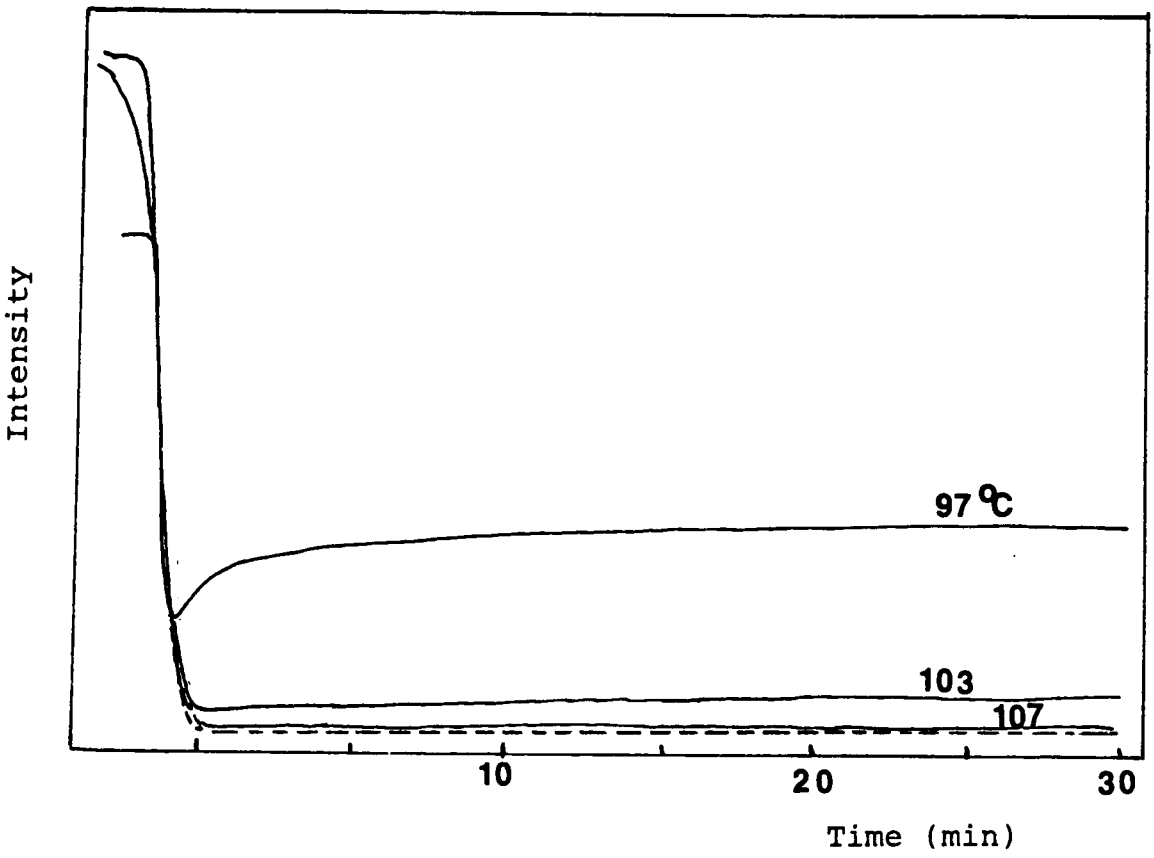

Figure 108 Light transmission intensity versus time plots of cable A1-8 gel annealed at the indicated temperatures.

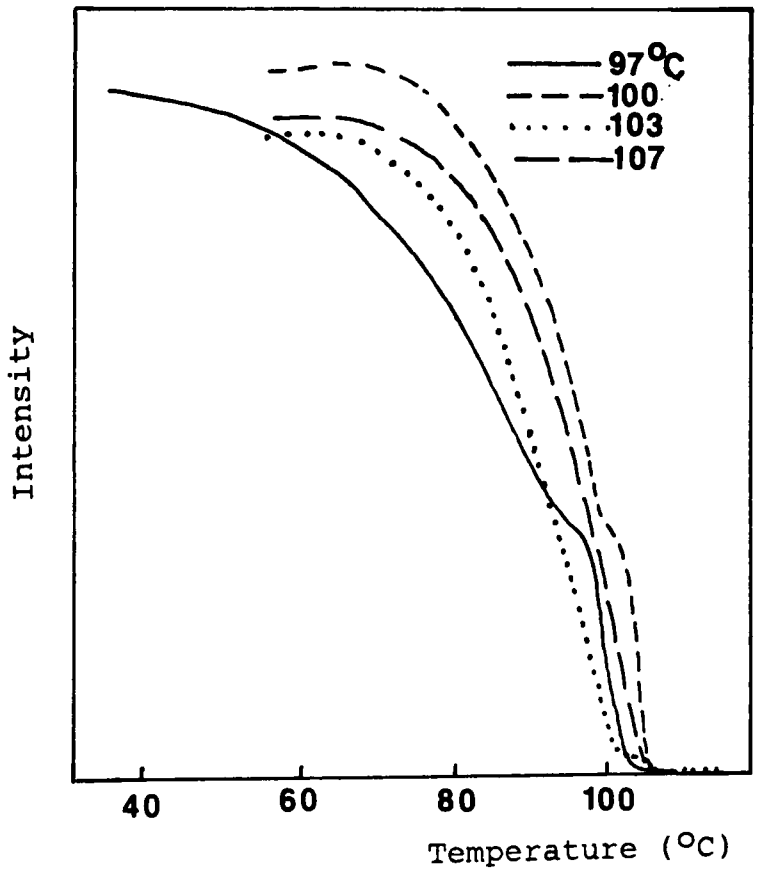

Figure 109 Light transmission intensity versus temperature plots of 10 deg/min heating of cable A1-8 gel annealed at the indicated temperatures.

carried out at 97, 100, 103 and 107 ^{o}C for the innermost layer of Cable A1. The dotted lines in Figures 106-109 are representative of crystallizations carried out by quenching from the melt in order to quantify the intensity levels. As can be seen from Figure 106, after reaching the annealing temperatures of 97 and 100 ^{o}C an increase in recorded transmitted light was observed. An increase in intensity due to recrystallization was observed during a 30 minute annealing. From Figure 92, p 214, it was found that about 76 % of the sample was melted at 97 ^{o}C. The intensity increase due to recrystallization was found to be about 11 % on the basis of the original crystallinity. By taking the amount of melted material as a basis, the recrystallized material was found to be 14 %. The remaining 86 % of the melt crystallizes on cooling. Figure 107 shows the transmitted light intensity versus temperature data obtained from a 10 deg/min heating of the sample annealed at 97 ^{o}C. The slight slope change around 95 ^{o}C correspond to the annealing temperature. Material crystallizing upon cooling from 97 ^{o}C was found to be 58 %. From Figure 106 for annealing at 100 ^{o}C, 91 % of the total material melted and crystallized upon cooling. 10 % of the melted material was found to have recrystallized during annealing. Higher temperature annealings at 103 and 107 ^{o}C did not show any evidence of recrystallization. At 103 ^{o}C only about 5 % of the material

was in the crystalline state while none could be detected at 107 ^{o}C.

A similar study was carried out for the gel fraction of Cable A1. At lower annealing temperatures, recrystallization was found to be more effective in the gel samples. Recrystallizations for 97 and 100 ^{o}C was recorded to produce 20 % and 32 %, respectively. 10 deg/min runs for annealings at 97, 100, 103 and 105 are shown in Figure 107. As can be seen, annealed samples have sigmoidal curves with humps corresponding to the annealing temperature (Figure 109).

4.3.3. X-Ray Studies

Degrees of crystallinity attained at annealing temperatures were determined using the high temperature cell equipped with temperature control units. Figure 110 shows the diffraction patterns obtained at the indicated annealing temperatures. Table 11 summarizes the available percent crystallinities for the indicated annealing temperatures. Percent crystallinity change during a 30 minute annealing was followed by keeping the diffractometer at the 2Θ value of 21.4 degree corresponding to the maximum point of the 110 crystalline peak. It shows that the increase in percent crystallinity is about 1.3 %.

SAXS analyses were carried out for cable A1 annealed at 90, 100 and 107 ^{o}C for two days. Scattering

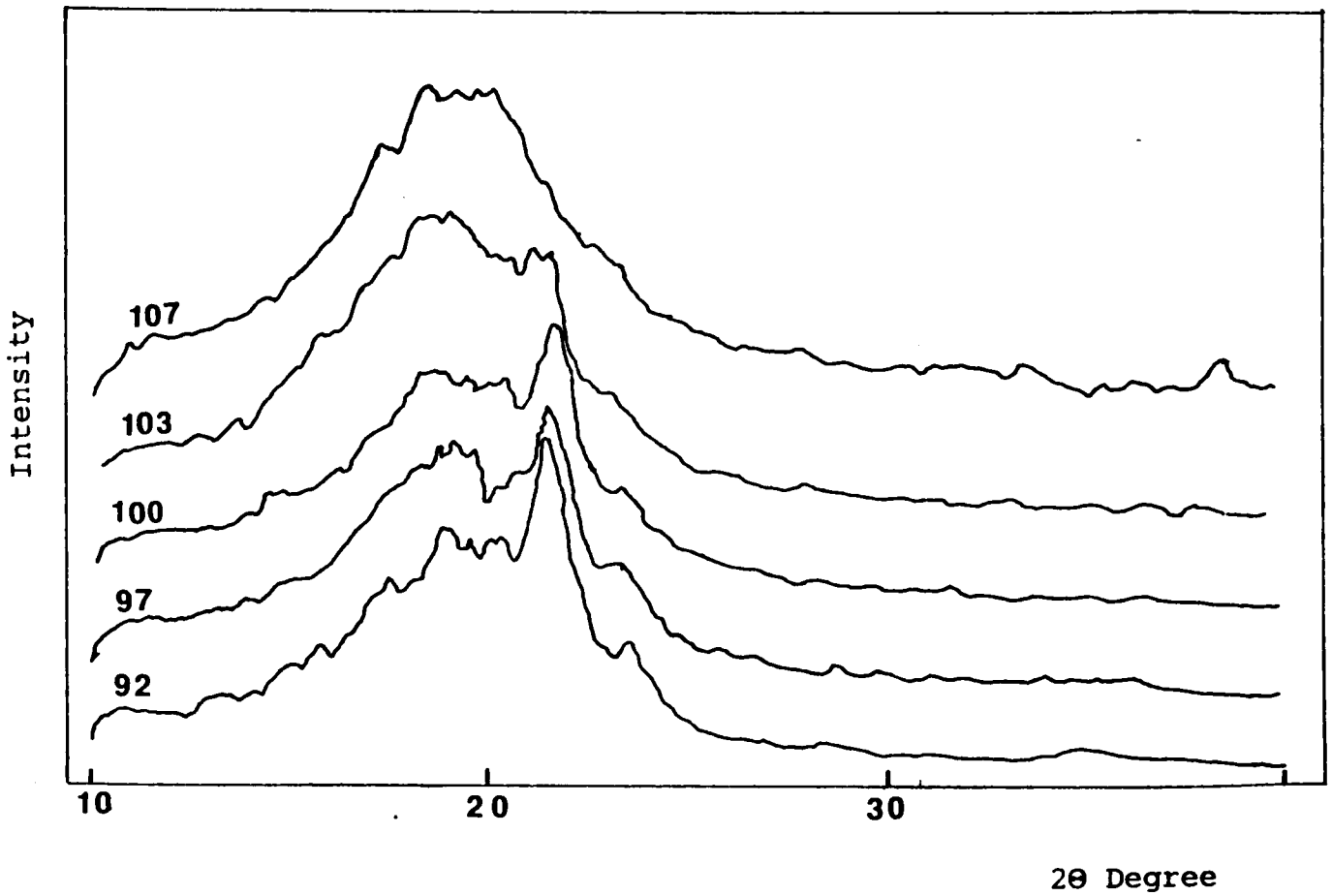

Figure 110 Wide angle X-ray diffraction patterns obtained at the indicated temperatures for cable A1-8.

Table 11 Percent crystalline material present at the indicated annealing temperatures for cable A1

Annealing Temperature (°C)	WAXS %
92	74
97	67
100	33
103	26
107	1

contours obtained from the outer and inner layers of the radial slab annealed at 107 ^{o}C are shown in Figures 111a-b. Scattering contours from the outer layer annealed at 90 ^{o}C and inner layer annealed at 100 ^{o}C are shown in Figures 112a-b. Slight orientation observed at the outer layer of cable A1 was found to disappear after annealing at 90 ^{o}C and 107 ^{o}C for two days. The inner layer was found to behave similarly to the original cable. Circumferentially averaged intensity versus scattering vector plots for 107, 100 and 90 ^{o}C annealings along with the original cable data are given in Figures 113 and 114. After recording the scattering data of the inner layer annealed at 107 ^{o}C the specimen was quenched from the melt to destroy its thermal history acquired during the 107 ^{o}C annealing. Circumferentially averaged scattering intensity data for quenched cable A1-8 is given in Figure 113. Long times of annealing of cable E1 at 90 ^{o}C resulted in long periods shorter than the values obtained for the original cable (Figure 115). After allowing the increase in crystallinity over 40 days annealing, lamellar thickness was found to remain essentially unchanged (Table 12).

4.3.4. Electron Microscopy

TEM micrographs from the inner layer of cable A1 annealed at 100 and 107 ^{0}C for two days showed similar texture to the same section of the original cable. The main

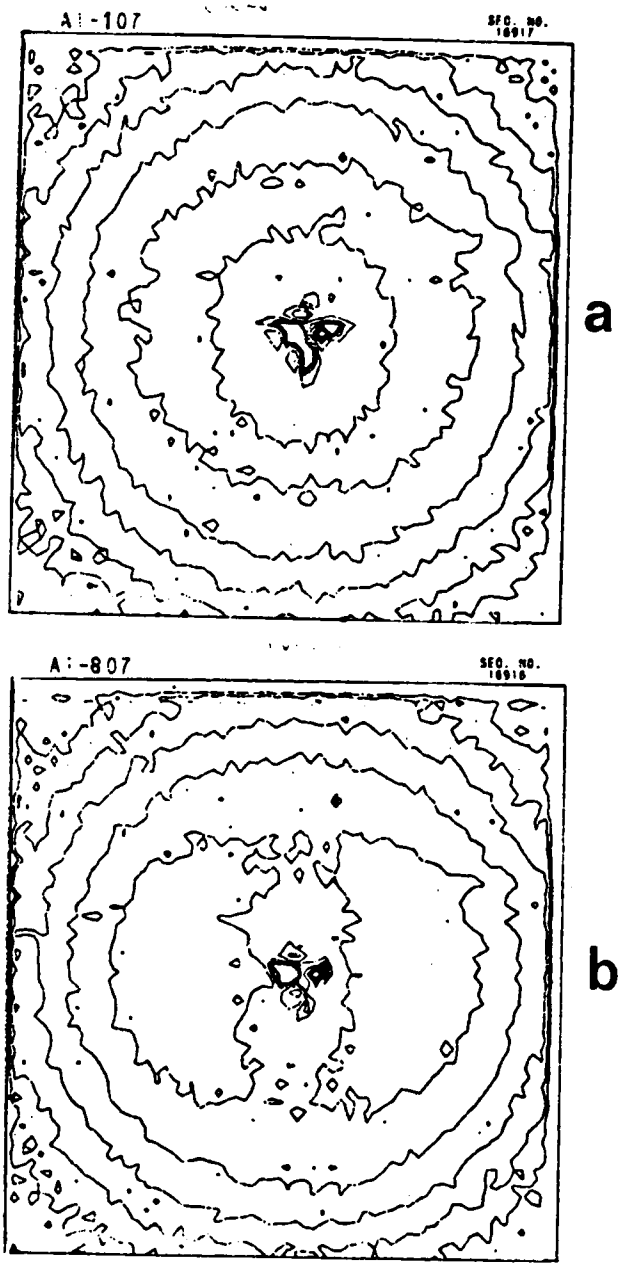

Figure 111 SAXS contours of cable A1 (a) outer layer (b) inner layer annealed at 107 ^{o}C for two days.

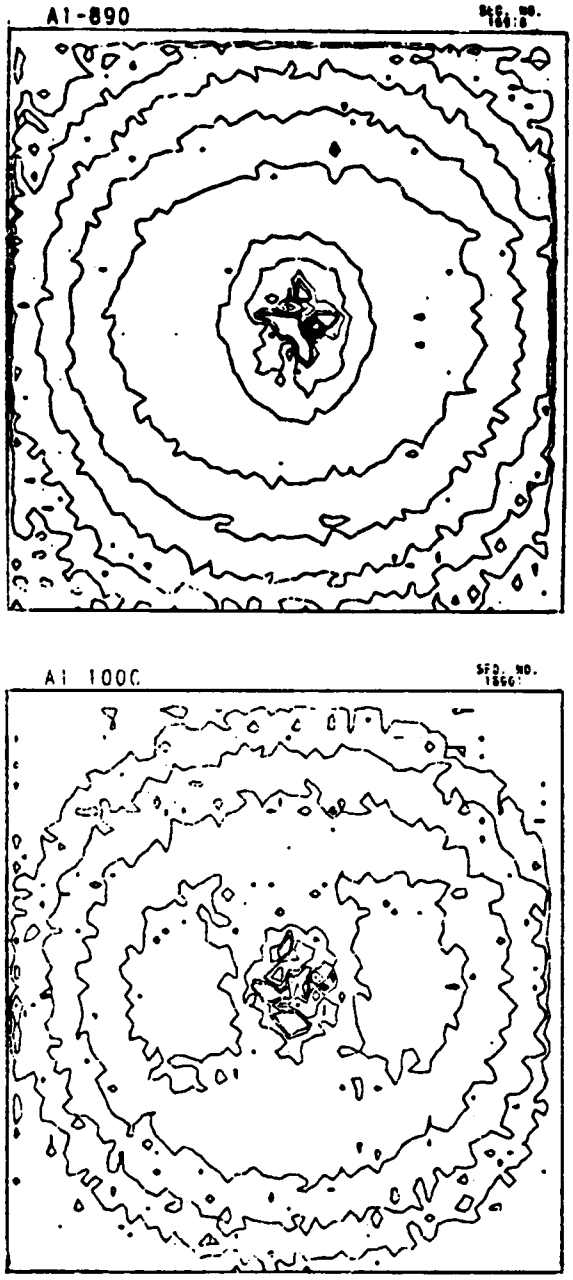

Figure 112 SAXS contours of cable A1 annealed at (a) 90 (b) 100 °C for two days.

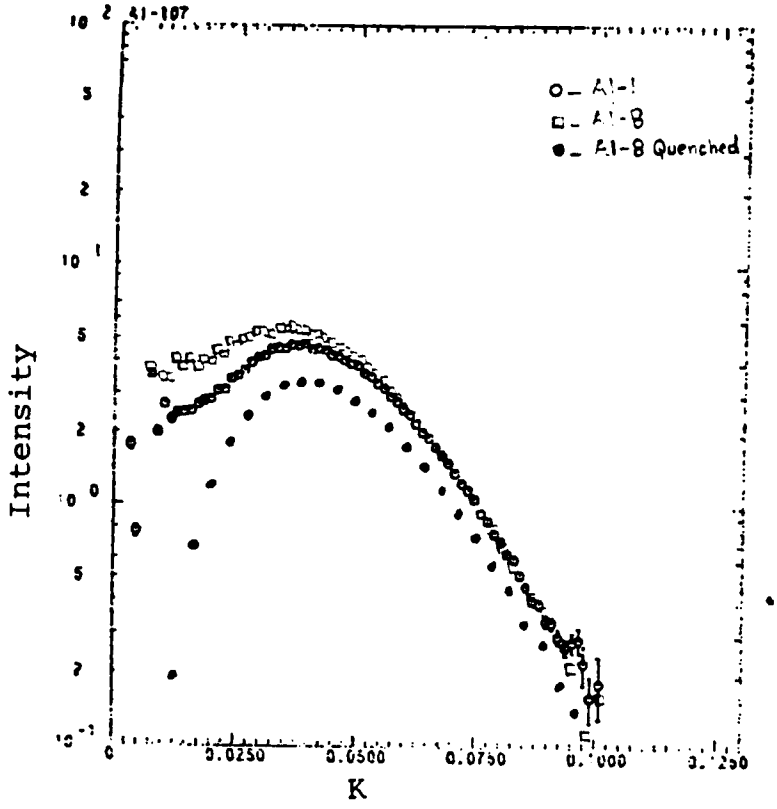

Figure 113 Circumferential average intensity versus scattering vector for (O) outer layer, (◘) inner layer, and (●) inner layer (quenched) for cable A1 annealed at 107 °C.

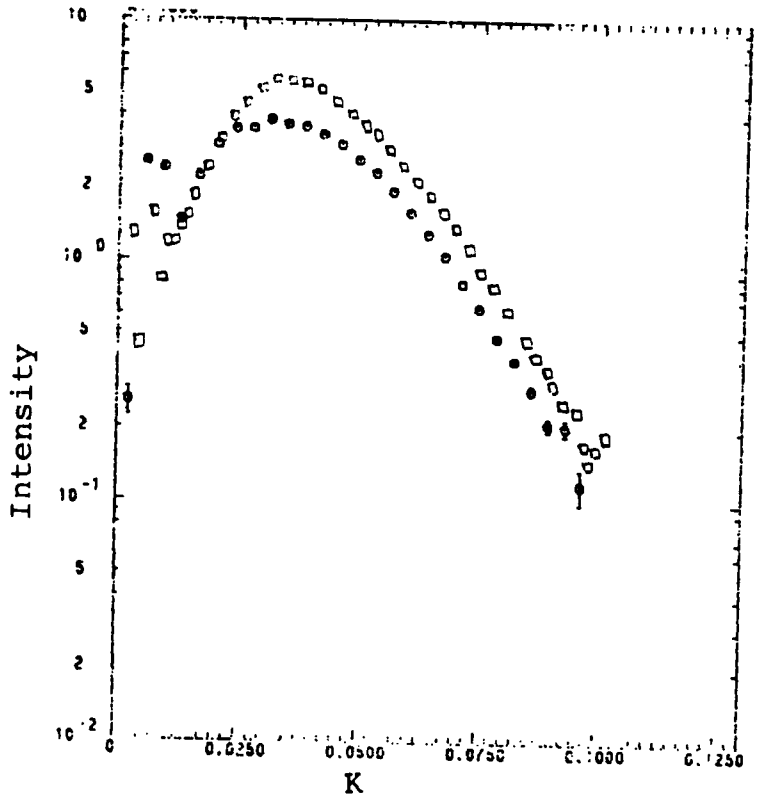

Figure 114 Circumferential average intensity versus scattering vector for cable A1 annealed at (□) 90 and (○) 100 °C for two days.

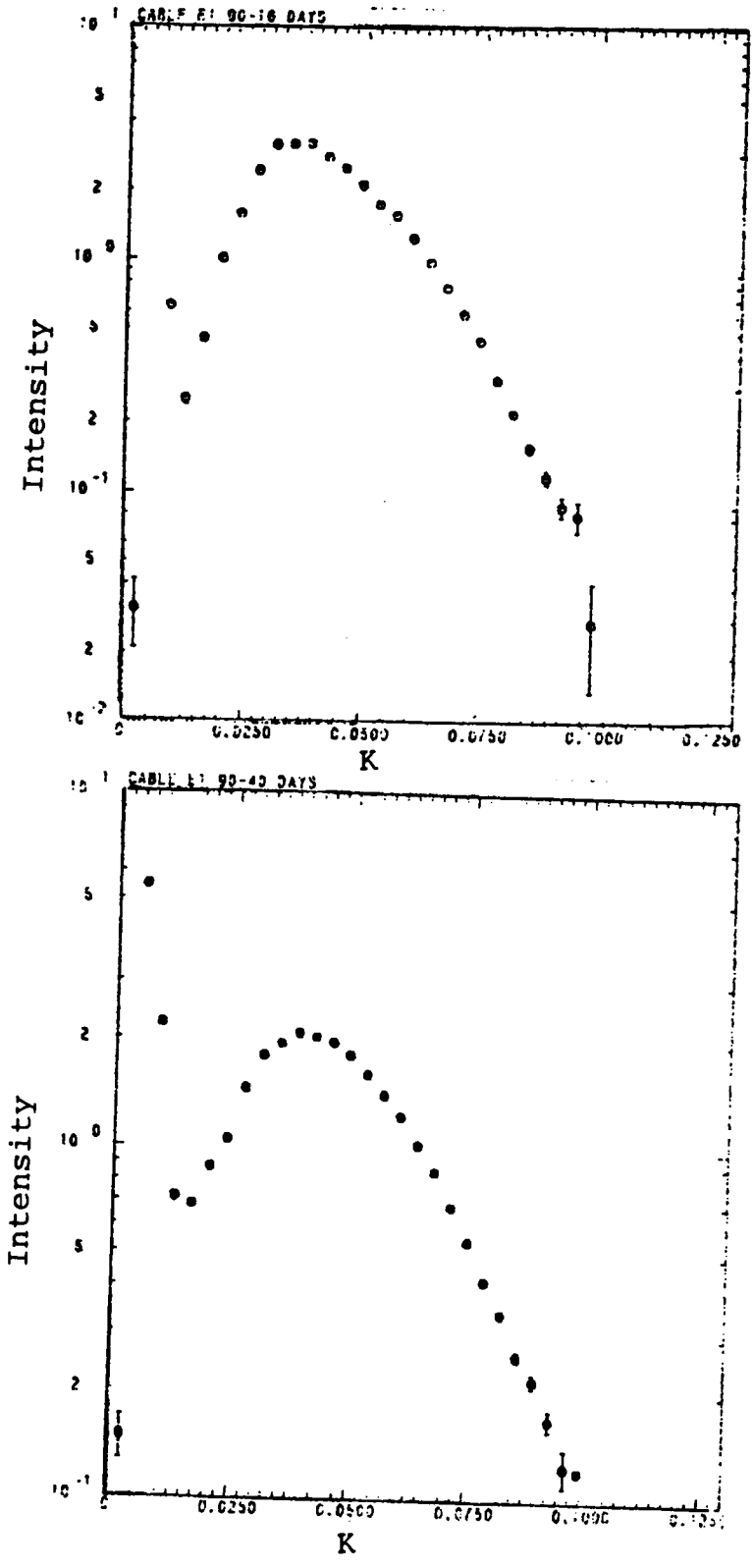

Figure 115 Circumferential average intensity versus scattering vector for cable A1 annealed at 90 °C for (O) 16 days and (●) 40 days.

Table 12 SAXS results obtained from annealed transmission cables

Cable	Annealing Temperature(^{o}C)	Annealing Time (days)	Long Period (^{o}A)
A1-1	107	2	174
A1-8	107	2	180
A1-8	Quenched	-	168
A1-8	90	2	193
A1-8	100	16	201
E1-8	90	2	209
E1-8	90	40	186

difference is the abundance of the thick lamellae observed for cable annealed at 107 ^{o}C. Similar effects are observed for 100 ^{o}C annealing but a fewer number of thick lamellae occur (Figures 116a-b and 117a-b).

LDPE air cooled from the melt resulted in banded spherulites typical of this material (Figures 118a-b). When original distribution cable D1 was subjected to the same thermal history, a similar morphology was observed (Figures 119a-b). 15 μm diameter impinging banded spherulites with a band periodicity of about three μm was observed to be the dominant morphological feature (Figures 119a-b).

4.3.5 Electrical Breakdown Studies

Thin films of crosslinked Union Carbide HFDE-4201 LDPE annealed for 30 minutes at 79, 85, 89, 93, 95, 100 and 107 ^{o}C were tested for their electrical breakdown strengths. Figures 120 show the DSC endotherms obtained for the annealed films. Narrowed versions of the original quenched peak are observed together with new peaks a few degrees above the annealing temperature, in each case, for annealings in the low temperature region (79-95 ^{o}C). High temperature peaks generated in 107 and 100 ^{o}C annealings were found to constitute 15 % and 68 % of the total peak area, respectively. These values are close to those obtained from cable A1 under similar conditions. Table 13 presents the breakdown voltage for 10 (or 9) test specimens annealed

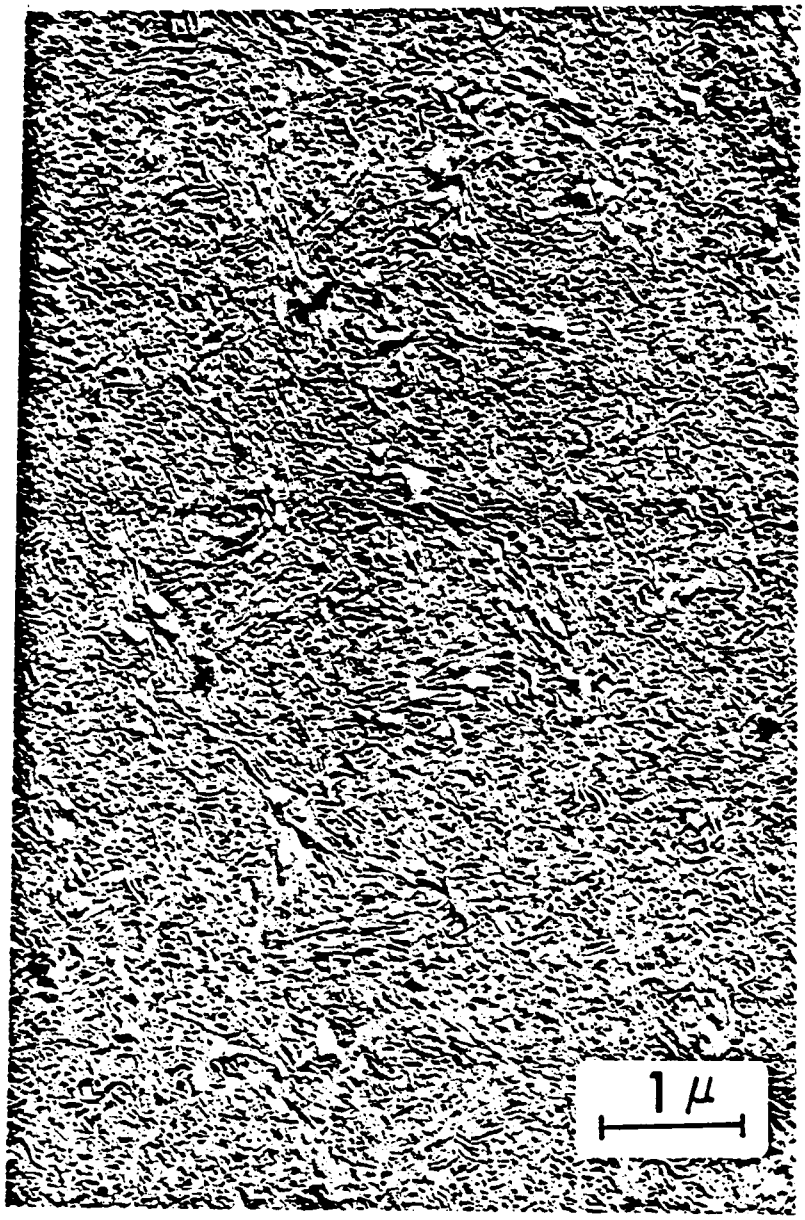

a

Figure 116 (a)(b) TEM pictures of cable A1-8 annealed at 107 °C for two days.

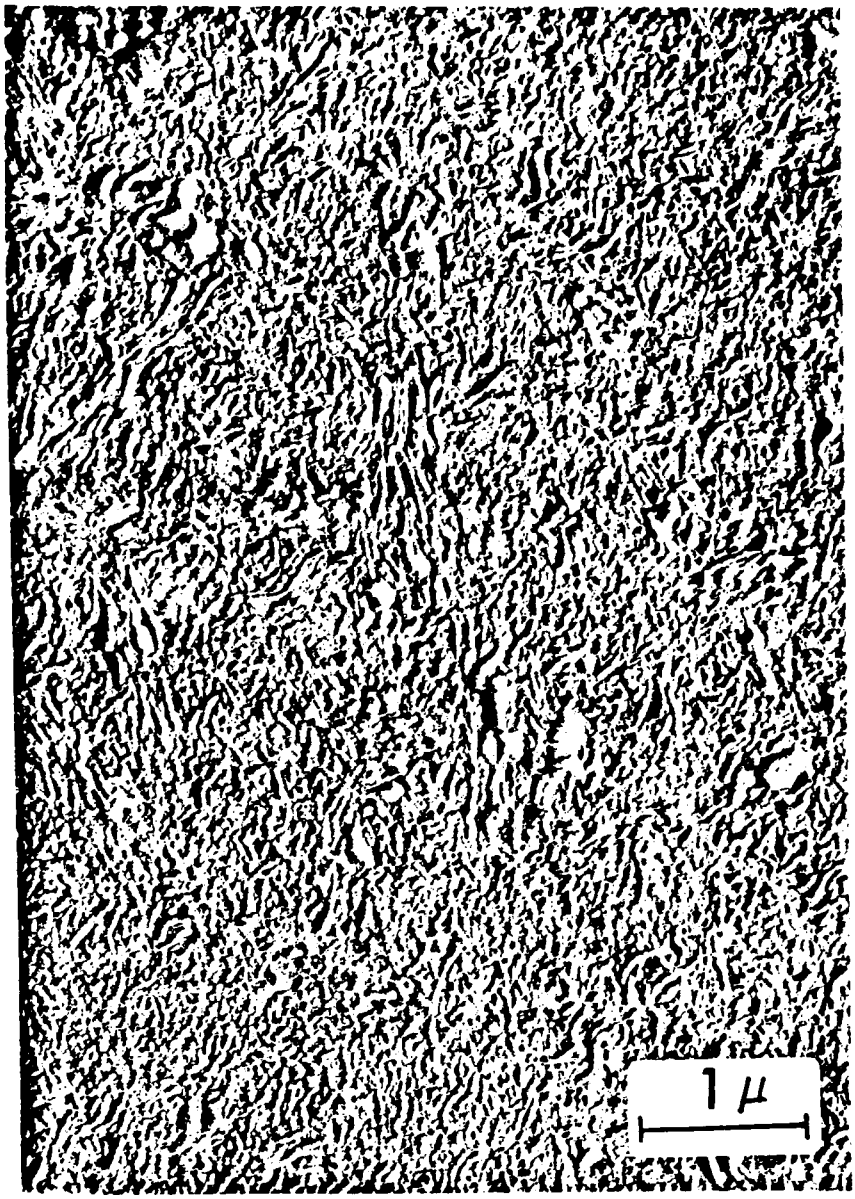

b

Figure 116 Continued

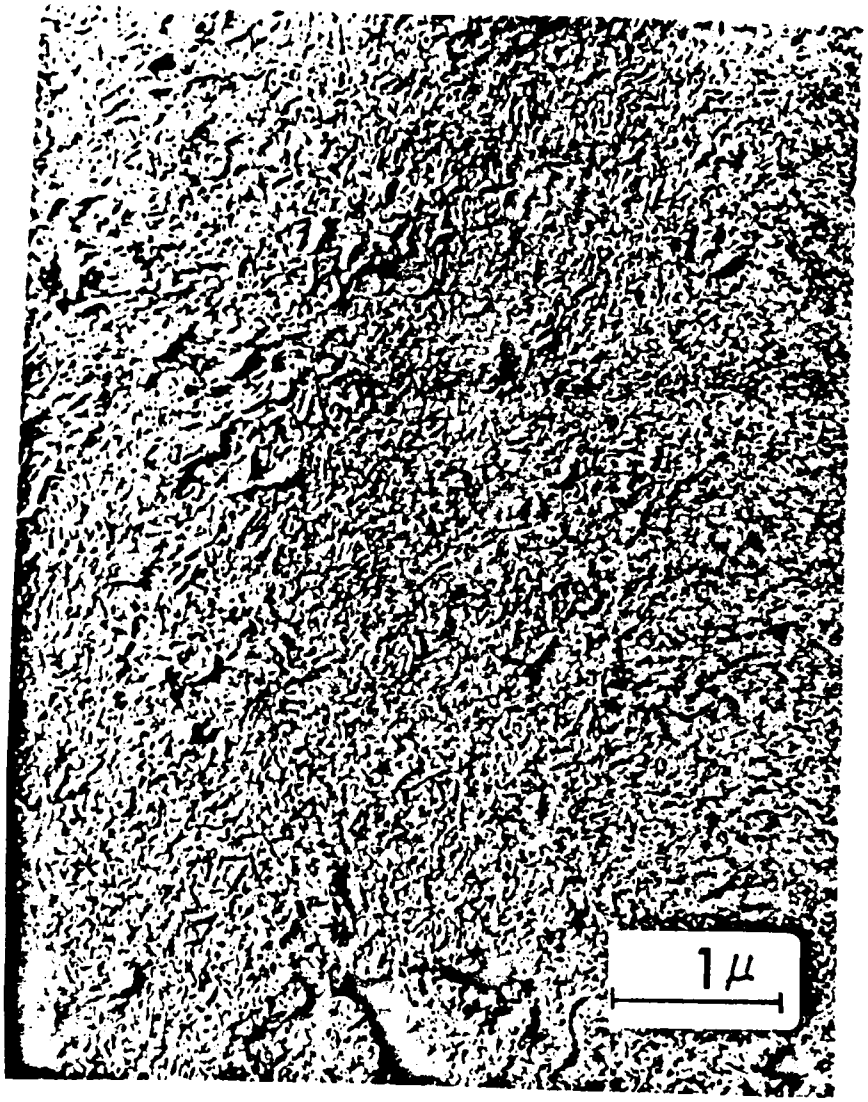

a

Figure 117 (a)(b) TEM pictures of cable A1-8 annealed at 100 °C for two days.

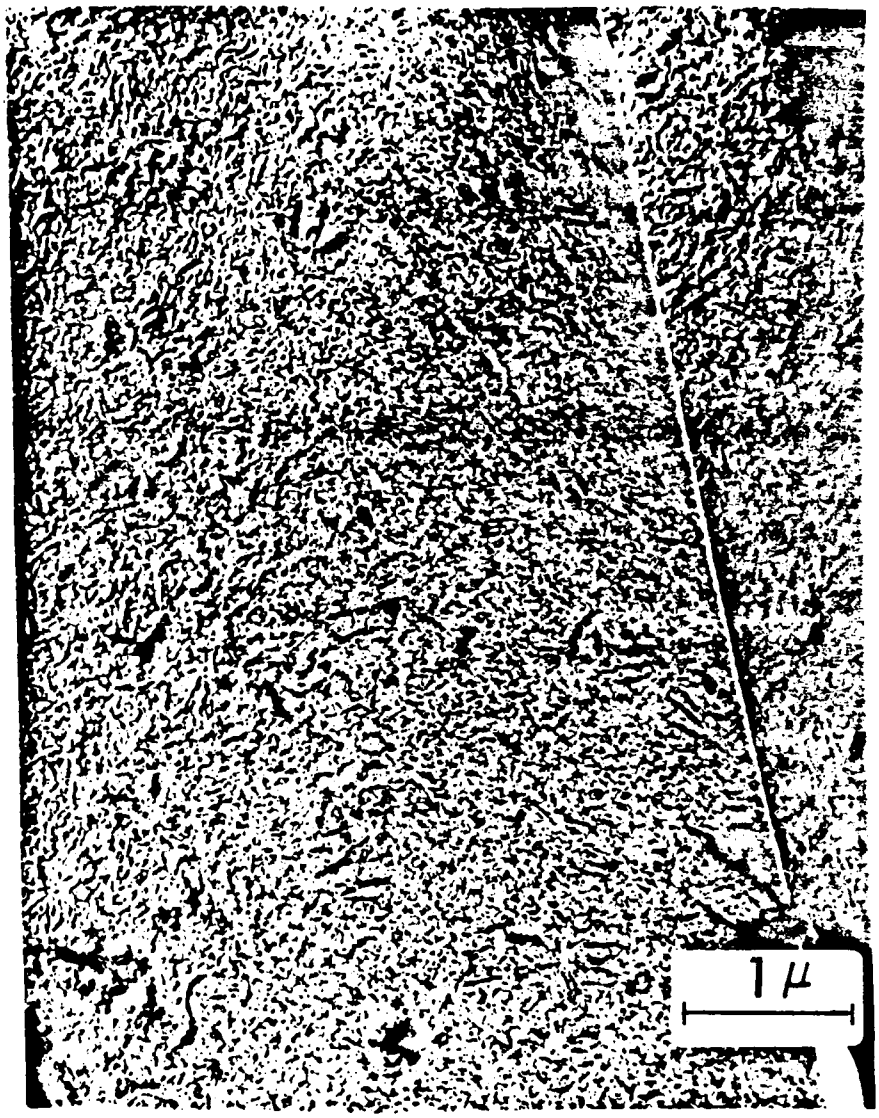

b

Figure 117 Continued

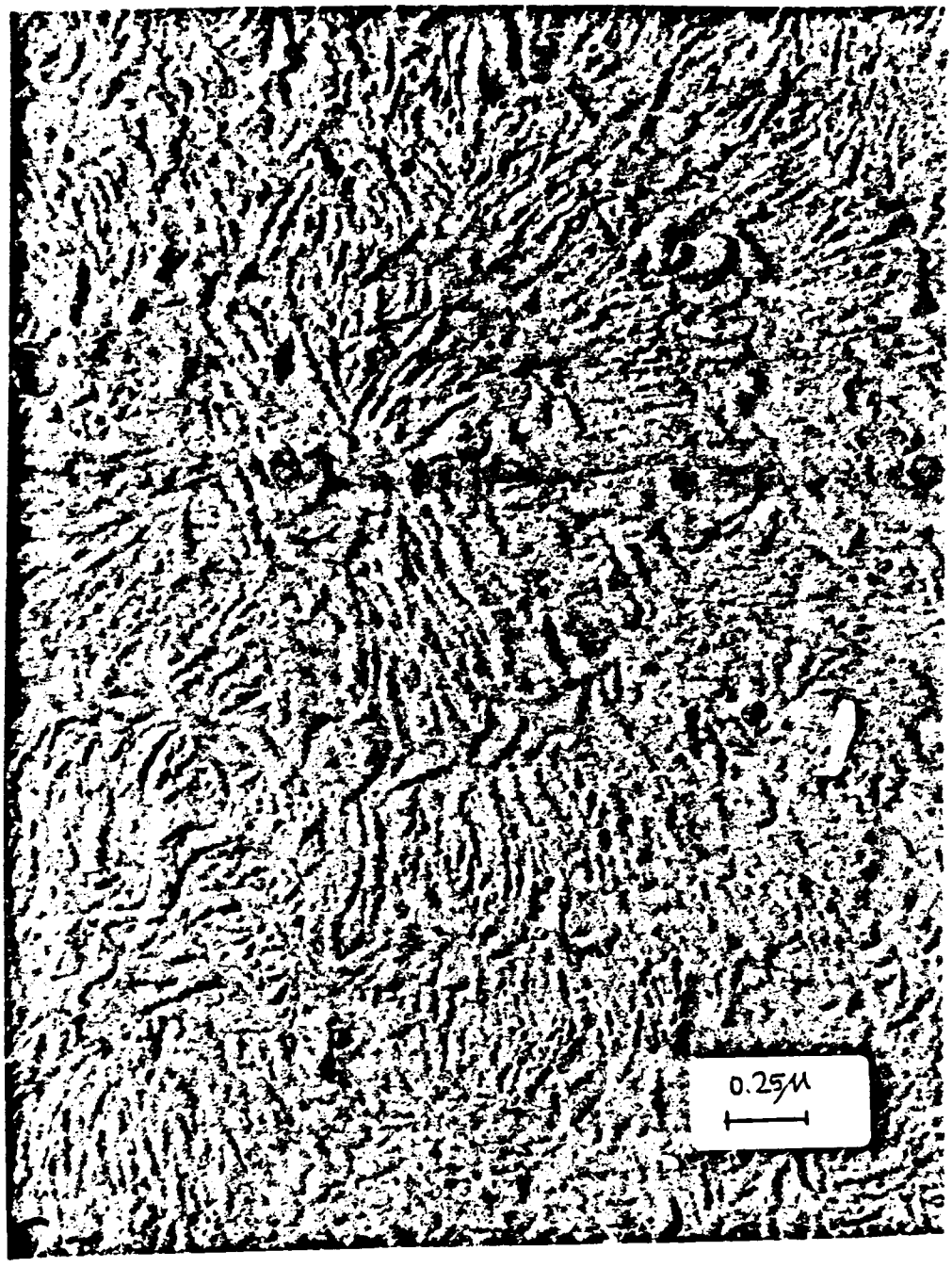

a

Figure 118 (a)(b) TEM pictures of LDPE samples air cooled from the melt.

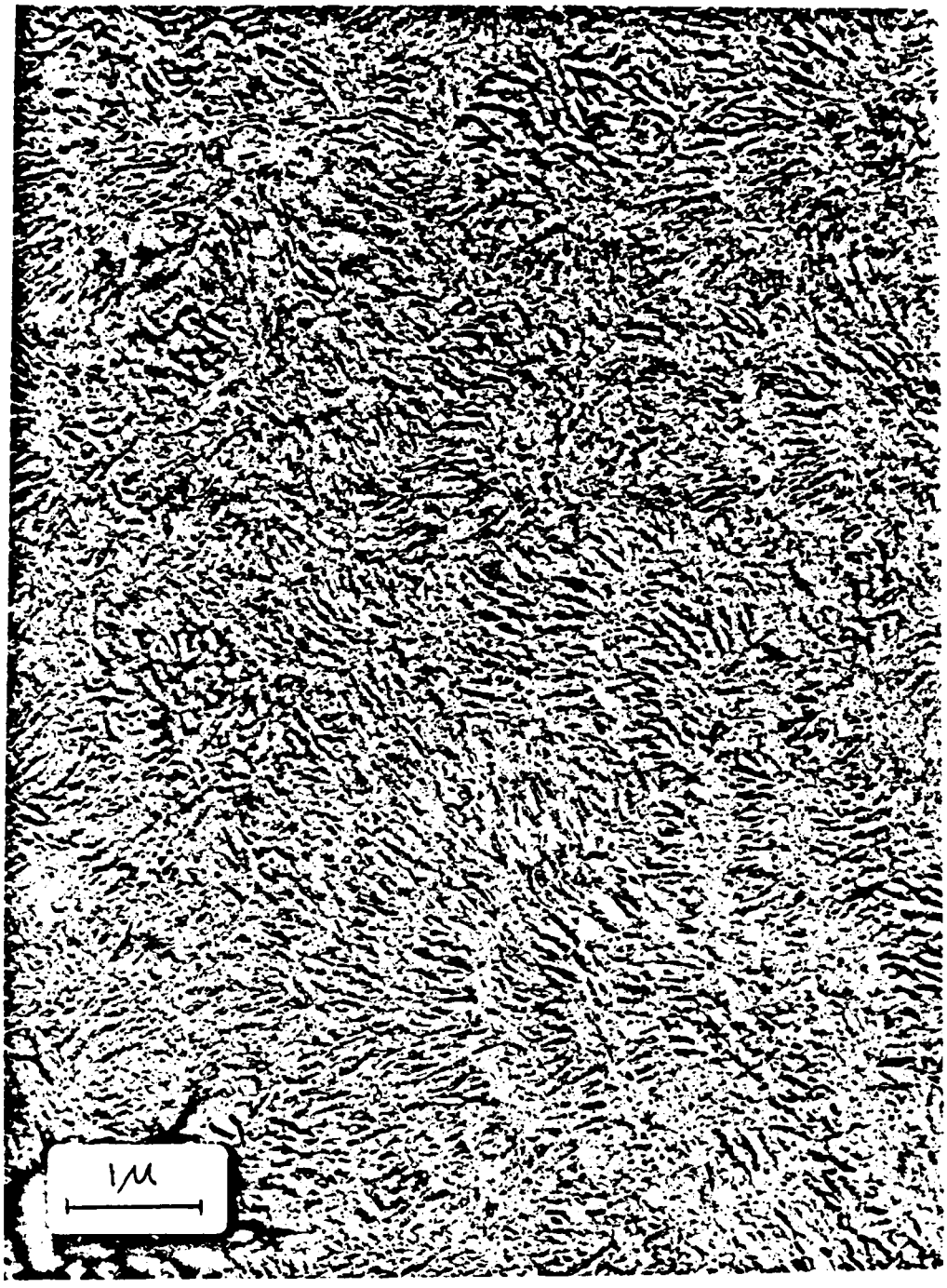

b

Figure 118 Continued

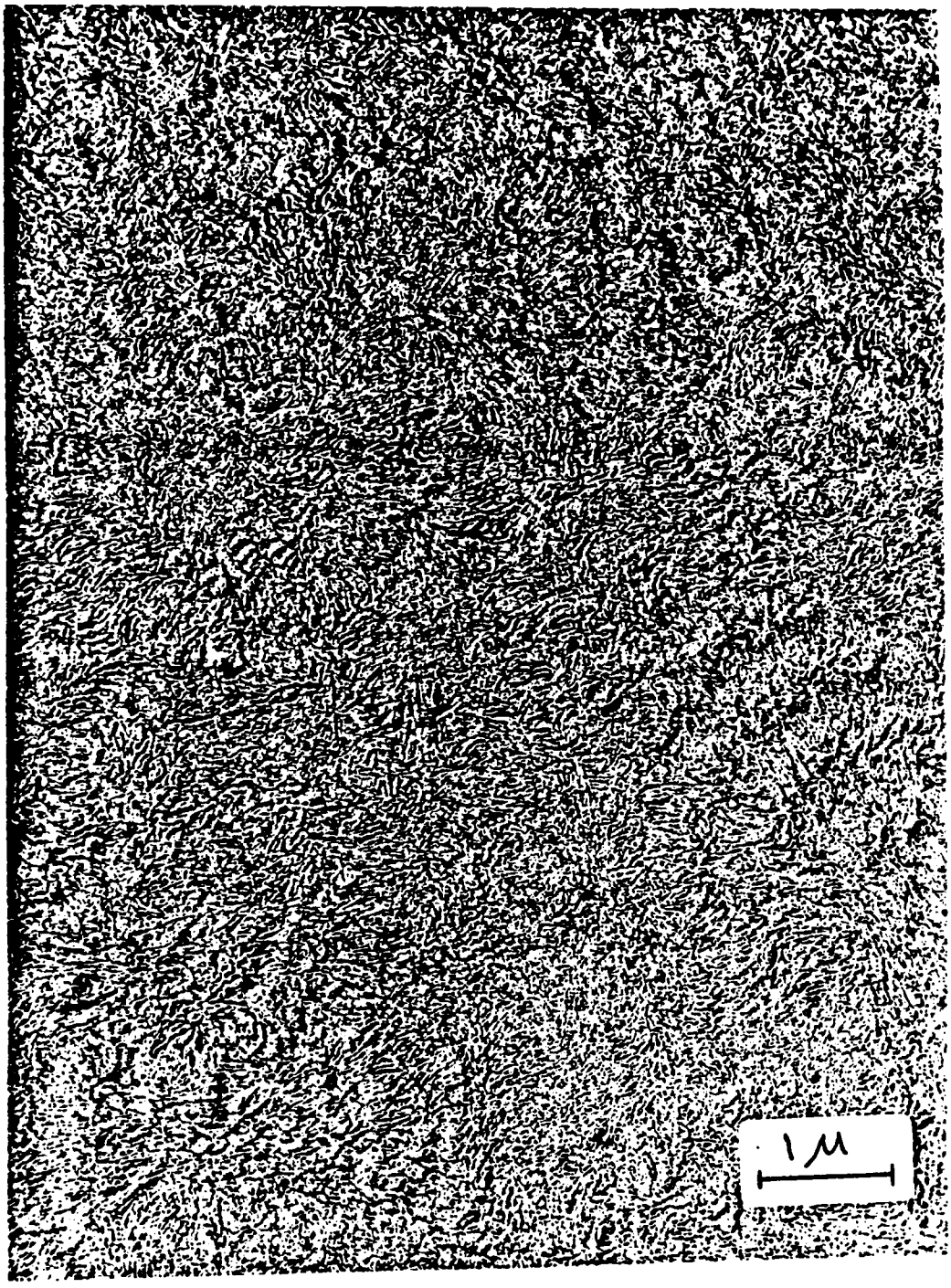

a

Figure 119 (a)(b) TEM pictures of distribution cable D1 air cooled from the melt.

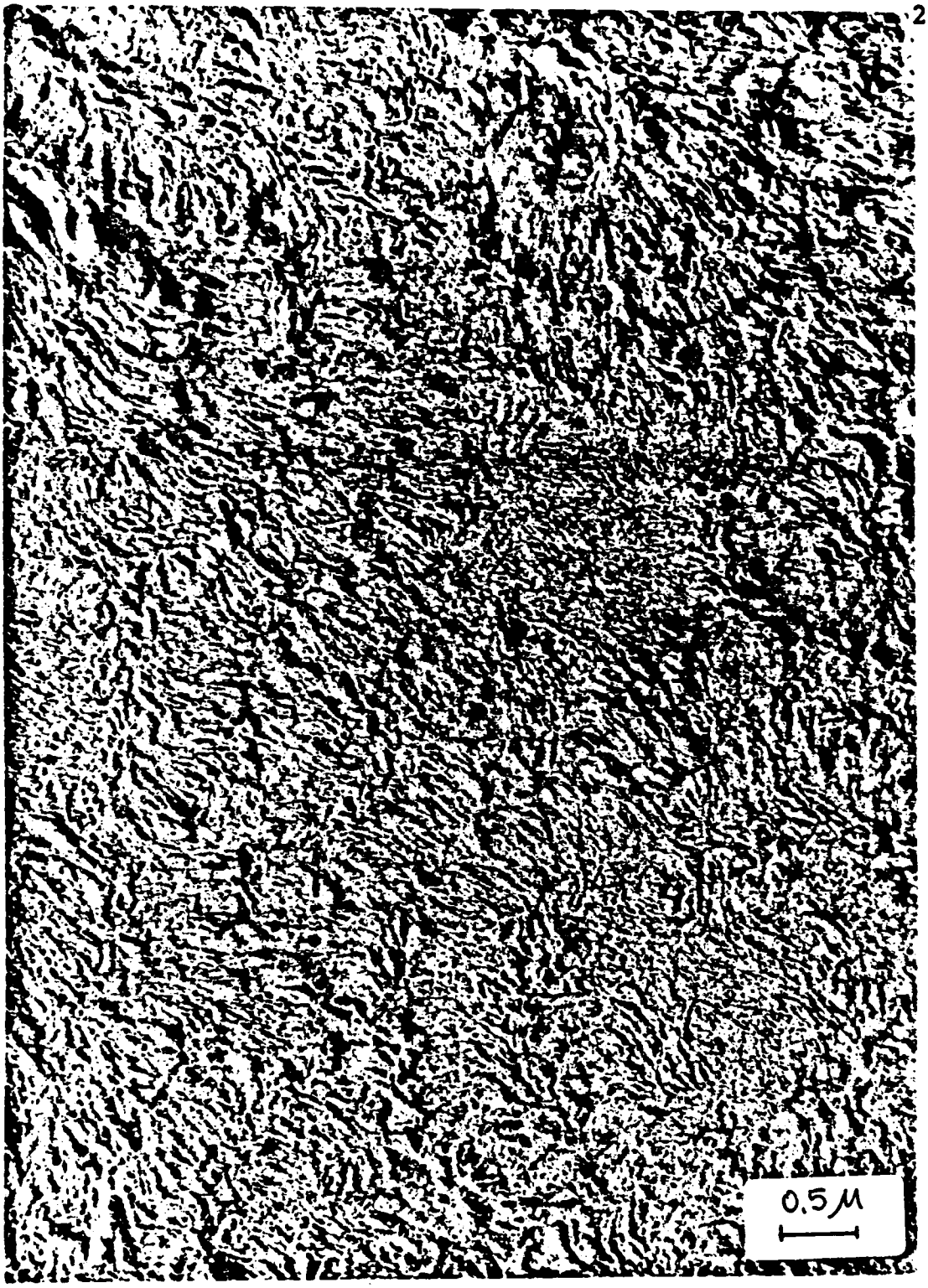

b

Figure 119 Continued

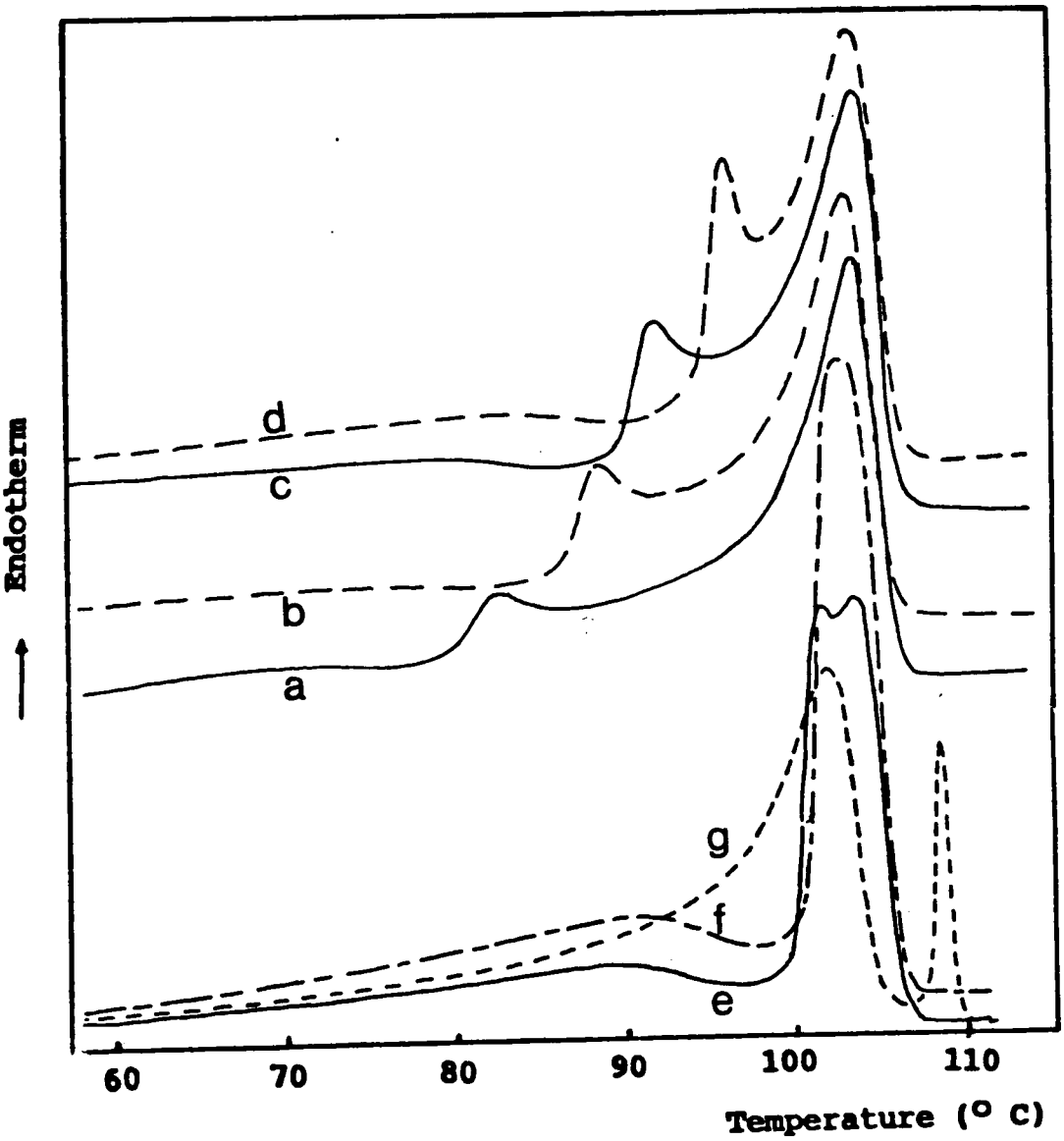

Figure 120 DSC thermograms of the XLPE thin films used in electrical breakdown tests annealed at a) 79, b) 85, c) 89, d) 93 , e) 95, f) 100 and g)107 °C for 30 minutes.

Table 13 Electrical breakdown data of XLPE thin films

Annealing Temperature (°C)	Breakdown Stress (V/mil) 1	2	3	4	5	6	7	8	9	10	Average
79	1663	1572	1921	1541	1442	1467	1400	1693	1733	-	1665
85	1468	1715	1591	1315	1550	1712	1449	1661	1835	-	1603
89	1584	1683	1484	1773	1720	1563	1823	1459	1327	-	1608
93	1736	1743	1959	1590	1485	1614	1421	1480	1616	-	1801
95	1725	2028	1845	1741	1768	2134	1693	1974	2159	2278	1627
100	1815	2187	1892	1669	1793	1822	1647	1650	1580	1720	1935
107	1833	1795	1735	1573	2008	1845	1905	1939	1973	1727	1774
Original	1793	1580	1655	1770	1699	1658	1603	1557	1718	1626	1833

at the indicated temperatures. As is seen from Table 13 the average breakdown stress for thin films annealed at temperatures of 95 ^{o}C and above were found to be higher than those of the original sample and of samples annealed at lower temperatures.

4.4 Field Aged Cables

4.4.1. Extraction Studies

The change in the amount of extractables in the innermost sections, #7 and #8, of the field aged cable E2 was followed by dividing each of these sections into four equal parts. While extractable levels remained almost constant throughout the radial sections of cable E1, an increase in extractables from 14 % to 18 % was recorded for the innermost two radial sections of the field aged version, E2 (Figure 121).

The radial distribution of extractables in the aged XLPE distribution cables was determined in a similar manner, except that the cables were divided into four equal radial sections. Table 14 presents the data obtained from the extraction studies of field aged distribution cables. While the average percent extractables over the entire radial direction of D12 field aged distribution cable was found to be 15.2 %, D9, D10 and D11 were found to have 23.1 %, 20.9 % and 20.2 %, respectively.

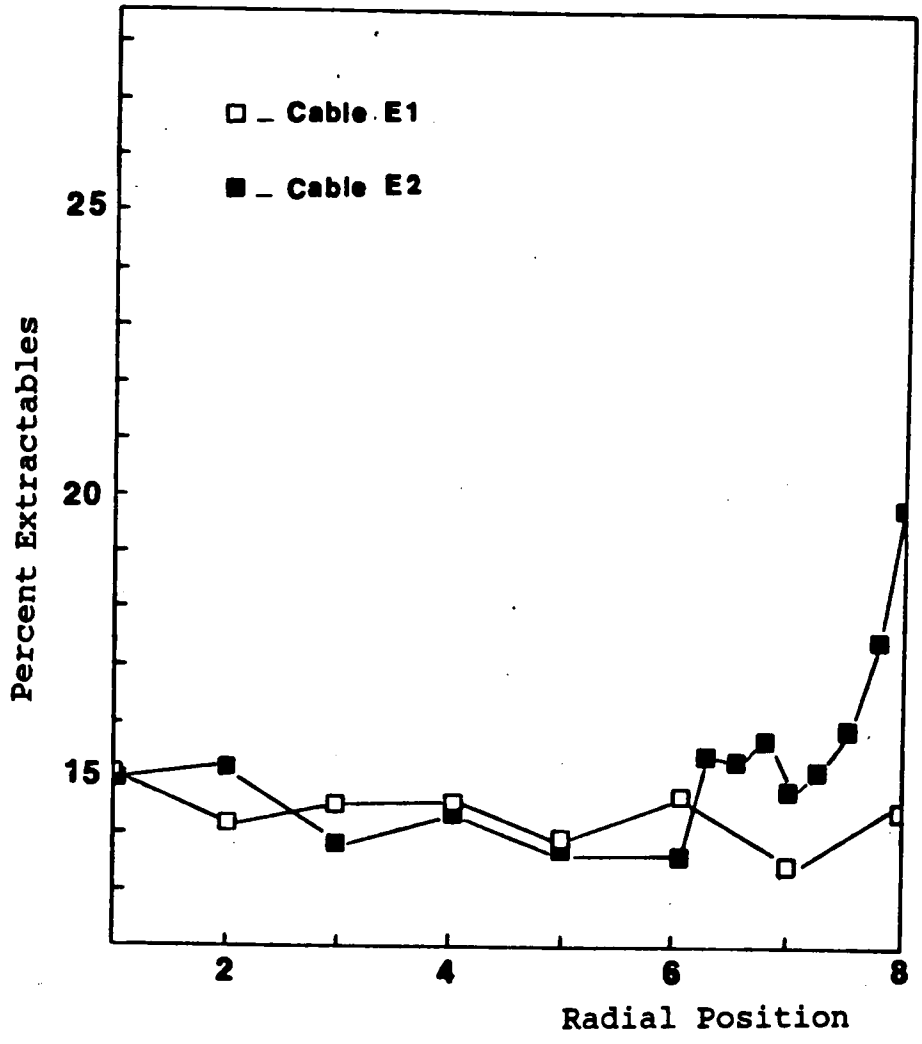

Figure 121 Percent extractables versus radial position for field aged (■) cable E2 and (□) original cable E1.

Table 14 Percent extractables versus radial position for the indicated distribution cables

	Percent Extractables			
Radial Position	D9	D10	D11	D12
1	23.6	20.0	21.2	15.4
2	23.5	19.8	20.6	14.8
3	22.9	20.5	19.2	15.0
4	22.3	23.1	19.8	15.4

4.4.2. Molecular Weight Studies of Extractables

GPC results of the extractables obtained from Cable E2 are given in Figure 122 and the related M_n, M_w and M_w/M_n data are presented in Table 15. Both Mn and Mw/Mn values for the inner layers were found to be lower than the values obtained for the outer layers.

4.4.3. Spectroscopic Studies

100 μm thick microtomed slices obtained from the outer and inner layers of cable E2 were studied for their molecular differences. As can be seen from Figures 123a-b and Table 16 an increase in carbonyl absorption was recorded for the inner layer compared to the values obtained for the outer layer. Carbonyl absorption of the inner layer was also found to be higher than the values recorded for the inner and outer layers of original cable E1. Although a noticeable increase in total unsaturation was recorded for the inner section of cable E2 compared to sections of cable E1, this increase was not as pronounced as for the carbonyl absorption (Figure 123a-b).

Similar analyses were carried out for the distribution cables. FTIR spectra from D2 and D4 aged LDPE distribution cables along with spectra for cable E2 are shown in Figures 123a-b. Given in Table 16, aged versions of both distribution cables have carbonyl and unsaturation

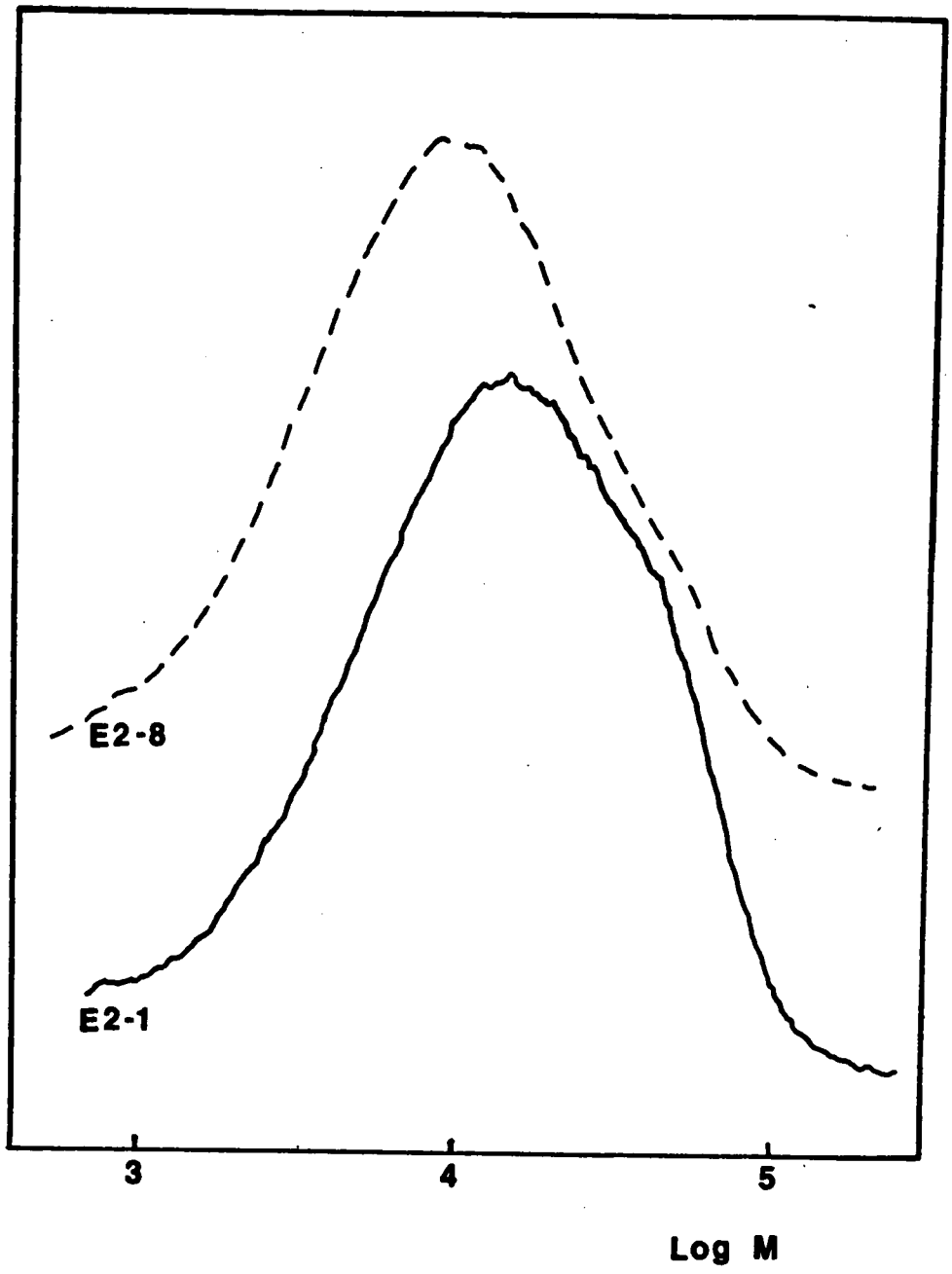

Figure 122 Molecular weight distributions of the extractables obtained from the inner (---) and the outer (——) radial sections of cable .

Table 15 GPC results on extractables obtained from the indicated radial positions of field aged cable E2

Cable	$M_n x10^{-3}$	$M_w x10^{-3}$	M_w/M_n
E2-1	7.14	22.9	3.21
E2-8	5.44	16.6	3.05

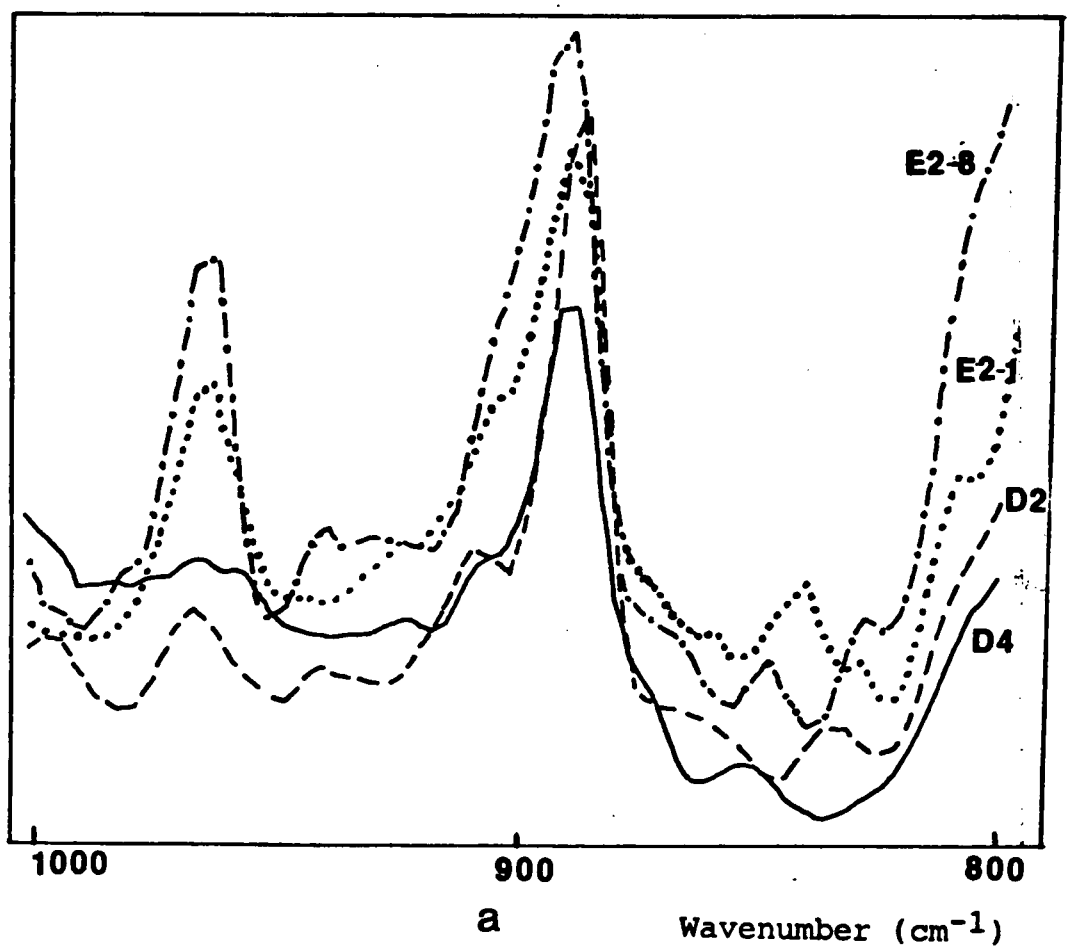

Figure 123 (a)(b) FTIR spectra of the field aged cables.

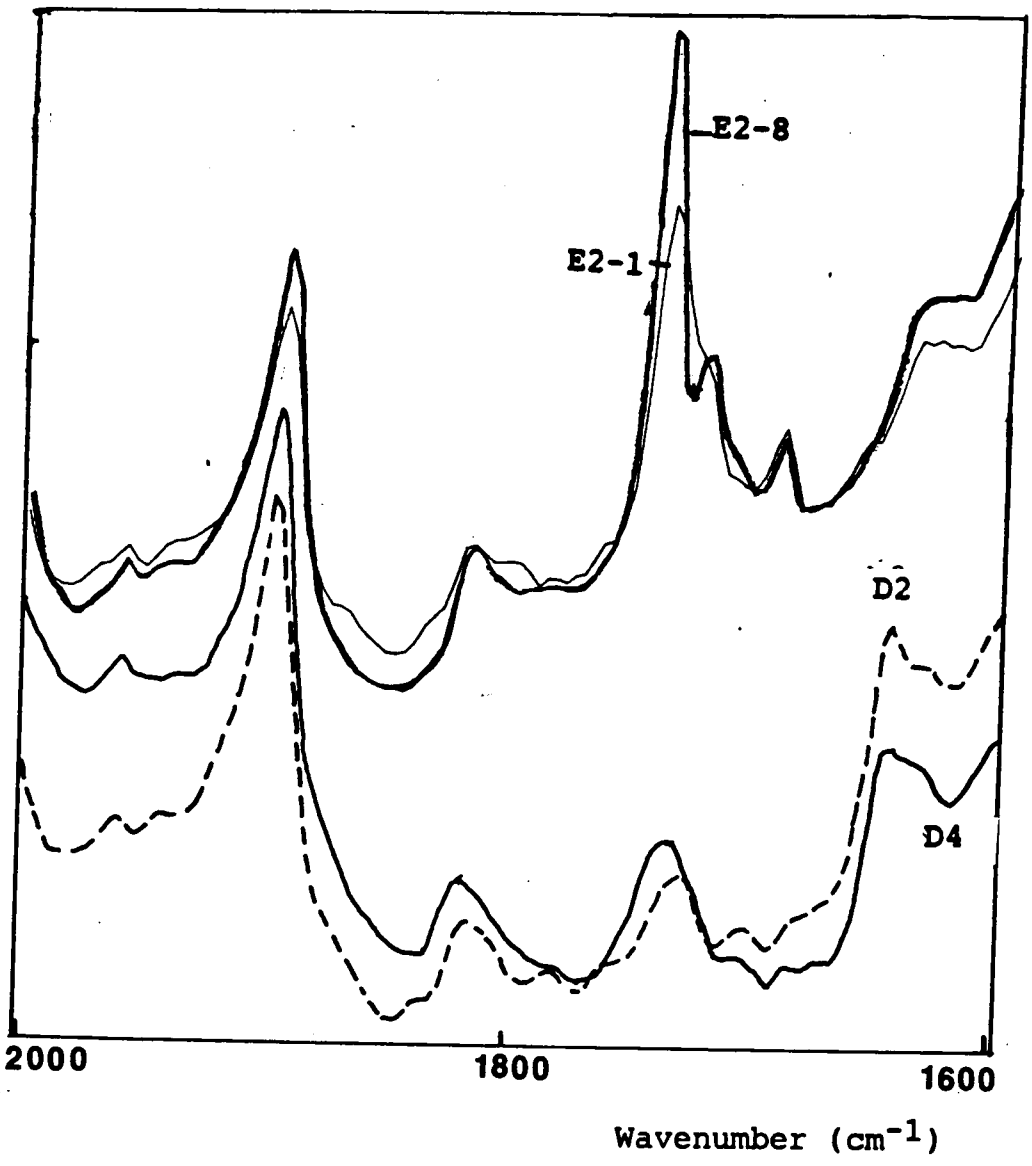

b

Figure 123 Continued

Table 16 FTIR data of the indicated field aged transmission and distribution cables

Cable	ABSORBANCE (a.u./mm)x10^{-2}			
	Carbonyl	Trans Vinylene	Vinyl	Vinylidene
E2-1	1.73	1.57	1.73	2.45
E2-8	3.90	1.99	1.38	2.56
D2	0.78	0.78	1.53	5.14
D4	1.13	0.39	1.21	3.45

absorption levels comparable to those of their unaged versions. The only exception is D3 which had only about one fifth of the carbonyl absorption level of its aged version. On the other hand, carbonyl absorptions of distribution cables, in general, were found to be in the range of 0.7-1.13x10^{-2} a.u./mm which is relatively lower than the levels observed in transmission cables (ca 0.95-9.61x10^{-2} a.u./mm) (Table 16, Figures 123a-b).

4.4.4. DSC Studies

The aging history of the field aged steam cured Cable E2 at the Waltz Mill aging facilities is given in Table 3, p 65.

The cable was first studied in eight radial sections. After detecting multiple-melting peak behavior in each section, in order to trace each individual peak closely, each section was further divided into four equal sub sections and DSC thermograms obtained. Progressive changes in the peaks' magnitude and position can be more closely followed from Figures 124-126 where all of the 1/32 sections are included. The sub designation nomenclature introduced here indicates the relative position of each 1/32 section in its 1/8 section (e.g. 8_1 refers to the outermost layer of radial section # 8 and 8_4 is the innermost layer of the same section and, so on). Figure 127 shows the DSC thermograms of 1/32 thick innermost layers from each 1/8

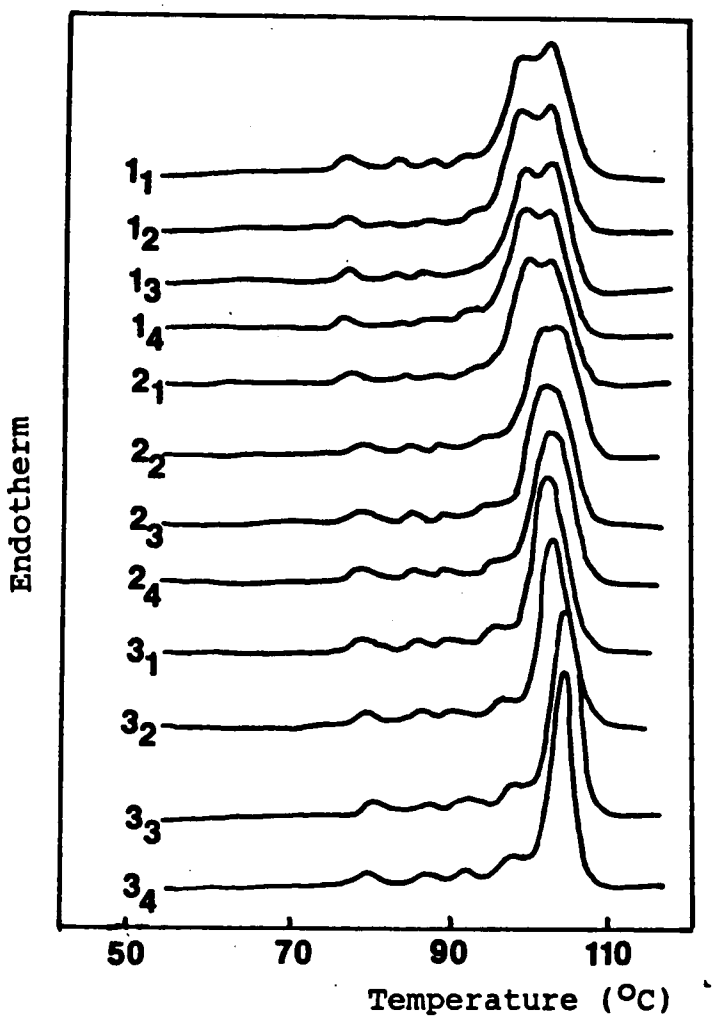

Figure 124 DSC thermograms obtained from the radial sections 1, 2 and 3 of field aged cable E2.

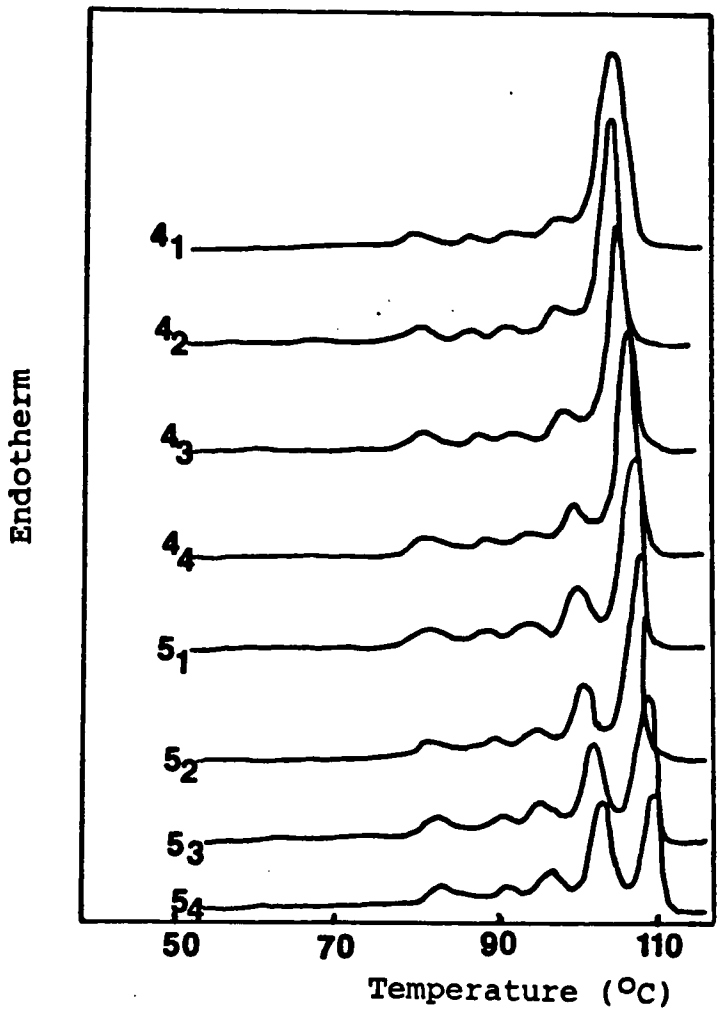

Figure 125 DSC thermograms obtained from the radial sections 4 and 5 of field aged cable E2.

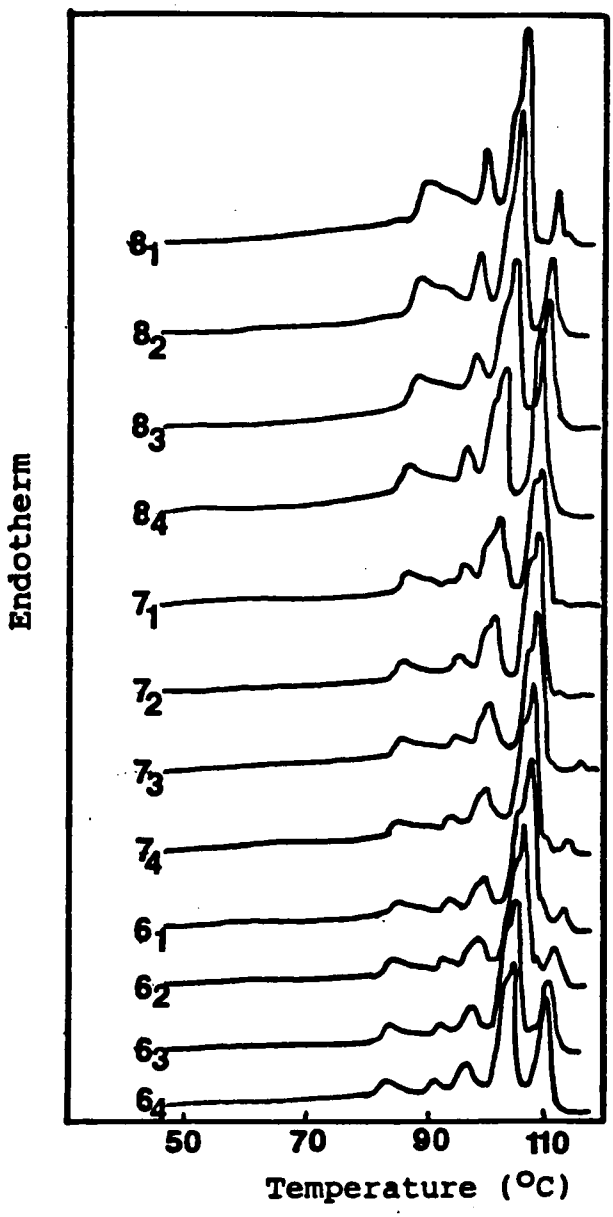

Figure 126 DSC thermograms obtained from the radial sections 6, 7 and 8 of field aged cable E2.

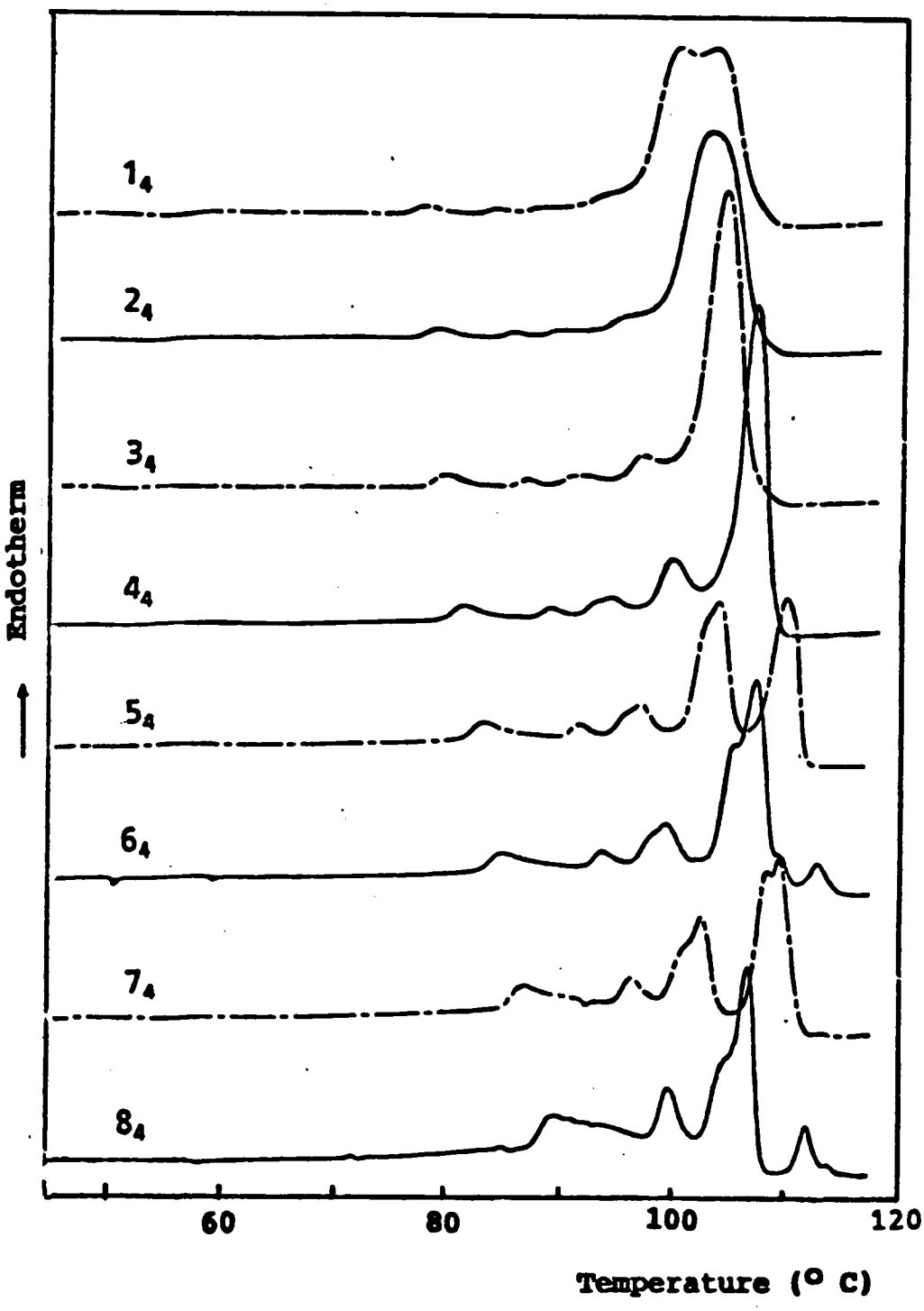

Figure 127 DSC thermograms representative of each one-eighth fraction of radial section of cable E2.

thick sections for a representative overall impression of the radial section. As is seen from these figures, the outermost layers result in endotherms with bimodal peaks and traces of lower melting subsidiary peaks. These subsidiary melting peaks increase in magnitude and temperature while the bimodal single peak first narrows then breaks up into newly generated peaks. The T_m s of each individual peak from Figures 124-126 are plotted in Figure 128. As can be seen from Figure 128, a progressive increase in T_m is disrupted around radial section #6, which has minor high temperature peaks, possibly generated at high annnealing temperatures.

Percent crystallinity as a function of radial position for each 1/32 section is given in Figure 129. In general, the crystallinity was found to be larger than forcable E1. While an even distribution of crystallinity along the radial direction of cable E1 was observed, cable E2 showed scatter. Crystallinity levels for the innermost and outermost layers were found to be comparable, while an increase in crystallinity was observed for the radial positions 5_3 to 7_4.

Melting endotherms obtained from the radial sections of field aged LDPE and XLPE distribution cables are presented in Figures 130-132. Each thermogram is representative of one fourth of the entire radial direction. T_m, T_{rb} and ΔH_f values are summarized in Table 17. Slight

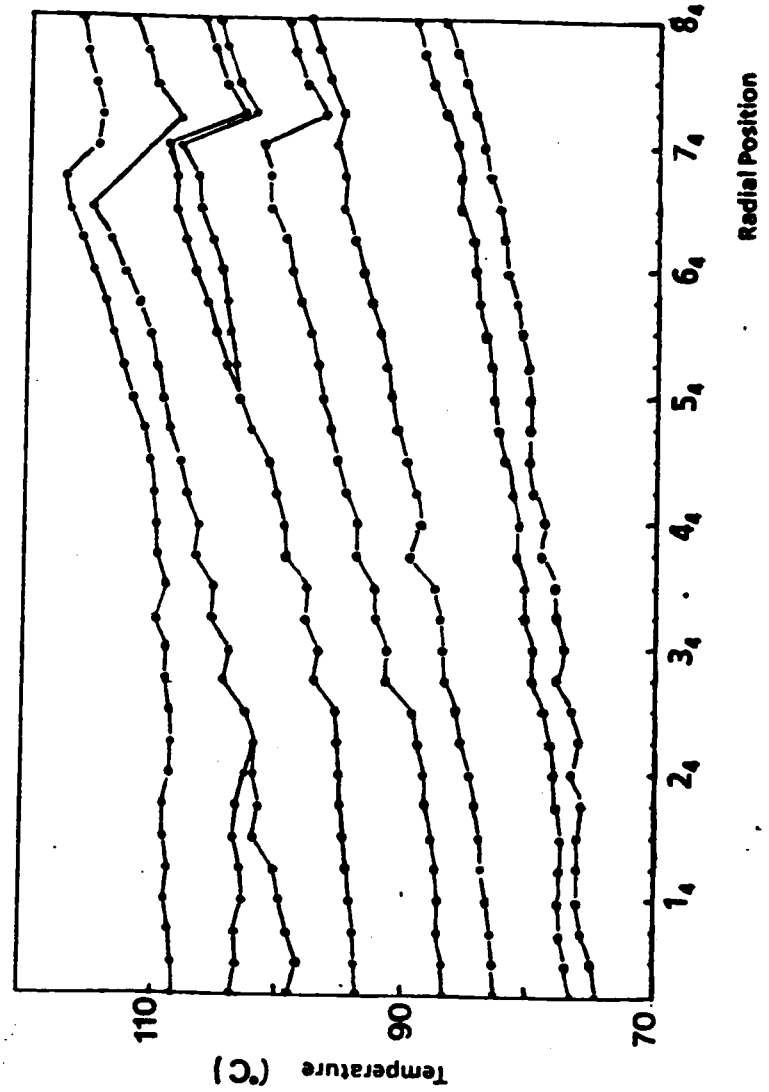

Figure 128 Melting temperature versus radial position obtained from the DSC thermograms of radial sections, each being 1/32nd of the entire radial section of cable E2.

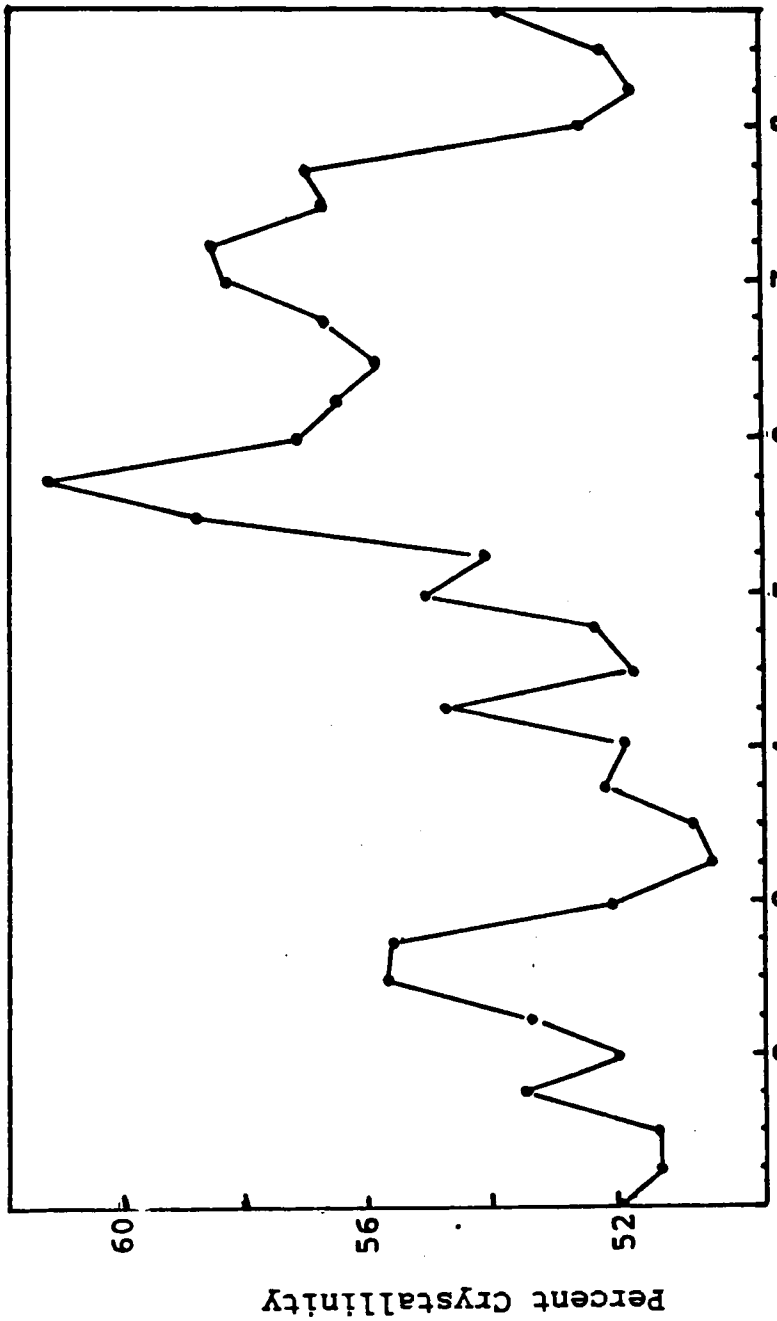

Figure 129 Percent crystallinity as a function of radial position for each 1/32nd fraction of the radial section of cable E2.

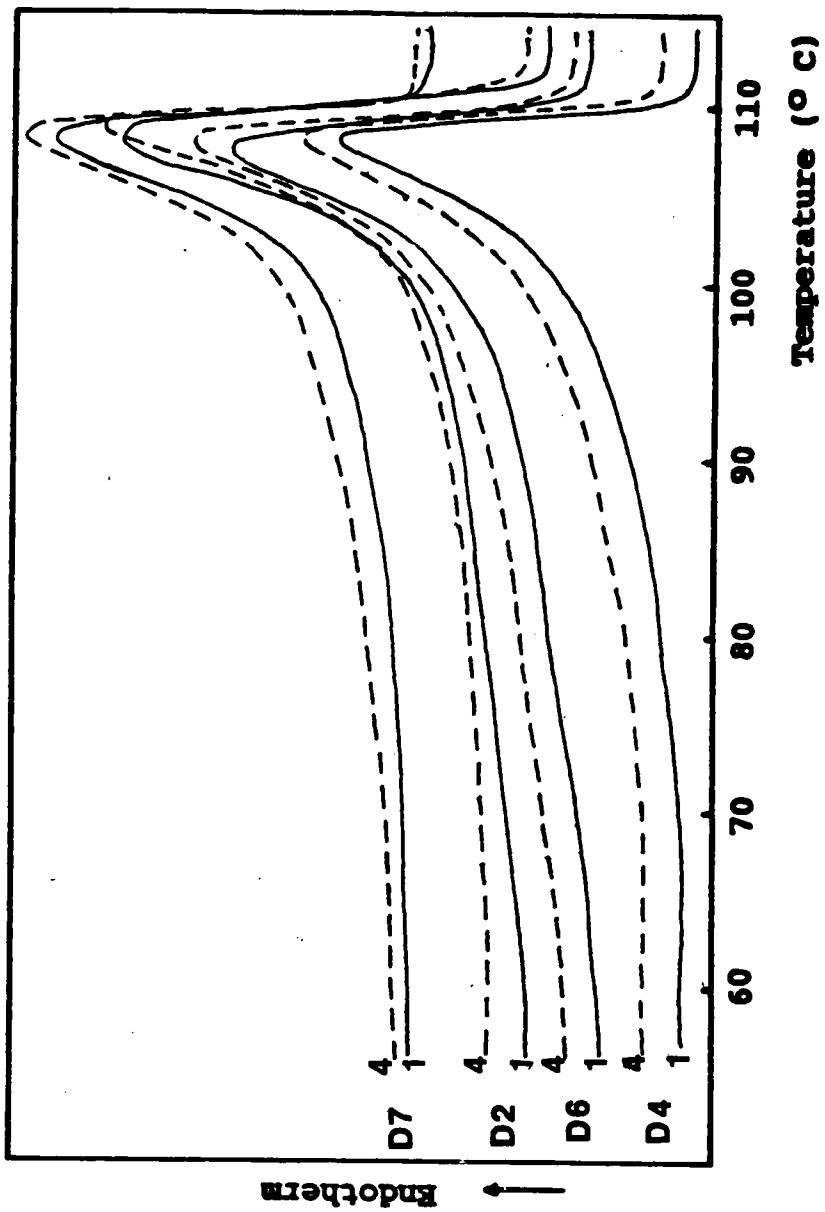

Figure 130 DSC thermograms of field aged distribution cables D2, D4, D6 and D7.

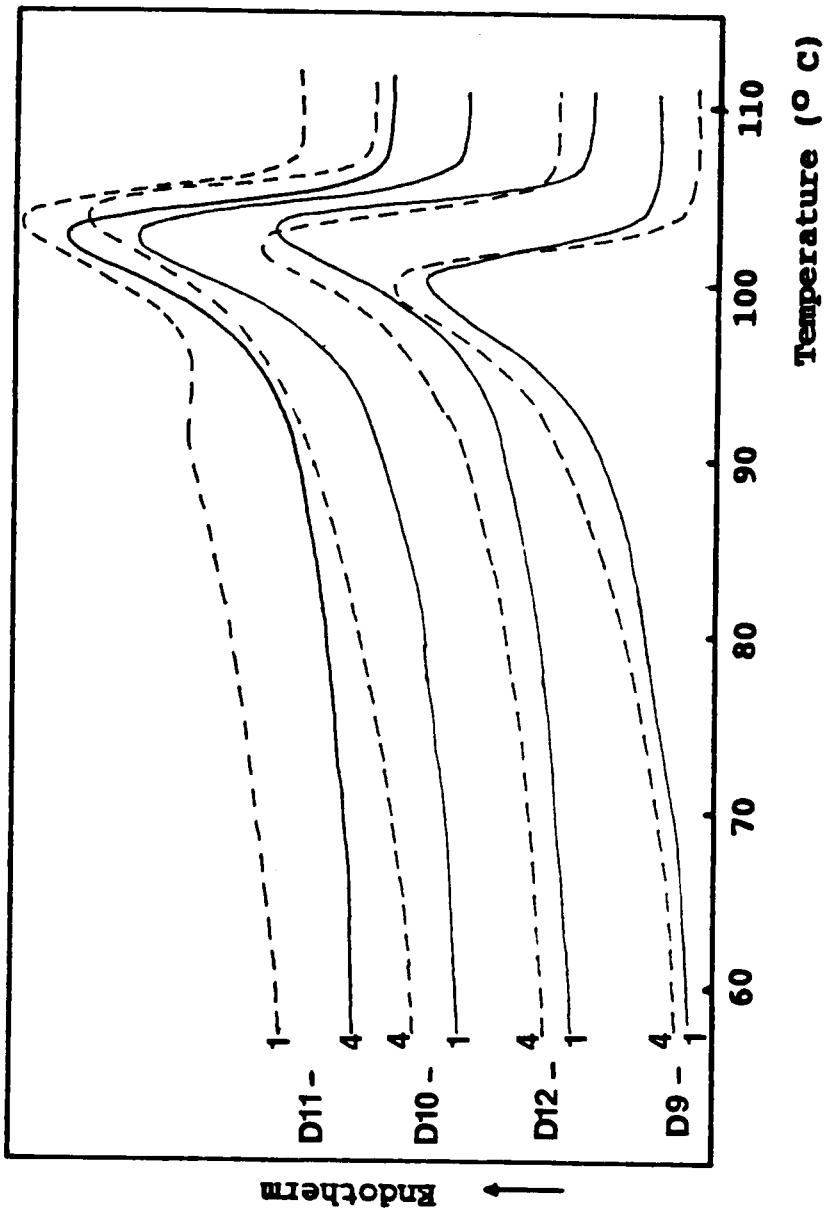

Figure 131 DSC thermograms of field aged distribution cables D9, D10, D11 and D12.

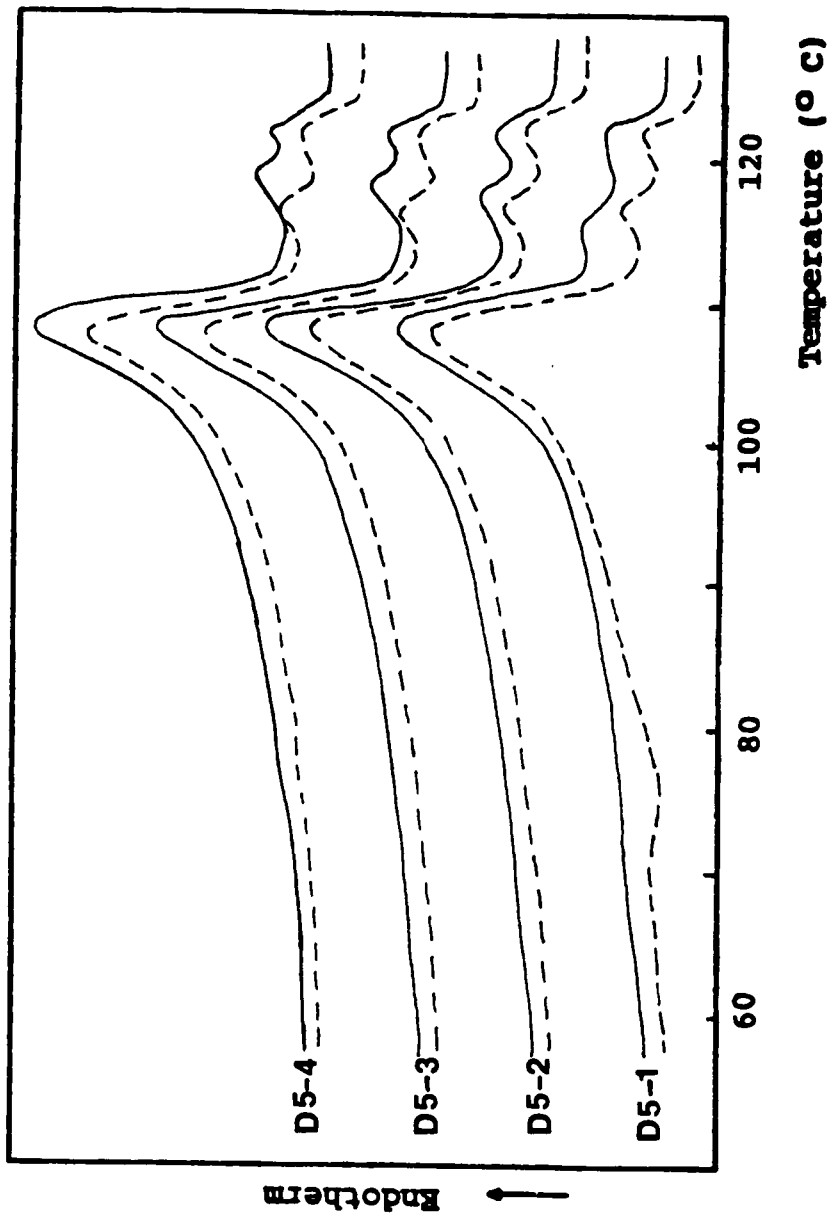

Figure 132 DSC thermograms of D5 field aged distribution cables.

Table 17 DSC results for the indicated field aged distribution cables

Cable	T_m (°C)	T_{rb} (°C)	ΔH (J/g)	Percent Crystallinity
D2-1	107.9	111.6	103 3	66.2
D2-4	108.6	111.9	91 .4	58.6
D4-1	108.2	111.3	98.3	63.0
D4-4	108.0	111.3	90.1	57.7
D5-1	108.0	124.8	102.3	65.4
D5-4	108.0	124.8	104.3	66.8
D6-1	107.6	111.6	97.3	49.6
D6-4	107.8	111.6	100.6	64.5
D7-1	108.3	111.6	77.4	49.6
D7-4	108.8	111.3	82.7	53.0
D9-1	100.0	105.2	71.6	45.9
D9-4	100.1	105.2	70.5	45.2
D10-1	102.4	107.1	75.9	48.6
D10-4	103.8	107.1	76.9	49.3
D11-1	102.4	107.1	79.0	50.6
D11-4	103.2	108.0	82.2	52.7
D12-1	102.8	107.4	79.8	51.2
D12-4	102.0	106.8	79.0	50.6

increases in T_m, T_{rb} and ΔH_f values for these field aged cables were observed compared to their original versions.

4.4.5. X-Ray Studies

Percent crystallinities of the inner and outer layers of cable E2 obtained from intensity versus 2θ WAXS patterns were found to be 50.7 and 50.4 %, respectively.

Small angle X-Ray scattering contours obtained for the inner and outer layers of Cable E2 are shown in Figures 133a-c. Circumferential average intensity versus scattering vector for the outer and inner layers are shown in Figure 134. Major differences between the scattering plots obtained for the inner and outer layers were observed at smaller scattering angles (Figure 134). Low angle scatterings are believed to result from the presence of extensive amounts of bow-tie trees at the innermost layer (Figure 135a-b). In order to prove this, cable samples were impregnated with mineral oil. As can be seen from Figure 136 low angle intensities were eliminated. These voids were found to be larger than 720 ^{o}A. The reduction in the scattering intensity over the high scattering angles indicates the effectiveness of oil diffusion. The relatively water tree free outside layer did not show any low-angle scattering.

Figures 137a-b are TEM pictures taken from the inner layer of Cable E2. In general, the morphology was observed to be similar to that of the original cable except

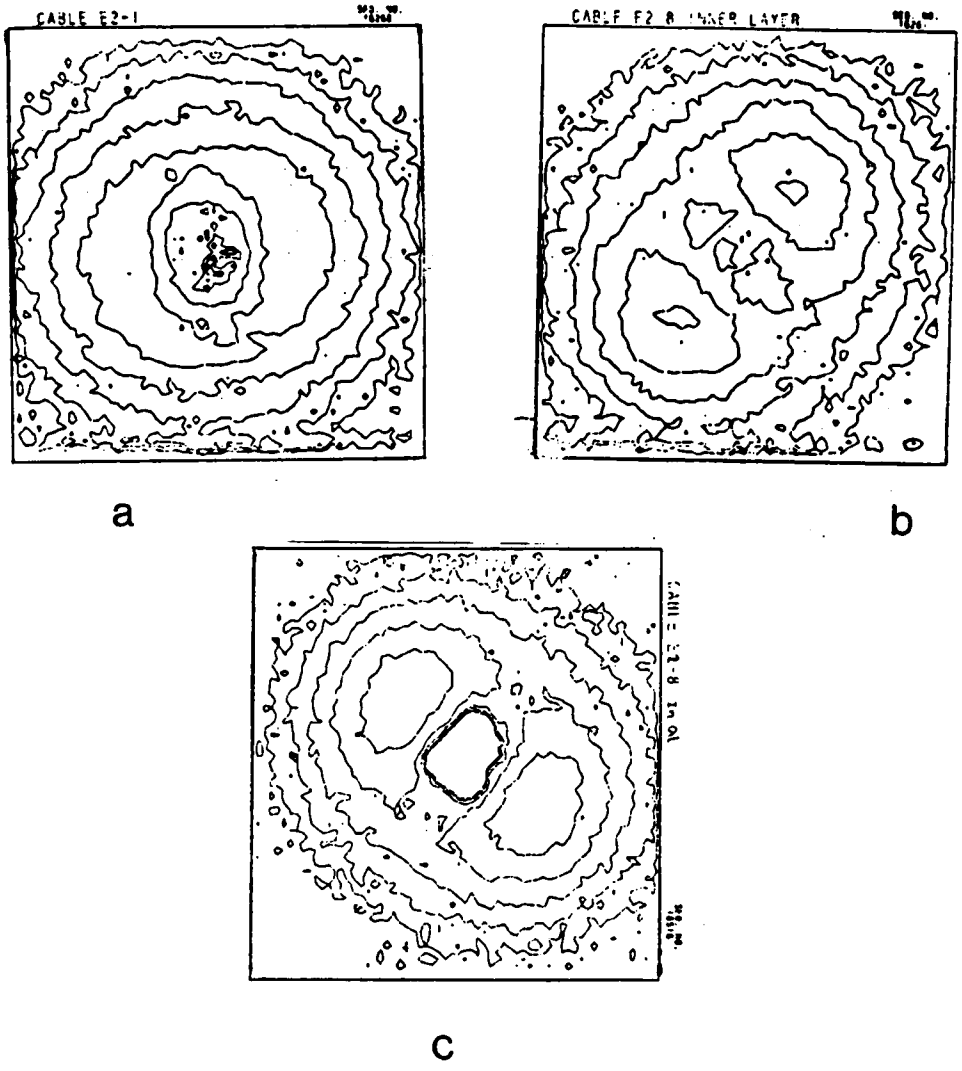

Figure 133 SAXS contours obtained from (a) outer and (b) inner layers of cable E2 and (c) inner layer soaked in oil.

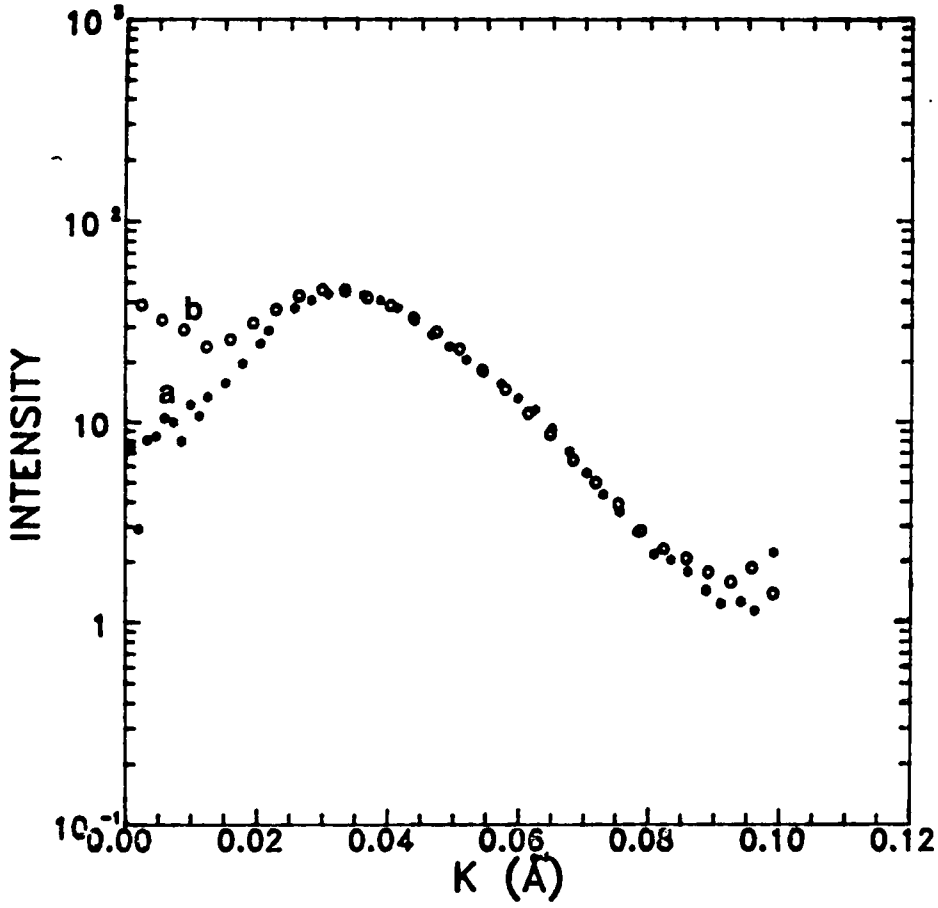

Figure 134 Circumferential average intensity versus scattering vector for (a) outer and (b) inner layer of cable E2.

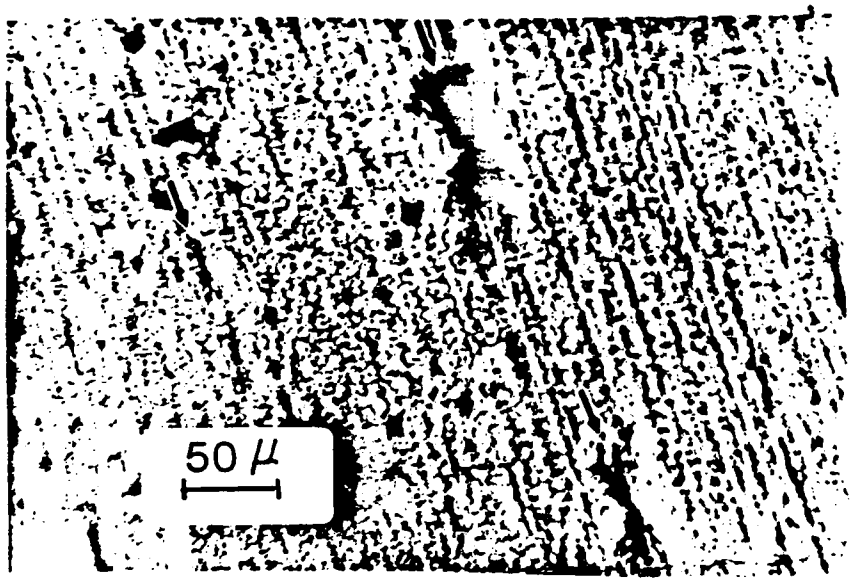

a

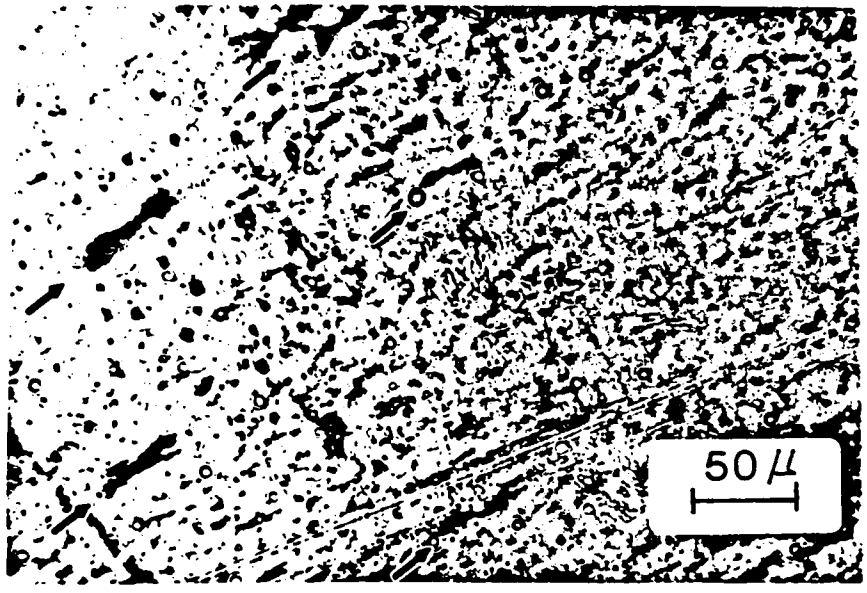

b

Figure 135 Bow-tie trees from the inner layer of cable E2.

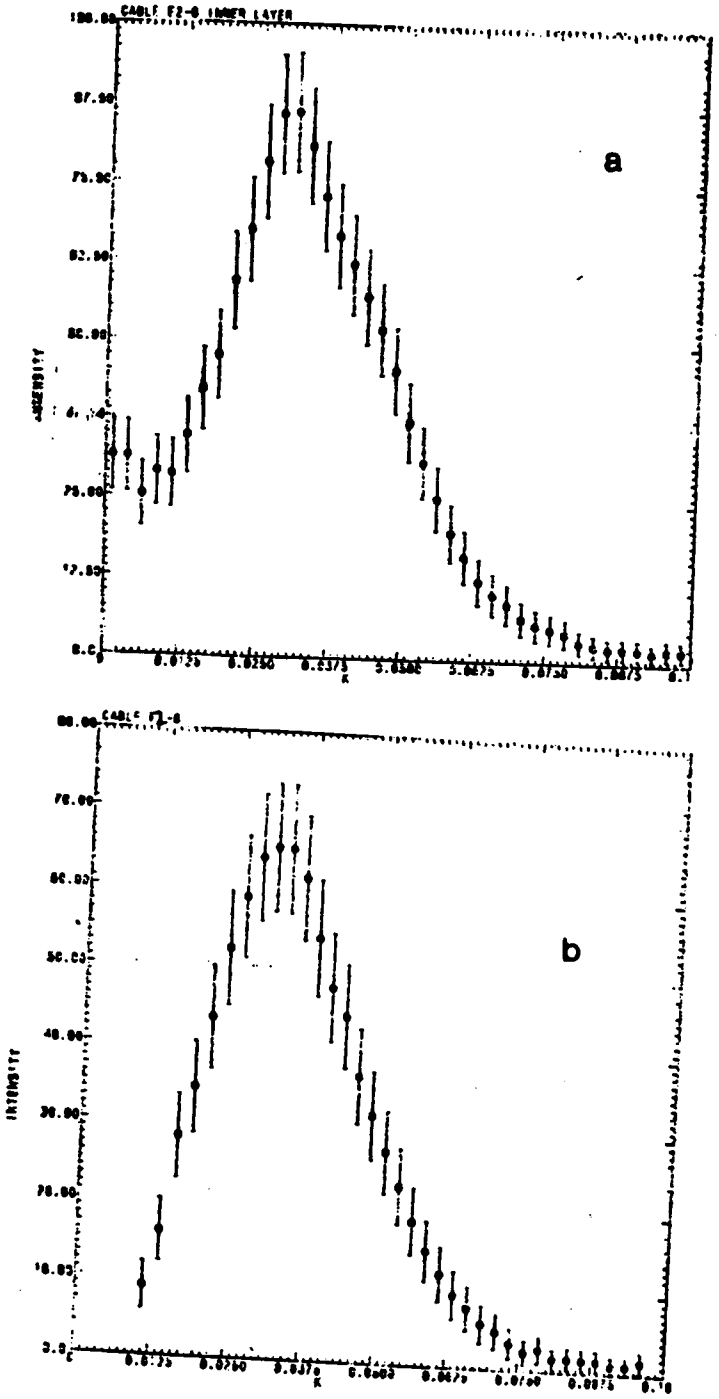

Figure 136 Angle average intensity versus scattering vector for (a) dry and (b) oil-soaked inner layer of cable E2.

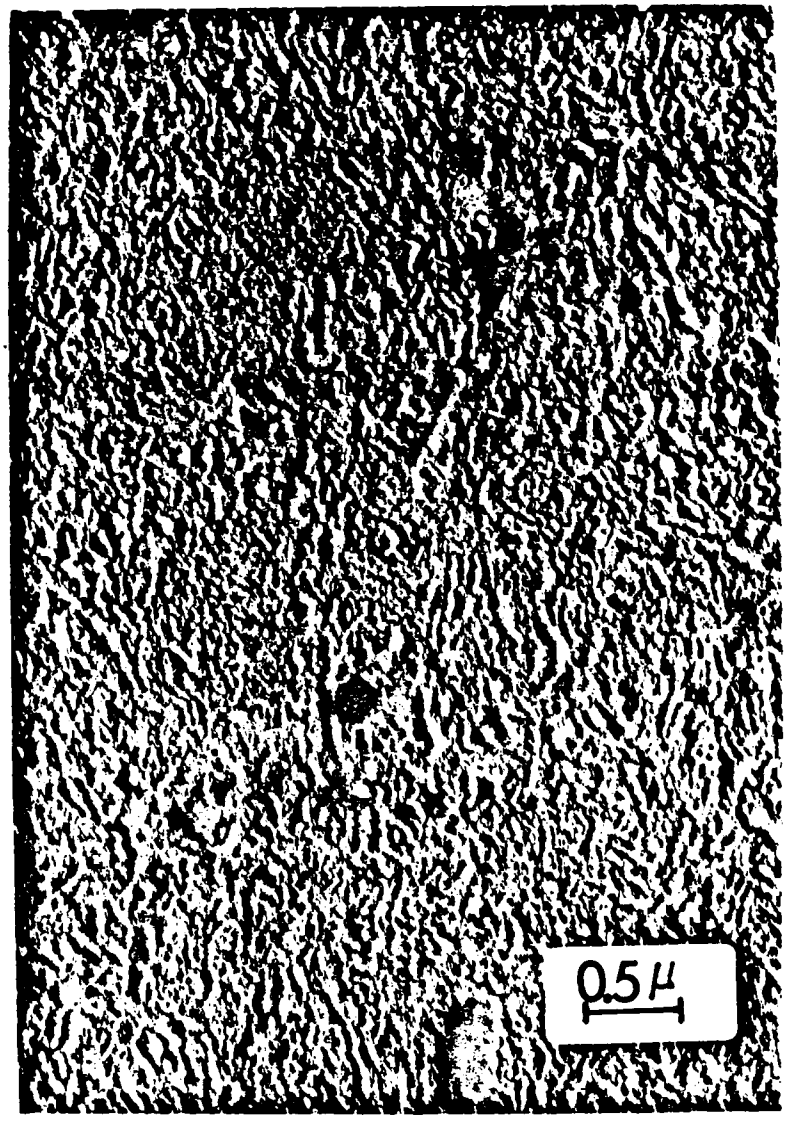

a

Figure 137 (a)(b) TEM pictures obtained from the inner layer of cable E2.

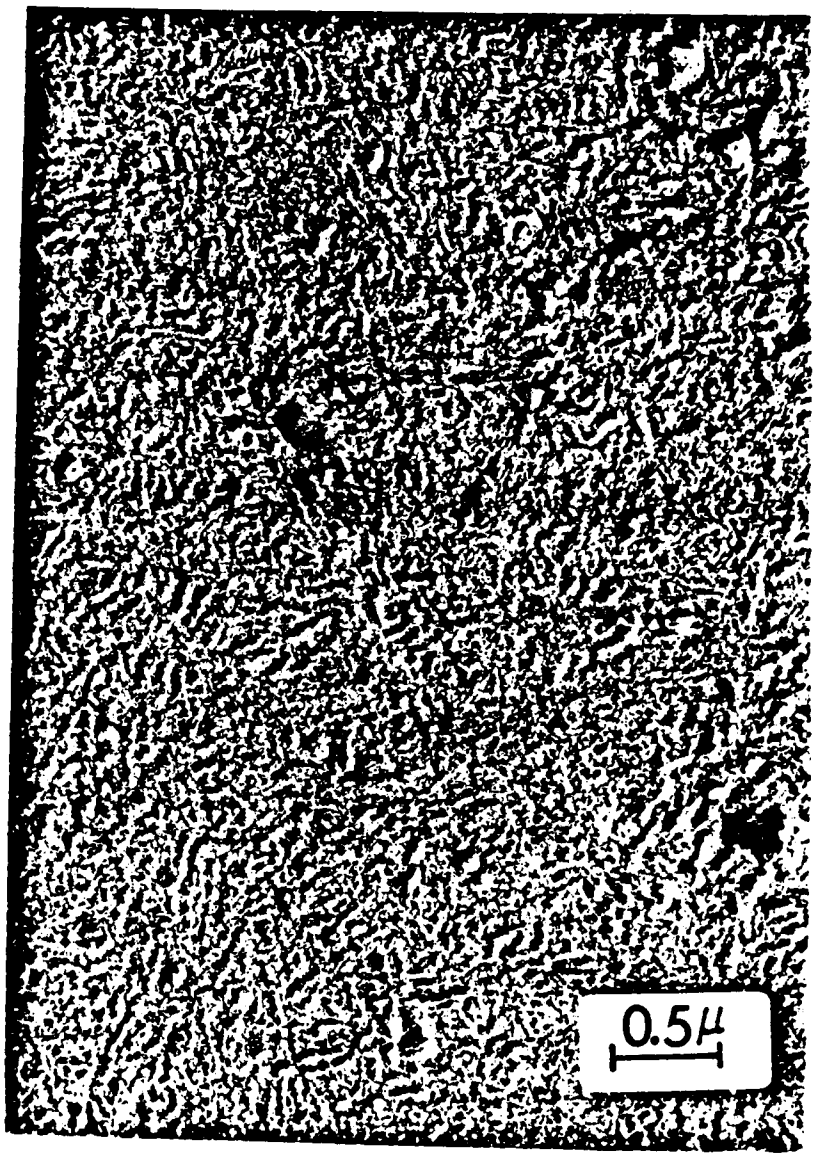

b

Figure 137 Continued

with more "C" and "S" type of relatively thicker lamellar organizations.

SAXS contours and circumferential average scattering intensity versus scattering vector plots for distribution cables D2 and D9 are given in Figures 138 and 139. Despite the complication caused by the distortion of the circumferential appearance of the isointensity contours at the lower angles, neither of the cables showed any sign of orientation. As can be seen from the circumferential average intensity versus scattering vector plots (Figure 139), broad maxima correspond to long periods of 186 and 155 ^{o}A for cables D2 and D9, respectively (Table 18). Low angle scatterings, similar to the ones observed for cable E2 are believed to result from the presence of voids.

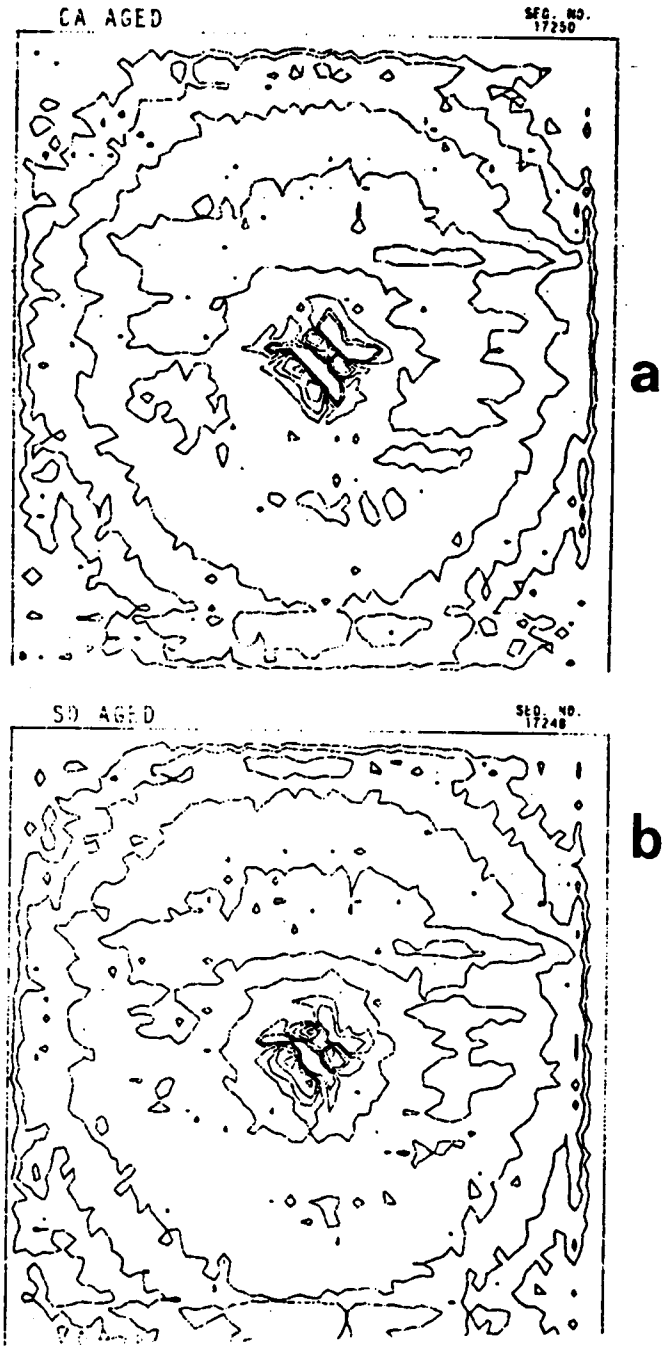

Figure 138 SAXS contours obtained from distribution cables (a) D2 and (b) D9.

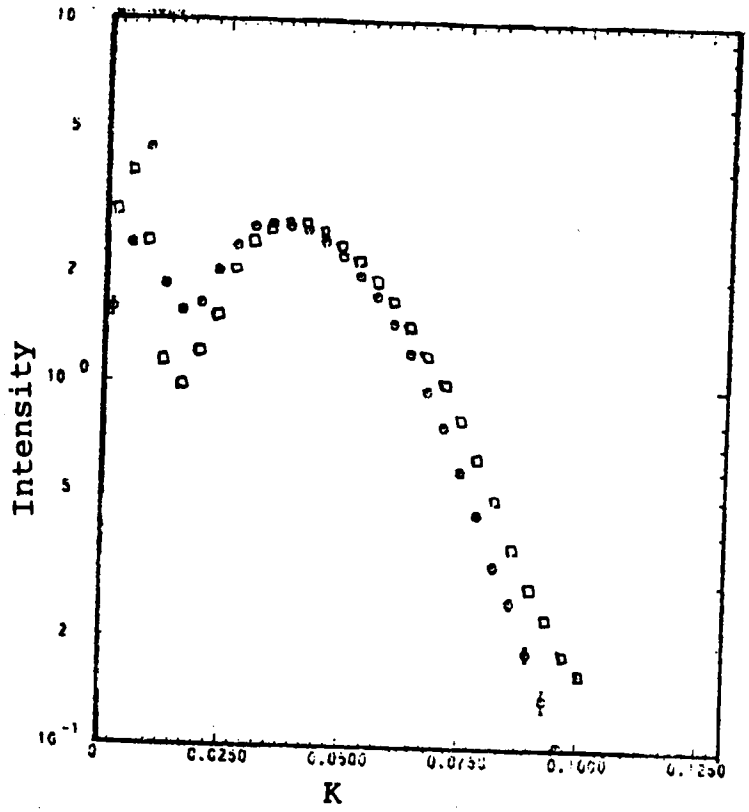

Figure 139 Circumferential average scattering intensity versus scattering vector obtained from distribution cables (O) D2 and (■) D9.

Table 18 SAXS results obtained from field aged cables

Cable	Long Period (^{o}A)
E2-1	198
E2-8	201
D2	186
D9	155

5. DISCUSSION

XLPE cable insulations produced from the chemical crosslinking of LDPE are composed of extractables (sol fraction) and network (gel fraction). The relative proportions of these phases are known to be dependent on the amount of crosslinking agent, DCP, the reaction conditions and the molecular nature of the LDPE.

HV XLPE cables prepared from the same blend of LDPE and 2 % (w/w) DCP were investigated structurally in order to be able to comment on the influence of the crosslinking process carried out during cable extrusion on the molecular structure of the insulation. After discussing the structural differences in relation to the processing conditions, the effect of such structural differences on the thermal annealing behavior of the cables will be discussed. Depending on the annealing temperature, the sol and the gel fraction were expected to anneal differently due to their molecular differences. Knowledge deduced from the characterization of the isothermally annealed cables was used to attempt the beginnings of an understanding of the microstructural changes taking place during field aging.

5.1. Original Cables

Knowing all the original cables were manufactured from the same resin preloaded with the same amount of crosslinking agent, sol-gel analyses were carried out in order to obtain information on the effectiveness of the different crosslinking processes, i.e. steam, dry, and poly ethylene glycol (PEG) medium curing.

Due to the statistical nature of the reactions taking place, i.e. propagation, disproportionation, chain scission, branching etc., during the crosslinking reaction, it was necessary to determine the molecular changes taking place and their effect on the microstructural organization. In turn, the effect of molecular differences on physical properties such as, crystallinity, melting, morphology, etc., were determined.

5.1.1. Sol-Gel Fractions

The extent of cure in DCP/PE systems is usually judged by determining the percent of extractables. From the extraction studies of XLPE cables prepared from 2 % DCP and LDPE mixtures it was found that the average amounts of extractables vary from cable to cable. Extractable levels vary from a minimum 13-14 % to a maximum of 30 % indicating that the efficiency of crosslinking in the production line is far from 100 %. The efficiency of crosslinking depends on

the extents of the competing reactions that lead to elastically effective crosslinks and to disproportionation. Insufficient curing temperatures are also another source of lower degrees of crosslinking. Assuming that high decomposition temperatures are maintained, due to the nature of the crosslinking reaction not every dissociated DCP molecule results in two macroradicals which eventually lead to one elastically effective crosslink. The levels of elastically effective crosslinks generated via intermolecular crosslinking, branching and transfer reactions all depend on the course of the reaction.

After finding extractable levels around 14-15 % to be common to many cables (Figures 21-23, pp 111-113), in order to understand the significance of the level of extractables, laboratory crosslinked samples were analyzed for their percent extractables. Blends of 2 % DCP and LDPE such as those used in cable production were fully cured in a hot press and analyzed for their extractable percentages. Similar levels of extractables obtained under laboratory conditions suggest that complete decomposition of DCP was achieved for the above mentioned cable sections. Due to the nature of the crosslinking reaction, 100% crosslinking is not possible for this blend composition. Kodres and Phillips (1981) simulated the variables of curing and calculations showed that a 40-50 minute curing duration is required at 200-250 ^{o}C for full size transmission cables.

Extractable amounts higher than 15 % which were observed for the one-third of the radial sections of cables A1 and A2 (Figure 22, p 112) and for the entire radial sections of cables B2 and B4 (Figure 23, p 113) are considered to be due to insufficient curing. Since the detailed extrusion conditions are not known to the cable manufacturers, it is difficult to correlate variables, such as cable geometry, extrusion rate, extrusion and curing time to the molecular properties. On the other hand, one of the known major differences in the production of the cables A1 and A2 than the rest of the processes was the curing medium. A 3,000 molecular weight polyethylene glycol, PEG, film in its melt state covering the extruded cable was used for facilitating the heat transfer. Obviously this heat transfer was not as effective as the heat transfer occurring in steam cured and dry (nitrogen gas) cured media. In steam curing, a water film develops naturally due to condensation at high steam pressures. This condensed water film plays a major role in dynamic heat transfer from the vapor phase to the condensed phase, thus to the cable via release of heat of condensation. As a result, having comparably higher amounts of extractables at the innermost layers than at the outermost layers of cables A1 and A2 suggests that the PEG process as used provided inadequate heat transfer. The problem could be solved through the use of a longer cure

stage, since only 50 ft was used which is much less than the 150 ft pipe used in the other processes.

5.1.2 Molecular Structure

Irrespective of cable curing method, extractable levels and swelling ratios were found to correlate with each other for each cable. A linear relationship was established between percent extractables and swelling ratios by considering the data obtained from cables A1, A2, C1 and E1 (Figure 25, p 117). While a reasonable trend was observed for cables A1, A2 and E1, a data scatter for cable C1 around 13.3-15.3 % extractables was found. It can be assumed that a liquid-like polymer melt has a statistically homogeneous structure, but this property of the melt diminishes as the crosslinking reaction proceeds. Since creation of a crosslink depends on recombination of macroradicals, adequate mobility of the macroradicals is necessary. As the viscosity increases due to the generation of crosslink points, physical entanglements, branching and inelastic crosslinking, the probability of macroradicals finding each other decreases. The statistical nature of the crosslinking process is even more complicated when chain-scission and radical migration along the chain are considered. Dole et al.(1954) proposed that the radical site on the PE chain migrates via a series of hydrogen abstraction reactions, either intra- or inter- molecularly. The relation of the

extent of the chain-scission reaction to crosslinking reactions in chemically crosslinked systems was established by Barton (1967). He related the extractable fraction to the inverse of the initiator concentration and MW of the polymer resin and also to the chain scission and crosslinking probability ratio. Karakelle (1986) found that six percent of the macroradicals led to chain scission for the Union Carbide LDPE used in XLPE cable production, utilizing Barton's relation. Both studies mentioned above, deducing the extent of chain-scission reactions, were based on changing the initiator concentration. The effect of the molecular structure on the crosslinking mechanism was studied by Narkiz and Miltz (1970) for branched and linear PE's and they found that chain-scission reactions are not common to linear PE. This suggests that branch points, being fewer in number in linear PE compared to LDPE, play a role in chain-scission reactions. Depending on the reaction conditions, domination of these competing reactions may result in statistically more random structures. For instance, more branching reactions involving the extractable low molecular weight fraction may affect the amount of extractables without causing much change in the swelling ratio. Despite its data scatter, cable C1 is thought to have a typical reaction scheme. As will be discussed later, thermal analyses of this cable also showed characteristics

different from those of the remaining cables indicating molecular differences in its network structure.

From the percent extractables versus swelling ratio graph (Figure 26, p 118), it is found that for a completely cured system having zero percent extractables the swelling ratio would be 2.6. This would correspond to the case when all molecules are incorporated in the network system and corresponds to a solvent volume fraction of 0.62 in equilibrium swelling. From the Flory-Rehner formula (Eq.3.2.3), the molecular weight between crosslinks and the crosslink density for such a system were found to be 258 and 387×10^{-5}, respectively.

Molecular weight studies of the extractables were found to reflect the statistical nature of the crosslinking reaction. As was found from GPC and viscosity studies, M_n and M_v values for the extractables obtained from highly crosslinked networks differ from the ones obtained from networks with lower crosslink density (Figure 27, p 124 and Tables 5 and 6, pp 121-122). Lower molecular weight sol fractions from highly crosslinked networks indicates that longer molecules are more easily trapped the crosslinking reaction than the shorter ones. This is obviously due to the fact that the number of sites available for radical creation is greater on a longer chain. Extractables obtained from XLPEs prepared from low DCP loadings in Union Carbide HFDE 4201 LDPE had higher viscosity average molecular weights

than the extractables obtained from the XLPEs with higher DCP loadings (Karakelle 1986). Failure to obtain a crosslinked network from the sol fraction containing 2 % DCP also indicates the effect of molecular weight on the statistical formation of crosslinks (Figure 19, p 108). Similar observations were reported for radiation crosslinked polymers. Patel (1975) reported that formation of 100 % gel with irradiation took longer for a low molecular weight fraction than for a high molecular weight fraction.

The outer layers of cable A1 and the entire radial sections of cables C1 and E1, all having comparable amounts of extractables showed different viscosity average molecular weights (Table 4, p 119). This difference in the molecular weight of extractables obtained from crosslinked networks with comparable crosslink densities confirms the earlier suggestion that different curing histories result in different molecular character in the extractables. This reasoning is again based on the assumption that the chemical environment was the same for each cable production.

FTIR studies of the cables were carried out in order to determine if any major structural variables resulted from the different curing techniques. For this purpose, the spectra of the outermost and innermost radial sections were studied without extraction. Carbonyl groups and unsaturated groups have been the major concern since they give information on effective molecular changes. While

carbonyl group formation can be taken as a sign of molecular degradation, the concentration of unsaturated groups gives information on the details of the crosslinking process. When radicals are formed along the chains, carbonyl formation is almost simultaneous in the presence of oxygen (Grassie and Scott 1985). The following reaction scheme can be given as the sequence taking place in reactions with oxygen.

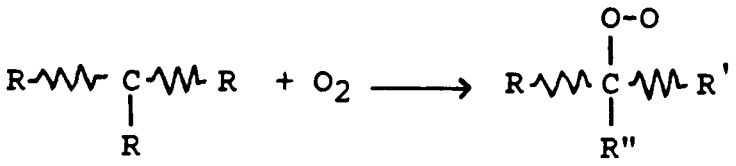

with intermolecular hydrogen abstraction and rearrangement

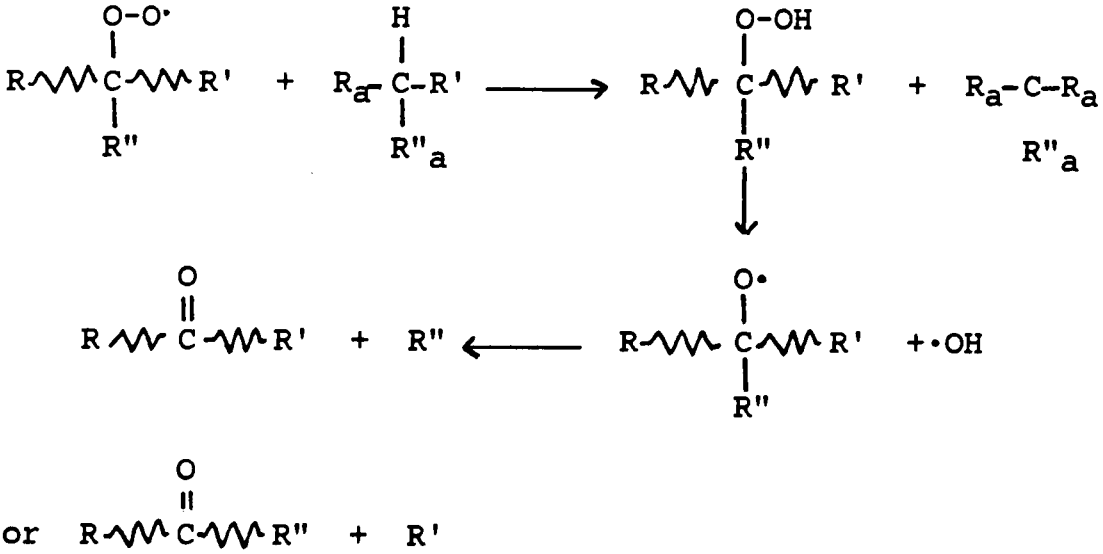

Due to the lower dissociation energy of C-H bonds compared to C-C bonds, C-H bond breakage takes place more

readily in the case of adequate energy supply. Tertiary hydrogens preferentially take part in radical formation since they are more stable than secondary and primary radicals (Hendrikson et al.1970).

Molecular weight reduction due to the oxidation reaction depends on the length of the radicals dissociating from the molecule during carboxy formation, i.e the molecular weight of R'(or R") in the reaction scheme.

Higher concentrations of carbonyl groups detected in both the inner and outer layers of cable C1, compared to cables A1 and E1, indicate that the dry cure process was more prone to oxidative degradation. One would expect lower oxidation levels for the dry cured cable since the curing process took place in a hot nitrogen atmosphere, but the purity of the nitrogen curing atmosphere is not known. The curing temperature for this particular process was around 260 ^{o}C which is within the temperature range, 150-300 ^{o}C, for extensive oxidation reactions. Lower M_v values found from viscosity studies also indicates that chain-scission reactions are accompanied with oxidative degradation (Table 5, p 121).

Higher concentrations of trans-vinylene and vinyl unsaturations found for the innermost layer of cable A1 compared to the outermost layer indicates premature curing. The presence of terminal vinyl concentrations has been proven to increase crosslinking efficiency (Rijke and

Mandelkern 1971). Comparable vinyl concentrations in the outermost layers of cables C1 and E1 (Table 7, p 129) correlate with their percent extractables data (Figure 24, p 115). It is reported in the literature that crosslinking efficiency depends on the initial vinyl concentration in the polymer. A change in vinyl concentration from 0.07 to 0.5 per 1000 carbons was found to increase the crosslinking efficiency from 20-40 % to 76 % (Hulse et al. 1981). On the other hand, vinyl group concentration in the final product cannot be taken as a direct measure in the calculation of the extent of crosslinking reaction, since disproportionation reactions also produce vinyl concentration especially at higher temperatures (Gedde 1986).

5.1.3.Thermal Behavior

All radial fractions from original cables A1, C1 and E1 and the remaining steam cured cables showed a broad melting peak characteristic of quenched LDPEs Figures 31-34, pp 131-134). Although the shapes of the thermograms from each cable look very much alike, differences lie in their T_m and T_{rb} values. T_m is the temperature at which the most populous crystals melt and T_{rb} is the temperature where the last traces of the thickest most perfect crystals are found. The area covered between T_{rb} and T_m is a measure of the thickest most perfect crystals present in the

semicrystalline matrix. cable A1 with varying percent of extractables along its radial direction showed the broadest T_{rb}-T_m range. An average value of 4.9 ^{o}C was found for cable A1 while this value is 3.1 ^{o}C for cable C1 and 3.6 ^{o}C for cable E1. The broadest T_{rb}-T_m range with high T_{rb} recorded for cable A1 indicates the presence of thicker crystals. The T_{rb}-T_m range was found to correlate with percent extractables. This relation can be easily followed for cable A1 along its radial direction. Increase in the T_{rb} and T_m values with percent extractables indicates that in a sol-gel two phase system more stable thicker crystals are developed in the presence of extractable molecules. In general, the isothermal crystallization rates of XLPE are known to be lower than the rates obtained for uncrosslinked versions under the same crystallization conditions (Kao 1983). Extension of such findings to the quench crystallization of XLPE systems leads to the conclusion that extractable fractions have the tendency to crystallize by themselves. The effect of extractables on T_m, T_{rb} and crystallinity is clearly demonstrated on the samples obtained from the innermost and outermost layers of cable A1 (Figure 40, p 143). The inner layer, with a higher amount of extractables, showed a 2.8 ^{o}C difference both in T_m's and T_{rb}'s for the extracted and unextracted samples. On the other hand, comparable T_m and T_{rb} values found for extracted and unextracted samples from the outer layer suggests that the

presence of about 14-15 % extractables does not change the crystal size distribution considerably. The increase in crystallinity observed for the extracted fraction from the inner and outer layers indicates easier crystallization of the gel network in the absence of the extractable materials (Table 8, p 144). In other words, extractables act as barriers to easy crystallization of the gel network and weaker crystals are developed from their cocrystallization. Slight broadening in the DSC thermogram of the extracted outer layer indicates both thicker and thinner crystals can develop in the absence of extractable materials (Figure 40, p 143). The 69.3 % crystallinity obtained for the gel network from the inner layer is typical of the uncrosslinked original LDPE (Table 8, p 144). Thus, lightly crosslinking the inner layer was found not to effect the percent crystallinity. Removal of the lower MW fraction by extraction can be thought of as fractionation of the original polymer. The presence of crosslinks in the fractionated network counterbalances the easier and more perfect crystallization of this relatively fractionated system resulting in percent crystallinities comparable to the unfractionated original uncrosslinked LDPE.

Steam cured cable E1 and dry cured cable C1 both showing even distributions of T_m and T_{rb} values over their radial directions is indirect correlation with the trends observed in their extraction analyses (Figures 35 and 36,

pp 135, 137). The different crosslinked nature of dry cured cable is reflected in different T_m and crystallinity values compared to cables A1 and E1. The higher T_m and crystallinities obtained over the entire radial direction suggests that relatively thicker and less defective crystals were developed. On the other hand, cable E1 with lower T_ms, but a higher percent of crystallinity compared to the outer six eighths of Cable A1, shows that comparatively thinner (or less perfect) crystals of cable E1 are more populous than the relatively thicker (or more perfect) crystals of cable A1.

The general trend in T_ms for these cables did not change much after they had acquired the same thermal history. Respectable drops in T_{rb}s of the thermally treated cables compared to T_{rb}s obtained from the original cables indicate that extractables are sensitive to thermal processes (Figure 39, p 141). Higher T_{rb}s obtained from the relatively slow cable quenching process indicates the existence of effective reorganization taking place in the sol fraction.

In order to understand the effects of the crosslinks produced by 2 % DCP on the crystallization behavior of LDPE and its related thermal properties, (e.g., T_m, T_{rb}, and percent crystallinity) LDPE was crosslinked in the DSC after recording its melting thermogram. The XLPE was rerun for its thermogram after acquiring the same thermal

history as its uncrosslinked version. A 4.5 ^{o}C drop in T_m, a 4.1 ^{o}C drop in T_{rb} and a 3 % drop in percent crystallinity of XLPE occurred suggesting that the introduction of crosslinks prevents formation of thicker more perfect crystals. These results are in accord with those of Kao and Phillips (1986) where the change in T_m with crosslink density was studied. The effects are due to the restricted molecular mobility imposed by the presence of crosslinks, especially in quench crystallization processes. Establishing a direct correlation between the crosslink density (Table 4, p 119) and the percent crystallinity (Figure 38, p 139) of the original transmission cables was not possible. The lower percent crystallinities recorded for the inner layer of Cable A1 with a relatively lower crosslink density compared to Cable C1 indicates that it is not simply crosslink density but also the amount of sol material, molecular structure and probably the different thermal histories that produced the resultant crystallinities. In the work carried out by Kunert et al. (1980) LDPE with 32,000 M_n and with short chain branching of 30 methylene per 1000 carbon atoms showed 33.1 % WAXS crystallinity. When this material was crosslinked with 2 % DCP, crystallinity was found to be 34.5 %. LDPE used in the cable production has M_n of around 20,600 and short chain methyl branching of 25 methyls per 1000 carbons (Karakelle 1986). Percent crystallinities found from our WAXS studies for quenched original and 2 % XLPE are

52 % and 49 % , respectively. This difference in percent crystallinity is expected to be due to methyl concentration assuming the rest of the variables, i.e. sample thermal history and data accusation, are the same. As was discussed earlier, the higher concentration of tertiary hydrogens at the methyl branching results in higher crosslink efficiencies. On the other hand, the methyl group is known to suppress crystallizability more than long chain branches. All these results show the importance of the chemical structure to the crystallization character of crosslinked systems.

DSC thermograms of original XLPE and LDPE distribution cables are again of quench crystallization (Figures 41 and 42, pp 145, 146). LDPE cables were quenched from about 120-130 ^{o}C to room temperature while the quenching processes for XLPE cables were carried out from 250-300 ^{o}C to room temperature. Depending on the rate of cooling the extent of crystal perfection would be expected to differ. Of course the major differences lie in the introduction of crosslinks. The 4-4.5 degree difference in T_ms and T_{rb}s of XLPE and LDPE distribution cables (Table 9, p 147) was found to correlate with the DSC thermograms obtained from uncrosslinked Union Carbide HFDE 4201 LDPE and its fully cured version (Figure 140).

One of the main differences between transmission and distribution cables lies in their geometry. Transmission

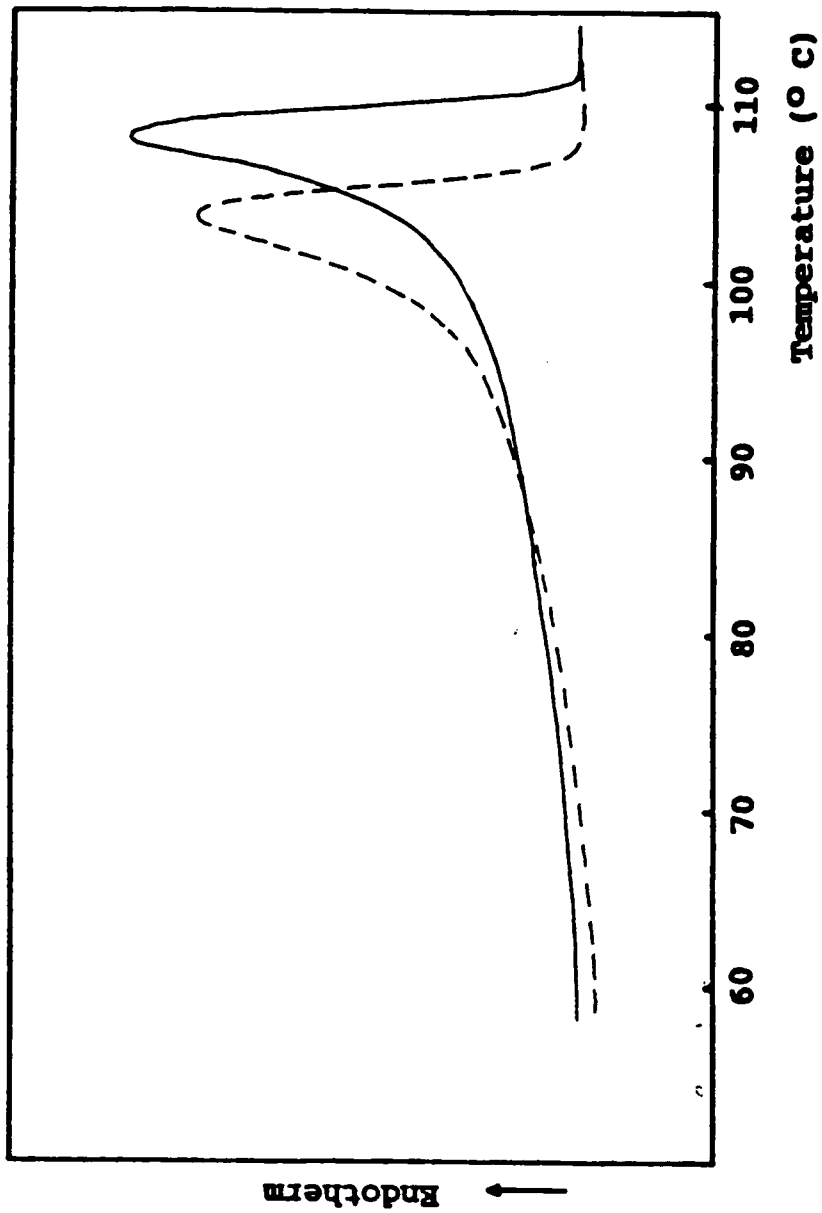

Figure 140 DSC thermograms of LDPE (——) and its crosslinked version (---).

cables with thicker insulation walls require more care for homogeneous morphological properties to be developed over the entire radial section. Variation in percent extractables found for distribution cable D8 is an indication that distribution cables with thinner insulation walls are also susceptible to inadequate curing, depending on the curing conditions.

5.1.4. Morphology

Spherulites, being the major morphological features of LDPE and linear PE, have been the subject to several previous studies on morphology-electrical property relationship in cable applications (Wagner 1974, Schultz 1974, Phillips 1978, Kolesov 1980). Pertinent morphological properties i.e. crystalline-amorphous content have been correlated with the electrical performance of the insulator. It was shown that bigger spherulites associated with wider imperfect boundaries had lower breakdown strengths whereas smaller spherulites associated with thinner, relatively less defect free boundaries resulted in higher breakdown strengths.

Introduction of even a slight amount of crosslinks to the original LDPE was found to prevent the development of spherulitic organization (Phillips and Gohil 1986). Instead sheaf-like morphologies are observed. Since sheaves are detected as being an early form of spherulites in most

linear polymers, having sheaves as fully formed characteristic features at even prolonged crystallizations for crosslinked systems indicates that spherulitic growth has been repressed. Well developed 10-12 μm banded spherulites observed for LDPE disappeared when the system was crosslinked with 0.9 % DCP and 2-3 μm banded sheaves were developed. Increasing the crosslink density with the addition of 2 % (w/w) DCP was found to eliminate banding completely (Phillips and Gohil 1986). Sheaves obtained from the crystallization of 2 % XLPE systems resemble bundles. A further decrease in sheaf size was observed due to increasing crosslink density. The growth of sheaves become almost impossible at crosslink levels achieved from 6.8 % DCP loading.

In accordance with Phillips and Gohil's study (1986) of laboratory crosslinked materials, spherulitic morphologies were found to be absent in all XLPE cables. Instead sheaf or bundle like organizations dispersed between wormlike background lamellae were found to be general morphological features (Figures 62-69, pp 174-187). The number of lamellae forming the bundle-like sheaves was found to be lower for original cables, which are quenched system, the cables than the number of lamellae forming the sheaves developed upon isothermal crystallization (Figures 60 and 61 p 171-173). This difference shows that controlled nucleation of crystals is facilitated around already formed lamellae

under isothermal crystallization conditions. Restricted branching possibilities finally result in bundle-like lamellae with restricted splaying. Well resolved sheaves with distinctly banded lamellar structures in laboratory crystallized samples of cable A1 correlates with crystallized laboratory cured samples (Figures 60 and 61). More distinct, better developed textures were found to be present in the outermost layers of dry cured cable C1. On the other hand, this texture was not observed in laboratory quenched specimens of cable C1 (Figure 68a-b, p 185). This indicates that unusual processing conditions affected the morphological nature of this cable. It is known that during cooling the insulation was first exposed to unheated nitrogen gas followed by quenching in water. The first cooling stage produced relatively slow cooling and these special textures, the second more drastic cooling stage produced the nonbanded sheaves typical of the rest of the insulation. Dispersed thicker lamellae observed in the inner layers of cable A1, compared to cables C1 and E1, correlates with its high extractable levels. The molecules can crystallize into better lamellar formations simply because of the relative ease of chain mobility in the sol molecules. The C or S type appearance of some of these thicker lamellae also suggests that they are associated with sol fractions that can accommodate themselves in

restrained crystallization areas caused by the crosslink network.

The long periods of lamellar crystals were calculated from the maxima of intensity versus scattering vector plots from SAXS studies using Eq. 3.5.4. Lamellar crystal thicknesses were calculated from long periods using the percent crystallinities found from WAXS studies (Table 10, p 153). As can be seen from Table 10, the lamellar thicknesses of the outer and inner layers of cable A1 were found to be 90 and 101 ^{o}A, respectively. On the other hand, the gel fraction of the inner layer was found to have a lamellar thickness of 81 ^{o}A. The intensity drop observed at lower scattering angles is an indication of the absence of extractable materials. With the consideration of ± 2 ^{o}A error involvement in the measurements, the inner and outer layers of cable C1 may be considered to have similar lamellar thicknesses. Cables E1 and C1 did not show as large a variation in lamellar thickness as the inner layer of cable A1 (Table 10, p 153). Although shorter long periods were observed for LDPE distribution cable D1, due to its higher crystallinity, lamellar thickness was found to be 105 ^{o}A. XLPE distribution cable D8 with cloudy morphological features was found to have the thinnest lamellar thickness, ca.81 ^{o}A. This result correlates with its low Tm and heat of fusion observed from the DSC study (Figure 42, p 146).

An estimate of the size of the crystalline regions in original transmission cables was determined using the Scherrer equation (Scherrer 1918, Alexander 1979)

$$L_{hkl}=K\lambda/\ \beta_o\ \cos\theta$$

where L_{hkl} is the mean dimension of the crystallites perpendicular to the planes (hkl), β_o is the breadth of the (hkl) peak at half maximum intensity in radians, K is a constant that is commonly assigned a value of unity. λ is the wavelength of X-ray source and θ is the Bragg angle for the particular reflecting plane (hkl). Table 19 summarizes the peak breadths of the (110) crystalline peak at half maximum of the original XLPE HV cables along with field aged cable E2. While original steam cured cable E1 has peak breadths around 0.9 ^{o}, the value is around ca. 0.7 ^{o}for the field aged version (cable E2) indicating improved crystalline order in cable E2. The relatively lower value of peak breadth (thicker crystal sizes) obtained for the outer layer of cable C1 correlates with DSC and morphology data. The relatively higher crystal size (lower peak breadth) for the gel fraction of cable A1-8 compared to the corresponding original radial section indicates better organized crystal structures for gel material. On the other hand, remembering that broadening also results from lattice distortions, which is not indicated in the Scherrer formula, estimates of the crystal size with this equation may be defective.

Table 19 Breadth of the (110) crystalline peak at half maximum in HV XLPE cables

Cable	(110) Peak Breadth (degree)
A1-1	0.82
A1-8	0.80
A1-8 T_a=107°C(2 days)	0.79
A1-8 Gel	0.70
C1-1	0.75
C1-8	0.82
E1-1	0.93
E1-8	0.90
E2-1	0.70
E2-8	0.68

Lamellar fold surface energies were found by using Eq. 2.6.5. In this equation, T_m^o, the equilibrium melting temperature for XLPE was taken as 138.3 ^oC (Kao 1983). Tm and ΔH_f heat of fusion values were obtain from the DSC studies of the cables. The volumetric heat of fusion was found by taking the density of XLPE as 0.922 kg/m^3. As can be seen from Table 10 a higher surface free energy was found for the gel fraction of cable A1 than for the inner and outer layers of the same cable. This higher value of surface free energy may be caused by the crosslinks giving rise to a stress in the interfacial region.

Dry cured cable C1 being the only cable with concentric isointensity contours, suggests that high processing temperatures are effective in reducing the stresses imposed during extrusion (Figure 47, p 155). The most highly stressed regions are expected to be at the inner layer where the drag force is higher along the cable core. This was observed to be the case in cable A1 (Figure 46 p 154). In steam cured cable E1 orientation was observed in both the inner and outer layers. Such orientation effects might result from mechanical forces exerting by the die on the outer layer during extrusion process (Figure 48 p 156).

Since the total scattered intensity results from the presence of phases with different electron densities the scattering curve for steam cured cable E1 is complicated by scattering from voids. Although the solubility of water in

XLPE and PE is very low at room temperature, higher water solubilities are attained at high temperatures. In the steam-cure process, the cable is usually quickly quenched. This rapid cooling induces voids due to abrupt density changes taking place and dissolved water precipitates as droplets. As a result, the number of voids generated in the steam cure process is known to be considerably higher than those of obtained in dry cure processes. In the case of cable E1 it was possible to evaluate void size distribution from electron microscopy (Figure 66, p 182) and to observe the effect of voids on SAXS at the appropriate scattering angles.

5.1.5 Evaluation of Original Cables

Since all the cables were manufactured from the same resin preloaded with the same amount of DCP, crosslinking agent, differences observed at a molecular level, e.g. amount of sol and gel fractions, molecular weight of extractables, crosslink density, unsaturation and carbonyl concentration, were thought to be due to differences in the processing conditions. Although the detailed histories of the extraction and curing process are not known, different curing media (steam,dry and PEG) and curing temperatures are expected to be the major factors affecting the curing process. Higher carbonyl concentrations, with extractables having lower molecular

weights, observed in dry cured cable C1 reflects the vulnerability of the curing process to molecular modification and degradation at high curing temperatures. On the other hand, the higher amounts of extractables observed for cables A1 and A2 are examples of inadequate curing due to heat transfer difficulties. The higher concentrations of highly reactive vinyl groups also indicate an incomplete curing process.

The influence of molecular structure on the thermal behavior of these cables was seen more clearly in cable A1 than in cable E1. The higher melting temperatures, T_m, and return to the base line temperatures, T_{rb}, observed for cable A1 were found to be related to its higher extractables levels resulting from inadequate curing. The effect of extractables is more meaningful when all the radial sections of that cable are considered. The decrease in T_m and T_{rb} values and in lamellar thickness (from SAXS studies) of gel fractions of cable A1 compared to values for the unextracted material clearly demonstrates the effect of extractables on morphology. Thicker isolated lamellae observed in TEM micrographs of the inner layer of cable A1 were not observed in other cables. On the other hand, the percent of extractables and molecular structure of cable C1 were comparable to those of cable E1. Having dry cured cable C1 with higher T_m and T_{rb} values than that of cable E1 and well developed sheaf structures suggests that curing and

cooling conditions influenced the thermal-morphological behavior. The absence of well formed sheaves in the lab quenched samples suggests that the two-stage quenching process from high curing temperatures generated conditions permitted better developed morphologies. Obtaining artifact-free resolution of the morphological details in XLPE systems is a the delicate process governed by the morphology itself. The sharp boundaries observed in low and high density PEs and PP are not observed in XLPE systems. Smaller interwoven crystalline entities lacking sharp boundaries result and may be one of the reasons for the improved dielectric properties of XLPE, compared to LDPE and PP, since crystal boundaries are known to be one of the factors reducing dielelectric performance (Phillips 1978, Kolesov 1980).

5.2. Thermally Aged Cables

In service, XLPE and LDPE insulated cables are subjected to temperatures corresponding to their effective annealing temperature region. Therefore, it is important to know the behavior of the insulation matrix, i.e. XLPE or LDPE, in the presence of thermal fields. Thermal fields experienced in practice are non-isothermal and the history of thermal changes is complicated. It is essential for isothermal annealing to be understood before attempts can be made at understanding non-isothermal annealing. Extension of

our understanding of the thermal processes taking place during annealing of XLPE is based on our isothermal and multistep successive isothermal annealing processes. Thermooptical analyses of the annealing event were also found to be useful.

5.2.1. Thermal Behavior

After observing single melting peak endotherms for water-quenched cables, the appearance of two or more endotherm maxima in isothermally annealed cable samples indicates that the original microstructural organization was altered (Figure 75 and 77, p 194, 197). This alteration is expected to be mainly due to perfection of some of the crystals and annihilation of defects because of the thermally activated molecular rearrangements.

Depending on the annealing temperature, two or three peaks were observed to develop on isothermal annealing. This dependence of the number of newly generated peaks and their broadness on annealing temperature suggests that there are several processes governing the microstructural changes.

One of the most important effects encountered during annealing is the irreversible thickening of crystals along the chain direction. This process is believed to occur either by means of diffusion of molecules in the solid state or in the melt due to recrystallization of partly or fully

melted crystals. These are the cases most commonly encountered in systems composed of linear and/or branched molecules. It was demonstrated by Bair et.al. (1967) that introducing crosslinks by irradiating PE single crystals suppresses the lamellar thickening process. The effectiveness of this suppression was found to be dependent on the irradiation dose. Therefore in a crosslinked network, the extent of rearrangement is expected to be reduced by the degree of crosslinking. In the case of XLPE prepared by chemical crosslinking, the system is composed of sol and gel phases, interpenetrating each other. The responses of these phases to annealing processes are expected to be different depending on the annealing temperature. The relative ease of rearrangement of uncrosslinked material might be expected to facilitate rearrangements of the crosslinked network. On the other hand, the presence of a network structure hinders easy rearrangement of uncrosslinked material. Depending on the annealing temperature, the generation of two peak or three peak endotherms indicates different molecular processes are taking place during annealing or at steps following the annealing procedure.

Three peak endotherms were found to be general for annealings carried out at temperatures relatively far below the major melting peak (Figure 141). These three peaks were generated at different times. Low temperature melting peaks with melting temperatures T_1 and T_2 (Figure 141)

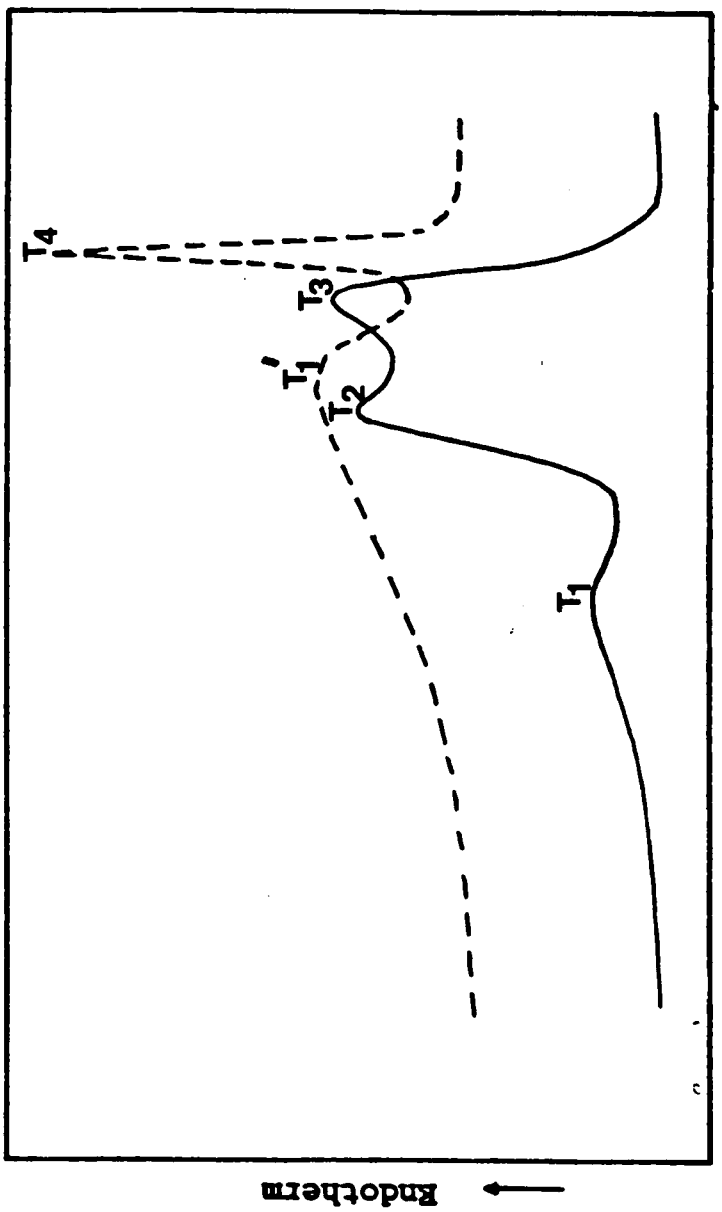

Figure 141 Schematic representation of multiple peaks generated from low (——) and high (- - - -) temperature annealings of original crosslinked polyethylene.

resulted from the annealing process. The peak melting at temperature T_3 was found to appear at the melting temperature of the original material and its position did not change much with annealing time. Crystals constituting this peak were in their solid state during low temperature annealings. The lowest melting temperature peak was developed after quenching the sample from the annealing temperature to room temperature. The magnitude of this peak, irrespective of the origin of the cable, was found to depend on annealing temperature and annealing time. Decrease in magnitude with annealing time indicates ongoing annealing processes at prolonged annealings. The presence of a low temperature peak even after 60 days annealing of steam cured cable E1 (Figure 95, p 217), indicates that the thinnest crystals forming this lowest temperature peak consist of molecular structures with the highest resistivity to molecular rearrangements. This suggests that they are the chain segments close to the crosslink points. Therefore these crystals are not expected to be isolated small crystals but thin crystals associated with the annealed crystals which are formed from the rejected chain segments close to the crosslink points.

The main event taking place during annealing is the crystallization of some of the molten material. When crystals, the ones poorly developed during quenching of the original cable in the extrusion line, are subjected to

reasonably high annealing temperatures they melt and some fraction of the melted material can recrystallize. An increase in melting temperature and magnitude of the recrystallization peak with annealing time indicate an ongoing crystal perfection process. In general, the magnitude of the recrystallization peak was found to be related to the amount of molten material attained at the annealing temperature and to the degree of crosslinking. The amount of available molten material depends on the molecular structure of the original material and also on the thermal history during quenching. Higher magnitudes of the recrystallization peak obtained from annealing of Cable A1 compared to similar annealings of C1 and E1 indicated that the reorganization of crystals is facilitated for low crosslink densities. Or as stated earlier, this might be due to a combination of effects resulting from easier reorganization of sol molecules. At higher annealing temperatures (e.g. 97 ^{o}C) more material is incorporated into the annealing process at the expense of the major melting peak. As the annealing temperature rises, more material molten at the annealing temperature fails to crystallize in the period of time available, due to the slow crystallization rates experienced at annealing temperatures close to the major melting temperature. The lowest annealing temperature at which two peak endotherms are developed was found to be 100 ^{o}C for all cables. A well separated narrow

high temperature peak and a broad low temperature peak indicate the generation of two major crystal groups with well separated melting points (Figure 75, p 194). At temperatures just below the major melting temperature, all the poorly crystallized material is melted and only thicker perfect crystals persist. Upon cooling from the high annealing temperature down to room temperature, these already existing crystals act as easy nucleating sites for the newly crystallizing molecules from the melt. An epitaxial type of growth of newly crystallizing molecules on the already existing ones is expected to be limited due to possible restrictions imposed by the crosslink points. On the other hand, the attainment of crystallographic register for some fraction of molecules relatively free from crosslink barriers is easy. Therefore the observation of a single melting peak representative of thicker crystals is a result of the merging of the recrystallization peak with the major melting peak of the original material.

As the annealing temperature is increased above the major melting peak, the breadth of the high temperature peak at half maximum was found to decrease (Figure 78 p 198). This indicates a narrow crystal size distribution. At these temperatures recrystallization rates are even lower than those of the ones attained at lower temperatures. From the comparative studies carried out for cables A1, C1 and E1 at an annealing temperature of 107 ^{o}C, it has been shown

that the magnitude of the high temperature peak generated at 107 ^{o}C is associated with the extractable materials available in the system (Figures 85, p 206, 91, p 213 and 101, p 225). The absence of a 107 ^{o}C annealing peak in the gel fractions of Cable A1 as well as in Cables C1 and E1 suggests a role of the extractable molecules in the generation of high temperature peak. The crystals formed at a 107 ^{o}C annealing melt around 112 ^{o}C and they correspond to the thicker crystals obtained from the crystallization of uncrosslinked original LDPE. A high temperature peak accounting for up to 36 % of the total crystallinity, (Figure 79 p 199), constitutes about 18 % of the entire material when the uncrystallizable amorphous fraction is included. This shows that some part of the sol fraction still contributes to the low temperature melting material and the amorphous fraction. This is expected since sol material, being a fraction of the original LDPE, can crystallize to some extent. The different magnitudes of the high temperature peaks obtained using different cooling rates from 107 ^{o}C annealing to room temperature indicate the separation of the sol material in the liquid state (Figure 104, p 228). Obtaining a smaller peak in slower cooling suggests that molten sol remixes with the molten gel during cooling. For a sol-gel separation to occur a positive enthalpy of mixing must arise from unfavorable chemical interaction between the sol and the gel molecules.

The rates of increase in the magnitude of the sharp high temperature peaks obtained from annealings carried out at 100, 103, 105 and 107 ^{o}C are given in Table 20. The magnitudes of the high temperature peaks are given as the percentage of the total area of the DSC thermograms. As can be seen from Table 20 at 107 ^{o}C annealing, the magnitude of the high temperature peak for Cable E1 increased at a rate of 0.0007 percentage/min, This is a very slow rate compared to 0.116 percentage/min observed for the peak generated from 107 ^{o}C annealing of Cable A1.

Annealings carried out at or above T_{rb} resulted in a quenched peak resembling the original ones obtained from the cable quenching process. This simply suggests that annealing processes do not take place in a completely molten polymer (Figures 96 and 97, pp 219, 220).

Multiple isothermal annealings were performed in order to understand the multiple melting behavior of some of the field aged cables. The generation of multiple peaks from two step successive annealings at 107 ^{o}C and then 100 ^{o}C (Figure 98 and 99, pp 221,222) led to the idea that successive drops in annealing temperature can help to reproduce the multiple melting peaks observed in the analysis of field aged cable E2. Multistep annealings carried out by successive increases in isothermal annealing temperature did not result in any multiple melting peak because, at each (higher) temperature annealing stage

Table 20 Rate of increase in percent crystallinty of the high temperature peak for cables A1-8 and E1-8 at the indicted annealing temperatures

Annealing Temperature (^{o}C)	Rate of increase of high temperature peak/minute	
	Cable A1-8	Cable E1-8
100	-	0.1030
103	0.169	0.1350
105	0.021	0.0240
107	0.116	0.0007

microstructural organizations developed during lower temperature annealing were destroyed. Sharpening of the individual melting peaks obtained from 107-103-100 and 95 ^{o}C successive annealings compared to 107-100 ^{o}C annealings indicates that the breadth of the individual peaks depends on the magnitude and distribution of the crystal population available in the annealing process. Resolution of the individual peaks is not as good as in isothermal single step annealings. The reason can be deduced from the 107-100 ^{o}C two step annealing. After generation of the 107 ^{o}C peak similar to 107 ^{o}C annealing, since temperature is dropped from 107 to 100 ^{o}C, instead of forming a low melting quenched peak, already melted material is subjected to a second crystallization period. Since material subjected to 100 ^{o}C annealing is already fractionated during 107 ^{o}C annealing the second step annealing does not lead to quenched peaks with well separated troughs. Still the troughs do correspond to the annealing temperatures. This character of the multiple annealing is used to trace back the annealing history of a thermally aged cable.

5.2.2. In-Situ Annealing Studies

Light transmission studies were conducted in order to monitor the changes taking place during the thermal treatments since all the thermal analyses described so far were carried out after the samples were thermally treated.

As described earlier, frozen-in stresses and form birefringence all contribute to the final transmitted intensity. On the other hand, scattering resulting from the presence of low molecular weight residues lowers the resultant intensity. Although freshly prepared chemically crosslinked PE systems contain low molecular weight organic byproducts from the crosslinking reaction, some diffuse out because of their high vapor pressure. On the other hand, the system is not homogeneous because of the deliberately added small molecules like antioxidants, voltage stabilizers, etc.. Therefore, some scattering effects are expected.

Since recrystallization is found to depend on annealing temperature and annealing time, the rate of annealing may be inferred from the intensity changes with time at a constant annealing temperature. From the data obtained from half hour annealings, the half times for 50 % annealing were calculated. A semiquantitative approach to the annealing rate can be obtained by plotting the reciprocal half times versus annealing temperature. Results for the annealings carried out at 92, 97 and 100 ^{o}C for original and gel samples of cable A1-8 are given in Table 21. While recrystallization rates for gel at 92, 97 and 100 ^{o}C annealing were found to be 0.492, 0.683 and 0.205 min^{-1}, corresponding values for the original cable were found to be 0.337, 0.363 and 0.182 min^{-1}, respectively. This suggests that the recrystallization process in the gel results in

Table 21 Recrystallization rates for the original and the gel fraction of the inner layer of cable A1

Annealing Temperature (°C)	Recrystallization rate (min^{-1}) A1-8 Original	A1-8 Gel
92	0.337	0.492
97	0.363	0.683
100	0.182	0.205

more perfect crystals in a shorter time than in the presence of sol molecules. DSC data are in accord with this suggestion.

The amount of available crystalline phase obtained from high temperature X-ray studies show that at low annealing temperatures, e.g. 92 ^{o}C, about 74 % of the original crystals are still present in the system. The presence of crystals dispersed throughout the crosslinked network in the temperature range of 90-92 ^{o}C acts as additional physical links along with crosslinks against mechanical forces. Mechanical stability at high temperatures is one of the reasons that makes XLPE superior to uncrosslinked PE insulations. Percent crystallinity drops steadily with increasing temperature (Table 11, p 237), finally, an amorphous peak obtained at 107 ^{o}C shows that the material is completely melted.

The development of the 107 ^{o}C high temperature annealing peak was not recorded in the high temperature X-ray annealing studies. Detection of the high temperature peak during 107 ^{o}C annealing in the in-situ thermo-optical study was not possible either. Around this temperature, the crystallization rates of both XLPE and its sol fraction were found to be very slow (Kao 1983). The development of 14 % high temperature peak upon cooling supports the reasoning for sol-gel separation derived from the thermal studies

involving coolings at different rates from the 107 ^{o}C annealing temperature down to ambient.

Incompatibility of sol and gel may arise because of the differences in their molecular structure. Major molecular structure differences are the network junction points, chain ends and unsaturation. While network junctions act as physical barriers for the continuation of the crystal register depending on their sizes, chain ends are also excluded from the crystal array. Chain ends containing initiator residues, bulky groups and/or unsaturation due to termination or transfer reactions alter the chemical nature of the chain. The presence of these chemical differences in the extractable molecules accentuates the incompatibility because of the higher entropy associated with the chain ends. Higher vinyl and vinylidene contents of the sol molecules compared to the gel could be another reason for sol separation. Large scale separation of sol molecules as a separate phase is not expected. Forces required for a complete sol separation would easily be opposed by rubber elastic forces which cover the entire network.

5.2.3. Morphology

Study of SAXS data of the annealed cables (Figures 113-115, p 241-243), shows major differences with annealing temperature. A change in crystal size distribution change is evident from the comparison of quenched Cable A1 with its

annealed version. The probable distribution of crystal sizes in the original material was found to change for high temperature annealings. A drop in the distribution maximum indicates lowering population numbers for the most populous crystals. On the other hand, an intensity increase at lower angles indicates an increase in the population of thicker lamellae. While the crystal thickness of the most populous crystals in the inner and outer layers of original Cable A1 were found to be 90 and 101 ^{o}A respectively, similar sections were found to have crystal thicknesses of 85 and 88 ^{0}A after annealing at 107 ^{o}C for two days, respectively. These observations correlate with the DSC study of the innermost layer annealed at 107 ^{o}C. The generation of a broad low temperature quenched peak is accompanied by thicker crystal development during 107 ^{o}C annealing (Figure 79, p 199). As discussed earlier, the newly generated quenched peak has a lower melting temperature than the original quenched peak.

A comparison of the SAXS data obtained for the innermost and outermost radial sections of Cable A1 annealed at 107 ^{o}C shows that the main difference is in the lower scattering angle side of the maximum. As was explained in the section on original cables, higher intensities at lower scattering angles are due to the presence of sol material in the original cable. Having the major maximum at almost the same scattering angle clearly suggests that in each case a

similar crystal distribution is attained for the quenched peak developed on cooling from the annealing temperature to room temperature. Since the only major difference between these two layers was found to be in their percent extractables, increased scattering intensity at low scattering angles reflects the rearrangements taking place mainly in sol fraction sites. In other words, the sol fraction separates out from the gel and forms thicker crystals. Higher and more diffuse intensity values at even lower angles are not observed for the outermost layer and are representative of void formations.

The rate of quenching was found to be very effective in altering the lamellar crystal distribution in the original cable. Much smaller lamellar crystals with broader distributions compared to the original cable were obtained from the laboratory quenched sample. Quenching following melting of the innermost layer of Cable A1, previously annealed at 107 ^{o}C, resulted in thinner lamellar crystals compared to the crystals obtained from 107 ^{o}C annealing (Table 10, p 153). The inner layer of Cable A1 annealed at 107 ^{o}C has 98 ^{o}A thick lamellae compared to a thickness of 77 ^{o}A in quenched material. As can be seen from intensity versus scattering angle plots, samples annealed at 90 and 100 ^{o}C have essentially the same crystal size distribution. The only noticeable difference lies in the slightly higher intensities observed at the lower angle side

of the main peak for 100 ^{o}C annealing. This confirms the presence of higher fractions of thicker crystals obtained in 107 ^{o}C annealing. Therefore two well resolved peaks observed in DSC analyses for samples annealed at 100 ^{o}C does not necessarily mean that two crystal populations exist with very different crystal sizes. These two crystal groups must be a result of different microstructural organizations, such as, fold surface nature thus surface free energy, or different concentration of defects.

SAXS data obtained from long term annealings of steam cured cable E1 at 90 ^{o}C showed that low temperature annealings did not alter the crystal size distribution of more populous crystals. Disappearance of low angle scattering is probably due to annihilation of crystal defects and voids.

5.2.4. Electrical Breakdown Studies

In order to understand the performance of polymeric insulation during its service life, accelerated aging tests are often performed. Acceleration of aging is achieved by the creation of severe environments with various combinations of voltage, frequency, temperature and chemical environment.

Despite the enormous efforts given to life time estimates, failure in estimating the exact life-time of insulation is due to lack of effective correlation of data

obtained from different laboratories and due to fundamentally different breakdown tests being used. The nature of the insulation material, mode of electrical stress (ac, dc or impulse), design of the experimental set-up, nature and design of the electrodes were all found to affect the breakdown tests (Nelson 1983).

For a long time understanding the breakdown problem from the material point of view was attempted at rather gross microstructural levels, such as correlations between spherulite size, weak paths in spherulitic structures and crystallinity with electrical breakdown strength. All these studies demonstrated that the morphological nature of the polymeric insulation is critical in its dielectric performance. Although these attempts increased the understanding of the dielectric behavior of some semicrystalline polymers forming spherulitic structures (e.g. PE, PP), the problem still needs to be understood in polymeric systems which do not exhibit those structures. XLPE, proven to be superior to PE insulations, does not exhibit spherulitic structures and the boundary problems arising between highly crystalline spherulites are not present. Sheaf-like morphological entities were found to be interwoven with the background lamellae. Experiencing similar aging problems in these structures suggests that problems stem from more intricate phase problems.

The results presented in section 4.3.5 for breakdown tests of the annealed specimens showed that average a.c. breakdown strengths were improved for annealing above 98 ^{o}C but slightly reduced for annealings below 98 ^{o}C. More information can be obtained using a Weibull statistical analysis. Weibull plots of the data are presented in Figures 142a-b. In order to use the Weibull probability (Equation 2.3.4), failure voltages for a given sample must be ordered from the smallest to the largest. The cumulative probability associated with the ith smallest voltage is

$$p = i/(n+1)$$

where n is the total number of samples tested. Thus the first failure has the lowest probability and the last failure has the highest probability which is not equal one. The scale parameter α in Equation 2.3.4 is considered as the voltage necessary for 63.2 % failure of the tested units and is usually taken as a measure for the strength of the material. In Figures 142a-b, this corresponds to an ordinate value of -1.4×10^{-4}. Finding exact values for 63.2 percent failures for samples annealed at high temperatures was complicated due to a non-linearity observed in the curves. Breaks in the Weibull plots for samples annealed at 95, 100 and 107 ^{o}C may be due to the presence of different mechanisms operating during breakdown. 95 ^{o}C annealing was

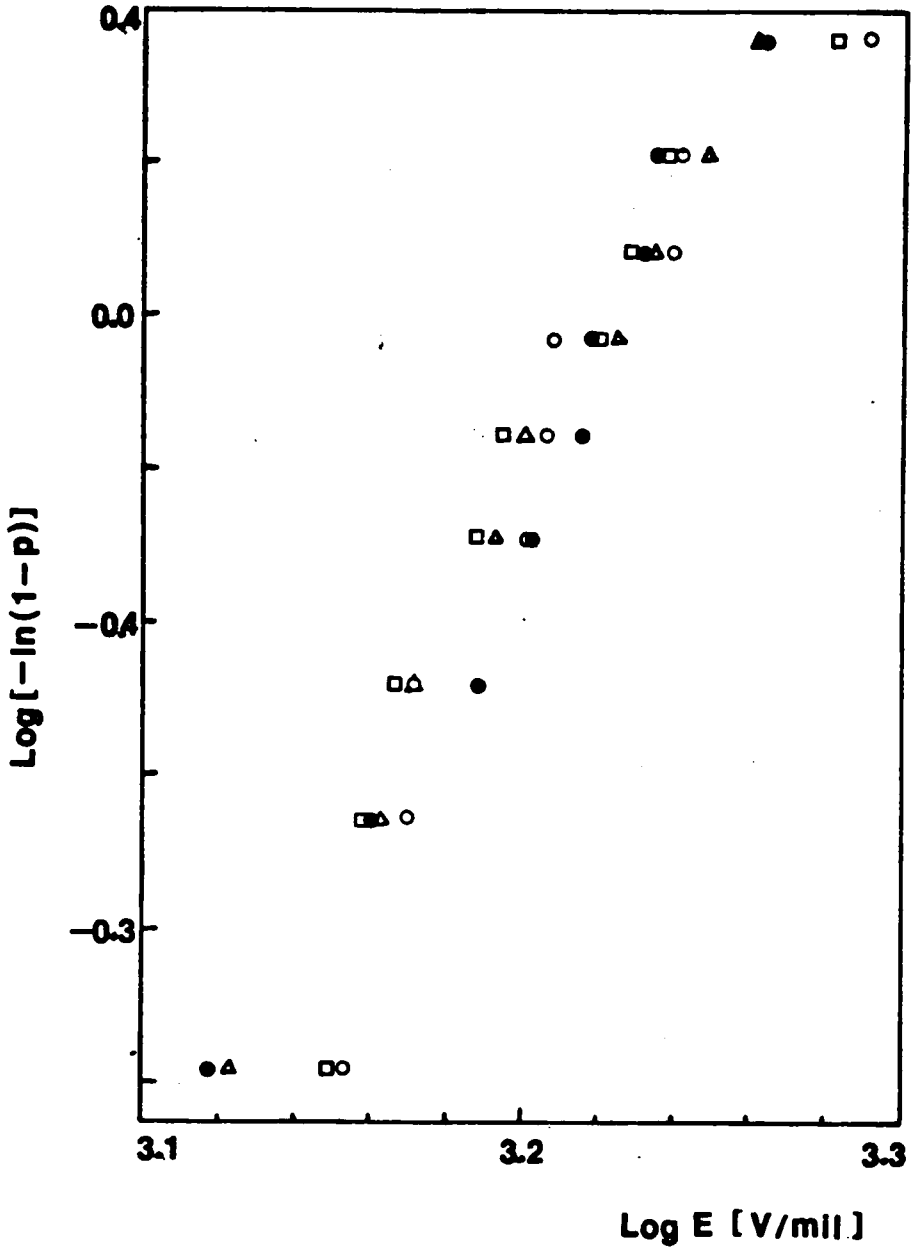

Figure 142 (a)(b) log (ln-(1-p)) versus logE Weibull plots for electrical breakdown tests of XLPE thin films annealed at (□) 79, (•) 85, (Δ) 89 and (○)93 °C for 30 minutes.

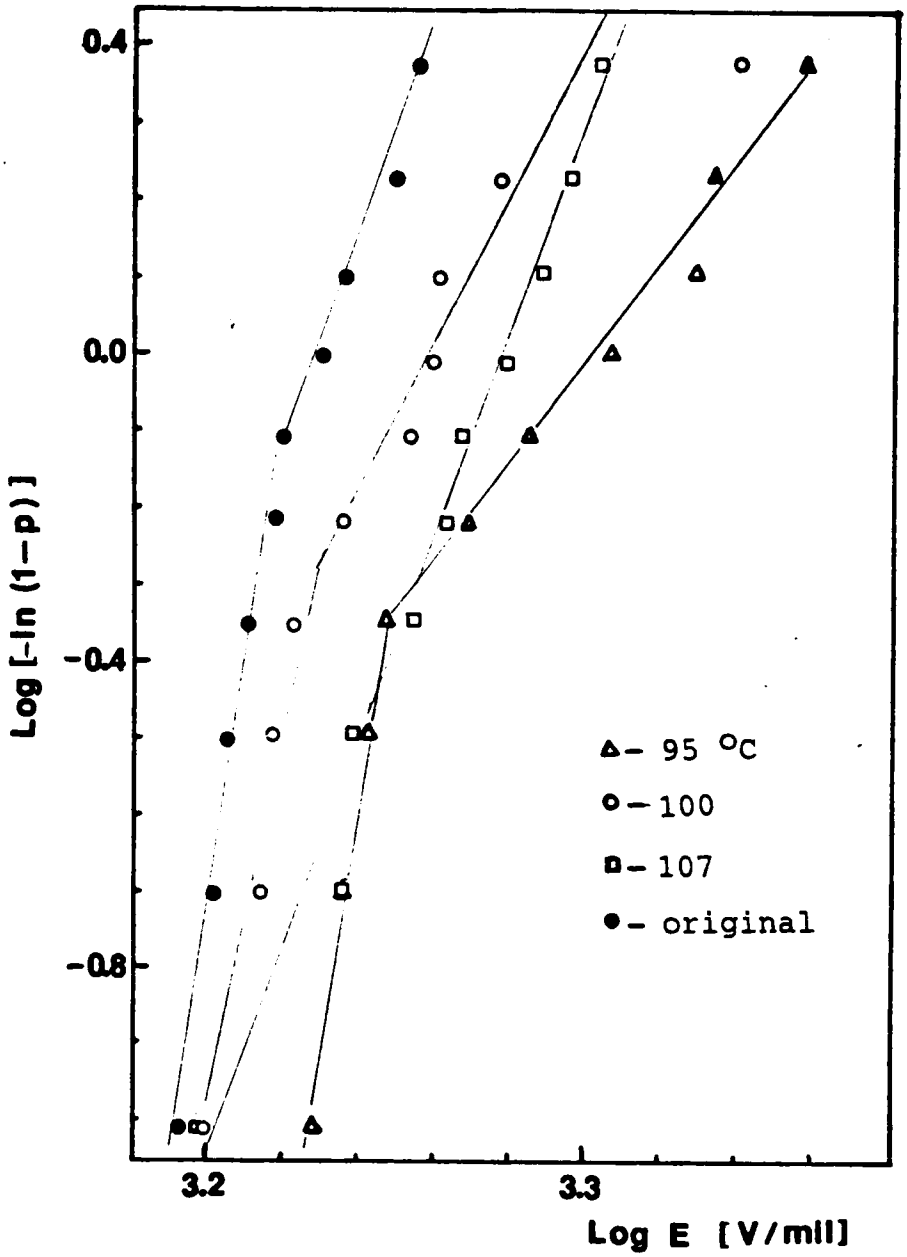

Figure 142 Continued

found to be the lowest limit for this behavior and the effect is best observed at this temperature. The recrystallization rate around 95 ^{o}C (ca 97 ^{o}C) for the original and the gel fraction of cable A1 was found to be the highest. Therefore, it is expected that large scale reorganizations in melt and solid state result in samples with higher breakdown strengths. Depending on the operating breakdown mechanism, a change in the breakdown strength causes a lack of linear behavior in breakdown plots. The increase in the inception voltage for 95 ^{o}C annealing is also indicative of improved dielectric behavior as a result of 95 ^{o}C annealing.

Electrical aging of annealed miniature cables prepared from the same base resin used in HV transmission cables showed dependence of water tree nucleation and water tree size on the annealing temperature (Karakelle 1986). Normally higher numbers of trees were observed for annealing temperatures lower than 96 ^{o}C. Golz (1985) found that XLPE's annealed at 80 ^{o}C exhibited higher growth rates of vented trees during electrical aging using needle-tip depression electrodes. Annealings carried out by Karakelle (1986) at high temperatures, around T_m, resulted in water trees bigger in size but fewer in number. Direct correlation of miniature cable studies with breakdown studies carried out on thin films of XLPE is difficult because of the different natures of the testing methods. While the former

study was on electrical aging of the annealed XLPE extruded miniature cable without breakdown, the current study uses a destructive electrical breakdown testing of annealed XLPE thin films. However, the reduction in breakdown strength of samples annealed at low temperatures parallels the deterioration rates observed for the miniature cables annealed at low temperatures. Since the XLPEs used was the same in both studies, equivalent microstructural changes are expected to have taken place at similar annealing temperatures. Therefore, the higher number of water trees generated during electrical aging of samples annealed at low temperatures can be related to lower breakdown strengths through the reasoning that microstructural developments such as microvoids result in weak points. Microstructural rearrangements taking place at low temperatures of annealing were found to reduce the breakdown strength. At low temperatures, only a small fraction of the crystals undergo recrystallization processes, the rest of the material being in the solid state. The slight reduction in the breakdown strength might be due to localized structural rearrangements taking place in the solid state at the imperfect regions. Improved breakdown strength at 95 ^{o}C and higher annealing temperatures show that slower annealing rates result in more perfect structures.

5.3 Field Aged Cables

Although cable E2 is referred to as a field aged cable, it was actually aged in the Waltz Mill aging facilities under severe experimental conditions. On the other hand distribution cables had actually served on the distribution line. They were removed from the line for maintenance purposes. Experimenting with a cable already in service on a time basis is impractical and expensive. Operation variables, cable environment i.e humidity, mineral content, mechanical stresses all need to be monitored carefully. Since cables are designed to survive relatively mild service conditions, long term experimentation on a pre-chosen area may not be conclusive in understanding dielectric breakdown. Therefore, forcing the aging of a dielectric material to its limits by accelerated aging can help to understand the physical changes taking place during degradation.

5.3.1 Changes in Molecular Structure

Extraction results were found to be the first evidence of molecular breakdown that took place during thermoelectrical aging of 138 kV steam cured cable. Increase in percent extractables in the radial section adjacent to the conductor compared to the corresponding section of the

original cable indicates molecular breakdown (Figure 121, p 257). On the other hand, increase in percent extractables cannot be taken as the only means of quantification of the extent of thermoelectric stresses reached during aging process. This is because of the statistical nature of the C-C bond cleavage. Not every C-C bond breakage will result in removal of the molecule from the network structure. One of the reasons for this is the recombination of created macroradicals due to their insufficient mobility in the solid state. Another consideration is that most of the molecules are attached to the network at least from two points. Breaking loose of a molecular segment from the network requires two C-C bond cleavages. The probability of such a cleavage is low especially at low breakdown fields. Therefore, it is thought that mainly the molecules with long branches are broken away from the crosslinked network during the early stages of electrical breakdown.

MW and MWD of the extractables obtained from the outermost and innermost layers of field aged steam cured cable, cable E2, provided clear evidence of molecular breakdown at the inner layer (Figure 122, p 260). The almost unchanged amount of extractables of the outer layer compared to the corresponding layer of the original material indicates that molecular changes did not take place to a large extent in this radial section. Decrease in M_n and narrowing of the MWD curve for the extractables obtained

from the degraded area, radial position #8, compared to the values obtained for radial section #1 suggests that the extractable fraction was also affected by the degradation process. Since breaking long molecular sections from the elastically bonded network is statistically more improbable, branch molecules attached to the network are expected to contribute to the increase in extractables and their final MW and MWD.

In another study, optical microscope examination of the XLPE thin films used in electrical breakdown tests showed spherulitic morphological features localized around the breakdown area (Lee 1986). Spherulitic morphologies being representative entities for the linear PEs their localized presence adjacent to the breakdown point in XLPE shows extensive molecular degradation. Such features were not observed in field aged cable simply because the are studied was not actually from the breakdown region, but was insulation from an adjacent area.

An increase in carbonyl concentration in the innermost layer confirms that oxidative degradation took place during aging of the cable. Crawther et al. (1979), in their work on effects of thermal and electrical stressing in polymeric dielectrics, found that the thermal field was more effective in molecular degradation than electrical stressing. They showed that molecular degradation resulting in low molecular weight material, through chain scission,

took place in a nitrogen atmosphere containing 1.16 % oxygen at high temperatures. They also showed that olefinic unsaturation increases with time, temperature and oxygen content. The vinyl and trans vinylene groups showed a larger increase than the vinylidene groups. A similar situation observed here for unsaturated groups in the inner layer of cable E2 compared with its outer layer suggests that a distribution of oxygen along the radial direction was attained during aging. For the case of distribution cables, comparably lower concentrations of trans vinylene and vinyl groups are indicative of their relatively mild aging environment compared to cable E2.

5.3.2. Thermal Behavior

The thermal history of field aged cable E2 was traced from the position of the multiple peaks using knowledge obtained from isothermal single step and isothermal multiple step annealing studies.

DSC thermograms obtained from the detailed sectioning of the field aged cable along the radial direction clearly show that the cable insulation was subjected to complicated thermal history. With the help of the electrothermal test history records (Table 3, p 65) and with the positions of multiple peaks the major thermal events taking place during aging were traced. The section of

the cable was close to the failure region but actually did not contain the major failure point.

In order to properly understand the temperature gradient attained along the radial direction during 80 ^{o}C jacket-110 ^{o}C conductor thermal field treatment following the equation is used to estimate temperature distribution; (Neher and McGrath 1957)

$$T_x = T_c - A \log (R_x / R_c)$$

where R_c is the radius of the conductor R_x, is the distance from the conductor and T_x and T_c are the temperatures at these points. Constant A was found by applying the jacket boundary conditions $T_x=T_j$ and $R_x=R_j$ with the assumption that semiconducting layer adjacent to the conductor and the jacketing material have the same conductivity the insulating material. The resultant temperature distribution is shown in Figure 143 for 80-110 ^{o}C and 80-120 ^{o}C thermal field applications together. As can be seen from this figure, during 80-120 ^{o}C thermal treatments about two eighths of the cable is above the T_{rb} of the original cable. Having the T_m and T_{rb} of the original cable E1 around 101 and 107 ^{o}C, respectively, development of subsidiary peaks with T_ms and T_{rb}s around 105-113 ^{o}C can not be produced from the 80-120 ^{o}C temperature field alone. One would normally expect single melting quenched peaks

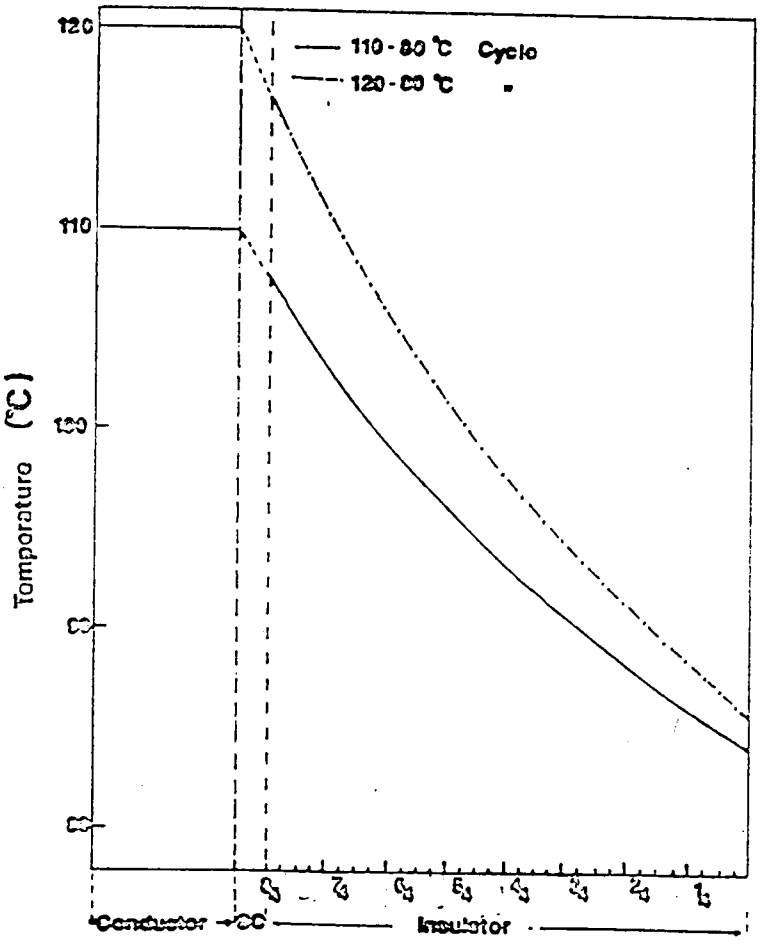

Figure 143 Calculated temperature distribution along the radial direction of cable E2 for (——) 110-118°C and (---) 120-80 °C temperature fields.

resulting from the innermost layers since they were treated at temperatures above their T_{rb}s. Figure 144 shows the comparative DSC thermograms of the original cable E1 and #1 and #8 radial positions from cable E2. As is seen from this figure, crystal population of the original cable was altered to a great extent. The overall shift in the melting range of cable E2 correlates with the early steps of its thermal history. As is given in Table 3, p 65, at the very start, for about seven months, relatively low temperature fields were applied from the inner and outer layers. As explained in section 5.3 related to the thermal aging of the original cables, 90 ^{o}C annealing induces bimodality to the melting endotherm while shifting the major melting peak to higher temperatures. Therefore, holding the conductor at 90 ^{o}C and the jacket at about 70 ^{o}C for about three months first must have created the bimodality at the inner layers. The application of 100 ^{o}C to the conductor split the bimodal peak from the high temperature peak site to further subsidiary peaks. Splitting of the high temperature peaks to some additional subsidiary peaks melting at even higher temperatures continues as a result of prolonged annealings carried out at 110 ^{o}C and 120 ^{o}C. The absence of broad quenched peaks in any of the above sections shows that the cooling process was not a quench process. In fact, it is reported that the 16 hour-cool down time period was not generally sufficient to reach ambient. A very slow cooling

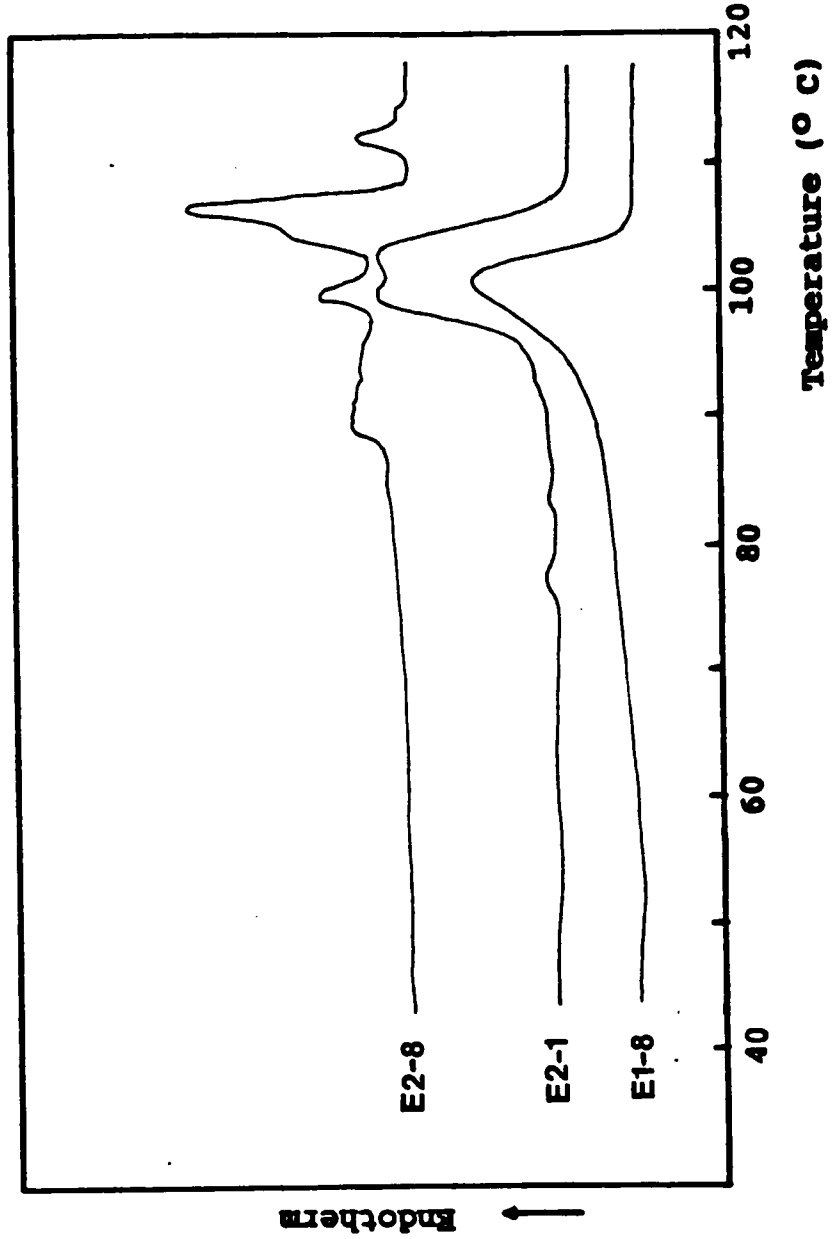

Figure 144 DSC thermograms from the inner and outer layer of cable E2 along with original cable E1.

experiment, 0.1 deg/min cooling, performed for radial section #8 from its melt did not show multiple melting behavior. Similar behavior was observed for a rapidly quenched sample, too. The absence of multiple peaks after slow cooling for about 14 hours from the melt suggests that subsidiary peaks are generated from step-wise cooling with temperature halts due to possible heat transfer difficulties.

For the case of the field aged distribution cables, except D5 and D11, all LDPE and XLPE cables showed characteristic quenched peaks. This might be due to a continuous cooling achieved following an overall melting. The other possibility is that none of these cables exceeded a 30-40 ^{o}C operating condition during their service lives. The slight bimodality observed for D11 field aged cable is expected to be the result of a short term annealing achieved around 95 ^{o}C.

Field aged LDPE distribution cable D2 demonstrated a typical example of molecular fractionation during aging. Double peaks appearing around 118 and 122 ^{o}C were observed to retain their shapes and positions after quenching the material from the melt and rerunning the DSC thermograms. At each crystallization temperature molecules with a molecular weight above the critical molecular weight for that crystallization temperature can crystallize (Mehta and Wunderlich 1975). Crystallization upon quenching results in

poorly formed crystals. When such poorly developed crystals are annealed in their crystallization region molecular fractions with different molecular characters, i.e. MW or branching, recrystallize at different rates. Thus, a more complete segregation of molecules takes place over a long annealing time.

5.3.5.Morphological Changes

From the WAXS and SAXS studies percent crystallinity, crystal and amorphous area thicknesses were found not to change a great deal compared to the unaged cables. 1 to 2 % increase in crystallinity shows that application of disruptive annealing procedures does not improve the crystallinity significantly. Amorphous and crystal thickness calculations from WAXS and SAXS data resulted in values similar to those of the original cable. Despite the facts that extractable levels increased and the molecular weight of the extractables decreased, demonstrating partial molecular breakdown in the matrix, the overall crystalline-amorphous phase distribution was found to be unchanged. Lamellar crystal thickness was found to be 10 ^{o}A higher for the inner layer of aged cable E2 compared to the corresponding layer of original cable E1. Despite the complicated DSC thermograms obtained for field aged cable E2, the lamellar thickness distribution of this cable was found to remain essentially the same. A slight change in the

scattering distribution curve is complicated by void formation which does not necessarily associated with the change in crystal thickness. Indeed, the only obvious consequence of the field aging process was the generation of voids in the deteriorated region of cable E2. It is also possible that the increase in SAXS intensity at the low angles is caused by the tree formation which was demonstrated in staining experiments. Increase in void fraction in the form of water trees adjacent to the conductor was probably the detrimental factor in the cable failure.

6. CONCLUSIONS

1- The polyethylene glycol medium cure process, as carried out in experimental form, has been found to result in incomplete curing of the cable insulation. This was judged by analyzing the amount of uncrosslinked material along the radial direction. Dry cure and steam cure processes, despite their effectiveness in achieving XLPE insulations with relatively uniform crosslink density, still do not result in a 100 % gel network.

2- Incomplete curing of the PEG medium cured cable is believed to be mainly due to its relatively short curing line. Therefore, depending on the length of the curing section, the rate of the extrusion has to be controlled to maintain dwell times long enough for complete curing. Higher carbonyl contents occured for the dry cure cable and high void contents for the steam cured cable. Further development of the PEG process should result in better cables than either of the two current processes.

3- From the laboratory cured samples, the level of extractables was found to be a function of the MW and MWD of

th PE base material as well as the amount of DCP and curing conditions.

4- Direct relations have been found between the amount of extractables, and the melting temperature of (a) the most populous crystals, T_m, (b) the thickest crystals, T_{rb}, (c) crosslink densities and (d) swelling ratios. Thus it is possible to deduce the extent of curing from a DSC experiment in relatively short time provided the molecular nature of the base material is known, i.e. linearity, MW, MWD etc.

5- A slow cooling step should be added to the processing line before the cured cable is quenched in water at room temperature, in order to minimize excessive void content introduced by rapid volume change during quenching. An alternative practice could be to heat the cable to a temperature above its melting range and to slow cool it to room temperature. This way more homogenous, more defect-free insulation matrices can be obtained.

6- The morphology of the XLPE samples was found to be sheaf-like. Development of these entities depends on the thermal history during crystallization. The dry gas cure process with slow quenching resulted in better developed sheaves compared to the other curing processes where more rapid quenching was practiced.

7- Processes taking place during isothermal annealings were found to be temperature dependent. At lower annealing temperatures the recrystallization process dominates. The magnitude of this process depends on the temperature and the amount of molten material available at that specific annealing temperature. Recrystallization rates were found to be higher for the gel fraction than for the unextracted material. This suggests that extractables impede the crystallization of the gel network. Perfection of already existing crystals is also possible through thickening mechanisms by solid state diffusion of the molecules. This process is complicated by the presence of crosslinks and its extent is much less from that observed in linear systems. At high annealing temperatures the sol separates out from the gel and crystallizes in separate microphases.

8- The breakdown strength of XLPE thin films annealed at temperatures higer than 95 ^{o}C was considerably greater than for unannealed films. Annealing of cables in the temperature range 100-110 ^{o}C would result in a higher breakdown strength.

9-The breakdown strength was reduced for annealings below 95 ^{o}C. Therefore, cable operating temperatures should be lower than 60 ^{o}C, not the 90 ^{o}C currently recomended.

10- Thermoelectrical aging was found to deteriorate XLPE cable insulation onthe molecular level. Deterioration also took place by disruption of the matrix through void formation in the form of bow-tie trees. Multiple melting behavior can be related to annealing temperatures based on the knowledge obtained from isothermal annealings. Multiple melting behavior is not caused by lamellar thickening, but by internal rearrangement processes.

11- In the presence of abnormally high sol contents, produced for instance by field aging, operation temperatures between T_m and T_{rb} should be avoided since this region (especially temperatures closer to T_{rb}) was found to be effective on sol separation. Generation of isolated phases with well defined boundaries is believed to promote stress intensification problems during electrical field applications.

12- Through observing the increase in the amount of extractables and changes in the chemical structure and MW and MWD of a the extractables of field aged cable compared to the original cable, estimates can be made of the extent of degradation experienced in the field.

7- SUGGESTIONS FOR FURTHER WORK

1- In order to understand further the development of multiple meltings in isothermal annealings, extraction of sol from the isothermally annealed samples at low temperatures, without disturbing the effective annealing history is expected to give further information on annealing process and perhaps relate melting peaks to molecular weight effects.

2- Further understanding of the sol-gel separation process can be followed by in-situ low intensity electron microscopy of thin films of XLPE with different amounts of sol at temperatures above the melting temperature of the material. In-situ SAXS annealing studies in connection with microscopy would help in understanding the events taking place on a microstructural level during annealing.

3- Radiation crosslinking may be utilized to control the behavior of extractables in already chemically crosslinked systems before thermal analyses. Such a study might give information on the role of sol fractions.

4- The dependence of electrical breakdown strength on percent of extractables (or crosslink densities) along with annealing history will help to understand the importance of having two phase systems as insulating materials. Such phase problems might also be followed using blends of polymers such as PE and PP.

5- The use of SAXS as a quantitative method of studying void content and tree formation could be explored using fractal analysis.

6- Temperature gradient annealing processes should be studied as they are important in practice, especially if accompanied by the imposition of an electric field. Such treatments of materials could be correlated with electric breakdown testing.

LIST OF REFERENCES

LIST OF REFERENCES

Alexander L.E. "X-Ray Diffraction Methods in Polymer Science", Kreiger Co., New York, (1979)

Anderson R.F., J. Appl. Phys., 35, 64 (1964).

Ashcraft A.C. and Eichorn R.M., IEEE Trans. EI, 13, 198 (1978).

Artbauer J. and Griac, Acta Technica CSAV No.3 416 (1966).

ASTM D 2765-68, 26, 830 (1971).

Auckland D.W. and Cooper R. CEIDP, 71 (1974).

Bahder G., Eager G.S., Silver D.A. and Lukac R.G., IEEE Trans. PAS-95 No.5 1552 (1973).

Bahder G., Katz C. Lawson J. and Vahstrom W., IEE Trans. PAS-93 977 (1974).

Baker W.P., Nature London V177 887 (1956).

Ball I.D.L., Proc. Inst. Elec. Eng.. Part 1, 99, 84 (1961).

Bamji S., Bulinski A., Densley J. and Garton A., IEEE Trans. EI-18 22 (1983).

Barton J. and Lazar M., J. Polym. Sci., 16, 361 (1967).

Bassett D.C. and Keller A., J. Polym. Sci., 40, 565 (1959).

Bassett D.C., "Principles of Polymer Morphology" Cambridge Univ. Press., (1981).

Bernstein B.S., IEEE Trans. Int. Symp. on Dielec. Insul. 11 (1984).

Bilmeyer F.W. Jr., "Textbook of Polymer Science", John Wiley and Sons Inc., New York, (1967).

Birks J.B. and Hart J. "Progress in Dielectrics" V.3, Academic Press, New York (1965).

Black R.M., "The History of Electric Wires and Cables", Pregrinus Ltd., London (1983)

Blais J.B.P. and Manley R.J., Macromol. Sc. B1 525 (1967).

Blodget R.B., Rubber Chem Tech., (2), 52, 410 (1979).

Buckley D.J., Berger M. and Poller D., J. Polym. Sci. , 56, 163 (1962).

Bunn C.W and Alcock T.C., Trans Faraday Soc., 41, 317 (1945).

Ceres B.V. and Schultz J.M., J. Appl. Polym. Sci., 29, 4283 (1984).

Charlesby A. and Pinner S.H., Proc. Roy. Soc.,Lond., Ser. A, 249, 367 (1967).

Charlesby A., Proc. Roy. Soc., Lond., Ser. A, 215, 187 (1952).

Chiang R. and Flory P.J., J. Am. Chem. Soc., 83, 2857 (1961).

Chiklis C.K. and Grasshoff J.M., J. Polym. Sci., Part A-2, 7, 1619 (1969).

Clark F.M. "Insulating Materials for Design and Engineering Practice" Wiley Interscience, NY (1962).

Crowdes G.J. Electr. World (1963).

Dannenberg E.M., Jordan M.E. and Cole H.M., J. Polym. Sci., 31, 127 (1958).

Dissado L.A., Fothergill J.F. and Wolfe S.V., IEEE, EE19 227 (1984).

Dougherty J.J., EPRI Journal, Jul./Aug. 50 (1984).

Dreyfuss P and Keller A., J. polym. Sci. B, 8, 253 (1970).

Eichhorn R.M. IEEE Trans. EI-12 18 (1977).

Eichhorn R.M. "Engineering Dielectrics" VII-A Ed. Bartnikas and Eichorn ASTM STP, 783, 355 (1983).

Epstein B. and Brooks H., J. Appl. Phy., 19, 544 (1948).

Fava R.A. "Treatise on Materials Sci. and Technology", Ed. Schultz J.M. V-10B, Academic Press, NY (1977).

Fava R.A., "Macromolecular reviews" V.5 John Wiley and Sons Inc., NY (1971).

Fisher P.H.H. and Nissen K.W., IEEE Trans. E1-11 37 (1976).

Fisher E.W., Naturforsh, 12-a, 753 (1957).

Fisher E.W. and Hinrichsen G., Kolloid Z., 213, 93 (1966).

Fisher E.W. and Schmidt G.F., Angew Makromol. Chem., 74, 551 (1962).

Flory P.J., J. Am. Chem. Soc., 84, 2857 (1962).

Geil P.H., J. Polym. Sci., C-13, 149 (1966).

Geil P.H. "Polymer Single Crystals", John Wiley and Sons, NY (1963).

Gohil R.M. and Phillips P.J., Polymer, 27(11), 1687 (1986).

Graneau P.,"Underground Power Transmission" Wiley Interscience, Canada (1979).

Grassie N. and Scott G., "Polymer Degradation and Stabilization", Cambridge Univ. Press, New York (1985).

Gravey B.S. Jr., ASTM Bull, 109, 19 (1941).

Harlang W.G., Khadr M.M. and Peters R.H., Polymer, 13, 13 (1972).

Harris I., J. Polym. Sci., 8, 353 (1952).

Hendrickson J.B., Donald J.C. and Hammond G.S. "Organic Chemistry", McGraw Hill, Tokyo (1970).

Hoffman J.D. and Weeks J.J., J. Res. Natl. Bur. Standard Sect. A 66, 13 (1962)

Howard P.R., Proc. IEEE Pt.II, 98, 365 (1951).

Ieda M., IEEE Trans. EI-12 18 (1977).

Ieda M. and Nawata M. Conf. on Elec. Insul. and Dielec. Phenom. 143 (1972).

Ishiki S., Yamamato M., Chabata S., Mizoguchi T. and Ono M., IEEE Trans. PAS-93 1419 (1974).

Kao Ye-Huan, M.S. Thesis, Univ. of Utah, 1983.

Kao Y.H. and Phillips P.J., Polymer, 27(11), 1669 (1986).

Karakelle M., PhD Thesis, Univ. of Utah, 1986.

Karash M.S., Fono A. and Nudenberg W., J. Org. Chem., 16, 105 (1951).

Kargin V.A., Podosenova N.G. Andvianova G.P. and Sazhin B.I., Polym. Sc. USSR, 9, 323 (1967).

Kawai T. and Keller A., Philos. Mag., 8, 1165 (1965).

Katz C. and Bernstein B.S., CEIDP 307 (1976).

Keller A., Phil. Mag., 8, No.2, 1171 (1957).

Kiss K.D., Dvepken H.C., Sirinivas N. and Bernstein B.S.,"Durability of Macromolecular Materials" Ed. Eby R.K., ACS Symp. Ser., 95, 433 (1979).

Kitchin D.W. and Pratt O.S., AIEE Trans. PAS-77 180 (1958).

Kolesov S.N., IEEE Trans. EI-15 No.5 382 (1980).

Lanctoe T.P., Wawson J.H., McVey W.L., IEEE Trans., PAS-98 912 (1979).

Lee Y.D. Private communication.

Lenz R.W., " Organic Chemistry of Synthetic Polymers", Wiley Interscience, NY (1967).

Loan L.D., J. Appl. Polym. Sci., 7, 2259 (1963).

Mason J.H., Proc. Inst. Elec. Eng., 102, Part-C, 254 (1955).

Mehta A. and Wunderlich B., Coll. Polym. Sci., 253, 193 (1975).

McKean A.L., IEEE Trans. PAS-95 (1), 253 (1976).

McKean A., IEEE Trans., EI-12 (1977).

McMahon E.J., IEEE Trans. EI-13, No.4, 277 (1978).

McMahon E.J. and Perkins J.R., IEEE Trans., PAS-83 1253 (1964).

Meares P.,"Polymers Structure and Bulk Propeties", Van Nostrand Co., London (1965).

Meyer C.T. and Chamel A., IEEE Trans., EI-15 (5), 389 (1980).

Miller A.A., J. Polym. Sci., 42, 441 (1960).

Miyoshi Y. and Saito N., J. Phys. Soc. of Japan, 24, 1007 (1968).

Mizukami T., Takahashi K., Ikeda C., Kato M. and Yoda B., IEEE Trans., EI-13(2), 130 (1978).

Munch J.P., Candau S. and Hild G., J. Polym. Sci., Polym. Phys. Ed., 15, 11 (1977).

Nagao M., Sawa G. and Ieda M., Trans. Inst. Elec. Eng. Japan, 96-A, 605 (1976).

Narkis M. and Miltz J., Israel Chem., 8, 7 (1970).

Naylor K.L. and Phillips P.J., J. Polym. Sci., Polym. Phys. Ed., 21, 2001 (1983).

Neher J.H. and McGrath M.H., A.I.E.E. Trans., 57, 660 (1957).

Nelson J.K. "Engineering Dielectrics" VII-A Ed. Bartnikas and Eichhorn ASTM STP, 783, 445 (1983).

Nichols J.B., J. Appl. Phys., 25, 840 (1954).

Nitta Y., IEEE Tran. EI 9(3), 109 (1974).

Nitta Y. and Funayama M., IEEE Trans. EI-13(2) 81 (1978).

Nitta Y., IEEE Trans. EI-15(2), 140 (1980).

Noto F., IEEE Trans. EI-15(3) 251 (1980).

Nunes S.L. and Shaw M.I., IEEE Trans. EI-15 No.6, 437 (1980).

Oakes W.G., J. Inst. Elec. Eng., Part 1, 95, 36 (1948).

O'Dwyer J.J., "The Theory of Electrical Conduction and Breakdown in Solid Dielectrics" Clarendon Press, Oxford, (1973).

Olley R.H., Hodge A.M. and Basset D.C., J. Polym. Sci. Polym. Phys. Ed. 17, 627 (1979).

Pasthuma A. and Pennings A.J., J. Polym. Sci. Polym. Phys. Ed. 14, 187 (1976).

Patsch R., Conf. on Elect. Insul and Dielect. Phenom. Annual Report, 323 (1975).

Patsch R., IEEE Trans EI-14 (4), 200 (1979).

Petermann J. and Gohil R.M., J. Macromol. Sci., Phys. B16 (2), 177 (1979).

Petermann J., Miles M. and Gleiter H., J. Macromol. Sci., Phys. B-12, 393 (1976).

Petermann J. and Schultz J.M., J of Mater. Sci.,13, 2188 (1978).

Phillips P.J., IEEE Trans EI-13 (2) (1978).

Phillips P.J., "Engineering Dielectrics" V. II-A Ed. Bartnikas and Eichhorn R.M., ASTM STP, 783 (1983).

Pohl H.A., "Electrostatics and Its Applications" Ed. Moore A.D., Willey Interscience,N.Y., (1973).

Proske G., Rubber Chem. Technol. 14, 489 (1941).

Rayner E.H., J. Institution of Elect. Eng., 49, 3 (1912).

Reneker D.H., J. of Polym. Sci. 59, 539 (1962).

Rijke A.M. and Mendelkern L., Macromolecules 4 594 (1971).

Rye J., Brown P.M. and Eeles W.T., J. of Physc. 8, L16 (1975).

Sabuni H. and Nelson J.K., J. of Materials Sci. 11, 1574 (1976).

Sasaki N., Yokoyama T. and Tanaka T., J. of Polym. Sci. Polym. Chem. Ed. 11, 1765 (1973).

Sazhin B.I. and Podosenova N.G., Polym. Sci. USSR, 6, 162 (1964).

Scherrer P., Gottinger Nachrichten, 2, 98 (1918).

Schultz J.M., "Polymer Materials Science" Prentice-Hall Inc. Canada (1974).

Seanor A.D., "Electrical Properties of Polymers" Academic Press, N.Y. (1982).

Seanor A.D., J. of Polm. Sci., A-2, 6, 463 (1968).

Sletbak J., IEEE Trans. PAS 98-4, 1358 (1979).

Sletbak J. and Erling I., IEEE Internat. Symp. on Elec. Insul., 29 (1984).

Srinavas N.N., Allam S.M. and Doepken H.C. Conf. on Elec. Insul. and Dielec. Phenom., 380 (1976).

Stark K.H. and Garton C.G., Nature, 176, 1225 (1955).

Starr W.T. and Endicott A., Trans AIEE PAS-80, 515 (1961).

Statton W.D. and Geil P.H., J. of Polym. Sci., 3, 357 (1960).

Stein R.S., Clough S. and Rhodes M.B., J. of Polym. Sci., 18, 1 (1967).

Tabata T., Fukuda T. and Iwata Z., IEEE Trans. PAS-91, 1361 (1972).

Tanaka T. and Fukuda T., Conf. on Elec. Insul. and Diel. Phenom., 239 (1974).

Tanaka T., Fukuda T. and Suziki S., IEEE Trans. PAS-95, 1892 (1976).

Tanaka T., Nitta Y. and Fukuda T., Conf. on Elec. Insul and Diel. Phenom. 1972, 216 (1973).

Trinh N.G. and Vincent C., IEEE PAS-99, 611 (1980).

Wagner H., Conf. on Elec. Insul. and Diel. Phenom., 62 (1974).

Wagner H. and Wartusch J., IEEE Trans IE-12 (6), 395 (1977).

Wargner K.W., AIEE Trans., 41,288 (1922).

Weedy B.M., "Underground Transmission of Electric Power" John Wiley & Sons England (1980).

Weibull W., J. of Appl. Mech., 18, 293 (1951).

Wintle H.J., in "Engineering Dielectrics" V.II-A Bartnikas and Eichhorn ED. ASTM STP 783 (1983).

Wunderlich B. and Sullivan P., J. of Polym. Sci., 61,195 (1962).

Wunderlich B., "Macromolecular Phiysics" V.2, Academic Press,N.Y. (1976).

Yahagi K., IEEE Trans. EI-15 (3), 241 (1980).

Varlow B.R., in "Methods of Experimental Physics" V.16-C, Ed. By Fava R.F., Academic Press, N.Y. (1980).

VITA

Ali Vatansever was born in Istip, Yugoslavia on July 13, 1954. He graduated from Bursa Ataturk High School in June of 1972. The following September he entered Middle East Technical University. Following a year of English preparatory school he received the Bachelor of Science degree in Chemistry in February of 1979. He started Master of Science studies in the same institution and received his M.Sc. degree in Polymer Chemistry in June of 1981.

In March 1982, the author entered the University of Utah at Salt Lake City, Utah and began to study toward a doctorate degree in Materials Science and Engineering. In December 13 1984, he transferred to the University of Tennessee at Knoxville, Tennessee along with his supervisor Professor Paul J. Phillips. He received the doctor of Philosophy degree in March 1987.